University of Strathclyde

NONLINEAR ESTIMATION FOR CONDITION MONITORING OF ADVANCED GAS-COOLED NUCLEAR REACTOR CORES

Santo Inzerillo

Industrial Control Centre,
Department of Electronic and Electrical Engineering,
University of Strathclyde,
204 George Street,
Glasgow G1 1XW

Thesis submitted in fulfilment of the requirements
for the degree of Doctor of Philosophy

August 2012

Declaration of Authenticity and Author's Rights

‘This thesis is the result of the author’s original research. It has been composed by the author and has not been previously submitted for examination which has led to the award of a degree.’

Santo Inzerillo

Signed:

Date:

Dedication

To my uncle Nino for inspiring me to undertake my study in the engineering field
(A mio zio Nino per avermi inspirato nell'intraprendere i miei studi nel campo ingegneristico)

To my parents Francesco and Rosa for their long life support
(Ai miei genitori Francesco e Rosa per avermi sostenuto tutta la vita)

To my sister Teresa for being always present in my life
(A mia sorella Teresa per essere stata sempre presente nella mia vita)

To my wife Joanna for her love and her patience
(A mia moglie Joanna per il suo amore e la sua pazienza)

Santo Inzerillo

Abstract

As the Advanced Gas-cooled Reactor (AGR) nuclear power stations are ageing, the nuclear core composed by graphite bricks can distort. The direct measurement of the core condition is costly and time-consuming, hence, alternative methods have been developed to provide the necessary information about the core condition.

This thesis presents a model-based technique for condition monitoring of AGRs cores using measurements obtained during routine core refuelling process. It has been demonstrated that Fuel Grab Load Trace (FGLT) data gathered during refuelling operations provides, through the magnitude of its friction component, information relating to the condition of the graphite bricks. Therefore, the condition monitoring of an AGR leads to the estimation of the friction force resulting from the interaction of the fuel assembly and the core channel. To this end the main objective of this work is to investigate estimation techniques that are needed in industrial applications and in particular can be used in the refuelling filtering problem. As a result of this study, a novel *LPV* estimator and robust estimator have been designed and implemented.

A model for the refuelling system was initially developed from the first principles of the process. Then its fuel assembly dynamics subsystem was identified to be used in a model based filtering application. Finally a H_∞ robust estimator was employed to estimate the friction force to be used for the core condition analysis.

Acknowledgements

Many people have contributed directly or indirectly to this thesis and at end of this journey I would like to give them a special thanks. Firstly, I would like to thank my supervisor Professor Mike Grimble for his excellent guidance over the years and for teaching me how to do research. His continuous feedback and encouragement have been essential for the completion of this work.

I also would like to thank my second supervisor Dr. Reza Katebi who gave me a lot of encouragement and comments during my research.

A special thanks is also due to Dr. Erfu Yang for useful discussion in the two years we worked in the nuclear project and for his contribution to the modelling section of this work.

Thanks to Sheila Campbell and Drew Smith for their help and nice chat and all my colleagues in the Industrial Control Centre who made my days more enjoyable.

I would like to acknowledge Prof. Stephen McArthur and Dr. Graeme West, coordinators of the AGR condition monitoring project in Strathclyde university, along with Dr Gordon Jahn and Chris Wallace all members of the Institute for Energy and Environment at the University of Strathclyde. Dr. Graeme West deserves a special mention for the useful discussions and suggestions which have had a significant impact on my understanding of the refuelling process.

This research was funded by EDF Energy under its monitoring programme. I therefore want to thank Graham Buckley, Ray Peacey, Michael Coghlan and Dave Towle from EDF Energy for their comments and technical support. I want to thank EDF for permitting me to publish the results of this research.

The contents, including any opinions and conclusions expressed in this thesis are those of the author alone. They do not necessarily represent the views of EDF Energy.

Santo Inzerillo

Table of Contents

Nomenclature

AGR	Advanced Gas-cooled Reactor
BETA	British Energy Trace Analysis
CBMU	Channel Bore Monitoring Unit
FGLT	Fuel Grab Load Trace
LPV	Linear Parameter Varying
NH_∞	Nonlinear H_∞ (Estimator)
NMV	Nonlinear Minimum Variance
pdf	Probability Density Function
PID	Proportional–Integral–Derivative (Controller)

Chapter 1

Introduction to Condition Monitoring for an AGR Nuclear Plant

The importance of condition monitoring for Advanced Gas-cooled Reactor nuclear power stations will be discussed and the previous works on this topic will be presented. The objectives of the thesis will be stated and a brief summary of each chapter will be given. Finally the main contributions achieved with this research and the list of publications resulting from this thesis will be presented.

1.1 Introduction

Most electricity currently generated by EDF Energy in nuclear plants is based on Advanced Gas-cooled Reactor (AGR) technology. The reactor core of an AGR plant is composed of a large number of graphite bricks that form channels, into which uranium fuel assemblies and control rods are inserted. This brick structure provides mechanical support for the fuel assemblies and control rods and helps to moderate the fission process in order to achieve a continuous and controllable nuclear chain reaction.

The graphite, used in the core structure, is a material that can tolerate the adverse conditions within the reactor relatively well, however it is not completely unaffected by the prolonged exposure to heat and radiation and therefore deteriorates over time. This core degradation, due to radiolytic oxidation and fast neutron doses, causes changes in the graphite properties and produce internal stresses in the core structure. As a result of this deterioration, cracks and deformations can occur in the graphite bricks that host the fuel assemblies components, however this process needs several decades to cause any significant damage to the core structure.

The AGR, second generation of UK commercial reactor systems, was designed during the late 60s and constructed during the 70s and early 80s (see Appendix A for an overview about AGR), hence the nuclear plants are approaching the end of their operating lives and the core may present the above-mentioned crack or deformation problems (see Appendix B for further details about graphite cracks). Although these distortions have remained within the expected and predicted limits, the condition of the reactor core bricks is increasingly becoming an important aspect of the monitoring phase [1-3].

The major concerns are about the effects that graphite brick cracking and deformation will have on the mechanical integrity of the core structure ([4, 5]) and if a distorted core structure can change the geometry of the control rod channels in such a way that the control of the fission would be jeopardized ([6]).

Detailed information relating to the condition of the graphite bricks can be obtained from channel inspections made every few years during routine outages (see Appendix C for further details). However, these inspections require the reactor to be shutdown and therefore cannot be executed on a regular basis without incurring a significant economical loss. Moreover the inspections can only cover a proportion of the core channels, thus consideration is being given to new methodologies for determining the core condition via routine monitoring of reactor parameters.

1.2 Condition Monitoring of AGR Nuclear Plant Research

To support the safety cases and extend the lifetime of an AGR nuclear plant, one of the main areas of research, that has been undertaken by the nuclear graphite team, is from the point of view of materials behaviour ([5]) and modelling the physical process of core degradation ([4]). The graphite failure, an ultimate result of internal shrinkages and thermal stresses generated during operational processes, depends not only on component geometry and size, but also on loading mode ([5]), as the nuclear graphite is a brittle and polygranular material. In [5], a continuum damage mechanics model was presented to predict the failures of nuclear graphite and this model was implemented into the commercial finite element analysis (FEA) software ABAQUS.

Recent studies have used measurements collected during routine refuelling of the reactor core called Fuel Grab Load Trace (FGLT). Each FGLT, collected whilst the

reactor remains in operation, describes in a dynamic way the force required to lift or lower each fuel assembly in and out of its fuel channel [7].

It has been proved that FGLT data can infer the condition of the channel being refuelled and therefore provides an indirect measurement of the core crack conditions. In fact, FGLT are influenced by the core bore geometry since part of the total load force represents the friction force between the fuel assembly and the graphite wall, which in turn is linked to the core crack conditions. Thus, by applying appropriate analysis techniques to the FGLTs useful information about the core crack condition can be extracted.

In recent years, many research studies have been made to assess the core condition using the refuelling process. An intelligent system for interpreting this process within an AGR reactor was developed in [7] by employing a knowledge-based system, Kohonen neural network-based classification, K-means clustering techniques, and rule induction methods. This system was designed to automate the process of data analysis by evaluating the large amounts of data produced during the refuelling process used to ensure the proper set-down of a fuel assembly within the given fuel channel. Currently engineers collate and assess the FGLT data.

Additionally a software system called BETA (British Energy Trace Analysis), that archives, visualizes and analyses data, has been developed to evaluate the condition of individual bricks and channels within the graphite cores ([8-11]).

In [12] a data mining approach was proposed to support graphite core condition monitoring by taking the FGLT data as the main source of information. A model of expected behaviour based on historical data was developed, which highlight events containing unusual features that may suggest the presence of brick cracking.

The FGLT data can also be used to infer the level of shrinkage within AGR reactor core bricks [13]. The refuelling measurements, versus the inspection data and theoretical ageing studies, confirms the expected shrinkage. The FGLT data is, moreover, used to build a predictive model of brick shrinkage. This allows for an understanding of how the graphite core bricks are ageing and gives an indication of the remaining useful life of the graphite core.

In [14] the effects of reactor parameters on the measured load of fuel assemblies during the refuelling process are considered.

The use of hidden Markov models (HMM) for anomaly detection in graphite core condition monitoring has been published recently ([15]). In this method, the presence of anomalous behaviour in candidate traces is inferred through the underlying statistical foundation of the HMM to give an observation likelihood averaged along the length of the input sequences. However, with the likelihood measure, the inference engine can only alert us to any anomalous behaviour and further detailed analysis will be needed.

Two benchmarking techniques were used in [16] to support the use of the FGLT data for the condition monitoring of graphite cores. The first technique was the minimum variance performance index method in which the traces that have performance indices out of the expected range are considered as abnormal. To identify the crack-related peaks in the traces, the recursive least squares (RLS) algorithm was employed as the second benchmarking technique. Like the data mining and HMM methods, the benchmarking techniques were also unable to directly separate the friction forces from the masked FGLT data. Their practical applications will be dependent on the availability of large data sets. The time-varying properties of the ageing core will also affect the scalability and generalization of the benchmarking techniques.

To separate out the friction forces from the masked FGLT data, model-based condition monitoring methods have attracted much attention over the last few years ([17, 18]).

In [19] a fault detection and isolation filter based on unknown input observer techniques is developed. The role of this filter is to estimate the friction force produced by the interaction between the wall of the fuel channel and the fuel assembly supporting brushes.

From this previous work it is clear that it is possible to estimate the friction forces from the masked FGLT data. However, in [17-19], the aerodynamic forces that are normally significant and varying were considered as system noises and as a result the estimate of friction force may be not accurate and reliable.

Due to the unknown properties of the aerodynamic forces involved in the model and filter as described above, the accuracy of estimating the friction forces will be affected significantly. A new approach is therefore required to reliably estimate the

friction force from the masked FGLT data obtained during the routine refuelling process.

1.3 Research Goals and Challenges

Obtaining consistent and reliable estimates of the friction force from FGLT data is difficult because the friction is just one of many physical phenomena that contribute to the final shape of the FGLTs. The weight of the fuel assemblies, the gas circulating in the channel and the fuel channel geometry are also components of the FGLTs and since their respective influence tend to vary in a seemingly random way the estimation of the friction force consequently becomes a challenging task.

This work proposes a strategy that deals with this challenge by developing 2 main areas of research, the model system identification and the estimator design, that converge in the estimation of the friction for the nuclear application (see Figure 1.1).

A summary of this approach is given below:

- System identification of the refuelling process by using the knowledge of the physical processes and the measurements gathered during the refuelling operation.
- Development of novel algorithm estimators that suits our system model specifications.
- Estimation of the friction force for the purpose of condition monitoring of the core channels.

1.4 Contributions of this Thesis

The main contributions of the thesis are summarized as follows:

- A linear parameter varying (*LPV*) model and nonlinear operator based approach to estimation and filtering is introduced for discrete-time multi-channel systems including time-delays. The validation of the theory and the design of the Nonlinear Minimum Variance (*NMV*) estimator for *LPV* system is done by using the Matlab/Simulink implementation for various case studies.
- Design and synthesis of a nonlinear operator based approach to H_∞ robust estimator. The estimator was implemented in Matlab/Simulink and the

simulation result proved that the H_∞ filtering problem is particularly appropriate for nonlinear uncertain systems.

- Design and synthesis of a robust optimal nonlinear estimator for uncertain systems. In the limiting case of a linear system the estimator has the form of a Wiener filter in discrete-time polynomial matrix system form. Simulations are carried out to corroborate the estimation algorithm theory.
- Development of a first principle model for the refuelling process of an AGR nuclear plant and identification of model parameters. Real data from an AGR nuclear power plant are employed to demonstrate the effectiveness of the nonlinear system identification approach.
- Estimation of the friction component of the FGLT data resulting from the interaction of the fuel assembly with the channel wall is performed by using a *NMV* estimator for a state-dependent model, particular class of the *LPV* estimator developed in Chapter 3 and the H_∞ estimator developed in chapter 4. The friction estimation, integrated in the BETA system ([8-11]), would be used to assess the condition of the nuclear core.

1.5 Organization of this Thesis

The thesis is organised as follows:

Chapter 1, gives an introduction to condition monitoring for an AGR nuclear plant, along with a background of related previous work. The motivation, organisation and main contributions of this thesis are presented. Finally the list of publications raised with this research are listed.

Chapter 2, provides an overview on the current state of the art in nonlinear estimation theories. The *NMV* estimation, the basic theory upon which this thesis is developed, is also introduced.

Chapter 3, describes the theory, design and simulation results, for a numerical and experimental case study, of the *LPV NMV* estimator.

Chapter 4, presents a robust nonlinear estimator for uncertain system and a H_∞ robust nonlinear estimator. Simulation results for 2 different case studies are also provided to validate the two novel estimators.

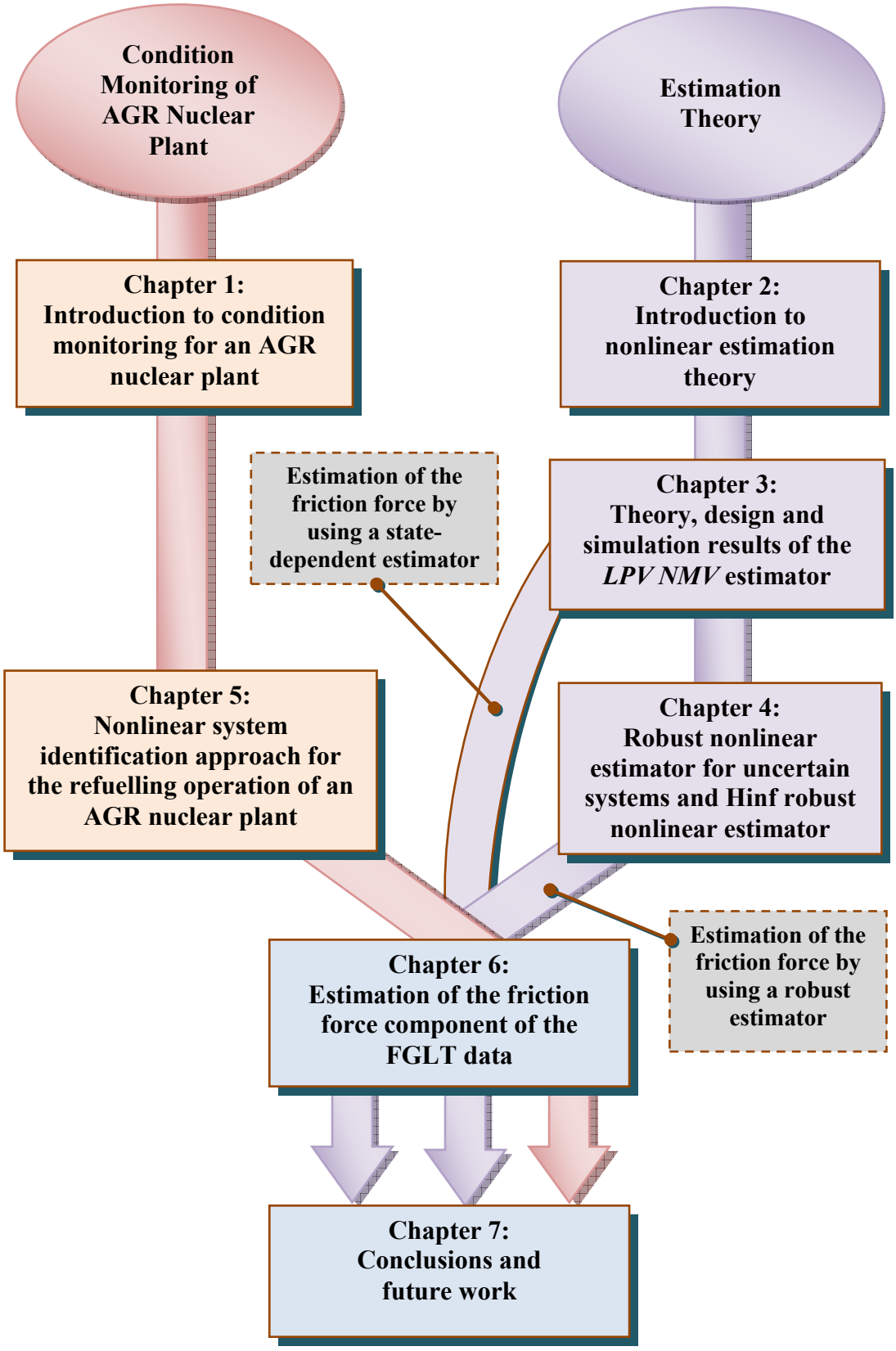

Figure 1.1: Outline of thesis

Chapter 5, describes a nonlinear system identification approach for the refuelling operation of an AGR nuclear plant. The model identification technique takes into account the physics law of the process and uses the Trust-Region Reflective Newton method to find the optimal parameters in the nonlinear refuelling model.

Chapter 6, presents the estimation of the friction force component of the FGLT data which can be used to assess the condition of the core channels. This estimation is obtained by using the filters designed in chapter 3 and chapter 4 and the nonlinear refuelling model identified in chapter 5. Simulation results for simulated cracks are also provided to highlight the efficacy of the method to evaluate the core condition.

Finally, Chapter 7 summarises the results presented in this thesis, draws some conclusions and discusses the proposed further work to be done in this area of research.

The outline of this thesis is visualized in Figure 1.1.

1.6 List of Publications

The outcomes of this thesis resulted in the following papers:

1. S. Inzerillo and M. J. Grimble, "H_∞ Robust Nonlinear Estimation for Condition Monitoring of AGR Nuclear Graphite Cores", to be submitted to IET signal processing.
2. S. Inzerillo and M. J. Grimble, "State-dependent Nonlinear Minimum Variance Estimation for Condition Monitoring of AGR Nuclear Graphite Cores", to be submitted to IEEE Transaction on Nuclear Science.
3. S. Inzerillo and M. J. Grimble, "Robust Wiener Optimal Nonlinear Estimation for Uncertain Systems" in 20th Mediterranean Conference on Control and Automation, Barcelona (Spain), July 3-6, 2012
4. S. Inzerillo and M. J. Grimble, "H_∞ Robust Nonlinear Estimation," in 18th IFAC World Congress, Milano (Italy), Aug 28-Sept 2 2011 pp. 6634-6639.
5. E. Yang, M. Grimble, S. Inzerillo, and M. Katebi, "Nonlinear model-based condition monitoring of advanced gas-cooled nuclear reactor cores," in 7th International Conference on Control & Instrumentation in Nuclear Installations, Lancaster University, UK, 2011.

6. E. Yang, M. Grimble, G. West, S. Inzerillo, M. Katebi, S. McArthur, "Model-based Estimation and Filtering for Condition Monitoring of AGR Nuclear Graphite Cores," in Proceedings of the UKACC International Conference on Control, Coventry, UK, 2010, pp. 1206-1211.

Chapter 2

Estimation Theory

The subject of nonlinear estimation is introduced by a very brief survey of the various nonlinear estimation methods. It represents only a limited survey but helps to put into context the new approach mentioned at the end of the chapter on which much of the rest of the thesis is based. A new nonlinear estimation paradigm which leads to simple filters, smoothers and predictors for classes of nonlinear stochastic systems is introduced. This new approach will be used in this thesis as the main theory for the design of a few novel estimators.

2.1 Introduction

Estimators like the Wiener ([20]) and Kalman filters ([21, 22]) provide well established solutions to the optimal linear filtering and estimation problems.

The Kalman filter has dominated the filter theory for decades in signal processing and control areas and it has been applied in various engineering and scientific areas. However its theory is for linear-Gaussian problem and since most of the real world systems are nonlinear and/or non-Gaussian many efforts have been made to develop nonlinear filtering methods.

Historically the first nonlinear filter was the extended Kalman filter (EKF) ([23]), which has the same structure as the Kalman filter but has a nonlinear model within the loop. To accommodate the nonlinearity the model is linearized at each time step to estimate the transition matrix and this is used to update the estimated covariance matrix. The EKF along with the dual EKF are the best known techniques for nonlinear estimation. The dual EKF uses two EKF's running concurrently (one for state estimation and one for neural network weight estimation).

The main problem of the EKF lies in the inherent approximations that are involved in its derivation mainly caused by the linearization of the nonlinear dynamic and/or measurement equations at each time-step.

Recently, there have been interesting developments in derivative-free nonlinear state estimation techniques as efficient alternatives to the extended Kalman filter. These include the so-called sigma point filters such as the unscented Kalman Filter (UKF) ([24, 25]), the central difference filter (CDF) ([26]), and the divided difference filter (DDF) ([27, 28]). The UKF is based on a set of discretely sampled sigma points that are used to parameterize the mean and covariance of the Gaussian random variables and the posterior mean and covariance are propagated through the true nonlinear function without the linearization steps so no explicit derivation of the Jacobian or Hessian matrix is necessary. The UKF approximation is generally much better than EKF (see [29]) and presents the same computation complexity.

The CDF and DDF compute the numerical derivative of a function at any point by approximating the function by some polynomial in the neighborhood of the selected point; this leads to efficient implementation of filters for nonlinear estimation applications.

The nonlinear filtering methods introduced so far, based on local linearization of the nonlinear system equations (EKF and dual EKF) or local approximation of the probability density of the state variables with the sampled sigma points (UKF, CDF and DDF), assume that the probability density of the state vector is Gaussian. For nonlinear and/or non-Gaussian filtering problems, the Gaussian sum filter (GSF) which approximates the posterior density function by a weighted sum of Gaussian densities has been adopted.

The main idea of the Gaussian sum filter is based on the principle that certain posterior densities can be approximated by a linear combination of Gaussian densities. However, this method may have a high computational complexity because a large number of densities could be necessary to approximate a non-Gaussian density. Another class of nonlinear and/or non Gaussian filter methods is based on the Monte Carlo approach. These estimators are flexible and relatively easy to design and they are promising candidates for a range of industrial problems ([30, 31]). Such methods are referred to as particle filtering because the continuous distributions are

approximated by a discrete set of weighted samples. These weighted samples are called particles, where each sample represents the system evolving through a random trajectory in the state-space. The weight represents the probability of the trajectory ([32, 33]). If the number of samples is large, the Monte Carlo approximation approaches a posterior probability density function (pdf) representation and the particle filter approaches the optimal Bayesian estimate. The main drawback with the particle filter (PF) is that it is very demanding computationally.

An overview of the main nonlinear filters methods introduced can be seen in Figure 2.1.

A direct numerical approximation to the optimal nonlinear filter can be employed. It calculates the Fokker-Planck equation (FPE) that is a partial differential equation governing the evolution of the probability density of the state conditioned on the measurements. Hence the approximation of this equation in real time can solve the nonlinear filter problem, however, the computational complexity grows exponentially with dimension of the state vector so the numerical solution of the FPE is feasible for low dimensional problems (see [34]).

An exact filter solves the nonlinear filtering problem by transforming a partial differential equation to a ordinary differential equation. In 1981 an exact filter for a special class of nonlinear problems was derived by Beneš ([35]), this filter was not as powerful as the Kalman filter for linear estimation problems. In 1986 this filter was generalized by Daum ([36]) to handle a much broader class of nonlinear problems and solving all Kalman filter problems.

In the following sections the Extended Kalman Filter, the Unscented Kalman Filter, the particle filter algorithms and the Nonlinear Minimum Variance (*NMV*) estimator are presented. To describe all the details of these algorithms is beyond the scope of this work, therefore, an algorithm description is presented omitting some theoretical considerations. The proposed *NMV* estimation theory, the base of this work, is rather different in nature of the above mentioned estimators, being model based and of a fixed structure.

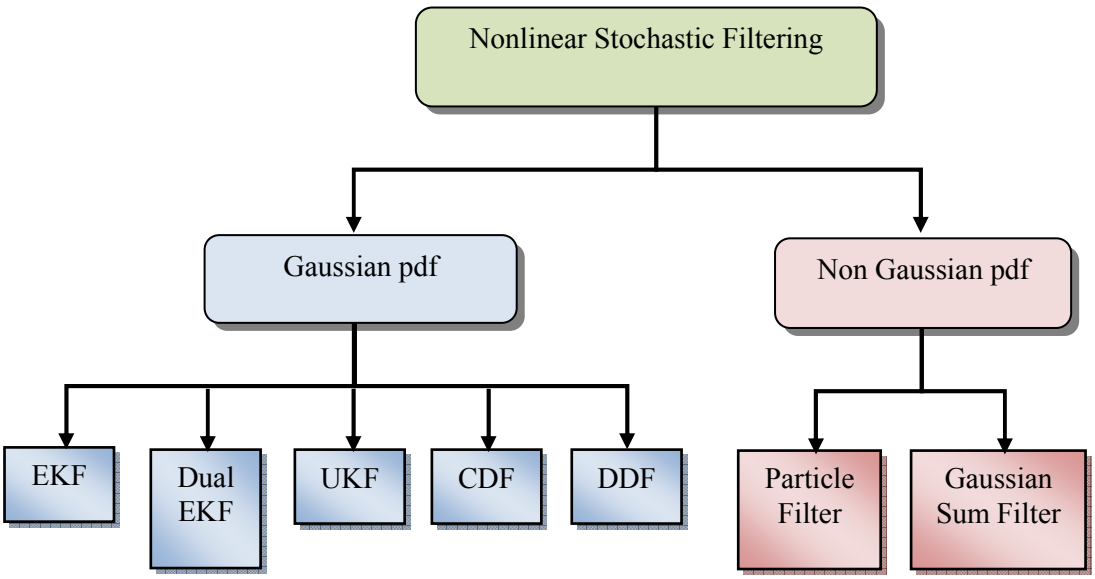

Figure 2.1: Nonlinear Stochastic Filtering Methods

2.2 Extended Kalman Filter

The extended Kalman filter is a set of mathematical equations that implement a predictor-corrector mechanism; it linearizes the process model at each step, calculates the current state of the system and then updates it by using the available sensor measurements.

Consider the following nonlinear system, described by the difference equation and the observation model with additive noise:

$$\begin{aligned} \mathbf{x}_k &= \mathbf{f}\left(\mathbf{x}_{k-1}\right) + \mathbf{w}_{k-1} \\ \mathbf{y}_k &= \mathbf{h}\left(\mathbf{x}_k\right) + \mathbf{v}_k \end{aligned} \tag{2.1}$$

The initial state $\mathbf{x}_0$ is a random vector with known mean $\mu_0 = E\left[\mathbf{x}_0\right]$ and covariance $\mathbf{P}_0 = E\left[\left(\mathbf{x}_0 - \mu_0\right)\left(\mathbf{x}_0 - \mu_0\right)^T\right]$.

We assume that $\mathbf{w}_k$ denotes the model uncertainties and $\mathbf{v}_k$ represents the measurement noise. These random vectors are uncorrelated, zero-mean and with known covariances and they are uncorrelated with the initial state $\mathbf{x}_0$.

Initially, since the only available information is the mean, μ_0, and the covariance, $\mathbf{P}_0$, of the initial state then the initial optimal estimate $\mathbf{x}_0$ and error covariance are:

$$\begin{aligned}\hat{\mathbf{x}}_0 &= \mu_0 = E\left[\mathbf{x}_0\right] \\ \mathbf{P}_0 &= E\left[\left(\mathbf{x}_0 - \hat{\mathbf{x}}_0\right)\left(\mathbf{x}_0 - \hat{\mathbf{x}}_0\right)^T\right]\end{aligned} \tag{2.2}$$

Assume now that we have an optimal estimate $\hat{\mathbf{x}}_{k-1} = E\left[\mathbf{x}_{k-1}\middle|\mathbf{y}_{k-1}\right]$ with $\mathbf{P}_{k-1}$ covariance at the time $k-1$, we can perform the prediction step that consists in deriving a priori state estimate $\hat{\mathbf{x}}_k^-$. This operation can be done by considering the first-order terms of the function $\mathbf{f}(\cdot)$ expanded in Taylor series in the point $\hat{\mathbf{x}}_{k-1}$ and after a straightforward derivation we have $\hat{\mathbf{x}}_k^- = \mathbf{f}(\hat{\mathbf{x}}_{k-1})$.

Then, we find that the a priori estimate of the error covariance matrix is:

$$\mathbf{P}_k^- = \mathbf{\Phi}_k \mathbf{P}_{k-1} \mathbf{\Phi}_k^T + \mathbf{Q}_k \tag{2.3}$$

where $\mathbf{Q}_k$ is the process noise covariance, $\mathbf{P}_{k-1}$ is the posteriori estimate of the error covariance, and $\mathbf{\Phi}_k$ is a Jacobian matrix which linearizes the process function $\mathbf{f}$:

$$\mathbf{\Phi}_k = \frac{\partial f_{(i)}}{\partial x_{(j)}}(\hat{\mathbf{x}}_k^-) \tag{2.4}$$

After the prediction step, the correction step calculates the posteriori state estimate using

$$\hat{\mathbf{x}}_k = \hat{\mathbf{x}}_k^- + \mathbf{K}_k\left(\mathbf{y}_k - \mathbf{H}_k \hat{\mathbf{x}}_k^-\right) \tag{2.5}$$

where $\mathbf{K}_k$ is the Kalman gain and $\mathbf{H}_k$ is the measurement matrix used to combine the measurement vector $\mathbf{y}_k$, obtained from the tracking device, with $\hat{\mathbf{x}}_k^-$. The Kalman gain is computed using

$$\mathbf{K}_k = \mathbf{P}_k^- \mathbf{H}_k^T \left(\mathbf{H}_k \mathbf{P}_k^- \mathbf{H}_k^T + \mathbf{R}\right)^{-1} \tag{2.6}$$

where $\mathbf{R}$ is the measurement noise covariance, and the measurement matrix is calculated using

$$\mathbf{H}_k = \frac{\partial h_{(i)}}{\partial x_{(j)}}(\hat{\mathbf{x}}_k^-) \tag{2.7}$$

a Jacobian matrix that linearizes around the nonlinear measurement function $\boldsymbol{h}$.

Finally, we compute the posteriori estimate of the error covariance using

$$\mathbf{P}_k = \left(\mathbf{I} - \mathbf{K}_k \mathbf{H}_k\right)\mathbf{P}_k^- \tag{2.8}$$

Further theoretical details can be found in [23].

The EKF is one of the most popular nonlinear estimators and this is justified for the simplicity of the linear approximation for nonlinear systems. However due to this linearization and the Gaussian assumption of the priori or posterior estimated mean and covariance, the mean and covariance are only an approximations to the true quantities.

2.3 Unscented Kalman Filter

In the UKF the probability density function, that it is assumed Gaussian, is sampled at a number of so-called sigma points to approximate the multidimensional integrals required ([37]). This process is called unscented transformation and it maps the sigma points using some weights in a way that yields a relationship between the moments of the input parameters and the weights of the sigma points; in other words the sigma points are chosen to have as mean and covariance $\hat{\mathbf{x}}_{k-1}$ and $\mathbf{P}_{k-1}$ respectively.

Consider the following nonlinear system, described by the difference equation and the observation model with additive noise:

$$\begin{aligned} \mathbf{x}_k &= \mathbf{f}\left(\mathbf{x}_{k-1}\right) + \mathbf{w}_{k-1} \\ \mathbf{y}_k &= \mathbf{h}\left(\mathbf{x}_k\right) + \mathbf{v}_k \end{aligned} \tag{2.9}$$

Initially, since the only available information is the mean, μ0, and the covariance, $\mathbf{P}_0$, of the initial state then the initial optimal estimate $\mathbf{x}_0$ and error covariance is:

$$\hat{\mathbf{x}}_0 = \mu_0 = E\left[\mathbf{x}_0\right]$$
$$\mathbf{P}_0 = E\left[\left(\mathbf{x}_0 - \hat{\mathbf{x}}_0\right)\left(\mathbf{x}_0 - \hat{\mathbf{x}}_0\right)^T\right]$$

Let $\mathbf{x}_{k-1}$ be a set of $2n+1$ sigma points (where n is the dimension of the state space) and their associated weights:

$$\mathbf{X}_{k-1} = \left\{\left(\mathbf{x}_{k-1}^j, W^j\right) \; for \; j = 0,1,....,2n\right\} \tag{2.10}$$

Consider the following selection of sigma points, selection that incorporates higher order information in the selected points ([38]):

$$
\begin{aligned}
&\mathbf{x}_{k-1}^{0} = \hat{\mathbf{x}}_{k-1} \\
&-1 < W^{0} < 1 \\
&\mathbf{x}_{k-1}^{i} = \hat{\mathbf{x}}_{k-1} + \left(\sqrt{\frac{n}{1-W^{0}} \mathbf{P}_{k-1}} \right)_{i} \quad for\ all\ i = 1,...,n \\
&\mathbf{x}_{k-1}^{i+n} = \hat{\mathbf{x}}_{k-1} - \left(\sqrt{\frac{n}{1-W^{0}} \mathbf{P}_{k-1}} \right)_{i} \quad for\ all\ i = 1,...,n \\
&W^{j} = \frac{1-W^{0}}{2n} \quad for\ all\ i = 1,...,n
\end{aligned}
\tag{2.11}
$$

where the weights must obey the condition:

$$\sum_{j=0}^{2n} W^{j} = 1$$

Each sigma point is propagated through the nonlinear process model:

$$\hat{\mathbf{x}}_{k}^{j-} = \mathbf{f}\left(\mathbf{x}_{k-1}^{j} \right)$$

The transformed points are used to compute the mean and covariance of the forecast value of $\mathbf{x}_k$:

$$
\begin{aligned}
\hat{\mathbf{x}}_{k}^{-} &= \sum_{j=0}^{2n} W^{j} \hat{\mathbf{x}}_{k}^{j-} \\
\mathbf{P}_{k}^{-} &= \sum_{j=0}^{2n} W^{j} \left(\hat{\mathbf{x}}_{k}^{j-} - \hat{\mathbf{x}}_{k}^{-} \right) \left(\hat{\mathbf{x}}_{k}^{j-} - \hat{\mathbf{x}}_{k}^{-} \right)^{T} + \mathbf{Q}_{k-1}
\end{aligned}
\tag{2.12}
$$

where $\mathbf{Q}$ is the process noise covariance.

Then the sigma points through the nonlinear observation model are propagated and their mean and covariance (innovation covariance) are computed:

$$\hat{\mathbf{y}}_{k}^{j-} = \mathbf{h}(\mathbf{x}_{k}^{j}) \tag{2.13}$$

$$
\begin{aligned}
\hat{\mathbf{y}}_{k}^{-} &= \sum_{j=0}^{2n} W^{j} \hat{\mathbf{y}}_{k}^{j-} \\
\mathbf{P}_{\hat{\mathbf{y}}_k \hat{\mathbf{y}}_k} &= \sum_{j=0}^{2n} W^{j} \left(\hat{\mathbf{y}}_{k}^{j-} - \hat{\mathbf{y}}_{k}^{-} \right) \left(\hat{\mathbf{y}}_{k}^{j-} - \hat{\mathbf{y}}_{k}^{-} \right)^{T} + \mathbf{R}_{k}
\end{aligned}
\tag{2.14}
$$

where $\mathbf{R}$ is the measurement noise covariance.

The cross covariance between $\hat{\mathbf{x}}_{k}^{-}$ and $\hat{\mathbf{y}}_{k}^{-}$ is:

$$\mathbf{P}_{\hat{\mathbf{x}}_k \hat{\mathbf{y}}_k} = \sum_{j=0}^{2n} W^{j} \left(\hat{\mathbf{x}}_{k}^{j-} - \hat{\mathbf{x}}_{k}^{-} \right) \left(\hat{\mathbf{y}}_{k}^{j-} - \hat{\mathbf{y}}_{k}^{-} \right)^{T} \tag{2.15}$$

The information obtained in the forecast step is now combined with the new observation measured $\mathbf{y}_k$.

Assume that the estimate has the same form as in the KF:

$$\hat{\mathbf{x}}_k = \hat{\mathbf{x}}_k^- + \mathbf{K}_k\left(\mathbf{y}_k - \hat{\mathbf{y}}_k\right) \tag{2.16}$$

where the Kalman gain is given by the following:

$$\mathbf{K}_k = \mathbf{P}_{\hat{\mathbf{x}}_k\hat{\mathbf{y}}_k}\mathbf{P}_{\hat{\mathbf{y}}_k\hat{\mathbf{y}}_k}^{-1} \tag{2.17}$$

The posterior covariance is updated by using the following:

$$\mathbf{P}_k = \mathbf{P}_k^- - \mathbf{K}_k\mathbf{P}_{\hat{\mathbf{y}}_k\hat{\mathbf{y}}_k}\mathbf{K}_k^T \tag{2.18}$$

2.4 Particle Filters

Particle filters include a large class of suboptimal nonlinear filters based on sequential Monte Carlo simulations, in which the distributions are approximated by weighted particles that are generated using pseudo-random number generators.
The general discrete-time model used in particle filters is as follow:

$$\begin{aligned}\mathbf{x}_{k+1} &= \mathbf{f}\left(\mathbf{x}_k\right) + \mathbf{w}_k \\ \mathbf{y}_k &= \mathbf{h}\left(\mathbf{x}_k\right) + \mathbf{v}_k\end{aligned} \tag{2.19}$$

Process noise $\mathbf{w}_k$ and the measurement noise $\mathbf{v}_k$ are not necessarily assumed to be Gaussian processes and this represents the main difference between particle filters and the other filters previously introduced. The distributions of $\mathbf{x}_0$, $\mathbf{w}_k$ and $\mathbf{v}_k$, denoted by $p\left(\mathbf{x}_0\right)$, $p\left(\mathbf{w}_k\right)$ and $p\left(\mathbf{v}_k\right)$, respectively, are assumed to be known and mutually independent. The probabilities $p\left(\mathbf{x}_{k+1}\middle|\mathbf{x}_k\right)$ and $p\left(\mathbf{y}_k\middle|\mathbf{x}_k\right)$ can be derived from the above model and are assumed to be available.

The state trajectory $\left\{\mathbf{x}_j\right\}_{j=0}^{k}$ and the measurement history $\left\{\mathbf{y}_j\right\}_{j=1}^{k}$, are denoted by the variables $\mathbf{X}_k$ and $\mathbf{Y}_k$ respectively. The discrete approximation of the posterior distribution $p\left(\mathbf{x}_k\middle|\mathbf{Y}_k\right)$ with N weighted particles $\left\{\mathbf{x}_k^{(i)}, \omega_k^{(i)}\right\}_{i=1}^{N}$ is given by

$$P_N\left(d\mathbf{x}_k\middle|\mathbf{Y}_k\right) \approx \sum_{i=1}^{N}\omega_k^{(i)}\delta_{x_k^{(i)}}\left(d\mathbf{x}_k\right) \tag{2.20}$$

where $\mathbf{x}_k^{(i)}$ are the particles drawn from the importance function or proposal distribution $q\left(\mathbf{x}_{k+1}\left|\mathbf{X}_k^{(i)},\mathbf{Y}_{k+1}\right.\right)$, $\omega_k^{(i)}$ are the normalized importance weights, satisfying $\sum_{i=1}^{N}\omega_k^{(i)}=1$, and $\delta_{x_k^{(i)}}\left(d\mathbf{x}_k\right)$ denotes the Dirac-delta mass located in $\mathbf{x}_k^{(i)}$. The importance weight is the ratio of the posterior distribution to the importance function evaluated at $\mathbf{x}_k^{(i)}$. The expectation of a known function $\mathbf{f}\left(\mathbf{x}_k\right)$ with respect to $p\left(\mathbf{x}_k\left|\mathbf{Y}_k\right.\right)$ is then approximated by $\sum_{i=1}^{N}\omega_k^{(i)}\mathbf{f}\left(\mathbf{x}\in_k^{(i)}\right)$.

After few iterations the samples tend to spread and the weights will be almost zero for most of them, which means that the samples do not contribute much to the estimation of the posterior distribution. This phenomenon is known as the degeneracy problem in the sequential importance sampling particle filter step. A solution to this problem is found by introducing a selection (resampling) step to eliminate samples with low importance ratios and multiply samples with high importance ratios.

The resampling step alleviates the inherent particle degeneracy of sequential importance sampling, but also reduces the number of distinct particles, which is often called the problem of particle impoverishment. Simple remedies for the impoverishment problem include roughening and regularization.

The particle $\left\{\mathbf{x}_k,\omega_k^{(i)}\right\}_{i=1}^{N}$ is updated recursively and at any step; first the sequential importance sampling step is calculated followed by the resampling step:

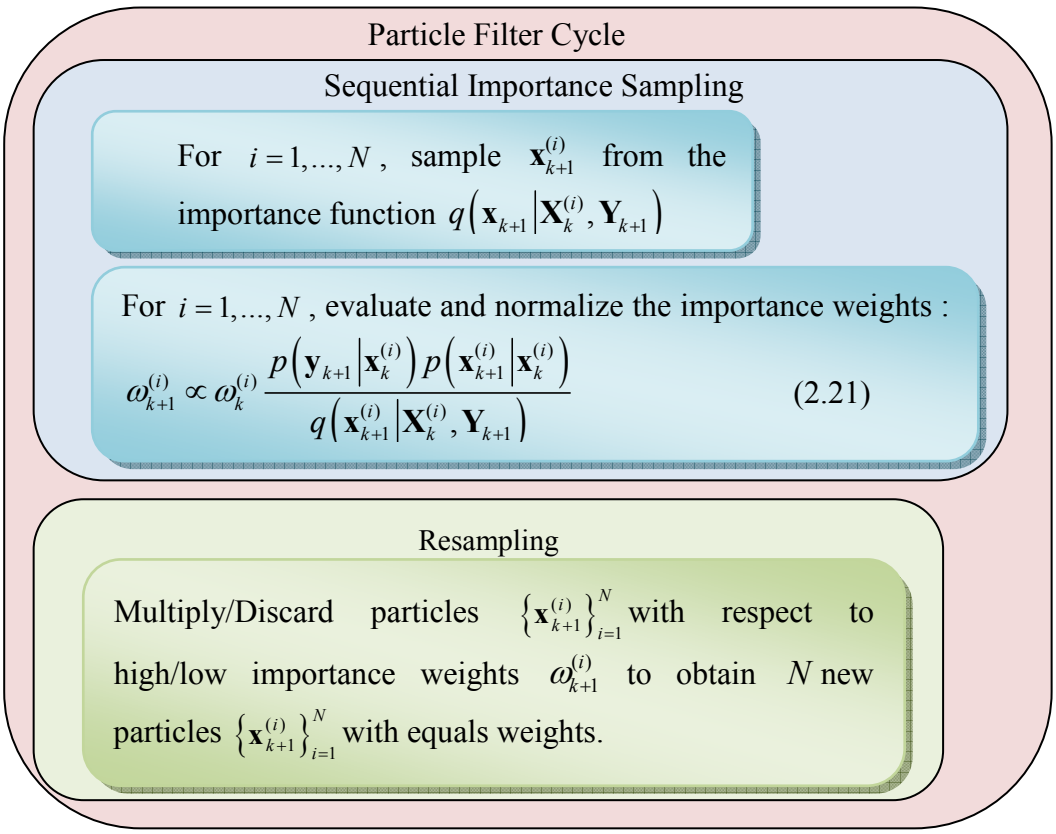

The importance function can be chosen from a large class of distributions. A popular suboptimal choice of the importance function is $q\left(\mathbf{x}_{k+1}^{(i)}\left|\mathbf{X}_k^{(i)},\mathbf{Y}_{k+1}\right.\right)=p\left(\mathbf{x}_{k+1}\left|\mathbf{x}_k^{(i)}\right.\right)$ and the resulting particle filter is called bootstrap filter (BF). Sampling $\mathbf{x}_{k+1}^{(i)}$ from $p\left(\mathbf{x}_{k+1}\left|\mathbf{x}_k^{(i)}\right.\right)$ is equivalent to the dynamic propagation of $\mathbf{x}_k^{(i)}$ to time t_{k+1}. The information contained in the measurement $\mathbf{y}_{k+1}$ is not employed in the sampling process. The corresponding update of the importance weight in Eq. (2.21) leads to the following simpler form:

$$\omega_{k+1}^{(i)} \propto \omega_k^{(i)} p\left(\mathbf{y}_{k+1}\left|\mathbf{x}_{k+1}^{(i)}\right.\right) \tag{2.22}$$

which is useful when the evaluation of $p\left(\mathbf{x}_{k+1}\left|\mathbf{x}_k\right.\right)$ is difficult.

2.5 Nonlinear Minimum Variance Estimator

The solution of a very special class of Nonlinear Minimum Variance estimation problems is considered here using least squares method. The generality of the

problem is restricted so that a simple nonlinear estimator algorithm is derived. This is the dual problem to the so-called NGMV optimal control approach introduced by Grimble (2005, [39]) and by Grimble and Majecki (2005, [40]). The cost-function to be minimised involves the variance of the estimation error and a relatively simple optimisation procedure and solution results. This was considered for systems represented by polynomial matrices by Grimble (2007, [41]), however, state equation methods of modelling are sometimes more natural when the system is represented by physical differential or difference equations and state models may also be preferable for larger systems because of numerical properties.

The filtering problem involves a signal that is generated by white noise into a colouring filter. The signal then goes through a nonlinear signal channel which is assumed to be stable but is otherwise quite general. One of the main strengths of the technique is that the nonlinear channel dynamics can be represented by a general nonlinear operator. This might involve a set of nonlinear equations or could even be a black box model containing unknown code or look-up tables. This black box model may be obtained from a neural or fuzzy-neural network. The delayed output of the communications channel is assumed to be measured but the measurements are corrupted by a signal representing either measurement noise or channel uncertainties.

The solution requires an assumption that a particular nonlinear operator has a stable inverse. This operator depends upon the nonlinear channel interference noise model which is included for design purposes and represents expected uncertainties. The uncertainty is modelled by a parallel communications path which can represent a possible interference signal. This may not be a physical path but is included for design purposes to shape the interference and measurement noise attenuation characteristics.

It has potential applications in control systems, fault monitoring, communications and signal processing systems.

Chapter 3

Linear Parameter Varying Estimation

A linear parameter varying (LPV) model and nonlinear operator based approach to estimation and filtering is discussed in this chapter. The problem involves a signal entering a communication channel that includes nonlinearities and transport delay elements. The measurements are assumed to be corrupted by a coloured noise signal which is correlated with the signal to be estimated. The communication channel may include either static or dynamic nonlinearities represented by a general nonlinear operator and/or a LPV model form. The theoretical solution does not involve empirical assumptions or linearization approximations. The resulting algorithm is relatively simple to derive and to implement. The validation of the nonlinear estimator theory is done by using a numerical example and a pursuit-evader problem case study.

3.1 Introduction

The control theories for linear time invariant systems are well established and dominant in the classical control theories, however real plants are often very complicated, thus control systems have to deal with nonlinear and/or time-variant systems; hence, over the last few decades the study of nonlinear systems have attracted considerable attention.

The gain-scheduling technique has been largely employed for nonlinear system controllers where linear models, obtained in different operating points, approximated the nonlinear model. The system controller is the combination of the controllers of the linear models, thus the well known theory of linear system synthesis is used for a nonlinear system. However, many of the gain scheduling techniques require a large

number of linear models and a slow varying operating point to guarantee that the closed loop specifications are achieved ([42]).

A solution to these problems may be the use of a particular type of time-varying model called Linear Parameter Varying (*LPV*) systems. An *LPV* model can be seen as a linear system where the system matrices depend upon a time varying parameter. Hence a nonlinear system can be brought to a *LPV* system by linearizing along a time-varying trajectory. A discrete *LPV* systems is represented in state space as:

$$\begin{aligned} x(k+1) &= A(p(k))x(k) + B(p(k))u(k) \\ y(k) &= C(p(k))x(k) + D(p(k))u(k) \end{aligned} \tag{3.1}$$

where $p(k)$ is the varying parameter, $x(k)$ is the state, $u(k)$ is the input, $y(k)$ is the output and $A(p(k)), B(p(k)), C(p(k)), D(p(k))$ are the parameter varying system matrices.

The terminology of *LPV* was first introduced in [43] and with the introduction of a Linear Fractional Transformation (LFT) structure for the *LPV* system ([44, 45]), advanced control synthesis techniques can be applied to these systems, such as the parameter dependent H_∞ controller introduced in [46, 47].

In the following sections the solution of a special class of Nonlinear Minimum Variance (*NMV*) estimation problems for *LPV* system is considered using *least squares* estimation methods. A simple nonlinear estimator algorithm is obtained which is a consequence of the choice of system structure and noise models. The estimation problem solution involves inferential estimation of a signal which enters a communication channel that contains transport delays and nonlinearities represented by nonlinear operator and an *LPV* set of nonlinear dynamics. It is assumed that the measurements are corrupted by a coloured noise signal correlated with the signal to be estimated. The cost-function to be minimized involves the variance of the estimation error and requires a very simple optimisation procedure ([48]).

3.2 Signal Processing System Description

The signal to be estimated passes through a transmitting channel which possesses a delay $z^{-\Lambda_0}$, a *LPV* model $\mathcal{W}_{co}$ and a general nonlinear operator $\mathcal{W}_{c1}$. The

measurements are assumed to be corrupted by a noise signal $n(t)$. The message signal to be estimated is at the output of a linear block: $s = \mathcal{W}_c y$.

For greater generality is introduced a dynamic cost weighting function that penalized the signal in particular frequency range: $s_q = \mathcal{W}_q s$ then is the signal to be estimated. The signal processing problem is illustrated in Figure 3.1. An additional nonlinear parallel channel with dynamics $\mathcal{F}_{c0}$ and delay $z^{-\Lambda_0}$ is also introduced in our nonlinear filtering problem (shown by dotted lines in Figure 3.1). This channel which is assumed to have a stable inverse will not exist physically but can be used to represent the uncertainties in channel, which provides additional design freedom. In Figure 3.1 the white noise signal ε is assumed to be zero mean.

3.2.1 Signal Processing System Equations

In this section is given a mathematical description of the signals in the system.

Input Signal:

$$y(t) = \mathcal{W}_s \varepsilon(t) \tag{3.2}$$

Disturbance Noise Signal:

$$n(t) = \mathcal{W}_n \varepsilon(t) \tag{3.3}$$

where $\varepsilon(t)$ is white driving noise

Channel input:

$$f(t) = y(t) + n(t) \tag{3.4}$$

Channel input:

$$f_0(t) = z^{\Lambda_0} f(t - \Lambda_0) \tag{3.5}$$

Input Channel Subsystem:

$$s_0(t) = (\mathcal{W}_{c0} f_0)(t) \tag{3.6}$$

Channel Interference:

$$n_c(t) = (\mathcal{F}_c \varepsilon)(t) \tag{3.7}$$

Nonlinear parallel channel:

$$\mathcal{F}_c(t) = \mathcal{F}_{c0}(t) z^{-\Lambda_0} \tag{3.8}$$

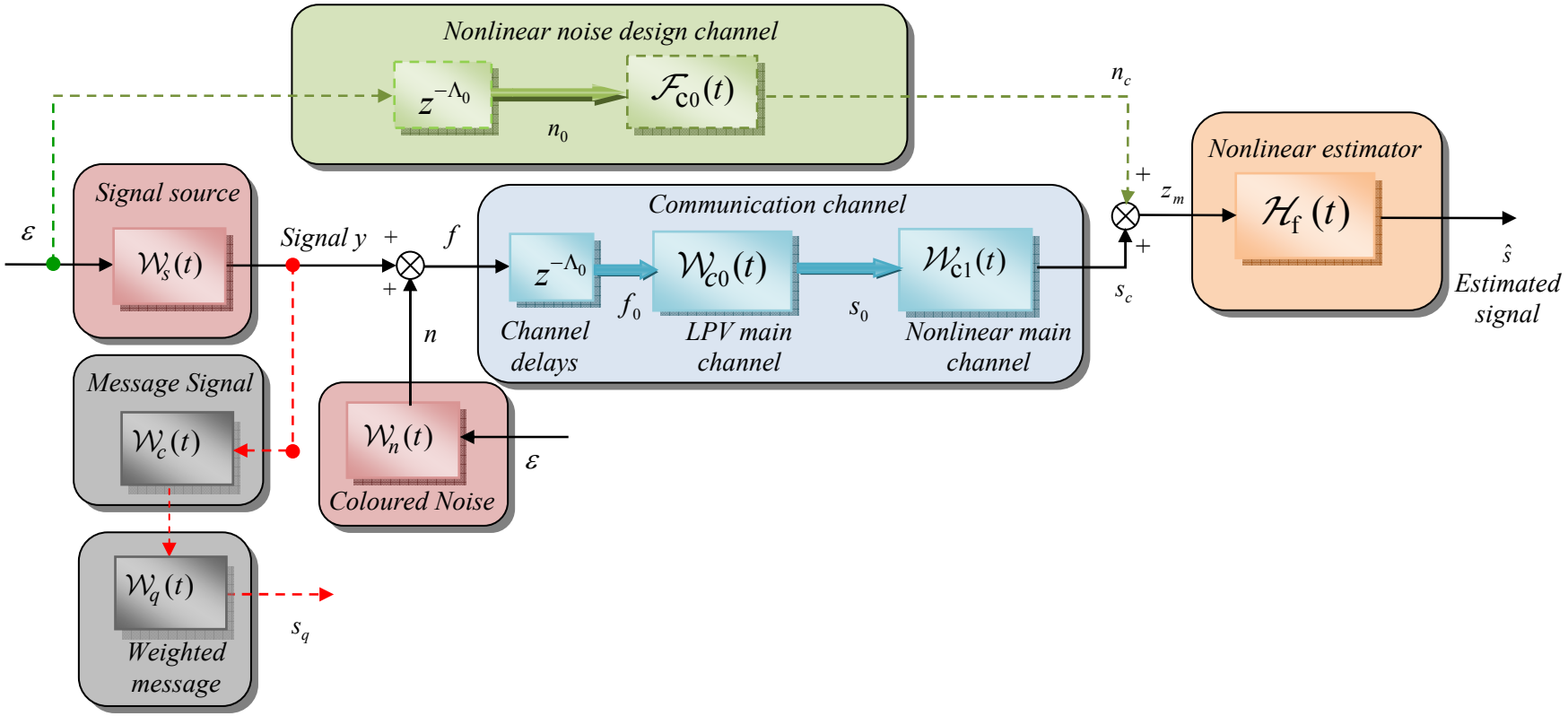

Figure 3.1: Canonical Nonlinear Filtering Problem with Noise Sources and Channel Interference

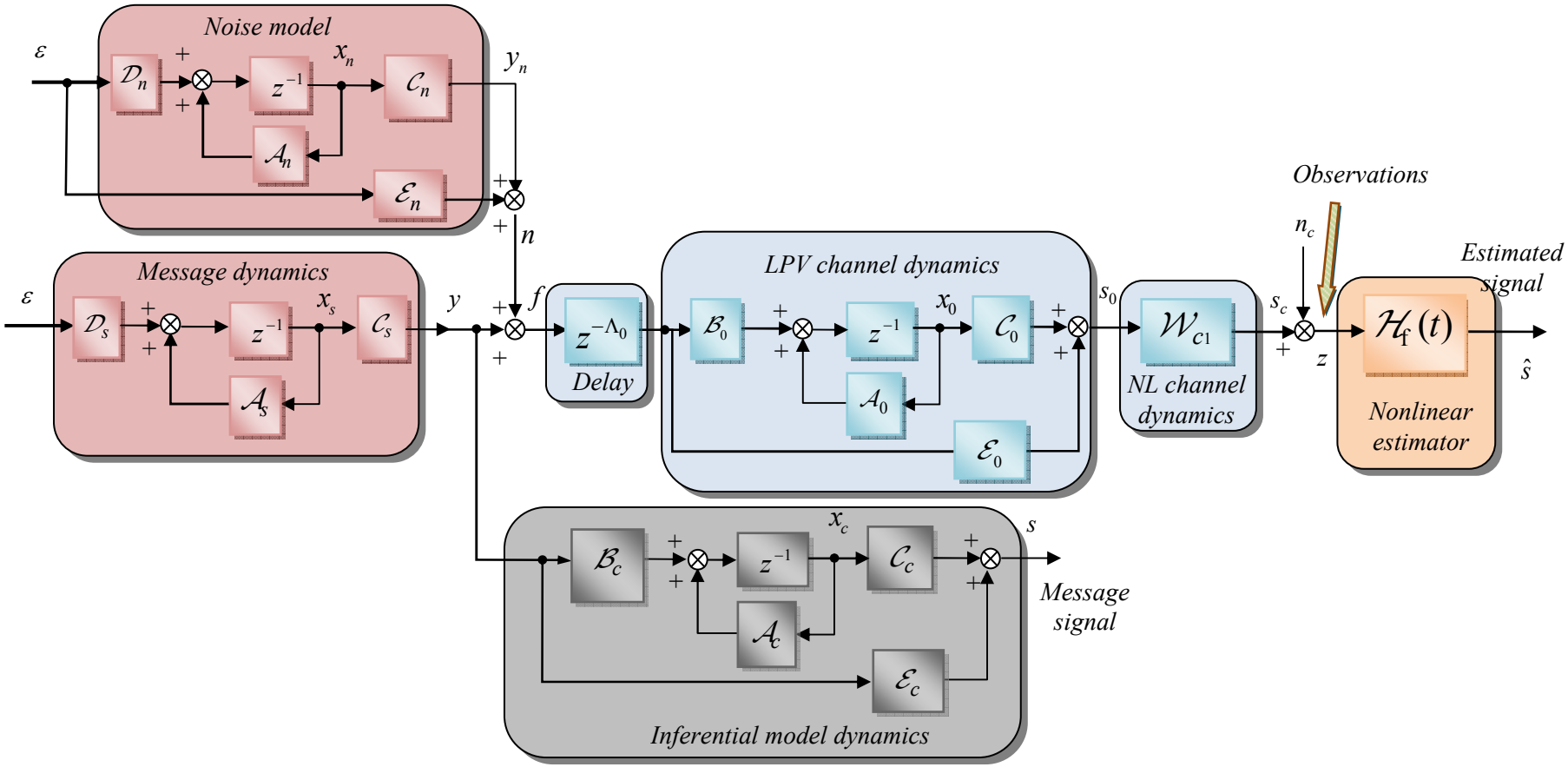

Figure 3.2: Linear Message and Noise Models and Linear and Nonlinear Channel Dynamics

Nonlinear channel subsystem output:

$$s_c(t) = \left(\mathcal{W}_{c1}\, s_0\right)(t) \tag{3.9}$$

Observations signal:

$$z(t) = n_c(t) + s_c(t) \tag{3.10}$$

Message signal to be estimated:

$$s(t) = \mathcal{W}_c y(t) = \mathcal{W}_c \mathcal{W}_s \varepsilon(t) \tag{3.11}$$

Weighted message signal:

$$s_q(t) = \mathcal{W}_q s(t) = \mathcal{W}_q \mathcal{W}_c y(t) = \mathcal{W}_q \mathcal{W}_c \mathcal{W}_s \varepsilon(t) \tag{3.12}$$

3.2.2 LPV Dynamics and Models

Consider now the various sub-systems which may be represented in either a linear state-space or a *LPV* state equation matrix form, as revealed more clearly in Figure 3.2. Recall the state-equation matrices are time-varying since they are allowed to depend upon the system parameters ([49]). This time dependence can be denoted $\mathcal{A}(t) = \mathcal{A}(p(t))$, or to simplify notation, simply as $\mathcal{A}$.

The total observations signal, representing the output of the communication channel, has the form:

$$z(t) = n_c(t) + s_c(t) = (\mathcal{F}_c \varepsilon)(t) + \left(\mathcal{W}_{c_1}\, s_0\right)(t)$$

The *signal and noise* entering the communication channel:

$$f(t) = y(t) + n(t) = \mathcal{C}_s(t) x_s(t) + \mathcal{C}_n(t) x_n(t) + \mathcal{E}_n(t)\varepsilon(t) \tag{3.13}$$

Note that all the models may be *LPV* with the exception of the cost weighting which is assumed to be linear and time-invariant. The state-space matrix form of the system models may therefore be listed as follows:

Signal generator:

$$x_s(t+1) = \mathcal{A}_s(t)\, x_s(t) + \mathcal{D}_s(t)\omega(t) \tag{3.14}$$

$$y(t) = \mathcal{C}_s(t) x_s(t) \;\; and \;\; operator \;\; \mathcal{W}_s(z^{-1}) = \mathcal{C}_s(t)(zI - \mathcal{A}_s(t))^{-1}\mathcal{D}_s(t) \tag{3.15}$$

Coloured input noise:

$$x_n(t+1) = \mathcal{A}_n(t) x_n(t) + \mathcal{D}_n(t)\varepsilon(t) \tag{3.16}$$

$$n(t) = \mathcal{C}_n(t)\, x_n(t) + \mathcal{E}_n(t)\, \varepsilon(t) \tag{3.17}$$

$$\mathcal{W}_n(t) = \mathcal{C}_n(t)\left(zI - \mathcal{A}(t)\right)^{-1}\mathcal{D}_n(t) + \mathcal{E}_n(t) \tag{3.18}$$

Note that if a through term $\mathcal{E}_n(t)$ is included then a white noise signal is present in the observations.

Inferential signal path:

$$x_c(t+1) = \mathcal{A}_c(t)x_c(t) + \mathcal{B}_c(t)y(t) = \mathcal{A}_c(t)x_c(t) + \mathcal{B}_c(t)\mathcal{C}_s(t)x_s(t) \tag{3.19}$$

$$s(t) = \mathcal{C}_c(t)x_c(t) + \mathcal{E}_c(t)y(t) = \mathcal{C}_c(t)x_c(t) + \mathcal{E}_c(t)\mathcal{C}_s(t)x_s(t) \tag{3.20}$$

$$\textit{and} \qquad \mathcal{W}_c(t) = \mathcal{C}_c(t)(zI - \mathcal{A}_c(t))^{-1}\mathcal{B}_c(t) + \mathcal{E}_c(t) \tag{3.21}$$

Input channel sub-system:

$$x_0(t+1) = \mathcal{A}_0(t)x_0(t) + \mathcal{B}_0(t)f_0(t) \tag{3.22}$$

$$s_0(t) = \mathcal{C}_0(t)x_0(t) + \mathcal{E}_0(t)f_0(t) \tag{3.23}$$

$$\mathcal{W}_{c0}(t) = \mathcal{C}_0(t)(zI - \mathcal{A}_0(t))^{-1}\mathcal{B}_0(t) + \mathcal{E}_0(t) \tag{3.24}$$

Weighting on message:

$$x_q(t+1) = \mathcal{A}_q x_q(t) + \mathcal{B}_q s(t) = \mathcal{A}_q x_q(t) + \mathcal{B}_q\mathcal{C}_c x_c(t) + \mathcal{B}_q\mathcal{E}_c\mathcal{C}_s x_s(t) \tag{3.25}$$

$$s_q(t) = \mathcal{C}_q x_q(t) + \mathcal{E}_q s(t) = \mathcal{C}_q x_q(t) + \mathcal{E}_q\mathcal{C}_c(t)x_c(t) + \mathcal{E}_q\mathcal{E}_c(t)\mathcal{C}_s(t)x_s(t) \tag{3.26}$$

$$\mathcal{W}_q(t) = \mathcal{C}_q(t)(zI - \mathcal{A}_q(t))^{-1}\mathcal{B}_q(t) + \mathcal{E}_q(t) \tag{3.27}$$

3.2.3 Combined LPV Models

First consider the sub-system involving the channel input signal and noise models with system states defined as: $x_f = \begin{bmatrix} x_s & x_n \end{bmatrix}^T$. Then the signal and noise equations may be expressed in a *LPV* equation form:

Combined state equation:

$$x_f(t+1) = \mathcal{A}_f(t)\,x_f(t) + \mathcal{D}_f(t)\,\varepsilon(t) \tag{3.28}$$

Signal plus noise:

$$f(t) = \mathcal{C}_f(t)x_f(t) + \mathcal{E}_f(t)\varepsilon(t) \tag{3.29}$$

where

$$\mathcal{A}_f = \begin{bmatrix} \mathcal{A}_s & 0 \\ 0 & \mathcal{A}_n \end{bmatrix} \textit{ and } \mathcal{D}_f = \begin{bmatrix} \mathcal{D}_s \\ \mathcal{D}_n \end{bmatrix} \tag{3.30}$$

$$\mathcal{C}_f = \begin{bmatrix} \mathcal{C}_s & \mathcal{C}_n \end{bmatrix} \quad \textit{and} \quad \mathcal{E}_f = \mathcal{E}_n \tag{3.31}$$

Also define the resolvent time-varying operator for the combined signal and noise as:

$\Phi_f(t) = (zI - \mathcal{A}_f(t))^{-1}$ and let $\mathcal{W}_f(t) = \mathcal{C}_f(t)\Phi_f(t)\mathcal{D}_f(t) + \mathcal{E}_f(t)$.

The *LPV* sub-system model that contributes to the weighted error:

$$s_q(t) = \mathcal{C}_q x_q(t) + \mathcal{E}_q s(t) = \mathcal{W}_q \mathcal{W}_c \mathcal{W}_s \varepsilon(t) \tag{3.32}$$

may also be introduced by defining the state vector as $x = \begin{bmatrix} x_s & x_c & x_q \end{bmatrix}^T$. Then the signal, inferential path and weighting equations may be expressed in the following combined *LPV* form:

$$x(t+1) = \mathcal{A}(t)\, x(t) + \mathcal{D}(t)\, \varepsilon(t) \tag{3.33}$$

Weighted output:

$$s_q(t) = \mathcal{C}(t)x(t) + \mathcal{E}(t)\varepsilon(t) \tag{3.34}$$

The augmented time-varying system matrices follow, using (3.16), (3.19) and (3.25) as:

$$\begin{aligned} \mathcal{A} &= \begin{bmatrix} \mathcal{A}_s & 0 & 0 \\ \mathcal{B}_c\mathcal{C}_s & \mathcal{A}_c & 0 \\ B_q\mathcal{E}_c\mathcal{C}_s & B_q\mathcal{C}_c & A_q \end{bmatrix} \quad \text{and} \quad \mathcal{D} = \begin{bmatrix} \mathcal{D}_s \\ 0 \\ 0 \end{bmatrix} \\ \mathcal{C} &= \begin{bmatrix} E_q\mathcal{E}_c\mathcal{C}_s & E_q\mathcal{C}_c & C_q \end{bmatrix} \quad \text{and} \quad \mathcal{E} = 0 \end{aligned} \tag{3.35}$$

The *resolvent operator* for the augmented system is defined as $\Phi(t) = (zI - \mathcal{A}(t))^{-1}$

3.3 NMV Estimation Problem

The *NMV* filter involves the minimization of variance of the estimation error (*Moir,* 1986 [50]):

$$\tilde{s}(t \mid t-l) = s(t) - \hat{s}(t \mid t-l) \tag{3.36}$$

where $\hat{s}(t \mid t-l)$ the optimal linear estimate of the signal $s(t)$ at time t, given observations $z(t)$ up to time $t-l$. The value of l may be positive or negative according to the following conditions:

$l = 0$, for estimation

$l > 0$, for prediction

$l < 0$, for fixed-lag smoothing

The criterion to judge optimality for the uncertain system models minimum variance estimation problem can be expressed as below:

$$J = trace\{E\{(\mathcal{W}_q\tilde{s}(t \mid t-\ell)(\mathcal{W}_q\tilde{s}(t \mid t-\ell)^T\}\} \tag{3.37}$$

where $E\{\cdot\}$ denotes the expectation operator. The $\mathcal{W}_q$ ([51]) denotes a linear dynamic weighting function matrix which is assumed to be strictly minimum phase, square and invertible.

3.3.1 Spectral Factorization

Assume a combined signal and noise model is defined so that the signal $f(t)$ may be realized as: $f(t) = \mathcal{Y}_f(t)\varepsilon(t)$, where $\mathcal{Y}_f(t) = \mathcal{W}_s(t) + \mathcal{W}_n(t)$ and that $\mathcal{Y}_f(t)$ is a stably invertible operator. If this assumption is not satisfied, $\mathcal{Y}_f(t)$ may be defined to be stably invertible using a time-varying spectral-factorization computation. If these sub-systems are time-invariant and linear a standard polynomial computation may of course be used to compute $\mathcal{Y}_f(t)$. However, for the state-space approach taken this operator may be found by exploiting the relationships from a Kalman filter for a time-varying plant (Grimble and Johnson, 1988 [51]).

Recall that if the signal $f(t)$ is measured the Kalman filter may be computed where the covariance matrix for the noise $\{\varepsilon(t)\}$ is $\text{cov}[\varepsilon(t), \varepsilon(\sigma)] = Q\delta_{t\sigma}$ and $\begin{bmatrix} \mathcal{D}_f Q \mathcal{D}_f^T & \mathcal{D}_f Q \mathcal{E}_f^T \\ \mathcal{E}_f Q \mathcal{D}_f^T & \mathcal{E}_f Q \mathcal{E}_f^T \end{bmatrix} \geq 0.$ The resulting Kalman filter gain matrix for such a time-varying system (Grimble and Johnson, 1988 [51]):

$\mathcal{K}_f = (\mathcal{A}_f \mathcal{P} \mathcal{C}_f^T + \mathcal{D}_f Q \mathcal{E}_f^T) R_f^{-1}$ where the Riccati equation solution satisfies the apriori covariance:

$\mathcal{P} = \mathcal{A}_f \mathcal{P} \mathcal{A}_f^T + \mathcal{D}_f Q \mathcal{D}_f^T - \mathcal{K}_f R_f \mathcal{K}_f^T$ and $R_f = (E_f Q E_f^T + C_f \mathcal{P} C_f^T)$,

and the spectral-operator of the combined signal and noise satisfies:

$\mathcal{Y}_f(t)\mathcal{Y}_f^T(t) = (\mathcal{W}_s(t) + \mathcal{W}_n(t))Q(\mathcal{W}_s^T(t) + \mathcal{W}_n^T(t))$

The spectral-operator may then be defined from the state models as:

$$\mathcal{Y}_f(t) = (I_r + \mathcal{C}_f \Phi_f(t) \mathcal{K}_f) R_f^{1/2} \tag{3.38}$$

3.3.2 NMV Estimation Solution

The estimator can be designed from the *spectral factor and by separating future and past terms* to minimize the variance of the estimation error ([39, 48]) given in equation (3.36).

The estimate $\hat{s}(t \mid t-\ell)$ can be generated from a nonlinear estimator of the form:

$$\hat{s}(t \mid t-\ell) = \mathcal{H}_f(t) z(t-\ell) \tag{3.39}$$

$$\mathcal{H}_f = \mathcal{W}_q^{-1} \mathcal{H}_0 (\mathcal{F}_{c0} + \mathcal{W}_{c1} \mathcal{W}_{c0} \mathcal{Y}_f)^{-1} \tag{3.40}$$

$\mathcal{H}_f(t)$ denotes a minimal realization of the optimal nonlinear estimator. The block diagram representation of $\mathcal{H}_f(t)$ will be as shown in Figure 3.3. The subsystems in this estimator that generate the signals $g(t)$ and $q(t)$ have *LPV* models that can be used for implementation.

The signal $g(t) = \mathcal{H}_0(t) m(t)$ has the *LPV* model form:

$$x_g(t+1) = \mathcal{A}(t) x_g(t) + \mathcal{D}(t) m(t) \tag{3.41}$$

$$\begin{aligned} g(t) &= \mathcal{C}(t+k+\ell) \prod_{j=1}^{k+l-1} \mathcal{A}(t+j)\, x_p(t+1) \quad \forall k+l \geq 1 \\ \prod_{j}^{m} &= 1 \; if \; m < j. \end{aligned} \tag{3.42}$$

and the signal $q(t) = \mathcal{Y}_f(t) m(t) = (I_r + \mathcal{C}_f \Phi_f(t) \mathcal{K}_f) R_f^{1/2} m(t)$ may be implemented as:

$$x_q(t+1) = \mathcal{A}_f(t) x_q(t) + \mathcal{K}_f(t) R_f^{1/2} m(t) \tag{3.43}$$

$$q(t) = \mathcal{C}_f(t) x_q(t) + R_f^{1/2} m(t) \tag{3.44}$$

3.3.3 State Space Prediction Results

Before presenting the proof of the estimator solution let consider a system which may or may not be time-varying. Assume for the present that the future values of the control signal are known, so that the future values of the system matrices may be computed. The future values of the states and outputs, at different times t may be obtained as:

$$x(t+1) = \mathcal{A}(t)x(t) + \mathcal{D}(t)\varepsilon(t)$$
$$y(t) = \mathcal{C}(t)x(t) + \mathcal{E}(t)\varepsilon(t)$$

$$x(t+2) = \mathcal{A}(t+1)[\mathcal{A}(t)x(t) + \mathcal{D}(t)\varepsilon(t)] + \mathcal{D}(t+1)\varepsilon(t+1)$$
$$= \mathcal{A}(t+1)\mathcal{A}(t)x(t) + \mathcal{A}(t+1)\mathcal{D}(t)\varepsilon(t) + \mathcal{D}(t+1)\varepsilon(t+1)$$
$$y(t+1) = \mathcal{C}(t+1)x(t+1) + \mathcal{E}(t+1)\varepsilon(t+1)$$
$$= \mathcal{C}(t+1)\mathcal{A}(t)x(t) + \mathcal{C}(t+1)\mathcal{D}(t)\varepsilon(t) + \mathcal{E}(t+1)\varepsilon(t+1)$$

$$x(t+3) = \mathcal{A}(t+2)[\mathcal{A}(t+1)\mathcal{A}(t)x(t) + \mathcal{A}(t+1)\mathcal{D}(t)\varepsilon(t) + \mathcal{D}(t+1)\varepsilon(t+1)]$$
$$+\mathcal{D}(t+2)\varepsilon(t+2)$$
$$= \mathcal{A}(t+2)\mathcal{A}(t+1)\mathcal{A}(t)x(t)$$
$$+\mathcal{A}(t+2)\mathcal{A}(t+1)\mathcal{D}(t)\varepsilon(t) + \mathcal{A}(t+2)\mathcal{D}(t+1)\varepsilon(t+1)$$
$$+\mathcal{D}(t+2)\varepsilon(t+2)$$

$$y(t+2) = \mathcal{C}(t+2)x(t+2) + \mathcal{E}(t+2)\varepsilon(t+2)$$
$$= \mathcal{C}(t+2)\mathcal{A}(t+1)\mathcal{A}(t)x(t) + \mathcal{C}(t+2)\mathcal{A}(t+1)\mathcal{D}(t)\varepsilon(t)$$
$$+\mathcal{C}(t+2)\mathcal{D}(t+1)\varepsilon(t+1) + \mathcal{E}(t+2)\varepsilon(t+2)$$

The expression for the i steps-ahead state-vector for $i \geq 2$ may be obtained by generalising the above result to obtain:

$$x(t+i) = \mathcal{A}(t+i-1)\mathcal{A}(t+i-2)....\mathcal{A}(t)x(t)$$
$$+\mathcal{A}(t+i-1)\mathcal{A}(t+i-2)...\mathcal{A}(t+1)\mathcal{D}(t)\varepsilon(t)$$
$$+ ... + \mathcal{A}(t+i-1)\mathcal{D}(t+i-2)\varepsilon(t+i-2) + \mathcal{D}(t+i-1)\varepsilon(t+i-1)$$

Generalising this result, obtain the state and output at the future times $t+i$ as:

$$x(t+i) = A_0^i(t)x(t) + \sum_{p=1}^{i} A_p^i \mathcal{D}(t+p-1)\varepsilon(t+p-1) \quad \forall i \geq 1$$
$$y(t+i) = \mathcal{C}(t+i)A_0^i(t)x(t) + \mathcal{C}(t+i)\left(\sum_{p=1}^{i} A_p^i \mathcal{D}(t+p-1)\varepsilon(t+p-1)\right) +$$
$$+\mathcal{E}(t+i)\varepsilon(t+i) \qquad \forall i \geq 1 \tag{3.45}$$
$$\text{where } A_p^i = \begin{cases} \prod_{q=p}^{i-1} \mathcal{A}(t+q) & p < i \\ 1 & p \geq i \end{cases} \qquad \forall i \geq 1, \forall p \geq 0$$

3.3.4 NMV Estimation Proof

An expression for the weighted estimation error: $\tilde{s}_q(t\,|\,t-\ell) = \mathcal{W}_q\,\tilde{s}(t\,|\,t-\ell)$ is required first. The weighted message signal is given by (3.12) as:

$$s_q(t) = \mathcal{W}_q\mathcal{W}_c y(t) = \mathcal{W}_q\,\mathcal{W}_c\mathcal{W}_s\,\varepsilon(t) \tag{3.46}$$

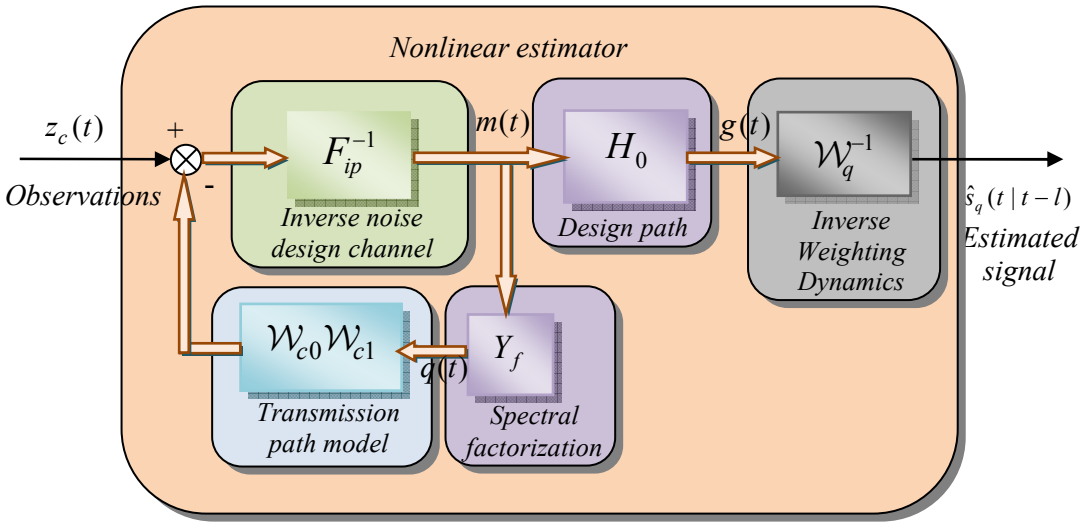

Figure 3.3: Nonlinear Estimator Structure

From equations (3.39) and (3.46) obtain the weighted estimation error:

$$\tilde{s}_q(t\,|\,t-\ell) = s_q(t) - \hat{s}_q(t\,|\,t-\ell) = \mathcal{W}_q\mathcal{W}_c\mathcal{W}_s\varepsilon(t) - \mathcal{W}_q\mathcal{H}_f z(t-\ell) \tag{3.47}$$

Recall from (3.10) that the observations $z = n_c + s_c$ and substituting from equation (3.47):

$$\tilde{s}_q(t\,|\,t-\ell) = \mathcal{W}_q\mathcal{W}_c\mathcal{W}_s\varepsilon(t) - \mathcal{W}_q\mathcal{H}_f(n_c(t-\ell) + s_c(t-\ell)) \tag{3.48}$$

From (3.4), (3.7), (3.5) and (3.9) obtain:

$$\begin{aligned}
\tilde{s}_q(t\,|\,t-\ell) &= \mathcal{W}_q\mathcal{W}_c\mathcal{W}_s\varepsilon(t) - \mathcal{W}_q\mathcal{H}_f\left((\mathcal{F}_c\varepsilon)(t-\ell) + (\mathcal{W}_{c1}s_0)(t-\ell)\right) \\
&= \mathcal{W}_q\mathcal{W}_c\mathcal{W}_s\varepsilon(t) - \mathcal{W}_q\mathcal{H}_f\left((\mathcal{F}_{c0}z^{-\Lambda_0}\varepsilon)(t-\ell) + (\mathcal{W}_{c1}\mathcal{W}_{c0}z^{-\Lambda_0}f)(t-\ell)\right) \\
&= \mathcal{W}_q\mathcal{W}_c\mathcal{W}_s\varepsilon(t) - \mathcal{W}_q\mathcal{H}_f\left((\mathcal{F}_{c0}\varepsilon)(t-\ell-\Lambda_0) + (\mathcal{W}_{c1}\,\mathcal{W}_{c0}f)(t-\ell-\Lambda_0)\right)
\end{aligned} \tag{3.49}$$

or advancing time:

$$\begin{aligned}
&\tilde{s}_q(t+\Lambda_0+\ell\,|\,t+\Lambda_0) = \mathcal{W}_q\mathcal{W}_c\mathcal{W}_s\varepsilon(t+\Lambda_0+\ell) - \\
&\mathcal{W}_q\mathcal{H}_f\left((\mathcal{F}_{c0}\varepsilon)(t) + (\mathcal{W}_{c1}\,\mathcal{W}_{c0}f)(t)\right)
\end{aligned} \tag{3.50}$$

The first term on the right of (3.50) must now be split into terms which depend upon the future and terms which depend upon the past white noise components $\varepsilon(t)$. Consider the case of the same channel delays of magnitude *k* so that $\Lambda_0 = kI$.

To obtain an expression for the weighted signal $s_q(t+\Lambda_0+\ell) = W_q \mathcal{W}_c \mathcal{W}_s \varepsilon(t+\Lambda_0+\ell)$ $(k+\ell \geq 1)$ that can be separated in future and past terms use (3.45) and applied it to this *LPV* system, for $i \geq 1$:

$$s_q(t+i) = \mathcal{C}(t+i)A_0^i(t)x(t) + \sum_{p=1}^{i} A_p^i \mathcal{D}(t+p-1)\varepsilon(t+p-1)\mathcal{C}(t+i) + \mathcal{E}(t+i)\varepsilon(t+i)$$

$$\text{where } A_p^i = \begin{cases} \prod_{q=p}^{i-1} \mathcal{A}(t+q) & p < i \\ 1 & p \geq i \end{cases} \qquad \forall\, i \geq 1, \forall\, p \geq 0$$

where the summation term is defined to be null when $i = 1$. Thence, obtain for the future times $k+\ell \geq 1$:

$$\begin{aligned} s_q(t+k+l) &= \mathcal{C}(t+k+l)A_0^{k+l}(t)x(t) \\ &+ \sum_{p=1}^{k+l} A_p^{k+l} \mathcal{D}(t+p-1)\varepsilon(t+p-1)\mathcal{C}(t+k+l) + \mathcal{E}(t+k+l)\varepsilon(t+k+l) \end{aligned} \tag{3.51}$$

For $k+\ell = 1$:

$$s_q(t+1) = \mathcal{C}(t+1)\mathcal{A}(t)x(t) + \mathcal{C}(t+1)\mathcal{D}(t)\varepsilon(t) + \mathcal{E}(t+1)\varepsilon(t+1)$$

For $k+\ell = 2$:

$$\begin{aligned} s_q(t+2) &= \mathcal{C}(t+2)\mathcal{A}(t+1)\mathcal{A}(t)x(t) + \mathcal{C}(t+2)\mathcal{A}(t+1)\mathcal{D}(t)\varepsilon(t) \\ &.....+ \mathcal{C}(t+2)\mathcal{D}(t+1)\varepsilon(t+1) + \mathcal{E}(t+2)\varepsilon(t+2) \end{aligned}$$

For $k+\ell > 2$ the lower term in the summation p=1 can be removed to obtain,

$$\begin{aligned} s_q(t+k+l) &= \mathcal{C}(t+k+l)A_0^{k+l}(t)x(t) + A_1^{k+l}\mathcal{D}(t)\varepsilon(t)\mathcal{C}(t+k+l) + \\ &+ \sum_{p=1}^{k+l} A_p^{k+l} \mathcal{D}(t+p-1)\varepsilon(t+p-1)\mathcal{C}(t+k+l) + \mathcal{E}(t+k+l)\varepsilon(t+k+l) \end{aligned}$$

First note that, $\mathcal{A}(t)\Phi(z^{-1}) + I = \left(\mathcal{A}(t) + (zI - \mathcal{A}(t))\right)\Phi(z^{-1}) = (I - \mathcal{A}(t)z^{-1})^{-1}$

Hence write:

$$s_q(t+k+\ell) = \mathcal{H}_0(z^{-1})\varepsilon(t) + \mathcal{F}_0(z^{-1})\varepsilon(t+k+\ell) \tag{3.52}$$

$$\begin{aligned}
&\text{where}: \mathcal{H}_0(z^{-1}) = \mathcal{C}(t+k+l)A_0^{k+l}(t)\Phi(z^{-1})\mathcal{D}(t) + \mathcal{C}(t+k+l)A_1^{k+l}\mathcal{D}(t) = \\
&\mathcal{C}(t+k+l)A_1^{k+l}(t)A(t)\Phi(z^{-1})\mathcal{D}(t) + \mathcal{C}(t+k+l)A_1^{k+l}\mathcal{D}(t) = \\
&\mathcal{C}(t+k+l)A_1^{k+l}(t)\left(A(t)\Phi(z^{-1}) + \mathrm{I}\right)\mathcal{D}(t) = \\
&\mathcal{C}(t+k+l)A_1^{k+l}(t)\left(I - \mathcal{A}(t)z^{-1}\right)^{-1}\mathcal{D}(t) \quad \forall\, k+l \geq 1
\end{aligned} \tag{3.53}$$

$$\begin{aligned}
&\mathcal{F}_0(t) = \mathcal{C}(t+k+\ell)\sum_{m=2}^{k+\ell}\left(A_m^{k+l}\mathcal{D}(t+m-1)z^{(m-1-k-l)}\right) + \mathcal{E}(t+k+\ell) \\
&\forall\, k+l \geq 1 \\
&\text{where } \sum = 0 \; for\, k+l = 1 \quad \text{and} \\
&A_m^{k+l} = \begin{cases} m < k+l & \prod_{q=m}^{k+l-1}\mathcal{A}(t+q) \\ m \geq k+l & 1 \end{cases} \qquad \forall\, k+l \geq 1, \forall\, m
\end{aligned} \tag{3.54}$$

It follows that the weighted signal to be estimated, for future times $k+\ell \geq 1$, may be expressed in the concise form:

$$s_q(t+k+\ell) = \mathcal{H}_0(t)\varepsilon(t) + \mathcal{F}_0\varepsilon(t+k+\ell) \tag{3.55}$$

where the stable filter $\mathcal{H}_0(t)$ and the finite pulse response estimation term $\mathcal{F}_0(z^{-1})$ may be defined as in the equations above. Reviewing the above results note that the signal $s_q(t+k+\ell) = \mathcal{W}_q\mathcal{W}_c\mathcal{W}_s\varepsilon(t+k+\ell)$ may now be represented in terms of the signals $\mathcal{H}_0(t)\varepsilon(t)$ and $\mathcal{F}_0\varepsilon(t+k+\ell)$, which involve terms dependent on past and future values of the white noise signal $\varepsilon(t)$, respectively.

***p(t)* Calculation**: Note that the sub-system $\mathcal{H}_0(t) = \mathcal{C}\left(t+k+l\right)\mathcal{A}^{k+\ell-1}(I - z^{-1}\mathcal{A})^{-1}\mathcal{D}$, defined in (3.53) forms part of the estimator and may conveniently be implemented, by the *LPV* equation model:

$$x_p(t+1) = \mathcal{A}(t)x_p(t) + \mathcal{D}(t)m(t) \tag{3.56}$$

$$\begin{aligned}
&\text{where}: \; p(t) = \mathcal{C}(t+k+\ell)\prod_{j=0}^{k+l-1}\mathcal{A}(t+j)\,x_p(t) \\
&+\mathcal{C}(t+k+\ell)\prod_{j=1}^{k+l-1}\mathcal{A}(t+j)\,\mathcal{D}(t)m(t) \\
&\forall k+l \geq 1; \; \prod_{j}^{m} = 1 \; if \; m < j.
\end{aligned} \tag{3.57}$$

The future values of the *LPV* matrices may not of course be known and in this case they may be assumed to be held constant at the values evaluated at time t.

***q*(*t*) Calculation**: Similarly, the spectral operator $\mathcal{Y}_f(z^{-1}) = (I_r + \mathcal{C}_f \Phi_f(z^{-1}) \mathcal{K}_f) R_f^{1/2}$, where $q(t) = \mathcal{Y}_f(z^{-1}) m(t)$, may be realized in the state equation form:

$$x_q(t+1) = \mathcal{A}_f(t) x_q(t) + \mathcal{K}_f(t) R_f^{1/2} m(t) \tag{3.58}$$

$$q(t) = \mathcal{C}_f(t) x_q(t) + R_f^{1/2} m(t) \tag{3.59}$$

After establishing the above properties we may return to the solution for the optimal nonlinear estimator. The weighted estimation error in equation (3.50) may be written, using the definitions of terms in (3.55) and the last assumption, as:

$$\tilde{s}_q(t+\Lambda_0+\ell \,|\, t+\Lambda_0) = \mathcal{W}_q \mathcal{W}_c \mathcal{W}_s \varepsilon(t+\Lambda_0+\ell) - \mathcal{W}_q \mathcal{H}_f \left((\mathcal{F}_{c0}\varepsilon)(t) + (\mathcal{W}_{c1}\, \mathcal{W}_{c0} f)(t) \right)$$
$$= \mathcal{F}_0 \varepsilon(t+\Lambda_0+\ell) + \left(\mathcal{H}_0 \varepsilon(t) - \mathcal{W}_q \mathcal{H}_f \left((\mathcal{F}_{c0}\varepsilon)(t) + (\mathcal{W}_{c1}\, \mathcal{W}_{c0} f)(t) \right) \right)$$

The assumption on the spectral-factor enables the combined signal and noise to be written as $f(t) = \mathcal{Y}_f(t) \varepsilon(t)$, so that:

$$\tilde{s}_q(t+\Lambda_0+\ell \,|\, t+\Lambda_0) = \mathcal{F}_0 \varepsilon(t+\Lambda_0+\ell) + \left(\mathcal{H}_0 - W_q \mathcal{H}_f (\mathcal{F}_{c0} + \mathcal{W}_{c1}\, \mathcal{W}_{c0} \mathcal{Y}_f) \right) \varepsilon(t) \tag{3.60}$$

This equation may be written in a form which is useful to define the block diagram of the estimator:

$$\begin{aligned} &\tilde{s}_q(t+\Lambda_0+\ell \,|\, t+\Lambda_0) = \\ &\mathcal{F}_0 \varepsilon(t+\Lambda_0+\ell) + \left(\mathcal{H}_0 - \mathcal{W}_q \mathcal{H}_f (I + \mathcal{W}_{c1}\, \mathcal{W}_{c0} \mathcal{Y}_f \mathcal{F}_{c0}^{-1}) \mathcal{F}_{c0} \right) \varepsilon(t) \end{aligned} \tag{3.61}$$

where $\Lambda_0 + \ell \geq 1$ or $\ell \geq 1 - \Lambda_0$ is assumed (meaning that the sum of the diagonal elements of Λ_0 plus $\ell \geq 1$).

It has been established that the first term in (3.61) is dependent upon the future values of the white noise signal components: $\varepsilon(t+1)$, $\varepsilon(t+2)$,..... The second group of terms in (3.61) are all dependent upon past values of the white noise signals. It follows that these two groups of terms are uncorrelated and the expected values of any cross terms are null. Also note that the first terms on the right hand sides of (3.60) or (3.61) are independent of the choice of estimator. It follows that the smallest variance is achieved when the remaining terms are set to zero ([48, 52]). Assuming the existence of a finite gain stable causal inverse to the nonlinear operator

(see Appendix G for more details) the optimal estimator is therefore obtained by setting this second group of terms to zero, giving:

$$\mathcal{H}_f = \mathcal{W}_q^{-1}\mathcal{H}_0\left(\mathcal{F}_{c0} + \mathcal{W}_{c1}\,\mathcal{W}_{c0}\mathcal{Y}_f\right)^{-1} \tag{3.62}$$

The optimal estimation error is defined by the terms that remain in (3.61) and these may be written as:

$$\tilde{s}_{q\min}(t+\Lambda_0+\ell\,|\,t+\Lambda_0) = \mathcal{F}_0\varepsilon(t+\Lambda_0+\ell) \tag{3.63}$$

3.4 Numerical Example

In this section, the estimator results for a fault detection problem are presented. Let us consider a fault-corrupted *LPV* system:

$$\begin{aligned} \dot{x} &= A(\delta)x(t) + B(\delta)u(t) + F(\delta)f(t) \\ y(t) &= C(\delta)x(t) + \mu(t) \end{aligned} \tag{3.64}$$

where u(t) is the system control command, $x^T = [x_1, x_2, x_3, x_4]$ is the state vector, f(t) is the unknown actuator fault to be detected and μ(t) is the sensor noise on the measurement y. The sensor noise μ(t) is added to the system output through the following noise design channel: $\mathcal{F}_{c0} = 375 * \left(1+z^{-1}\right)\big/\left(z-0.9048\right)$.

In this example the matrices **F** and **C** are considered constant. The matrices in equation (3.64) can be defined as:

$$A(\delta) = \begin{bmatrix} -0.046+\delta & 0.027 & 0.065 & -0.455 \\ 0.058 & 1.010+\delta & 0.028 & -2.020 \\ 0.140 & 0.390 & 0.070+\delta & -0.619 \\ 0 & 0 & 1 & \delta \end{bmatrix},$$

$$B(\delta) = \begin{bmatrix} -0.181+\delta \\ -2.564 \\ 1+\delta \\ 0 \end{bmatrix}, \quad C = \begin{bmatrix} 0 & 1 & 0 & 0 \end{bmatrix}, \tag{3.65}$$

$$F = \begin{bmatrix} 1 & 0 & 0 & 0 \end{bmatrix}^T$$

where the parameter δ varies as follow:

$$\delta(x_1) = \begin{cases} -0.15 & -0.7 < x_1 \\ -0.1 & -0.7 \le x_1 < -0.5 \\ -0.05 & -0.5 \le x_1 < -0.3 \\ 0.05 & -0.3 \le x_1 \end{cases}$$

In order to validate the estimator the simulations are carried out for 4 different fault signals. In the simulations the unknown message signals are estimated by using the *LPV* filter introduced above.

The state variable x_1 values, over the 30 sec simulation and the corresponding parameter δ, whose value depends on x_1, are shown in Figure 3.5 for the fault f_1.

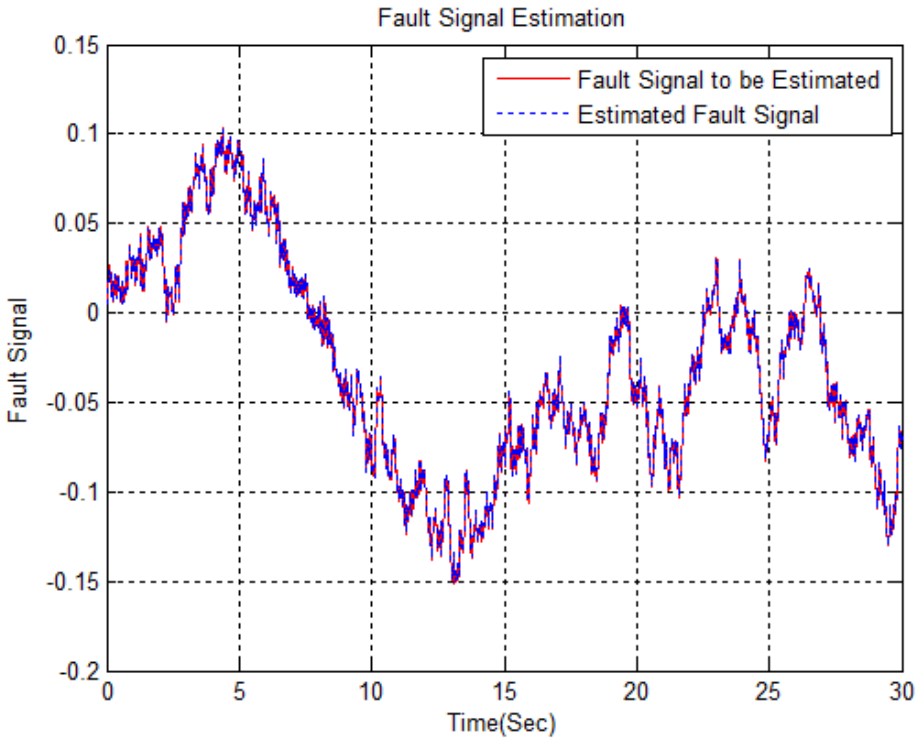

Figure 3.4: The unknown fault signal f1 vs its estimation

Table 3.1: Variance of estimation error for the 4 unknown faults detection cases.

Unknown Signal	Variance of
Fault f1	1.3146e-007
Fault f2	1.4558e-007
Fault f3	1.4346 e-007
Fault f4	1.3097e-007

The estimated fault signal and the actual signal are shown in Figure 3.4. It can be seen that the actuator fault is greatly estimated and its estimation error variance is $J = 1.3146 \times 10^{-7}$. Table 3.1 presents the results of the 4 case studies in terms of estimation error variance, confirming the efficacy of the *LPV* estimator.

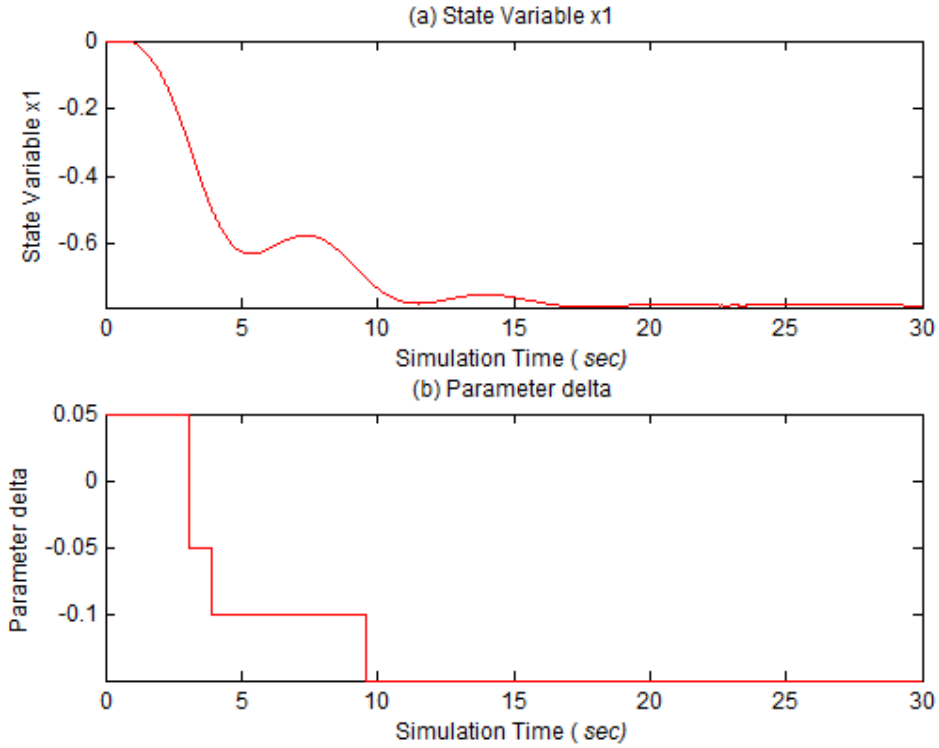

Figure 3.5: State variable x_1 (top) and parameter δ (bottom) over the 30s simulation (fault f_1 case)

3.5 Experimental Results

In this section, the estimator results for a pursuit-evader problem are presented.

This pursuit-evader problem represents an endgame of intercepting a maneuverable target by a guided missile (see [52, 53] for more details). The optimal missile guidance implementation law requires knowledge of the lateral acceleration of the target. This information cannot be directly measured so there is a need to estimate this variable. Since the lateral acceleration depends on the evader command signal, its value becomes the objective of the estimation.

The pursuer-evader system can be written as a fault-corrupted linear parameter-varying system:

$$\begin{aligned}\dot{\mathbf{x}}(t) &= \mathbf{A}\mathbf{x}(t) + \mathbf{B}u(t) + \mathbf{L}v(t)\\ \mathbf{y}(t) &= \mathbf{C}(\rho)\mathbf{x}(t) + \mathbf{E}\mu(t)\end{aligned} \tag{3.66}$$

Where u(t) is the pursuer command, v(t) is the unknown evader command, and μ(t) is the sensor noise on the first measurement, y_1. The state vector $\mathbf{x}^T = [y, \dot{y}, a_E, a_P]$ is composed by relative position, relative speed, evader acceleration and pursuer acceleration respectively.

In equation (3.66) the matrices can be defined as below:

$$\begin{aligned}\mathbf{A} &= \begin{bmatrix} 0 & 1 & 0 & 0 \\ 0 & 0 & 1 & -1 \\ 0 & 0 & -1/\tau_E & 0 \\ 0 & 0 & 0 & -1/\tau_P \end{bmatrix}, \qquad \mathbf{B} = \begin{bmatrix} 0 \\ 0 \\ 0 \\ a_P^{\max}/\tau_P \end{bmatrix}\\ \mathbf{C} &= \begin{bmatrix} 1 & 0 & 0 & 0 \\ \rho & 1 & 0 & 0 \end{bmatrix}, \qquad \mathbf{E} = \begin{bmatrix} 1 \\ 0 \end{bmatrix}\\ \mathbf{L} &= \begin{bmatrix} 0 & 0 & a_E^{\max}/\tau_E & 0 \end{bmatrix}^T\end{aligned} \tag{3.67}$$

Where $\rho = 1/(t_f - t)$, τ_E and τ_P are the time constants and $a_E^{\max}$ and $a_P^{\max}$ are the maximal achievable acceleration of the evader and pursuer respectively.

The simulation presents the last few second of a pursuer–evasion endgame where the unknown input, the evader input change is estimated by using the *LPV* filter above introduced.

The measurement of relative position y_1 and relative speed y_2, between evader and pursuer is shown in Figure 3.6, and the pursuer control input signal is shown in Figure 3.7.

The estimated evader command input and estimated lateral evader acceleration are compared to the actual message signals in Figure 3.8 and Figure 3.9 respectively.

It can be seen that the unmeasured evader command is sufficiently estimated and its estimation error variance is $J = 2.5723 \times 10^{-5}$.

Software implementation details can be found in Appendix F.

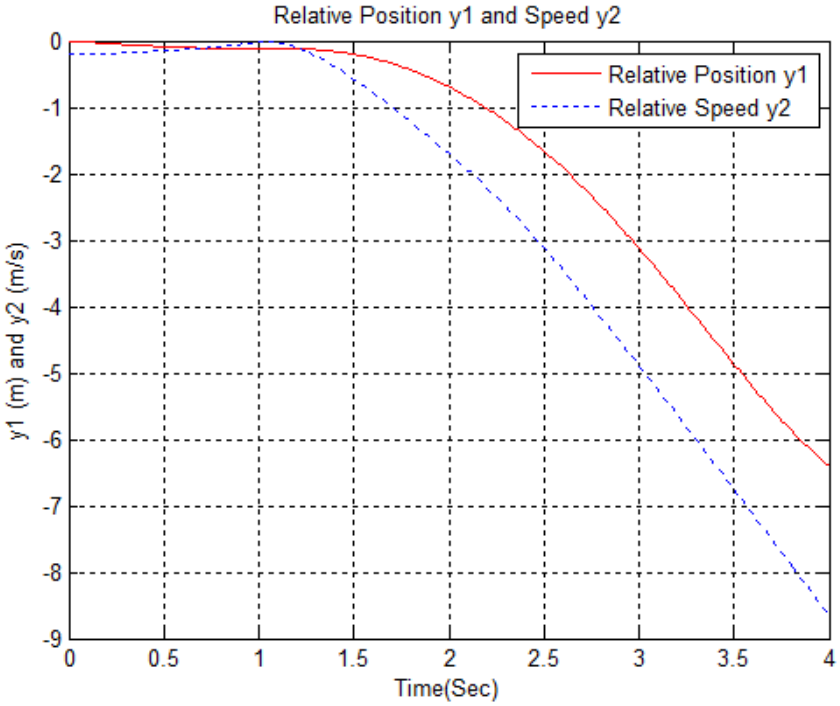

Figure 3.6: Measurement of relative positive y_1 and relative speed y_2 between evader and pursuer

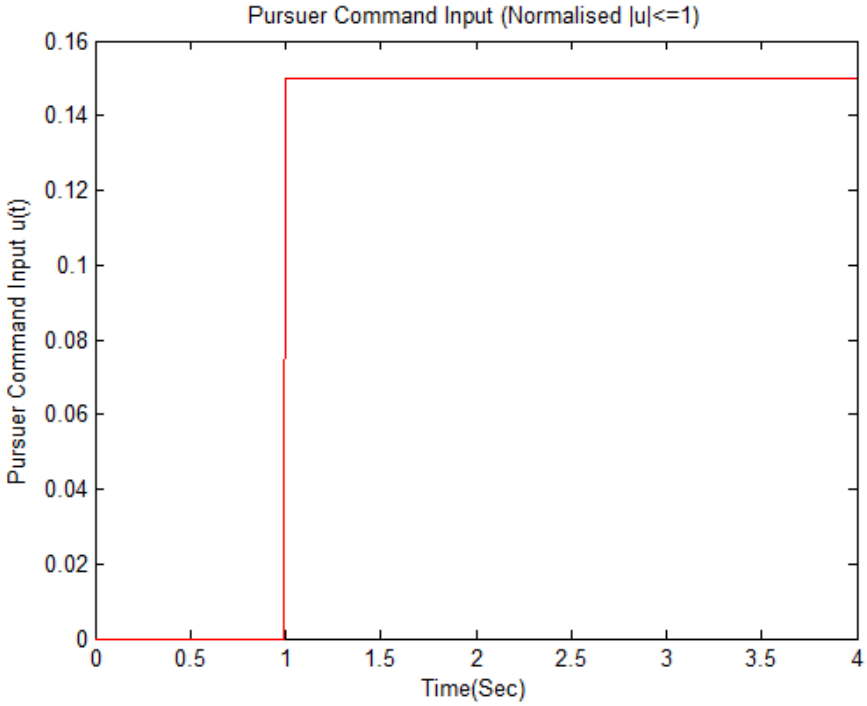

Figure 3.7: Pursuer command input

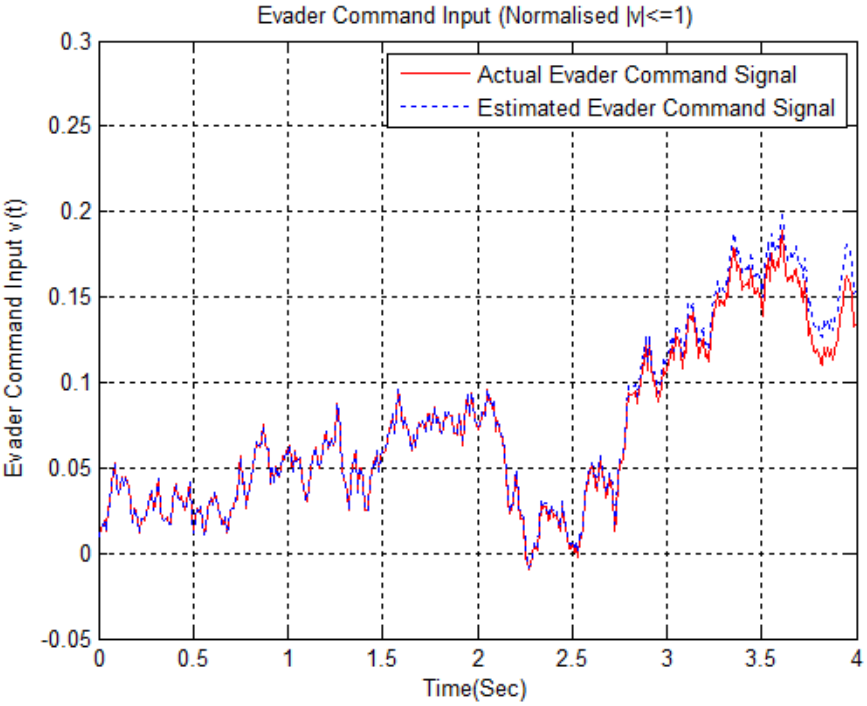

Figure 3.8: Actual evader command input vs estimated evader command signal

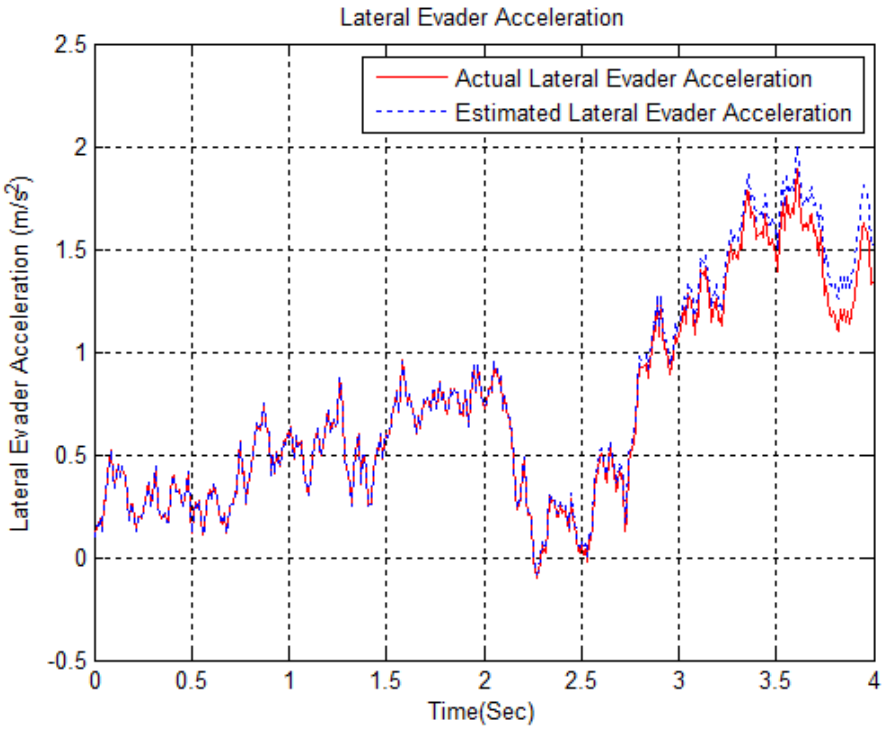

Figure 3.9: Actual evader acceleration vs estimated evader acceleration

3.6 Conclusions

The proposed nonlinear filter is easy to understand and to implement and its resulting block structure can be explained intuitively. The new *LPV* approach introduced here for modelling various sub-systems adds considerably to the generality of the results, in fact previously only the unstructured channel sub-system $\mathcal{W}_{c_1}$ (see Figure 3.1) was assumed to be nonlinear. The uncertainties were represented in a parallel channel that also introduces design freedom.

An advantage of the general philosophy is that the nonlinear subsystem in the signal channels can be represented by either a set of known nonlinear equations or can be replaced by a neural network to provide learning features.

The potential can be exploited in applications that currently use or are exploring *LPV* models such as in the wind turbine, flight control and the automotive engine control industries. The potential in fault detection applications still has to be explored and there is also a role for the estimator in feedback control systems.

It is worth noticing that an extension can be done to assume the system matrices are also functions of system known inputs or system states (the estimator results can therefore be extended to include so-called state-dependent systems). That is, a system with time-varying linear state-space matrix $\mathcal{A}(x(t), u(t), p(t))$, which might be considered a state-dependent system.

Chapter 4

Robust Nonlinear Estimation

A nonlinear operator based approach to robust estimation is first introduced for discrete-time systems. The signal and noise model parameters are assumed to be subject to perturbations represented by random variables with known means and covariances. In the limiting case of a linear system the estimator has the form of a Wiener filter in discrete-time polynomial matrix system form. A nonlinear operator based approach to H_∞ robust estimation is then presented for discrete-time multichannel systems. The H_∞ filtering problems can be solved by using a NMV embedding procedure. That is, an auxiliary minimum variance filtering problem can be solved for a cost function with dynamic weighting. A Lemma linking the solutions of the NMV and H_∞ problems can then be employed to provide the desired solution.

4.1 Introduction

In the last couple of decades the study of robust signal estimation methods has attracted considerable attention. Plant equations provide only an approximation of the real systems and the development of robust theory can deal with these model errors. In [54] was introduced a robust Kalman filtering problem for systems with bounded parameter uncertainty; this problem was solved in [55, 56] for systems with bounded parameter uncertainty in both the state and measurement matrices. In [57] a state estimator with guaranteed cost bounds for linear systems with parametric uncertainties was proposed.

In the first part of this chapter a robust Wiener optimal nonlinear estimation is presented for frequency domain or polynomial system whose signal and noise

models present uncertainties. The solution requires the introduction of an average spectral factorization and minimization of an error variance cost criterion.

The H_∞ filtering problem was pioneered by Grimble ([58]) and by Elsayed and Grimble ([59, 60]). A filter was derived using a polynomial systems model and a frequency-domain-based solution. The role that the H_∞ filter could play in signal processing problems was recognized since its early development. However, its importance in the robust control problem was only realized in more recent work by Doyle et al. ([61]), where a state-space solution of the problem was employed.

The state-space solution of H_∞ filtering problems has also been considered by Shaked ([62]) and Yaesh and Shaked ([63]).

The solution of the optimal H_∞ smoothing problem was considered by Grimble ([64]) using a polynomial system analysis.

In the H_∞ estimation the filter is designed to minimize the H_∞ norm of an operator that relates the external input signals with the estimation errors to make it below a defined threshold. When the systems under consideration are subject to some uncertainties, a robust estimator can be designed to guarantee good performance for all the tolerated range of uncertainties. To solve the robust H_∞ estimation problem many approaches have been employed such as algebraic Riccati equation based approach ([56, 65, 66]) and Linear Matrix Inequalities (LMI) based approach ([67-69]).

In this chapter an H_∞ filtering problem is solved by using an *NMV* embedding procedure ([48]). That is, an auxiliary minimum variance filtering problem is solved for a cost function with dynamic weighting. A Lemma linking the solutions of the *NMV* and H_∞ problems can then be employed to provide the desired solution.

4.2 Robust Wiener Optimal Nonlinear Estimation for Uncertain System

In the following a related frequency domain or polynomial system approach to robust nonlinear estimation problems is presented. The system, signal and noise models are assumed to include uncertain elements that can be represented by linear models with probabilistic parameter deviations. The optimal robust filter, smoother, or predictor

can be obtained from the results of a frequency weighted estimation problem. The estimation problem involves inferential estimation of a signal which enters a communication channel that contains nonlinearities and transport delays. The measurements are assumed to be corrupted by a colored noise signal correlated with the signal to be estimated ([70]). The solution of the nonlinear estimation problem is obtained using nonlinear operators. The cost-function to be minimized involves the averaged variance of the estimation error and requires a very simple optimization procedure ([48]). The averaged mean square error has been previously used in literature by Grimble ([71]), Speyer and Gustfson ([72]), and Sternad and Ahlén ([73]). In the latter was demonstrated that if the uncertainty in the system elements is described by soft bounds, the optimal robust estimator can be found for the solution of the minimum variance problem.

4.2.1 Signal Processing System Description

The signal and noise models are assumed to be time-invariant, asymptotically stable and discrete-time and represented in transfer-function or polynomial matrix form.

The signal to be estimated passes through a transmitting channel which possesses a delay z^{-k}, linear dynamics W_l and nonlinear dynamics W_{nl}. The signal generated by white noise goes into a colouring filter and then enters the linear subsystem W_l representing part of the channel dynamics which can be non-minimum phase (inverse unstable). It then enters the nonlinear subsystem W_{nl} which is assumed to be stable. The measurements are assumed to be corrupted by a noise signal $n(t)$. The message signal to be estimated is at the output of a linear block $s = W_c y$.

For greater generality a dynamic cost weighting function is introduced that penalizes the signal in a particular frequency range $s_q = W_q s$ and this becomes the signal to be estimated. The signal processing problem is illustrated in Figure 4.1. An additional nonlinear parallel channel with dynamics F_{ip} and delay z^{-k} is also introduced in our nonlinear filtering problem (shown by dotted lines in Figure 4.1). This channel will not exist physically but can be used to represent uncertainties in the nonlinear subsystem. This provides additional design freedom.

In Figure 4.1 the white noise signals ε and ω are assumed to be mutually independent and trend free.

The covariance matrices for the white noise signals are defined as $\mathrm{cov}[\varepsilon(t), \varepsilon^T(t)] = Q_s \delta_{t\tau}$ and $\mathrm{cov}[\omega(t), \omega^T(t)] = Q_n \delta_{t\tau}$, respectively, where $\delta_{t\tau}$ denotes the Kronecker delta function.

4.2.2 System Equation

In this section a mathematical description of the signals in the system is introduced. The estimation problem shown in Figure 4.1 is first modified to the problem in Figure 4.2.

The mathematical justification and derivation of the innovation signals in Figure 4.2 is described in [74, 75].

Input Signal:

$$y(t) = W_s Q_s C_s^* D_{f0}^{*-1} \varepsilon(t) \tag{4.1}$$

Disturbance Noise Signal:

$$n(t) = W_n Q_n C_n^* D_{f0}^{*-1} \varepsilon(t) \tag{4.2}$$

where $\varepsilon(t)$ is white driving noise

$$W_s(t) = A_0^{-1}(t) C_s(t), \tag{4.3}$$

$$W_n(t) = A_0^{-1}(t) C_n(t) \tag{4.4}$$

$$\textit{and} \qquad W_l(t) W_s(t) = A_0^{-1}(t) C_{ls}(t) \tag{4.5}$$

Linear channel subsystem output:

$$s_0(t) = W_l y(t) = W_l W_s Q_s C_s^* D_{f0}^{*-1} \varepsilon(t) \tag{4.6}$$

Channel input:

$$f(t) = s_0(t) + n(t) \tag{4.7}$$

Nonlinear parallel channel:

$$F_c(t) = F_{ip}(t) z^{-k} \tag{4.8}$$

Channel Interference:

$$n_c(t) = (F_c f)(t) \tag{4.9}$$

Nonlinear channel input output:

$$s_d(t) = z^{-k} f(t) = f(t-k) \tag{4.10}$$

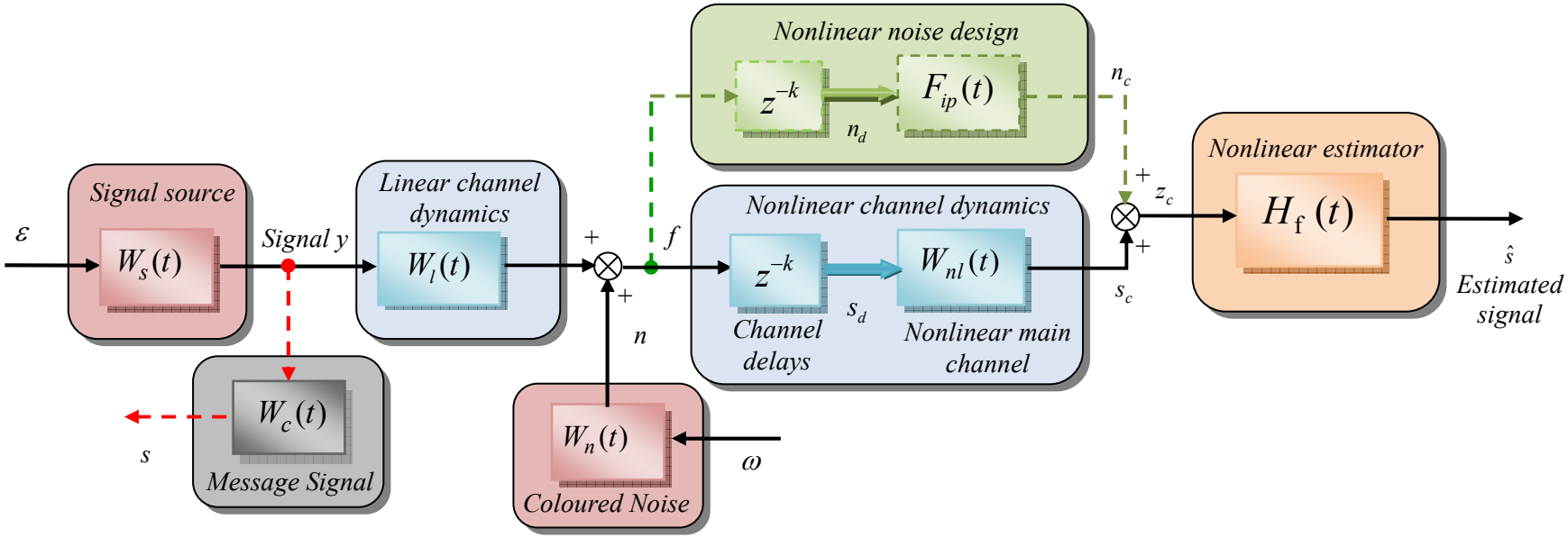

Figure 4.1: Signal Source, Noise Sources and Nonlinear Communication Channel Dynamics

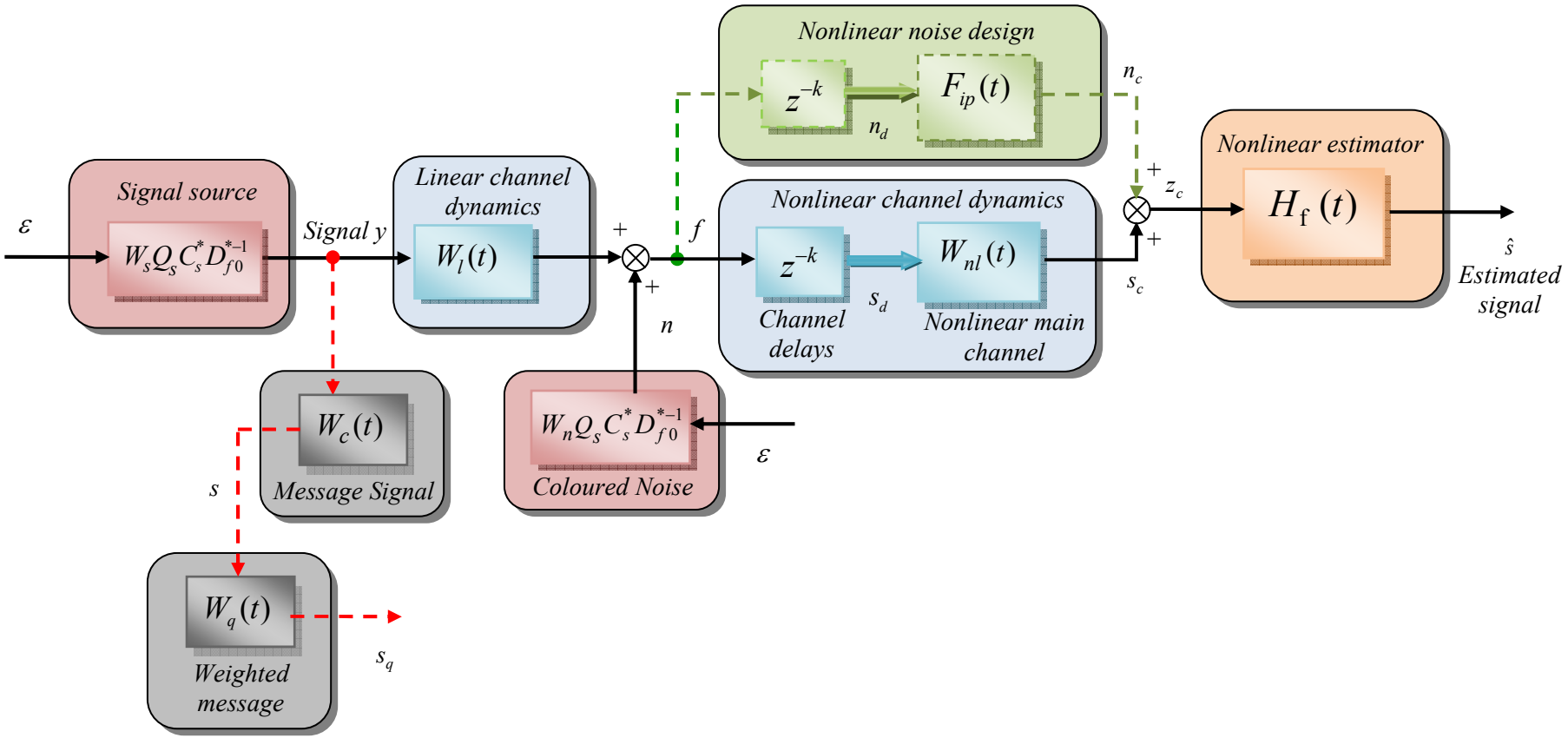

Figure 4.2: Nonlinear Filtering Problem with Innovation Signals

Nonlinear channel subsystem output:

$$s_c(t) = \left(W_{nl}\, s_d\right)(t) \tag{4.11}$$

Observations signal:

$$z_c(t) = n_c(t) + s_c(t) \tag{4.12}$$

Message signal to be estimated:

$$s(t) = W_c y(t) = W_c W_s Q_S C_s^* D_{f0}^{*-1} \varepsilon(t) \tag{4.13}$$

Weighted message signal:

$$s_q(t) = W_q s(t) = W_q W_c y(t) = W_q W_c W_s Q_S C_s^* D_{f0}^{*-1} \varepsilon(t) \tag{4.14}$$

4.2.3 Uncertain System Model Representation

The system models W_s, W_n and W_l are assumed to be uncertain, hence the notation for their models will now be modified to allow for the uncertainty:

$$W_s = \bar{W}_s \delta W_s$$

$$W_n = \bar{W}_n \delta W_n$$

$$W_l = \bar{W}_l \delta W_l$$

where $\bar{W}_i$ for $i = s,n,l$ represents the nominal model and δW_s, δW_n and δW_l are linear in the random parameters.

For simplicity a scalar uncertain problem is considered. Let $E_p\{\cdot\}$ denote the expectation taken with respect to the random parameters, then for the scalar system the transfer function of the uncertainty $\delta W_i \; for\, i = s,n,l$ is assumed to have the following polynomial form:

$\delta W_i = \delta W_{inum} / \delta W_{iden}$, where $E_p\{\delta W_{inum}\} = E_p\{\delta W_{iden}\} = 1$

The numerator and denominator terms, denoted as δW_{inum} and δW_{iden} respectively, can be written in the form $\delta W_{inum} = 1 + \delta \tilde{W}_{inum}$ and $\delta W_{iden} = 1 + \delta \tilde{W}_{iden}$ where $E_p\{\delta \tilde{W}_{inum}\} = E_p\{\delta \tilde{W}_{iden}\} = 0$.

For example, the second-order uncertain polynomials δW_{inum} and δW_{iden} may be represented in the linear form:

$$\delta W_{inum} = (1 + \alpha_1 z^{-1} + \alpha_2 z^{-2})$$

$$\delta W_{iden} = (1 + \beta_1 z^{-1} + \beta_2 z^{-2})$$

where the means and the variances of the random parameters are as follow:

$$E_p\{\alpha_1\} = E_p\{\alpha_2\} = E_p\{\beta_1\} = E_p\{\beta_2\} = 0$$
$$E_p\{\alpha_1^2\} = \sigma_{n1}^2, E_p\{\alpha_2^2\} = \sigma_{n2}^2, E_p\{\beta_1^2\} = \sigma_{d1}^2, E_p\{\beta_2^2\} = \sigma_{d2}^2$$

These random parameters are, for simplicity, taken to be independent.

The work by Grimble ([71]), reveals that the solution of the Wiener filter problem for an uncertain system in the form described is very similar to the traditional Wiener filtering problem. However, the spectral factor involving products of random variables include the corresponding covariance terms. The remaining polynomial models describing the plant, signal and noise transfers functions are simply the polynomials with mean levels of parameters included.

In the limiting case when the channel dynamics are absent and the problem reverts to a Wiener filtering problem we require the nonlinear proposed estimator to be identical to the optimal Wiener filter for the uncertain system.

The approximation taken is therefore to make these substitutions before solving the nonlinear estimation problem. For simplicity of notation it will assumed the polynomials therefore include mean values but where products of uncertain terms are present the expectation $E_p\{\cdot\}$ will be included which signifies the variances of uncertain parameters will be involved.

4.2.4 Robust Optimal Estimator

The *NMV* filter involves the minimization of variance of the estimation error:

$$\tilde{s}(t \mid t-l) = s(t) - \hat{\bar{s}}(t \mid t-l) \tag{4.15}$$

where $\hat{\bar{s}}(t \mid t-l)$ denotes the average with respect to the random parameters of the weighted estimation signal at time *t*, given observations $z_c(t)$ up to time $t-l$. The value of *l* may be positive or negative according to the following conditions ([50]):

$l = 0$, for estimation

$l > 0$, for prediction

$l < 0$, for fixed-lag smoothing

The criterion to judge optimality for the uncertain system models minimum variance estimation problem can be expressed as below ([76]):

$$J = trace\{E_s\{(W_q\tilde{s}(t\,|\,t-\ell)(W_q\tilde{s}(t\,|\,t-\ell)^T\}\} \tag{4.16}$$

where $E_s\{\cdot\}$ denotes the expectations with respect to the stochastic signals. The W_q ([48]) denotes a linear dynamic weighting function matrix which is assumed to be strictly minimum phase, square and invertible and may be represented in polynomial matrix form as: $W_q(z^{-1}) = A_q^{-1}(z^{-1})C_q(z^{-1})$.

4.2.5 Spectral Factorization

The solution of the nonlinear estimation problem requires the introduction of an average spectral factorization of the signal f. The *power spectrum* for the combined linear models can be calculated by using the Parseval's theorem ([48])

$$\Phi_{ff} = E_p\left\{(W_l W_s\varepsilon + W_n\omega)(W_l W_s\varepsilon + W_n\omega)^*\right\} \tag{4.17}$$

where the notation for the adjoint of W_s implies $W_s^*(z^{-1}) = W_s^T(z)$, and in this case the z denotes the z-domain complex number. The *averaged generalized spectral-factor* Y_f that is required may be computed using

$$Y_f Y_f^* = \Phi_{ff} \tag{4.18}$$

$$\text{where} \quad Y_f = A_0^{-1} D_{f0} \tag{4.19}$$

The system models are assumed such that D_{f0} is a *strictly Schur* polynomial matrix ([72, 77]) satisfying:

$$D_{f0}D_{f0}^* = E_p\left\{C_{ls}Q_s C_{ls}^* + C_n Q_n C_n^*\right\} \tag{4.20}$$

A realization of the averaged signal $\overline{f}$ with respect to the random parameters can be obtained from the average spectral factor:

$$\overline{f}(t) = E_p\left\{f(t)\right\} = Y_f\varepsilon(t) \tag{4.21}$$

4.2.6 The Robust Wiener Optimal Estimator Solution

The estimator can be designed from the *spectral factor and Diophantine equation* to minimize the variance of the estimation error ([41, 74]) given in equation (4.15).

The estimate $\hat{\tilde{s}}(t\,|\,t-\ell)$ can be generated from a nonlinear estimator of the form:

$$\hat{\tilde{s}}(t\,|\,t-\ell) = H_f(t)z_c(t-\ell) \tag{4.22}$$

and it is shown in the next section that for an uncertain system this will be of the form:

$$H_f(t) = G_f A^{-1} Y_f^{-1}(\mathrm{F}_{ip} + W_{nl})^{-1} \tag{4.23}$$

$H_f(t)$ denotes a minimal realization of the optimal nonlinear estimator. The block diagram representation of $H_f(t)$ will be as shown in Figure 4.3.

The generalized spectral factor $Y_f = A_0^{-1} D_{f0}$ used in this filter can be obtained from the equation (4.20) where D_{f0} is required to be asymptotically stable. The *minimal degree* solution of G_0 and F_0 can be obtained with the help of the following Diophantine equation:

$$A_{cs} A_q F_0 + G_0 D_{f0}^* z^{-g} = E_p \left\{ C_{cs} Q_s C_s^* z^{(k+l-g)} \right\} \tag{4.24}$$

The minimum value of theoretical variance in this case will be as follows:

$$J = trace\left\{ F_0 D_{f0}^{*-1} D_{f0}^{-1} F_0^* \right\} \tag{4.25}$$

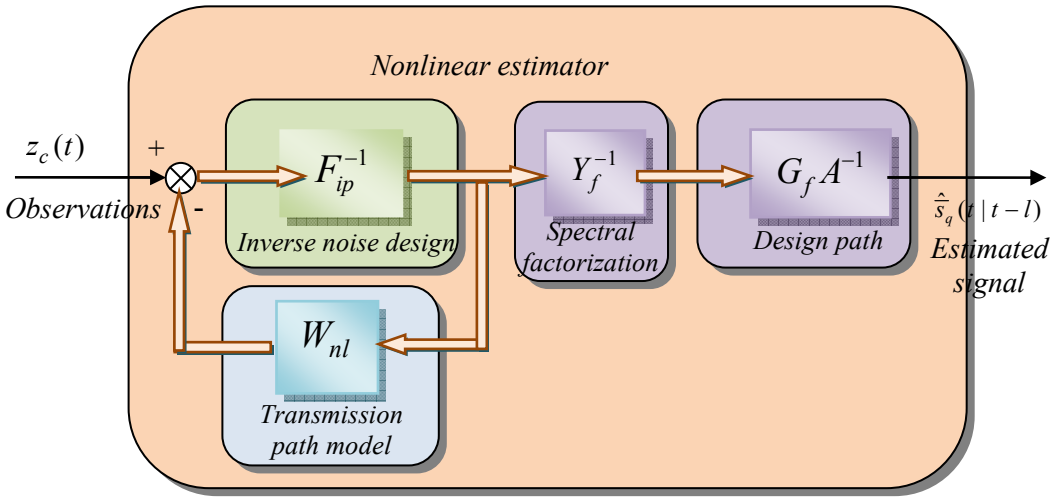

Figure 4.3: Block Diagram of the Robust Optimal Estimator for Uncertain System

4.2.7 The Robust Wiener Optimal Estimator Solution Proof

To obtain a proof of the estimator we start from the expression of the weighted estimation error:

$$\tilde{s}_q(t \mid t-l) = s_q(t) - \hat{\tilde{s}}_q(t \mid t-l) \tag{4.26}$$

Using equation (4.14) and (4.22):

$$\tilde{s}_q(t\,|\,t-l) = s_q(t) - \hat{\tilde{s}}_q(t\,|\,t-l) = \\ E_p\left\{W_q W_c W_s Q_s C_s^* D_{f0}^{*-1}\varepsilon(t)\right\} - E_p\left\{W_q H_f z_m(t-l)\right\} \tag{4.27}$$

Recall (4.12) and substitute in (4.27):

$$\tilde{s}_q(t\,|\,t-l) = E_p\left\{W_q W_c W_s Q_s C_s^* D_{f0}^{*-1}\varepsilon(t)\right\} - E_p\left\{W_q H_f (n_c(t-l) + s_c(t-l))\right\} \tag{4.28}$$

Considering equation from (4.8) to (4.11) and after simple manipulations we obtain:

$$\tilde{s}_q(t\,|\,t-l) = E_p\left\{W_q W_c W_s Q_s C_s^* D_{f0}^{*-1}\varepsilon(t)\right\} - W_q H_f (F_{ip} + W_{nl}) E_p\left\{f(t-k-l)\right\} \tag{4.29}$$

Recall (4.21) and substitute in (4.29):

$$\tilde{s}_q(t\,|\,t-l) = E_p\left\{W_q W_c W_s Q_s C_s^* D_{f0}^{*-1}\varepsilon(t)\right\} - W_q H_f (F_{ip} + W_{nl}) Y_f \varepsilon(t-k-l) \tag{4.30}$$

Advancing by $t+l+k$ in (4.30) we obtain:

$$\tilde{s}_q(t+k+l\,|\,t+k) = E_p\left\{W_q W_c W_s Q_s C_s^* D_{f0}^{*-1} z^{(k+l)}\varepsilon(t)\right\} - W_q H_f (F_{ip} + W_{nl}) Y_f \varepsilon(t) \tag{4.31}$$

Now introduce the left-coprime polynomial matrices for the weighted signal model ($W_q = A_q^{-1} C_q$):

$$A_{cs}^{-1} C_{cs} = C_q W_c W_s \tag{4.32}$$

Using (4.32) in (4.31) we can write:

$$\tilde{s}_q(t+k+l\,|\,t+k) = E_p\left\{A_q^{-1} A_{cs}^{-1} C_{cs} Q_s C_s^*\right\} D_{f0}^{*-1} z^{(k+l)}\varepsilon(t) \\ -W_q H_f (F_{ip} + W_{nl}) Y_f \varepsilon(t) \tag{4.33}$$

The equation in (4.33) can be simplified using the Diophantine equation defined in (4.24):

$$\tilde{s}_q(t+k+l\,|\,t+k) = (F_0 D_{f0}^{*-1} z^g + A_q^{-1} A_{cs}^{-1} G_0)\varepsilon(t) - A_q^{-1} C_q H_f (F_{ip} + W_{nl}) Y_f \varepsilon(t) = \\ F_0 D_{f0}^{*-1}\varepsilon(t+g) + A_q^{-1}\left[A_{cs}^{-1} G_0 - C_q H_f (F_{ip} + W_{nl}) Y_f\right]\varepsilon(t) \tag{4.34}$$

The second group of terms in the square brackets in (4.34) is all dependent upon past values of the white noise signals, whereas the first term depends only upon future values. It follows that these two groups of terms are statistically independent and the expected value of the cross terms is null.

Also note that the first term of (4.34) is independent of the choice of estimator. It follows that the smallest variance is achieved when the remaining terms are set to zero.

The *optimal estimator* is obtained by setting this second group of terms to zero for any sequence of $\varepsilon(t)$:

$$A_q^{-1}\left[A_{cs}^{-1}G_0 - C_q H_f(F_{ip}+W_{nl})Y_f\right]\varepsilon(t)$$

Assuming the existence of a finite gain stable causal inverse to the nonlinear operator, this equation is satisfied if the optimal estimator is defined as:

$$H_f = C_q^{-1}A_{cs}^{-1}G_0 Y_f^{-1}(\mathrm{F}_{ip}+W_{nl})^{-1}$$

There may normally be difficulties in guaranteeing the existence of the inverse. However, this may be achieved by construction. That is, we know we can produce an inverse of the operator $(\mathrm{F}_{ip}+W_{nl})$ if it is assumed F_{ip} can be chosen so that inverse is stable.

This relationship may be simplified by defining the following right coprime polynomial matrix as:

$$C_q^{-1}A_{cs}^{-1}G_0 = G_f A^{-1}$$

So that we obtain the result shown in the previous section:

$$H_f(t) = G_f A^{-1} Y_f^{-1}(\mathrm{F}_{ip}+W_{nl})^{-1}$$

See Appendix G for further details about the realization of the inverse operator. This can be realized easily through a block structure implemented in Simulink.

4.2.8 Experimental Results

The robust filter is computed below for a typical application and a simulation is used to verify the results.

Consider a system having linear non-minimum phase channel characteristics as:

$$W(t) = 0.3482 + 0.8704z^{-1} + 0.3482z^{-2}$$

The model is generally used in channel equalization case studies. The nonlinearity in the signal channel is modelled as $z(t) = \tanh\left(f(t-\Lambda_0)\right)$, where Λ_0 is the channel delay. The nonlinearity is a function of the signal output of the linear channel dynamics $W(t)$, and takes into account, saturation effects due to the transmitting amplifier.

The overall system when implemented with the robust Wiener filter will be as shown in Figure 4.5.

Software implementation details can be found in Appendix F.

In Figure 4.4 is shown a comparison between actual and estimated signals using the *Wiener NMV* estimator ([74, 75]) and robust Wiener estimator for the system described above without any uncertainty. The results from the estimators are the same as we could have expected from the theory, in fact with no uncertain models the robust wiener filter correspond to the *Wiener NMV* filter. When the system plant differs from the nominal model, the estimation using the robust estimator is lower in term of variance of estimation error than the *Wiener NMV* filter (see Figure 4.6 for 2 different case of studies).

In Figure 4.7 is introduced an uncertainty in the signal and noise model. The robust filter variance error for this simulation also happens to be less than the variance error for the *Wiener NMV* estimation.

Simulations are also carried out for either system plant and signal/noise models differing from their nominal models (see Figure 4.8 for 2 different case of studies).

All the above simulations are summarised in Table 4.1 where a comparison between *Wiener NMV* estimation and robust optimal estimation are carried out for two different case of studies which differ 7% and 15% respectively from their nominal models.

The expectation is that the robust estimator has benefits compared to the *Wiener NMV* estimator since it can have less sensitivity to dynamic model uncertainties.

It is useful to consider the limiting form of the estimator so that it may be related to existing filter solutions. In the limiting case as the nonlinear channel dynamics tend to the identity and the uncertainty weighting F_{ip} tends to zero, the estimator becomes equivalent to a *Wiener deconvolution estimator* with uncertain models in the linear polynomial matrix equation form $H_f = G_f A^{-1} Y_f^{-1}$.

Table 4.1: Variance of estimation error for Wiener NMV and Robust Wiener estimators

Variance of Estimation Error			
Deviation from Nominal Value	***Uncertainty Type***	**Wiener NMV Filter**	**Robust Wiener Filter**
	None	0.0187	0.0187
CASE 1 (7%)	*Plant Model*	0.0725	0.0314
	Signal & Noise Models	0.0221	0.0202
	Signal, Noise & Plant	0.0777	0.417
CASE 2 (15%)	*Plant Model*	0.1044	0.0823
	Signal & Noise Models	0.0231	0.0228
	Signal, Noise & Plant	0.1135	0.1034

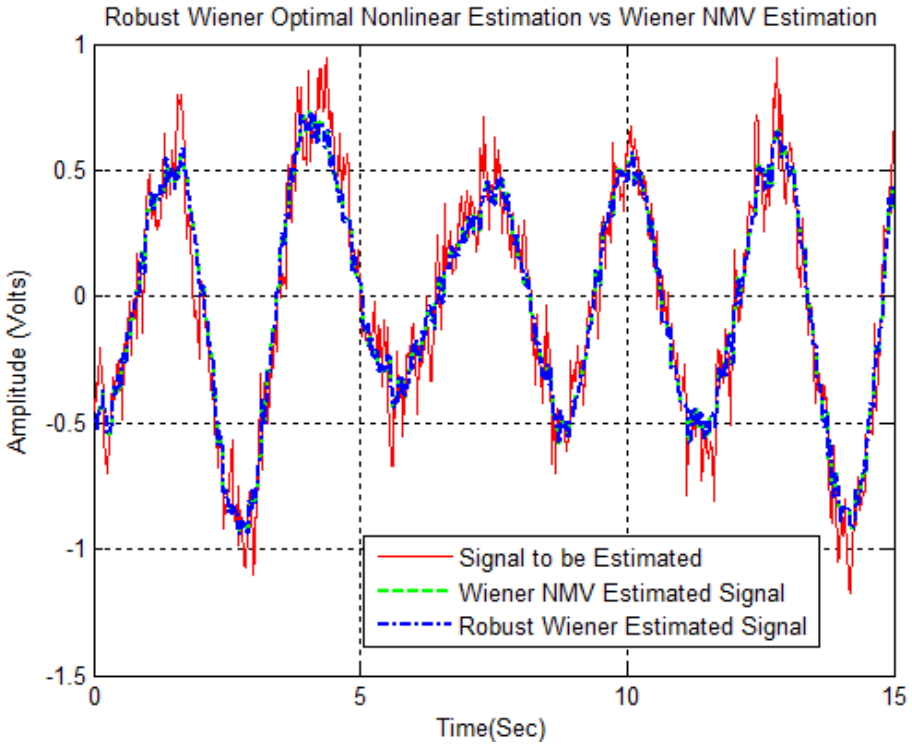

Figure 4.4: Comparison between actual and estimated signals using Wiener NMV and Robust Wiener estimators without any uncertainty.

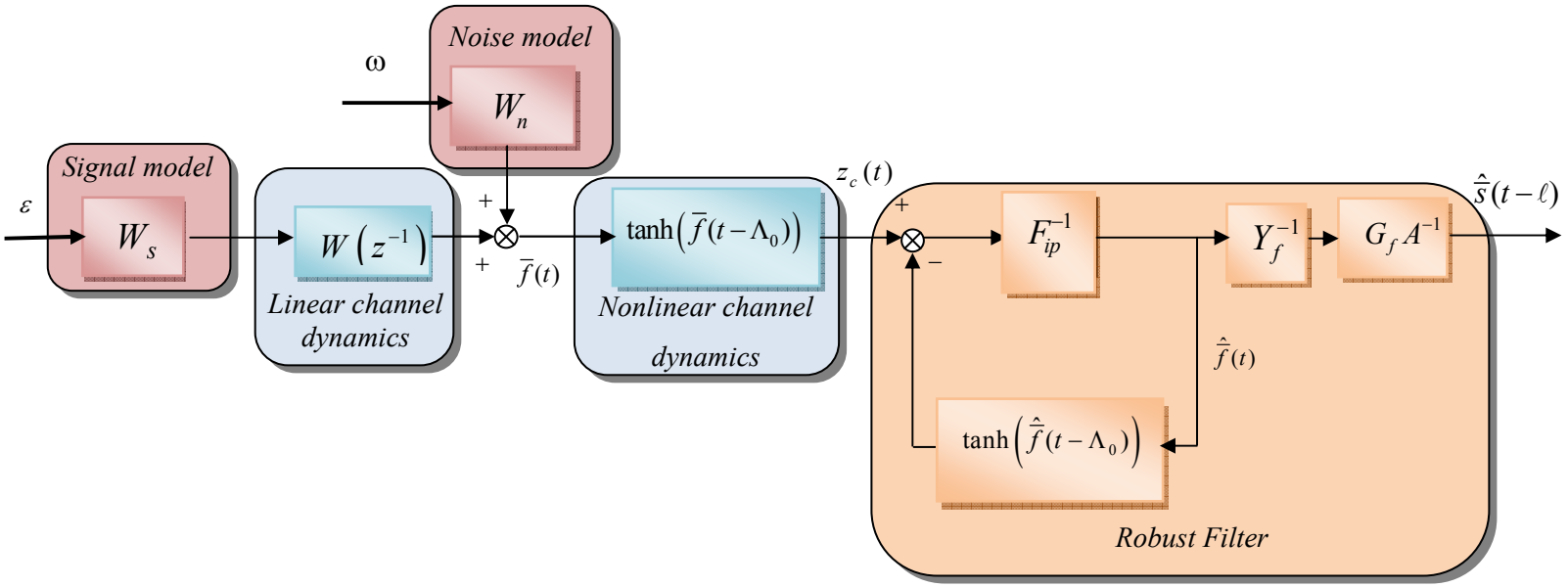

Figure 4.5: System Model Along with Channel Dynamics and Robust Estimator

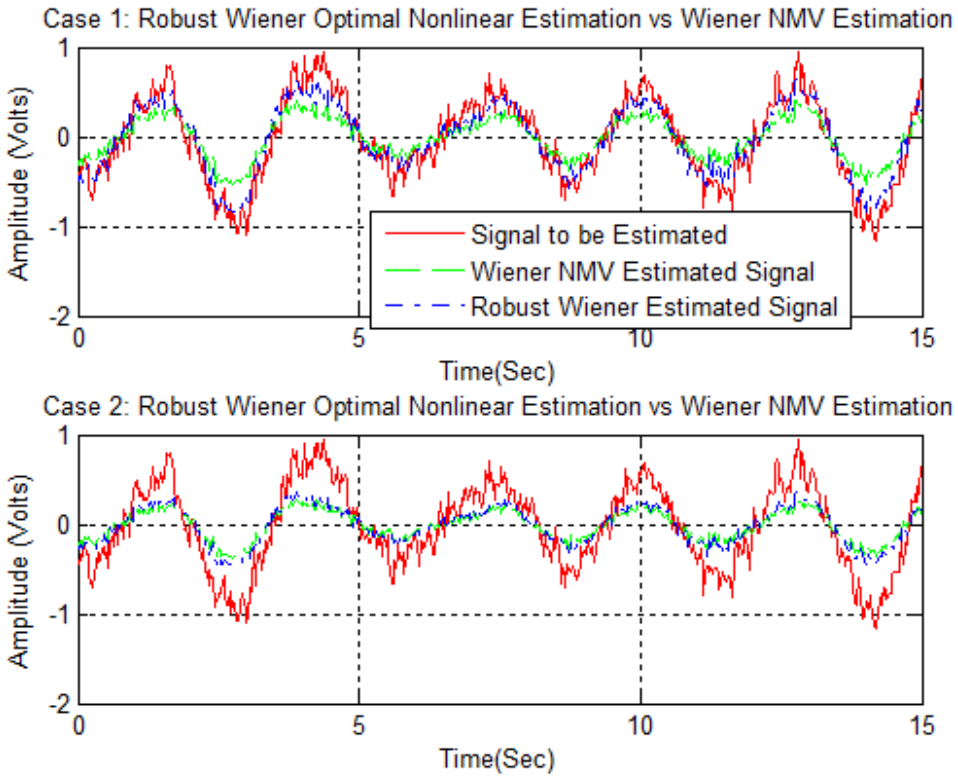

Figure 4.6: Comparison between actual and estimated signals using the Wiener *NMV* and the robust Wiener estimators with plant differing from its model.

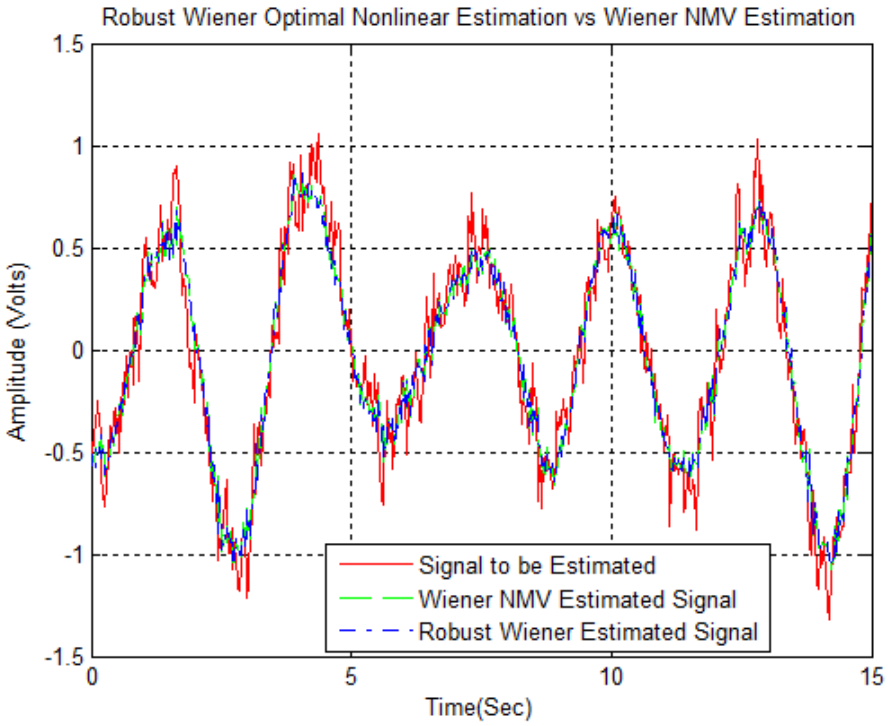

Figure 4.7: Comparison between actual and estimated signals using the Wiener *NMV* and the robust Wiener estimator for signal and noise uncertainty.

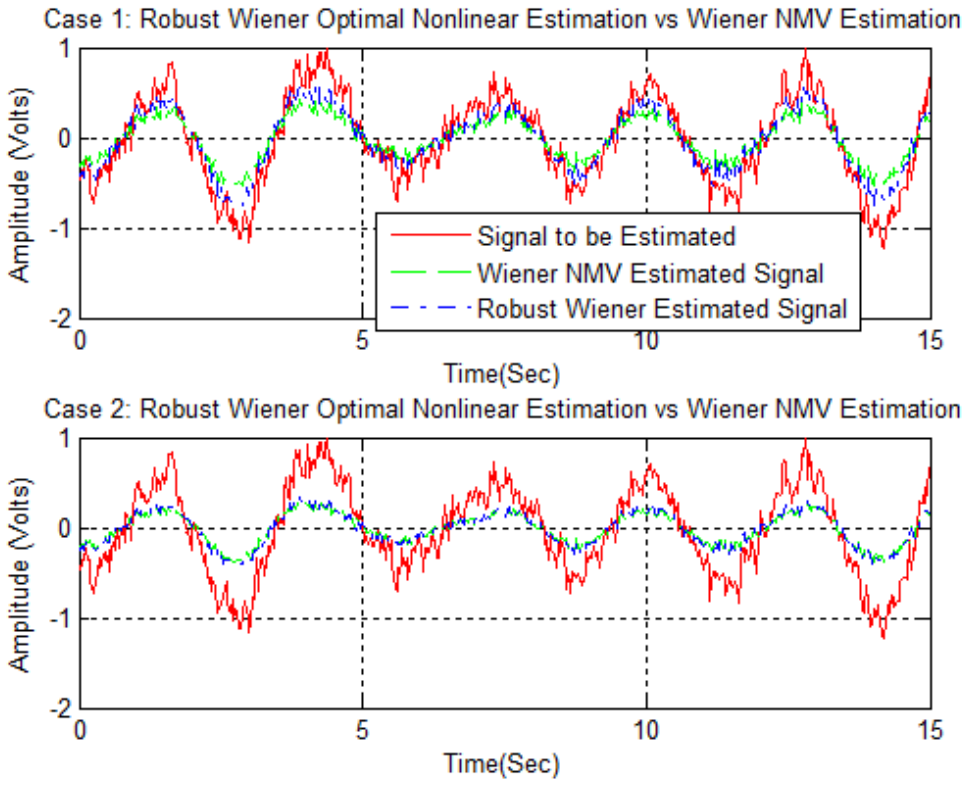

Figure 4.8: Comparison between actual and estimated signals using the Wiener *NMV* and the robust Wiener estimator for either plant and signal/noise uncertainty.

4.3 H_∞ Robust Nonlinear Estimation

In the following the solution of a H_∞ robust nonlinear estimation problems is considered.

The solution presented allows for the presence of a nonlinear communication channel between the signal and the measurement. Uncertainties can also be represented in a parallel noise or interference signal channel. The channel includes an operator or "black box" subsystem. It is well known that uncertainties can often be bounded in a frequency response way. For a linear system this suggests frequency response shaping certain sensitivity functions and this can best be achieved by minimizing an H_∞ norm. For a nonlinear system the sensitivity functions are replaced by sensitivity operators but frequency response shaping of estimator responses still has some significance.

An optimal robust estimation problem is therefore defined, where the H_∞ norm of a cost index is to be minimized. This includes a frequency response weighting

function. There is also design freedom introduced by the way the model for uncertainty is included. The resulting estimator is relatively simple to understand and to implement. It has potential applications in control systems, fault monitoring, communications and signal processing systems.

4.3.1 Signal Processing System Description

The signal and noise models are assumed to be time-invariant, asymptotically stable and discrete-time and represented in transfer-function or polynomial matrix form.

The signal to be estimated passes through a transmitting channel which possesses a delay z^{-k}, linear dynamics W_l and nonlinear dynamics W_{nl}. The measurements are assumed to be corrupted by a noise signal $n(t)$. The message signal to be estimated is at the output of a linear block: $s = W_c y$.

For greater generality is introduced a dynamic cost weighting function that penalized the signal in particular frequency range: $s_q = W_q s$ then is the signal to be estimated. The signal processing problem is illustrated in Figure 4.9. An additional nonlinear parallel channel with dynamics F_{ip} and delay z^{-k} is also introduced in our nonlinear filtering problem (shown by dotted lines in Figure 4.9). This channel which is assumed to have a stable inverse will not exist physically but can be used to represent the uncertainties in channel, which provides additional design freedom. In Figure 4.9 the white noise signal ε is assumed to be zero mean.

4.3.2 System Equations

In this section is given a mathematical description of the signals shown in Figure 4.9.

Input Signal:

$$y(t) = W_s \varepsilon(t) \tag{4.35}$$

where $\varepsilon(t)$ is white driving noise.

Disturbance Noise Signal:

$$n(t) = W_n \varepsilon(t) \tag{4.36}$$

$$\text{where} \quad W_s(t) = A_0^{-1}(t) C_s(t) \tag{4.37}$$

$$\text{and} \quad W_n(t) = A_0^{-1}(t) C_n(t) \tag{4.38}$$

Channel input:

$$f(t) = y(t) + n(t) \tag{4.39}$$

Nonlinear parallel channel:

$$F_c(t) = F_{ip}(t) z^{-k} \tag{4.40}$$

Channel Interference:

$$n_c(t) = (F_c \varepsilon)(t) \tag{4.41}$$

Linear channel subsystem output:

$$s_0(t) = \left(W_l z^{-k} f\right)(t) \tag{4.42}$$

Nonlinear channel input output:

$$s_d(t) = z^{-k} s_o(t) = s_o(t-k) \tag{4.43}$$

Nonlinear channel subsystem output:

$$s_c(t) = \left(W_{nl} s_d\right)(t) \tag{4.44}$$

Observations signal:

$$z_m(t) = n_c(t) + s_c(t) \tag{4.45}$$

Message signal to be estimated:

$$s(t) = W_c y(t) = W_c W_s \varepsilon(t) \tag{4.46}$$

Weighted message signal:

$$s_q(t) = W_q s(t) = W_q W_c y(t) = W_q W_c W_s \varepsilon(t) \tag{4.47}$$

4.3.3 Nonlinear Minimum Variance Estimation

The Nonlinear Minimum Variance estimator must first be considered since its solution will provide the results upon which the robust H_∞ estimator solution will be based.

The *NMV* filter involves the minimization of variance of the estimation error:

$$\tilde{s}(t \mid t-l) = s(t) - \hat{s}(t \mid t-l) \tag{4.48}$$

where $\hat{s}(t \mid t-l)$ denotes the estimate of the signal $s(t)$ at time t, given observations $z_m(t)$ up to time $t-l$. The value of l may be positive or negative according to the following conditions:

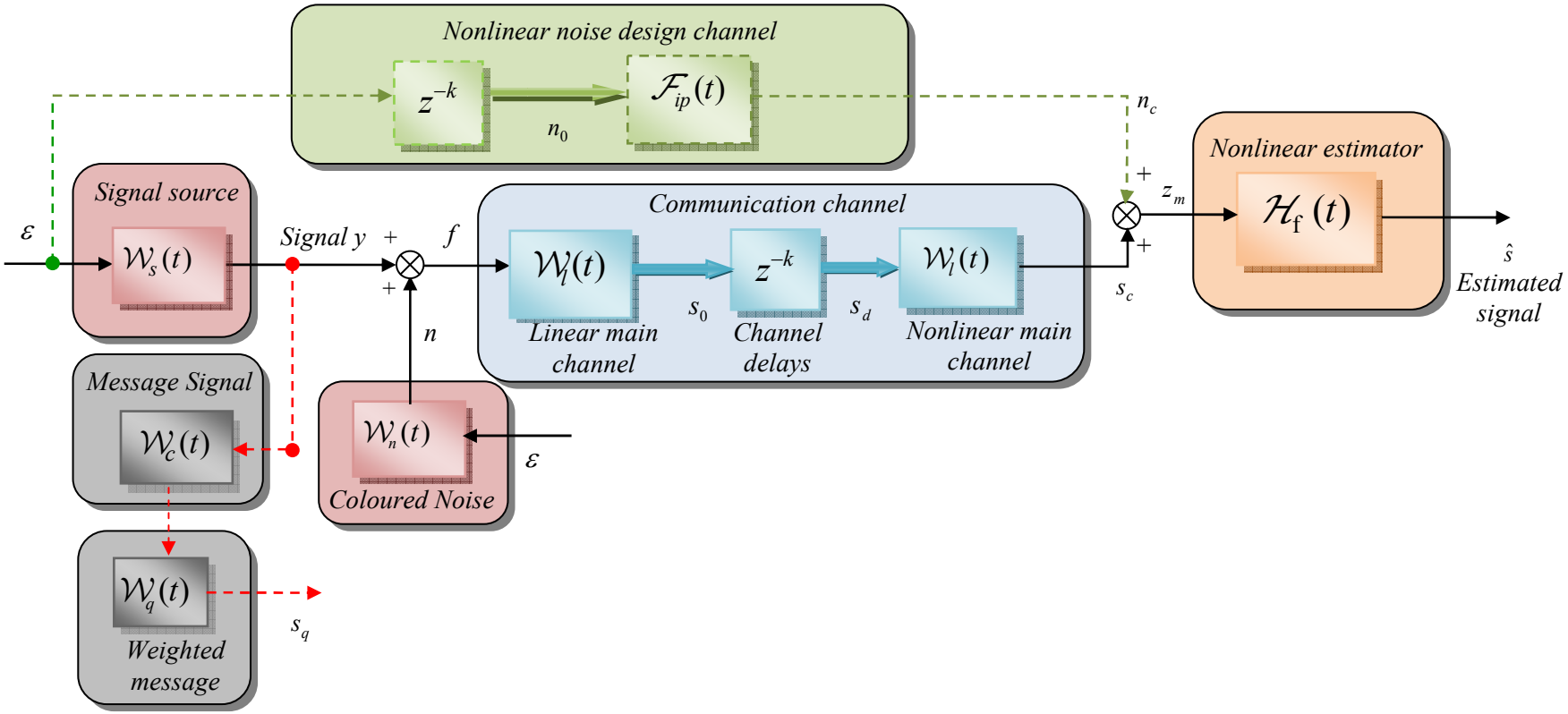

Figure 4.9: Signal Sources, Noise Sources and Nonlinear Communication Channel Dynamics

$l = 0$, for estimation

$l > 0$, for prediction

$l < 0$, for fixed-lag smoothing

The criterion to judge optimality for the minimum variance estimation problem can be expressed as below:

$$J = trace\{E\{(W_q \tilde{s}(t \mid t-\ell)(W_q \tilde{s}(t \mid t-\ell)^T\}\} \tag{4.49}$$

where $E\{\cdot\}$ denotes the expectation operator and W_q ([78]) denotes a linear strictly minimum-phase dynamic cost-function weighting function matrix which is assumed to be strictly minimum phase, square and invertible.

The above equation at the optimum can be written in complex integral form, in fact one of the estimator properties is that, at the optimum the system is behaving like a linear system:

$$J = trace\left\{\frac{1}{2\pi j}\oint_{|z|=1} W_q \Phi_{ee} W_q^* \frac{dz}{z}\right\} \tag{4.50}$$

where Φ_{ee} denotes the power spectrum of the estimation error $e(t) = \tilde{s}(t \mid t-l) = s(t) - \hat{s}(t \mid t-l)$.

The solution of the nonlinear estimation problem requires the introduction of the spectral factorization of the signal *f*. The *power spectrum* for the combined linear models can be calculated by using the Parseval's theorem ([48]):

$$\Phi_{ff} = (W_s + W_n)(W_s^* + W_n^*) \tag{4.51}$$

where the notation for the adjoint of W_s implies $W_s^*(z^{-1}) = W_s^T(z)$, and in this case the z denotes the z-domain complex number. The generalized spectral-factor Y_f that is required may be computed using $Y_f Y_f^* = \Phi_{ff}$, where

$$Y_f = A_0^{-1} D_{f0} = D_f A^{-1} \tag{4.52}$$

The system models are assumed such that D_{f0} is a strictly Schur polynomial matrix ([74, 79]) satisfying:

$$D_{f0} D_{f0}^* = (C_s + C_n)(C_s^* + C_n^*) \tag{4.53}$$

The right-coprime polynomial matrix may now be defined as:

$$\begin{bmatrix} C_f & D_f \end{bmatrix} A^{-1} = \begin{bmatrix} W_c W_s & Y_f \end{bmatrix} \tag{4.54}$$

According to *NMV* filter theory the estimate $\hat{s}(t \mid t-\ell)$, assuming the existence of a finite gain stable causal inverse to the nonlinear operator $(F_{ip} + W_{nl} W_l Y_f)$, can be generated from a nonlinear estimator of the form:

$$\hat{s}(t \mid t-\ell) = H_f(t,\, z^{-1}) z_m(t-\ell) \tag{4.55}$$

where $$H_f(t, z^{-1}) = W_q^{-1} G_0\, A^{-1} (F_{ip} + W_{nl} W_l Y_f)^{-1} \tag{4.56}$$

The proof is given in [41, 74, 80]. $H_f(t, z^{-1})$ denotes a minimal realization of the optimal nonlinear estimator. The block diagram representation of $H_f(t, z^{-1})$ will be as shown in Figure 4.10.

The *NMV* estimator given in (4.56) can be designed from the spectral factor and Diophantine equation to minimize the variance of the estimation error given in (4.48) . The generalized spectral factor $Y_f = A_0^{-1} D_{f0}$ used in this filter can be obtained from the equation (4.53) where D_{f0}^{-1} is required to be asymptotically stable. The minimal degree solution of G_0 and F_0 can be obtained with the help of the following Diophantine equation:

$$F_0 A + G_0 z^{-k-l} = W_q C_f \tag{4.57}$$

while the minimum value of theoretical variance in this case will be as follows:

$$J = trace\left\{ \frac{1}{2\pi j} \oint_{|z|=1} F_0 F_0^* \frac{dz}{z} \right\} \tag{4.58}$$

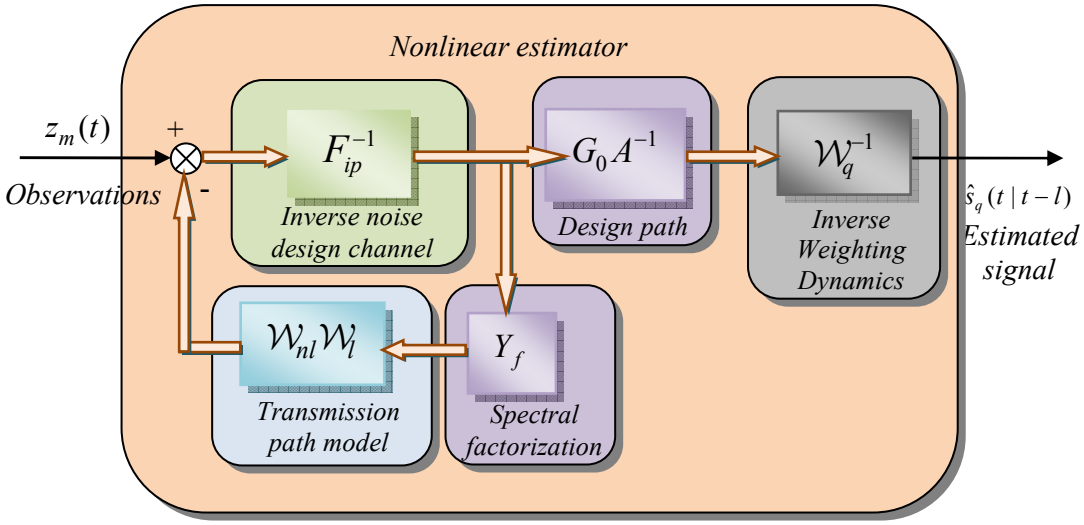

Figure 4.10: Block Diagram of the *NMV* Estimator

4.3.4 The H_∞ Robust Nonlinear Estimator

In this section the *Nonlinear* H_∞ (NH_∞) cost-function is proposed and minimized. The NH_∞ filtering problem can be solved by using a *NMV* embedding procedure. This enables most of the attention to be focused on the auxiliary *NMV* problem which can be solved for a cost function with dynamic weighting. The NH_∞ cost-function to be minimized includes the same type of weighted error and control terms in the *NMV* criterion (4.50) but employs the H_∞ norm.

To relate the two problems let the dynamics weighting function W_q in equation (4.50) be written as:

$$W_q = W_\lambda W_0 \tag{4.59}$$

The term W_0 is a dynamic weighting function introduced on the estimation error and it is selected by the designer to shape the frequency response of the estimation error spectrum. The weighting W_λ is necessary to link the *NMV* and H_∞ problems.

The function $X(z^{-1})$ to be minimized can be defined in terms of the weighted estimation error as:

$$X \triangleq W_0 \Phi_{ee} W_0^* \tag{4.60}$$

where Φ_{ee} is a positive definite function.

Hence the cost-function to be minimized is given as:

$$J_\infty = \sup_{|z|=1}\left\{\sigma_{\max}\left\{X(z^{-1})\right\}\right\} = \sup_{|z|=1}\left\{\sigma_{\max}\left\{W_0 \Phi_{ee} W_0^*\right\}\right\} \tag{4.61}$$

A lemma, linking the solution of the *NMV* and the NH_∞ problems, can then be used to obtain the desired solution.

4.3.5 Auxiliary problem and linking lemma

Lemma: Consider the auxiliary problem of minimizing the variance J of the estimation error in the NMV filtering problem for the system introduced in the previous section and represented in Figure 4.9:

$$J = trace\left\{\frac{1}{2\pi j}\oint_{|z|=1} W_\lambda(z^{-1}) X(z^{-1}) W_\lambda^*(z^{-1}) \frac{dz}{z}\right\} \tag{4.62}$$

Suppose that for some real-rational matrix:

$W_\lambda^*(z^{-1})W_\lambda(z^{-1}) \geq 0$ the cost function J is minimized by a function $X(z^{-1}) = X^*(z^{-1})$, for which $X(z^{-1}) = \lambda^2 I_r$ (a real constant matrix on $|z| = 1$). Then the function $X(z^{-1})$ also minimizes:

$$J_\infty = \sup_{|z|=1} \left\{ \sigma_{\max}(X(z^{-1})) \right\} \tag{4.63}$$

Proof: The proof of the above lemma is derived by contradiction. Assume that there exists a function $X_0(z^{-1}) = \Lambda\Lambda^T = \lambda^2 I_r$ which minimizes the cost function *J*:

$$J_{\min} = trace\left\{ \frac{1}{2\pi j} \oint_{|z|=1} W_\lambda(z^{-1}) X_0(z^{-1}) W_\lambda^*(z^{-1}) \frac{dz}{z} \right\} \tag{4.64}$$

In the above equation λ is a scalar and Λ is a diagonal matrix that at the optimum solution for the estimator reduces to λI_r. Then according to the Lemma the function $X_0(z^{-1})$ also minimizes J_∞ (the H_∞ norm of itself, see (4.63)).

Let P denote the assertion: $X_0(z^{-1})$ minimizes the cost function J_∞. Now assume that there exists another function $X_1(z^{-1})$ that also minimizes the cost function J but with a lower H_∞ norm. It follows that at the optimum:

$$J_{1\infty} = \sup_{|z|=1} \left\{ \sigma_{\max}(X_1(z^{-1})) \right\} < J_{0\infty} = \sup_{|z|=1} \left\{ \sigma_{\max}(X_0(z^{-1})) \right\} = \lambda^2 \tag{4.65}$$

From the above equation: $X_1(z^{-1}) < X_0(z^{-1}) = \lambda^2 I_r$ hence the cost function related to $X_1(z^{-1})$ is as below:

$$J_{1\min} = trace\left\{ \frac{1}{2\pi j} \oint_{|z|=1} W_\lambda(z^{-1}) X_1(z^{-1}) W_\lambda^*(z^{-1}) \frac{dz}{z} \right\} < J_{0\min} \tag{4.66}$$

This contradicts the assumption that the function $X_0(z^{-1})$ minimizes the cost function *J*. Then, since the negation of the assertion P implies a contradiction, it follows that the assertion P is true.

4.3.6 Solution strategy and weighting

The problem is now to determine the function W_λ which when substituted into the results of the *NMV* estimation will ensure the conditions of the above lemma are satisfied.

The function W_λ is calculated using an equalizing solution between the *NMV* and the auxiliary problem cost-functions. This solution corresponds to an equalizing solution $X(z^{-1}) = \lambda^2$. The H_∞ estimator solution then follows.

Assume that the scalar λ in the above W_λ must now be found which leads to an equalizing solution:

$$X(z^{-1}) = \Lambda\Lambda^T = \lambda^2 I_r \quad on \quad |z| = 1 \tag{4.67}$$

From a comparison of the integrand of the auxiliary problem cost-function (4.62) and the cost-function for the *NMV* estimator (4.58) we obtain:

$$F_0 F_0^* = W_\lambda \Lambda\Lambda^T W_\lambda^* \tag{4.68}$$

Let F_{0S} denote a Schur polynomial matrix which satisfies:

$$F_{0S} F_{0S}^* = F_0 F_0^* \tag{4.69}$$

Then the equation (4.67) is satisfied if $W_\lambda \Lambda = F_{0s}$ or

$$W_\lambda = F_{0S} \Lambda^{-1} \tag{4.70}$$

4.3.7 The H_∞ Nonlinear Minimum Variance Estimator

The H_∞ estimator, which minimized the criterion (4.61), for the system shown in Figure 4.9, can be computed from the solution ($G_0, F_0, F_{0s}, \lambda$) of the following *generalized eigenvalue problem*:

$$F_0 A + G_0 z^{-k-l} = F_{0s} \Lambda^{-1} W_0 C_f \tag{4.71}$$

The polynomial matrix F_0 has to be of minimal degree and $|\lambda|$ a minimum. To obtain (4.71) we start from the expression of the weighted estimation error:

$$\tilde{s}_q(t \mid t-l) = s_q(t) - \hat{s}_q(t \mid t-l) \tag{4.72}$$

Using equation (4.47) and (4.55):

$$\tilde{s}_q(t \mid t-l) = s_q(t) - \hat{s}_q(t \mid t-l) = W_q(W_c W_s \varepsilon(t) - H_f z_m(t-l)) \tag{4.73}$$

Recall (4.59) and consider the expression of W_λ (see (4.70)) which ensures satisfaction of the above lemma:

$$\begin{aligned} \tilde{s}_q(t \mid t-l) &= W_\lambda W_0 W_c W_s \varepsilon(t) - W_\lambda W_0 H_f z_m(t-l)) \\ &= F_{0s} \Lambda^{-1} W_0 W_c W_s \varepsilon(t) - F_{0s} \Lambda^{-1} W_0 H_f z_m(t-l)) \end{aligned} \tag{4.74}$$

Define the equation below:

$$\begin{bmatrix} C_f & D_f \end{bmatrix} A^{-1} = \begin{bmatrix} W_c W_s & Y_f \end{bmatrix} \tag{4.75}$$

Substituting (4.75) in (4.74):

$$\tilde{s}_q(t \mid t-l) = F_{0s}\Lambda^{-1}W_0 C_f A^{-1}\varepsilon(t) - F_{0s}\Lambda^{-1}W_0 H_f z_m(t-l)) \tag{4.76}$$

The first term in equation (4.76) can be simplified by using the following Diophantine equation:

$$F_0 A + G_0 z^{-k-l} = F_{0s}\Lambda^{-1}W_0 C_f \tag{4.77}$$

which represents the generalized eigenvalue problem in (4.71). The NH_∞ estimator can now be found from (4.56), (4.59) and (4.70):

$$\begin{aligned} H_f(t,z^{-1}) &= W_q^{-1}G_0 A^{-1}(F_{ip} + W_{nl}W_l Y_f)^{-1} = (W_\lambda W_0)^{-1}G_0 A^{-1}(F_{ip} + W_{nl}W_l Y_f)^{-1} \\ &= (F_{0s}\Lambda^{-1}W_0)^{-1}G_0 A^{-1}(F_{ip} + W_{nl}W_l Y_f)^{-1} = W_0^{-1}\Lambda F_{0s}^{-1}G_0 A^{-1}(F_{ip} + W_{nl}W_l Y_f)^{-1} \end{aligned} \tag{4.78}$$

In the above is it assumed the existence of a finite gain stable causal inverse to the nonlinear operator $(F_{ip} + W_{nl}W_l Y_f)$.

The block diagram representation of the H_∞ version of $H_f(t,z^{-1})$ is shown in Figure 4.11.

The minimal cost is:

$$J = trace\left\{\frac{1}{2\pi j}\oint_{|z|=1} W_0 \Phi_{ee} W_0^* \frac{dz}{z}\right\} = \lambda^2 \tag{4.79}$$

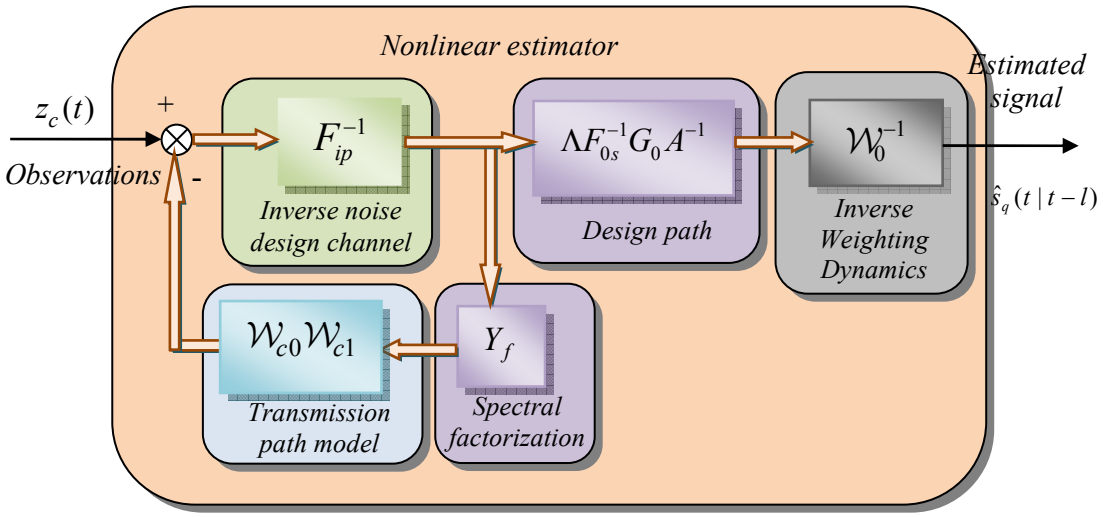

Figure 4.11: Block Diagram of the NH_∞ Estimator

4.3.8 Design and Experimental Results

First we illustrate the procedure to solve the generalized eigenvalue problem (4.71). For this purpose we use an example which matrices are in parameterized form. Let

$$D_k = k - l,$$
$$A = a_0 + a_1 z^{-1} + a_2 z^{-2},\ C_f = c_0 + c_1 z^{-1}$$
$$W_0 = w_0 + w_1 z^{-1}$$

We are looking for the solution of smallest degree therefore $\deg(F_0) < D_k = 2$. The latter implies $F_0 = f_0 + f_1 z^{-1}$ and hence $F_{0s} = f_1 + f_0 z^{-1}$. To balance the degrees of the first and second member of (4.71) G_0 has to be of order *1*: $G_0 = g_0 + g_1 z^{-1}$

We can write $W_0 C_f = c_{00} + c_{01} z^{-1} + c_{02} z^{-2}$.

From the above equations follow:

$$(f_0 + f_1 z^{-1})(a_0 + a_1 z^{-1} + a_2 z^{-2}) + z^{-2}(g_0 + g_1 z^{-1}) = (f_1 + f_0 z^{-1})(c_{00} + c_{01} z^{-1} + c_{02} z^{-2}) / \lambda$$

Equalizing the coefficients in $z^{-i}\,(i = 0,1,2)$ we can write the above equation in matrix form:

$$\left\{ \begin{bmatrix} 0 & 0 & a_0 & 0 \\ 0 & 0 & a_1 & a_0 \\ 1 & 0 & a_2 & a_1 \\ 0 & 1 & 0 & a_2 \end{bmatrix} - \lambda^{-1} \begin{bmatrix} 0 & 0 & 0 & c_{00} \\ 0 & 0 & c_{00} & c_{01} \\ 0 & 0 & c_{01} & c_{02} \\ 0 & 0 & c_{02} & 0 \end{bmatrix} \right\} \begin{bmatrix} g_0 \\ g_1 \\ f_0 \\ f_1 \end{bmatrix} = 0$$

This equation can be written as $(T_1 - \lambda^{-1} T_2)x = 0$ where T_1 is in Toeplitz form, which guarantee that its inverse exist and the equation can be written as: $(\lambda I - T_0)x = 0$ where $T_0 = T_1^{-1} T_2$. This is a classic eigenvalue/eigenvector problem, which can be solved for the eigenvalue of smallest magnitude. The corresponding eigenvector is the solution of the Diophantine equation: $x^T = [g_0 \quad g_1 \quad f_0 \quad f_1]$ where the solution $F_0 = f_0 + f_1 z^{-1}$ is non-Schur.

4.3.8.1 **Automotive Lambda Sensor Estimation Problem**

An important sensor in an automotive engine fuel control feedback loop is the exhaust gas oxygen sensor or lambda sensor. The sensor measures the residual

oxygen in the exhaust gas and passes the information to the engine control unit, and according to this information the engine control unit regulates the air/fuel ratio in order to achieve an optimum performance. There is a significant delay in the measurement since the lambda sensor is some distance from the point of interest (see Figure 4.12). Two types of lambda or Air/Fuel ratio sensor are used in the automotive industry; the Universal Exhaust Gas Oxygen (UEGO) and the Exhaust Gas Oxygen (EGO) sensors. The static nonlinear characteristics of the EGO and UEGO sensors are shown in Figure 4.13 and Figure 4.14 respectively.

In Figure 4.15 and Figure 4.16 are shown a comparison between actual and estimated signals using *NMV* and NH_∞ , respectively for EGO and UEGO sensors. In Table 4.2 the results of the 3 case studies illustrated in Figure 4.15 and Figure 4.16 are summarized. If system uncertainties are not present (Case study 1) the variance of the *NMV* estimator is, of course, lower than NH_∞**,** but if the system differs from the nominal model as in Case Study 2 and 3, where some uncertainties are introduced through the design parallel channel, this is not necessarily the case as can be seen in the previous figures and in Table 4.2

The NH_∞ estimator does not of course aim to minimize variances but the visual performance often accords with variance so it is a useful measure to assess.

In Figure 4.18 the results are shown for the same situation where the UEGO sensor characteristic is the one shown in Figure 4.17. The NH_∞ variance error for this simulation also happens to be less than the variance error for *NMV* estimation (see Table 4.3). The expectation is that NH_∞ estimator has benefits compared to the *NMV* estimator since it can have less sensitivity to dynamic model uncertainties.

Software implementation details can be found in Appendix F.

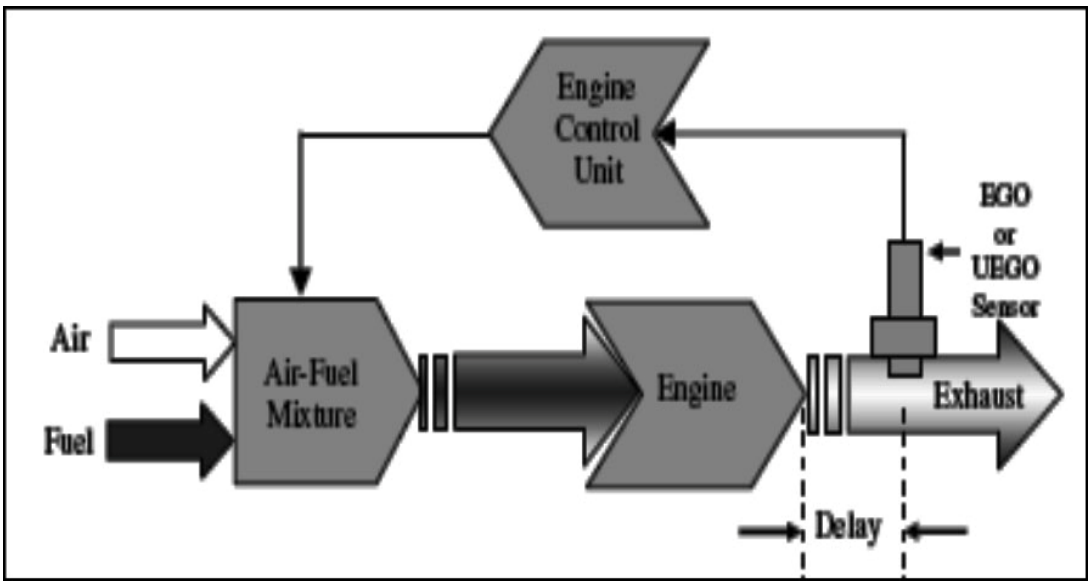

Figure 4.12: Location of Lambda or Oxygen Sensor in Automobile Engine

Table 4.2: Variance of estimation error for EGO and UEGO sensors for 2 different case studies

Variance of Estimation Error			
		EGO Sensor	**UEGO Sensor**
CASE STUDY 1 No Uncertainties	***NMV Estimation***	$J=3.0611\times10^{-4}$	$J=8.4408\times10^{-5}$
	NH_∞ Estimation	$J=4.0198\times10^{-4}$	$J=1.0804\times10^{-4}$
CASE STUDY 2 $F_{ip}=\frac{1+1.212z^{-1}}{1-0.7788z^{-1}}$	***NMV Estimation***	$J=4.8506\times10^{-4}$	$J=1.7093\times10^{-4}$
	NH_∞ Estimation	$J=4.1080\times10^{-4}$	$J=1.1303\times10^{-4}$
CASE STUDY 3 $F_{ip}=10\frac{1+1.212z^{-1}}{1-0.7788z^{-1}}$	***NMV Estimation***	$J=6.8022\times10^{-4}$	$J=2.7789\times10^{-4}$
	NH_∞ Estimation	$J=4.2442\times10^{-4}$	$J=1.1864\times10^{-4}$

Table 4.3: Variance of estimation error for *NMV* and NH_∞ estimation for EGO sensor

Variance of Estimation Error	**EGO Sensor**
NMV Estimation	$J=5.5445\times10^{-4}$
NH_∞ Estimation	$J=4.1413\times10^{-4}$

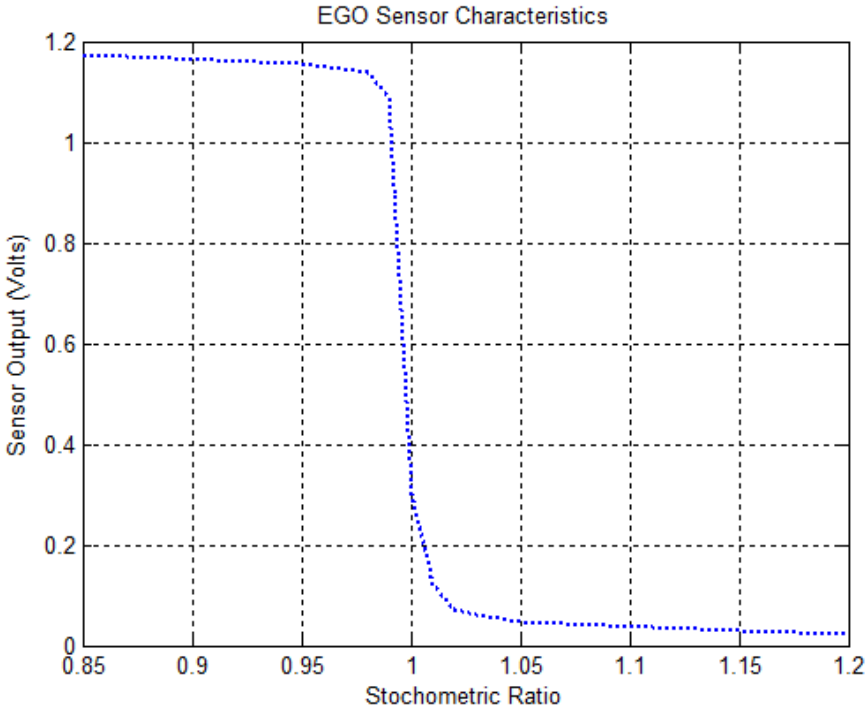

Figure 4.13: EGO Lambda Sensor Nonlinear Behaviour

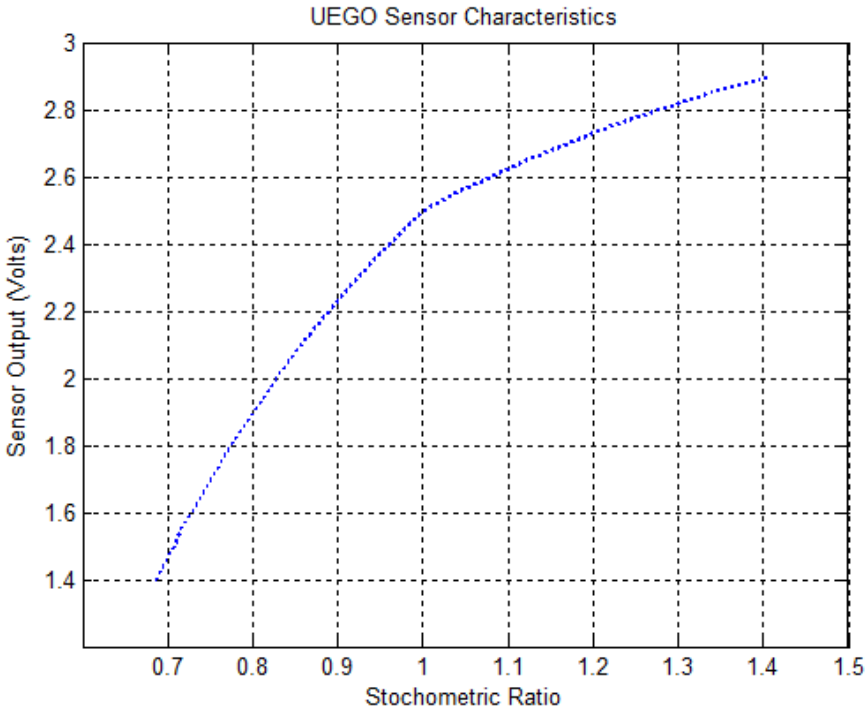

Figure 4.14: UEGO Lambda Sensor Nonlinear Behaviour

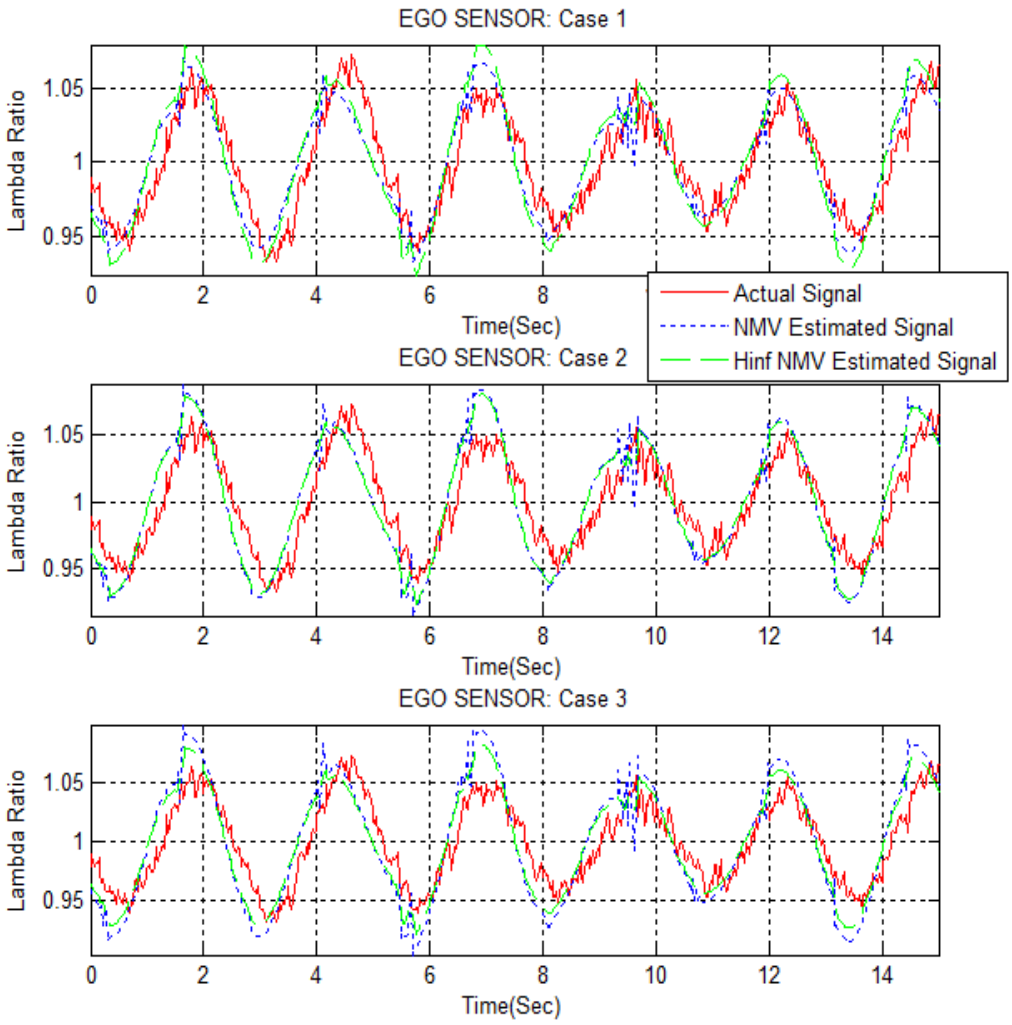

Figure 4.15: Comparison between actual and estimated signals using *NMV* and NH_∞ for EGO sensor

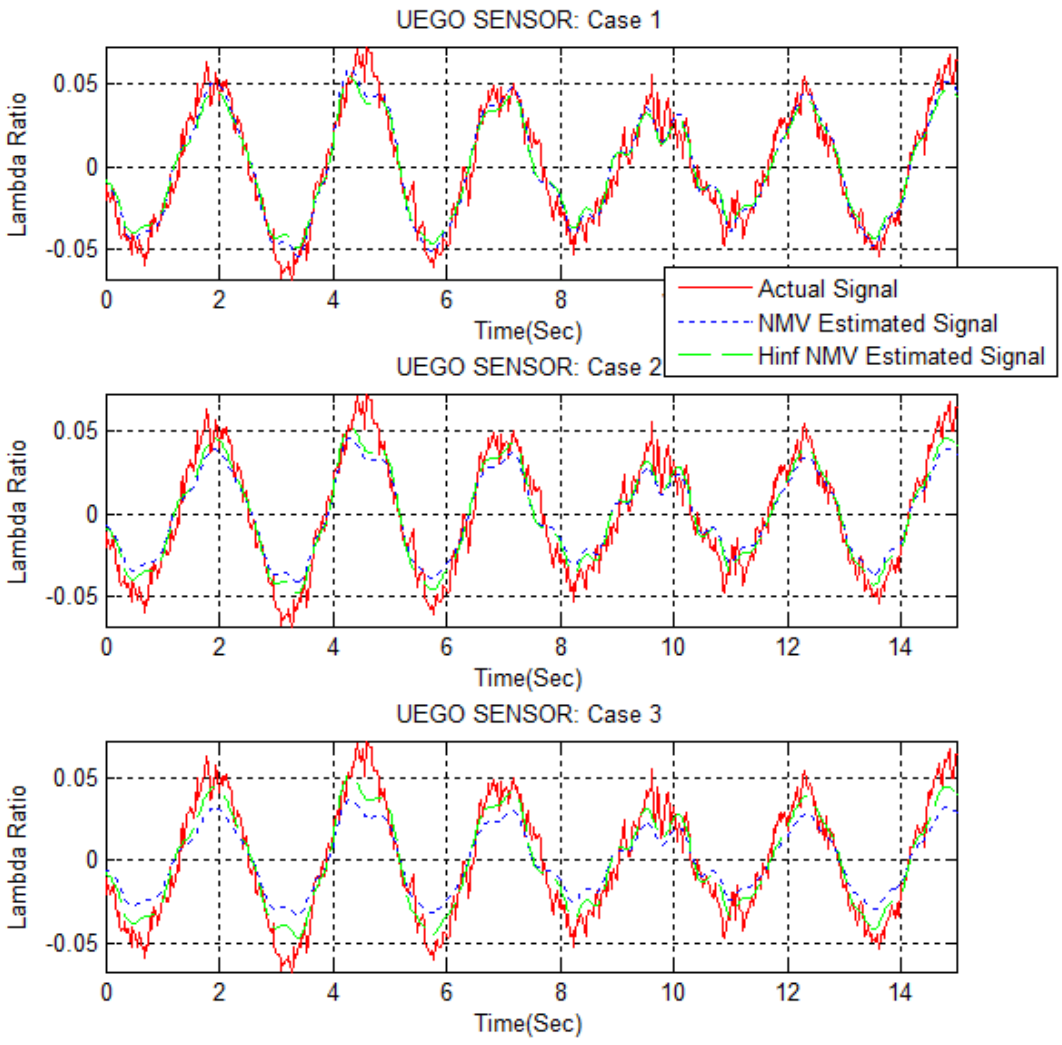

Figure 4.16: Comparison between actual and estimated signals using *NMV* and NH_∞ for UEGO sensor

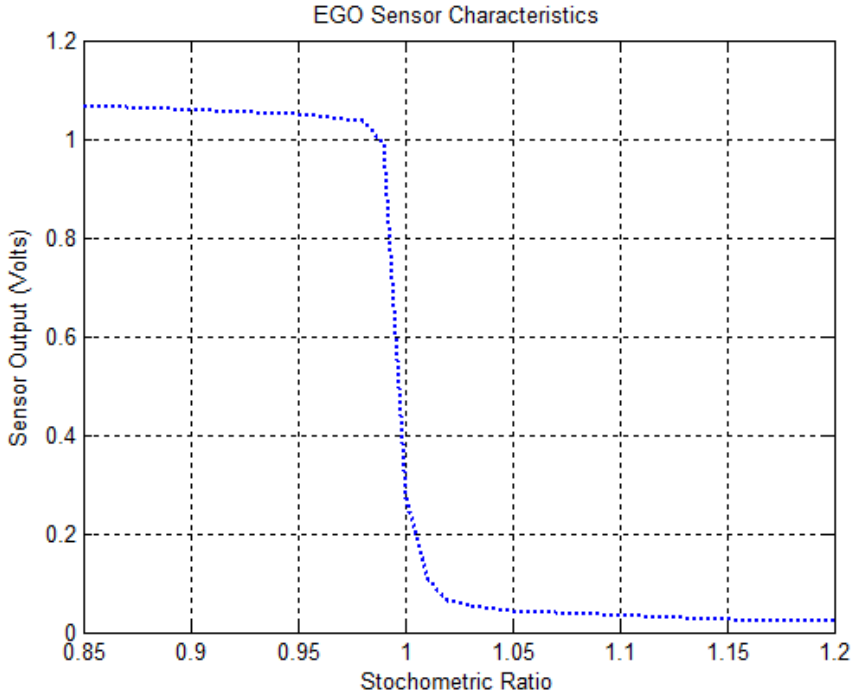

Figure 4.17: EGO Sensor Characteristic in practice may differ from its mathematical model

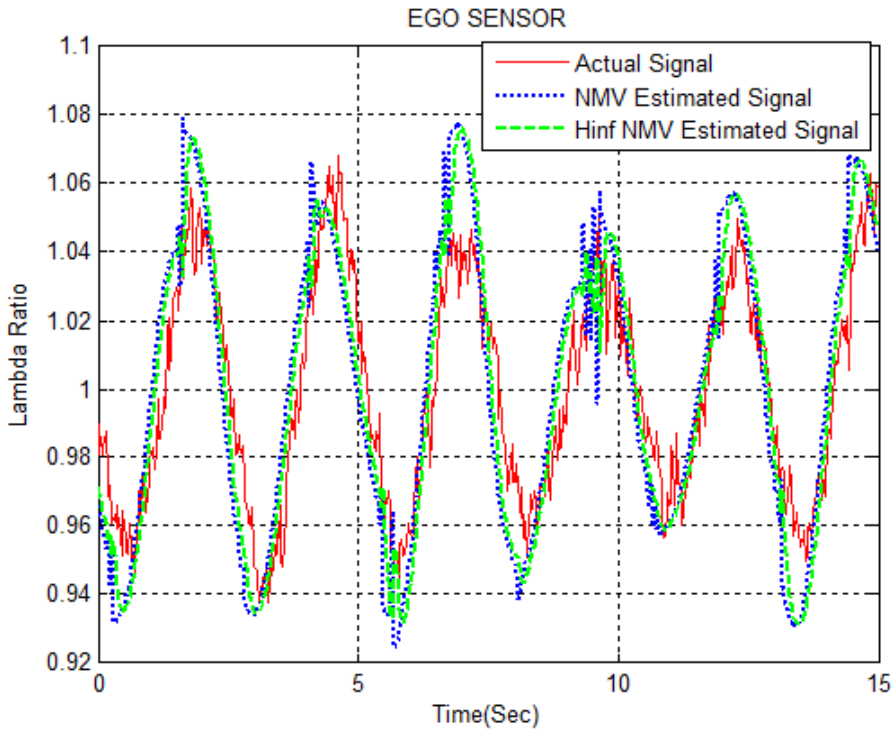

Figure 4.18: Comparison between actual and estimated signals using *NMV* and NH_∞ for EGO sensor which characteristic is shown in Figure 4.17

4.4 Conclusions

In this chapter, the theory, design and the implementation of two robust polynomial based estimators have been investigated. The robust filtering problems introduced are particularly appropriate for nonlinear uncertain systems. The system, for both cases, presents a channel sub-system W_{nl} represented by a nonlinear operator, which is a very general approach. Possible nonlinear channel dynamics uncertainties are represented in a parallel channel that also introduces design freedom.

For the robust Wiener optimal estimator the uncertainty in signal, noise and plant are represented by a probabilistic system description and the variances are assumed to be given. In the limiting case when the dynamics are linear, the estimator has the form of a Wiener filter in polynomial system description form.

The H_∞ filtering problems solution is based on the so-called *NMV* embedding procedure, where an auxiliary minimum variance filtering problem is solved for a cost function with dynamic weighting and a linking lemma is introduced. The dynamic weighting is chosen to relate the two problems, that is, when it is substituted into the results of the auxiliary *NMV* estimation will ensure the conditions of the linking lemma which in turn guarantees the minimization of an H_∞ norm. This H_∞ norm minimization provides different opportunities for tailoring the response of the estimator to uncertainties that can only be frequency response bounded. It may therefore have potential in applications.

The advantage of the above robust estimation solutions is the relative simplicity of the theoretical approach and ease of implementation.

Chapter 5

A Nonlinear System Identification Approach to Condition Monitoring of AGR Nuclear Cores

A nonlinear first principles model is initially developed to describe the refuelling process. Secondly, the friction effects are mathematically investigated and comparatively evaluated under the static friction model, LuGre friction model, and Dahl friction model, respectively. Finally, a nonlinear system identification method, the trust-region reflective Newton, is used to find the optimal parameters in the nonlinear refuelling model.

5.1 System Identification Overview

In control engineering applications a description of the dynamic behaviour of the system is necessary for synthesis or analysis studies. However most of the work of the research community has focused on linear identification that presents elegant solution ([81, 82]), the real-life systems always present nonlinear dynamic behaviour and a linear model can only describe such a system for a small range of input and output values. Therefore, a considerable interest in identification methods for nonlinear systems has risen over the last twenty years. Nonlinear dynamic models can be built using solely the laws of physics, in a so-called first principles model or white model. However, due to the complex nature of many systems and processes, such models are difficult to develop and usually require detailed understanding of physical processes.

Another method to derive a model for a process is using the system identification technique. In this approach dynamic models are built directly from measured data and this usually leads to compact accurate models.

An important task in system identification is the choice of the model that will represent the system examined; this decision is based on knowledge of the system and properties of the model. Attention has been focused on black-box methods such as neural networks ([83]). The models identified from the black-box approach have some drawbacks, in fact they cannot be extrapolated in general, it is difficult to interpret the black-box models and their parameters do not have direct physical interpretations. Therefore, other model structures have received considerable attention over the years.

The most noteworthy models are control-affine models ([84]), Volterra models ([85]), Hammerstein models ([86]), Wiener models ([87]), nonlinear autoregressive moving average models with exogenous inputs (NARMAX), nonlinear autoregressive models with exogenous inputs (NARX), and nonlinear additive autoregressive models with ex-ogenous inputs (NAARX).

Another important class of system identification is the grey-box approach ([88, 89]) where the model structure of the system is derived from the first principles and the system identification is used to estimate the unknown parts or parameters of the model. A grey-box model utilises the measured data for the system identification part and a priori knowledge of physical laws of the process to create a model structure that has an interpretable representation compared to the artificial structure of the black-box. Hence this approach, which is in between the first principles and the black-box, is used in this work as it should offer advantages over those methods.

5.2 Refuelling Process

Within an AGR nuclear power plant each reactor has hundreds of channels that house over 300 fuel assemblies and control rods (see Figure 5.1 and Figure 5.2). The fuel assembly needs to be removed when its irradiation level becomes less than a predefined threshold. The refuelling is the process by which the original fuel assembly is first removed and then a new fuel assembly is inserted to the same fuel channel by a refuelling machine (see Figure 5.3 and Figure 5.4). Over a period of about 5 to 7 years, every fuel channel in the AGR reactor is refuelled. In Figure 5.5 we can see a cross view of a graphite moderator brick with fuel element.

The refuelling process consists of a charge (insertion) operation and a discharge (vacation) operation. In the charge stage, the fuel assembly is lowered by a charge machine into a fuel channel, as opposed to the discharge stage when the exhausted or part exhausted fuel assembly is removed from the channel by the hoist machine.

The aim of this chapter is to establish the refuelling model by working from first principles in the AGR refuelling process and identifying the model parameters using the FGLT data ([90]). The range of interest is the core region of approximately 300 channels, each of which comprises 12 graphite brick layers. The depth of the graphite stack is approximately 11m. On top of the brick stacks each channel presents tundishes, guide tubes and standpipes. During the refuelling process, the fuel assembly has to travel through all of these components to achieve full set down at approximately 30m at the bottom of the channel. It should be noted that reactor dimensions and attributes vary depending on which power station is being discussed.

During the refuelling process, each time the fuel assembly is inserted or removed, two load cells directly measure and record the grab load. The height of the fuel assembly in the brick stack is also recorded.

To drive the fuel assembly through the channel and prevent any contact between the channel wall and the assembly, the latter is equipped with two sets of stabilizing brushes (see Figure 5.6). Their interaction with the channel wall generates a frictional force whose magnitude contributes to the load value. Any variation in the wall geometry results in a corresponding change in the frictional force, and therefore in the FGLT data. An analysis of the refuelling data can provide information about the channel shape and thus it can be used for channel condition monitoring.

The value of the measured load is usually affected by a number of factors, such as the weight of the fuel assembly, friction forces, and the upthrust of the gas (aerodynamic forces) circulating through the core and wall geometry. All these components are considered to develop a nonlinear system model, using a grey model based approach, for the refuelling process which will be used to estimate the friction forces.

In Figure 5.7 a schematic drawing of the simplified nuclear refuelling machine is given. From this figure the nonlinear first principle model is derived in the following sections.

In this work, the refuelling model is used in a model-based filtering application, however, it can also be used to simulate the whole refuelling system in which a controller, such as a PID controller is also included. Figure 5.8 illustrates such an application for the developed nonlinear first principles models, in which a speed feedback closed-loop control is employed. It should also be noted that in the figure the symbol "s" is used as a derivative operator for the purpose of simplifying the representation.

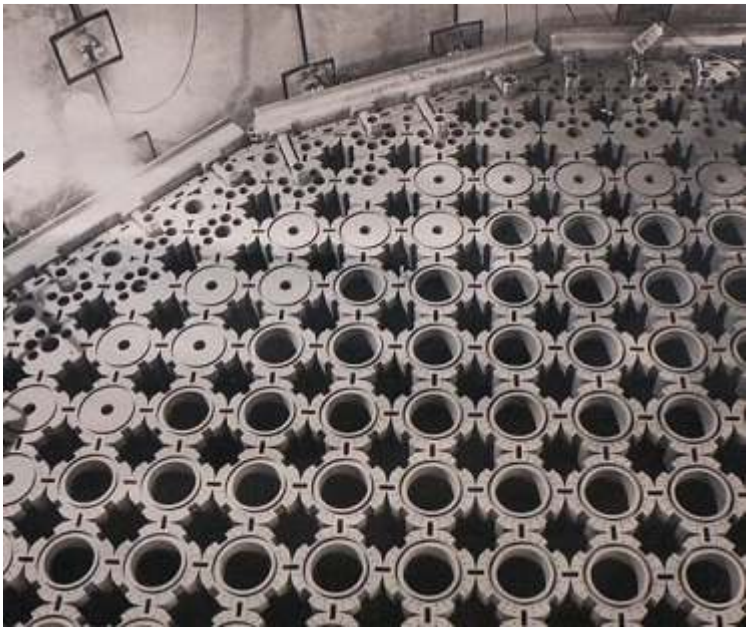

Figure 5.1: Partially complete AGR Graphite Core (Source: [91])

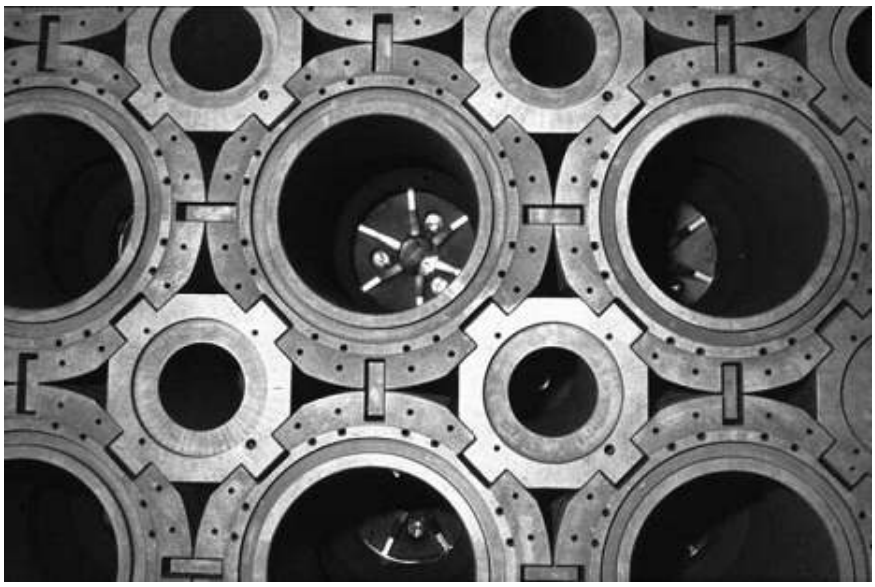

Figure 5.2: AGR System of Radial Keys and Keyways (Source: [91])

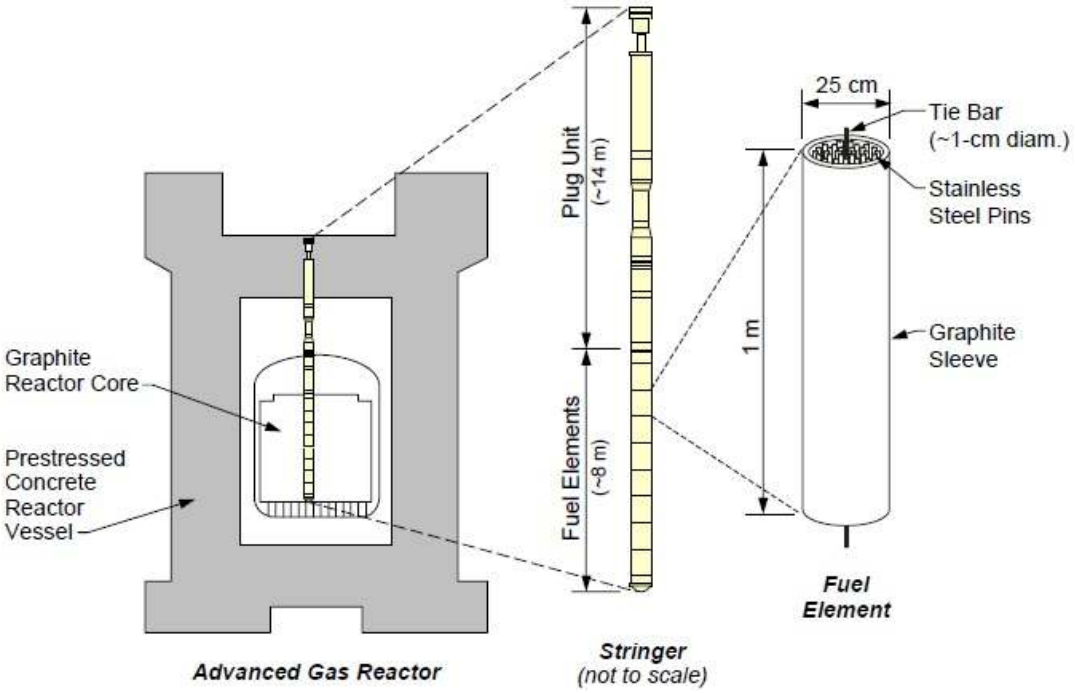

Figure 5.3: AGR core and fuelling assembly (Source: [92])

Figure 5.4: Dungeness B Refuelling Machine (Source: [92])

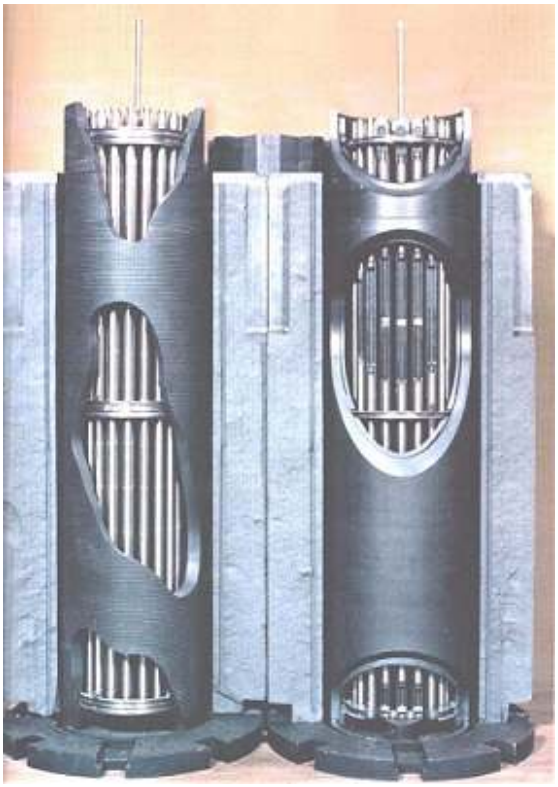

Figure 5.5: Graphite Moderator Brick with Fuel Element (Source: [93])

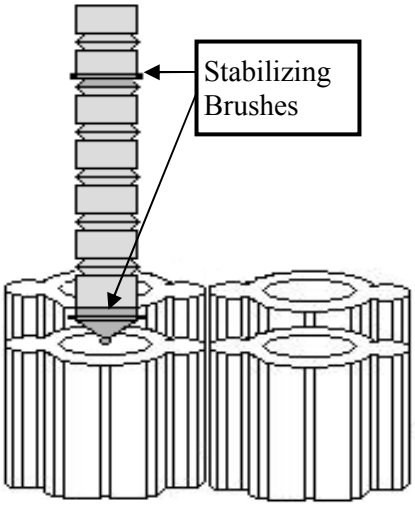

Figure 5.6: AGR Fuel assembly elements and Brick Keying Arrangement

5.2.1 Fuel Assembly Dynamics

The most significant elements that contribute to the value of the net load are the following:

- the weight of the fuel assembly;
- frictional force generated by the interaction between the stabilizing brushes of the fuel assembly and the channel wall;
- up-thrust effect of the gas circulating through the core.

The weight of the fuel assembly depends on its mass, which is known in the charge process and unknown during the discharge, but can be determined once the fuel assembly is extracted from the channel.

The magnitude of the frictional force is directly linked with the wall geometry, because it is created by the interaction between the fuel assembly stabilizing brushes and the channel wall. That means that any possible distortion in the channel will affect the frictional force. The sign of the frictional force changes depend on the operation performed, but always in opposite direction of the fuel assembly. Thus, during the reactor discharge operation, the frictional force opposes the extraction of the fuel assembly from the channel resulting in an apparent load raise. The opposite is true obviously for the fuel charging, when the frictional force support the weight of the channel.

The gas circulating in the core generates a buoyancy force that makes the fuel assembly weight appear lighter.

All the above forces act simultaneously during the refuelling process and therefore all affect the dynamical behaviour of the fuel assembly, as apparent when Newton's Law is applied to the fuel assembly motion:

$$\begin{aligned} \dot{h} &= v \\ \dot{v} &= \frac{1}{m}[mg - F + \mathrm{sgn}(v)F_f - F_a] \end{aligned} \tag{5.1}$$

where sgn(v) denotes the discharge ("+") and charge ("−") stage, h, v, and m denote the height, velocity, and mass of the fuelling assembly, respectively, F represents the grab load force, F_f and F_a denote the frictional and aerodynamic force, respectively.

5.2.2 Aerodynamic model

The net between the upthrust and the downthrust is the main aerodynamic force experienced by the fuel assembly. Because the downthrust is much smaller than the

upthrust during the normal operation of AGR power plant, the upthrust is therefore considered as the main aerodynamic force in this work ([94]).

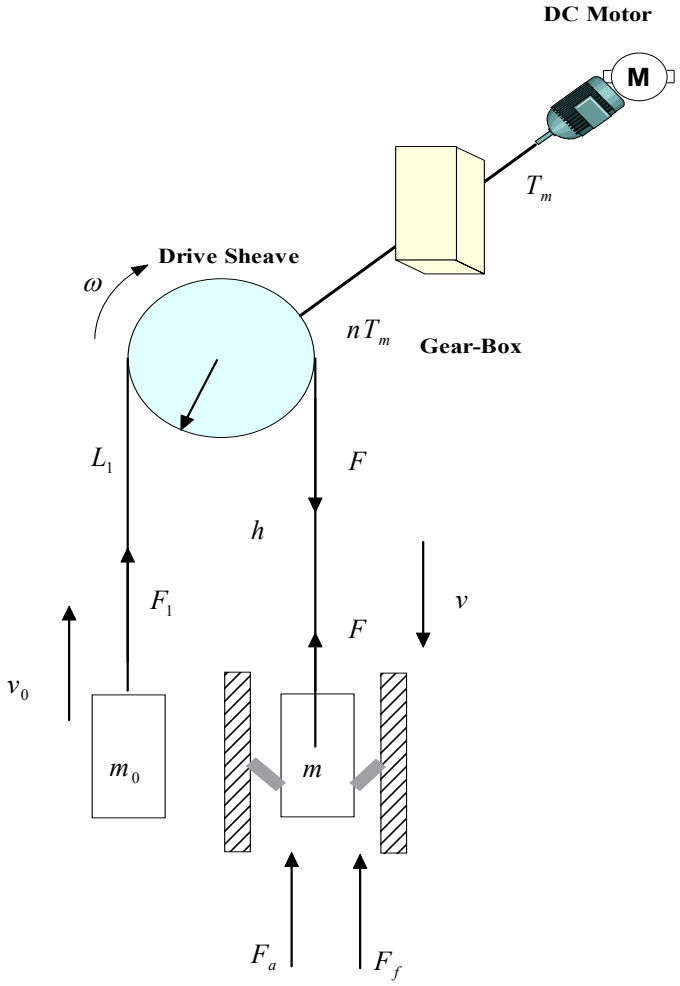

Figure 5.7: Schematic drawing of the simplified nuclear refuelling process

The aerodynamic force in this study is modelled by ([94]):

$$F_a = \frac{1}{2}\rho C_d A[U + \text{sgn}(v)v]^2 \tag{5.2}$$

where,

ρ: mass density of the coolant gas;

U: speed of the coolant gas;

A: crossing sectional area;

C_D: drag coefficient.

If all the parameters ρ, C_d, and A are unknown and need to be identified, then it is unlikely to estimate them separately by only using the input-output data set.

However, for the purpose of the condition monitoring we can treat the term $\rho C_d A / 2$ as a new parameter, i.e., generalised aerodynamic coefficient ψ ,

$$\psi = \frac{1}{2}\rho C_d A \tag{5.3}$$

5.2.3 Friction modelling

In order to reliably derive the estimates of the core cracking conditions from the FGLTs it is critical to understand how the friction force between the fuel assembly's guide brushes and the fuel channel walls can be mathematically modelled and analysed.

Currently there have been many friction models available in different engineering domain to deal with diverse application problems. In this work, we will investigate the three popular friction models, i.e., static friction model, LuGre friction model, and Dahl friction model to examine if they can describe the friction phenomenon in the nuclear refuelling process. Toward this end, a comparative study will be carried out against real plant data sets.

5.2.3.1 **Static Friction Model**

The general friction model for describing the average behaviour of the bristle deflection between two contacting surfaces has the following form:

$$F_f = \sigma_0 z + \sigma_1 \frac{dz}{dt} + \sigma_2 v \tag{5.4}$$

where F_f is the friction force, z is the average deflection of the bristles, v is the relative velocity between the two surfaces; σ_0 is the stiffness, σ_1 is the damping coefficient, and σ_2 is the viscous coefficient.

The static friction model describes how the friction force depends only on the velocity in the sliding regime. It is given by

$$F_f = \sigma_2 v + sign(v)(F_c + (F_s - F_c)e^{-\left|\frac{v}{V_s}\right|^{\delta}}) \tag{5.5}$$

where F_s is the static force, F_c represents the Coulomb force, V_s is the Stribeck velocity, and δ is a shape factor. The first term in (5.5) gives the viscous friction force, whereas the second term models the Stribeck effect.

5.2.3.2 **Dahl Friction Model**

The Dahl model was a first attempt by Dahl ([95]) to describe the friction behaviour in the presliding regime. It is given by

$$\frac{dF_f}{dt} = \sigma_0 v \left| 1 - \frac{F_f}{F_c} sign(v) \right|^{\kappa} sign(1 - \frac{F_f}{F_c} sign(v)) \tag{5.6}$$

where κ is a shape factor. In the Dahl model, the Stribeck effect is not considered. It also exhibits a hysteretic behaviour with nonlocal memory.

A Dahl friction model is relatively simple to identify as it is only determined by three parameters, i.e., the stiffness σ_0, the Coulomb friction F_c, and the shape factor κ.

5.2.3.3 **LuGre Friction Model**

In 1995, Canudas de Wit ([96]) proposed a new dynamic friction model, i.e., the LuGre friction model. It is given as follows:

$$\begin{aligned} \frac{dz}{dt} &= v - \sigma_0 \frac{|v|}{s(v)} z \\ s(v) &= F_c + (F_s - F_c) e^{-\left|\frac{v}{V_s}\right|^{\delta}} \\ F_f &= \sigma_0 z + \sigma_1 \frac{dz}{dt} + \sigma_2 v, \end{aligned} \tag{5.7}$$

The LuGre friction model is able to describe both the presliding and sliding regime. Therefore, it is popular in many areas such as control engineering, mechanical application, and robotics. The internal state variable z is used to represent the average deflection of the bristles. The first-order nonlinear part in (5.7) describes the friction lag in sliding regime.

Unlike the static and Dahl friction model, there are seven parameters in the LuGre friction model. Therefore, it often raises more challenging issues in identifying these parameters in practice due to its hysteresis-like behaviour in presliding and varying breakaway force. Since the LuGre friction model cannot be transformed into a linear form of its unknown parameters, the traditional linear system identification methods cannot be applied.

5.2.4 Hoist Dynamics

From Figure 5.7 we can derive the following differential equations for the hoist machine (for further details see [94]):

$$m_0 \frac{dv_0}{dt} = m_0 \dot{v}_0 = F_1 - m_0 g \tag{5.8}$$

$$\frac{dL_1}{dt} = \dot{L}_1 = -v_0 \tag{5.9}$$

$$L_1 \frac{dF_1}{dt} = L_1 \dot{F}_1 = R(EA_p - F_1)\omega - EA_p v_0 \tag{5.10}$$

$$\frac{dh}{dt} = \dot{h} = v \tag{5.11}$$

$$h \frac{dF}{dt} = h\dot{F} = R(EA_p - F_1)\omega + (EA_p - F)v \tag{5.12}$$

where,

m_0 : equivalent counterweight and tensioning mass (ECTM);

v_0 : velocity of the ECTM;

F_1 : tension of the left hoist rope;

L_1 : length of the left hoist rope;

R : radius of the drive shave;

ω : angular velocity of the drive shave;

E, A_p : tension coefficient and crossing area of the hoist rope.

F : tension of the right hoist rope;

v : velocity of the grab;

h : height position of the grab.

5.2.5 Motor Dynamics

From Figure 5.7 we can write the following differential equations for the motor dynamics:

$$\begin{aligned} &\frac{J}{R}\frac{d\omega}{dt} = \frac{J}{R}\dot{\omega} = \frac{n \cdot T_m}{R} - F_1 + F - B\omega R \\ &T_m = k_m I_a \end{aligned} \tag{5.13}$$

where,

n: ratio of motor gear-box;

J: inertia of the motor

T_m: torque exerted by the motor;

B: viscous friction coefficient of the motor shaft system;

k_m: motor torque coefficient.

From (5.13), a linear transfer function can be derived as follows:

$$\frac{\omega(s)}{n \cdot T_m(s) + [F(s) - F_1(s)]R} = \frac{K_m}{1 + \tau_m s}$$

In which, $K_m = 1/B$ is the mechanical gain and $\tau_m = J/BR^2$ is the mechanical time constant.

$$\frac{dI_a}{dt} = \dot{I}_a = -\frac{R_a}{L_a} I_a - \frac{k_\omega}{L_a}\omega + \frac{v_a}{L_a} \tag{5.14}$$

where,

I_a : current of the motor amature;

v_a : voltage of the motor amature;

L_a : inductance of the motor electric circuit;

R_a : resistance of the motor electric circuit.

Since (5.14) is linear, the following transfer function can be obtained as well:

$$\frac{I_a(s)}{v_a(s) - e(s)} = \frac{K_a}{1 + \tau_a s}$$

in which, $e(s) = k_m \omega(s)$, K_a is the rotor gain, $\tau_a = L_a / R_a$ is the rotor time constant.

5.3 Nonlinear system identification

Since there are a number of unknown parameters in the nonlinear dynamic model developed for the refuelling process, it is paramount to identify these parameters from noisy input/output data to implement the nonlinear first principles model in the condition monitoring of nuclear graphite cores.

The nonlinear system can be described by the following continuous-time SISO (single-input single output) form:

$$\begin{aligned} \dot{\mathbf{x}} &= \mathbf{f}(\mathbf{x}, u, \mathbf{p}) \\ y &= h(\mathbf{x}, u, \mathbf{p}) \end{aligned} \tag{5.15}$$

where $\mathbf{x}$ is the state vector, y and u are the scalar output and input, respectively; $\mathbf{f}(\cdot)$ is a nonlinear vector field, $h(\cdot)$ a nonlinear scalar function; $\mathbf{p}$ is a parameter vector with a appropriate dimension.

In this study, the nonlinear system identification is directly performed in continuous-time domain because it can allow us to have a better understanding of the physical behaviour of the nuclear refuelling system under consideration. The models of the nuclear refuelling system are derived from the first principles, therefore they are inherently continuous in time. Moreover, the parameters in the continuous-time models are strongly linked with the physical properties of the nuclear refuelling system. However, the main difficulty in dealing with the continuous-time system with conventional methods is the presence of the derivative operators associated with the noisy input and output data ([97, 98]). To avoid this difficulty in the nonlinear system identification of the continuous-time nuclear refuelling models, a simulation-based optimization method is adopted in this study. The optimization method will be detailed in the next section.

The complete system for the refuelling process is very complex. If the entire system is considered, the number of unknown parameters is very large. This would be a very challenging task for the nonlinear system identification, i.e. large-scale identification problem. Therefore, a system decomposition strategy is adopted in this study. The key idea here is to decompose the whole system into smaller sub-systems and for each sub-system the aim is to use an efficient nonlinear system identification method, given an input-output measurement data trend, to tune its parameters such that the output data trend can be reproduced by the model under the input data traces.

5.3.1 Trust-Region Reflective Newton method

The nonlinear system identification problem can be solved by finding the solution to the nonlinear constrained optimization with the following form:

$$\begin{aligned} &\min_{\mathbf{x}\in R^n} f(\mathbf{x}) \\ &s.t. \qquad l_i \le x_i \le u_i, i = 1, 2, \cdots, n \end{aligned} \tag{5.16}$$

where $f(\mathbf{x})$ is a real scalar function to be minimized, l_i and u_i are the lower and upper boundedness for the optimization variable x_i, respectively.

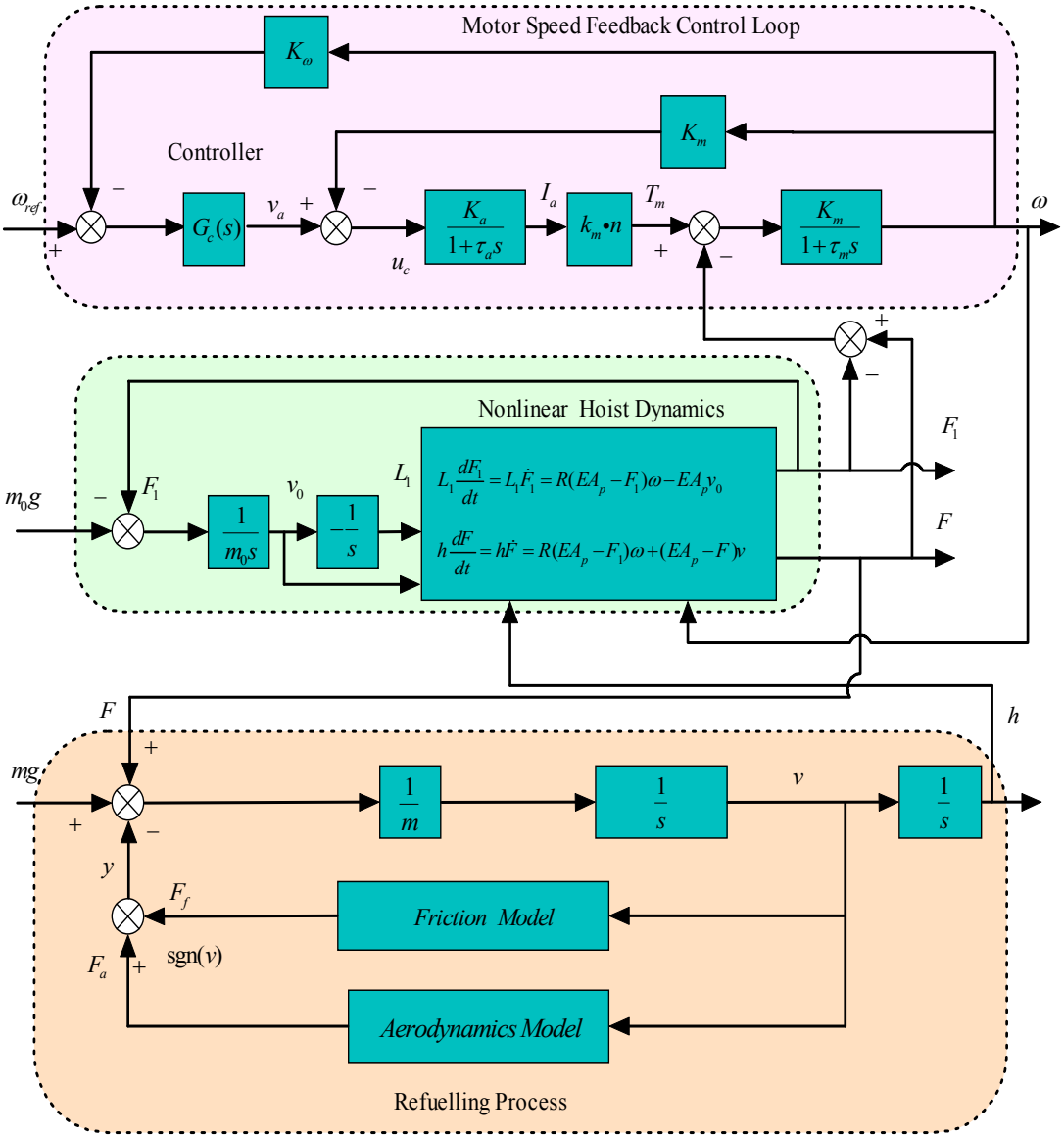

Figure 5.8: Speed feedback closed-loop control block diagram

To solve the above optimization problem, the classic methods are the line search algorithms. The descent direction can be found by solving a sub-problem which approximates the original optimization problem near the current iteration. Therefore, the major drawback for the line search methods is that they cannot guarantee a descent direction can be always found.

In this work the trust-region method is used to solve the nonlinear optimization problem (see Appendix D for theory details).

5.3.2 Numerical experiments

In this section, a case study for the fuel assembly subsystem is performed (see Figure 5.9). In Appendix F the software implemented for this case study is presented.

The objective is to have a comparative study for the three different friction models, i.e., static friction model, LuGre friction model, and Dahl friction model. The aerodynamic force will be also fully considered in the case study. In all the numerical experiments, the cost function to be minimised is defined as the sum of squares of errors between the measured and simulated outputs. Because the fuel assembly subsystem is considered in this case study, the input and output are the FGLT and height, respectively, which can be measured and collected for each fuel channel during the routine refuelling activities.

The FGLT and height data used in this case study are chosen from one channel in an AGR nuclear power station, as given in Figure 5.10. If the parameters in the developed models are not correctly estimated, none of these models are able to properly describe the true output (height measurements) under the true, noisy input (FGLT data traces). Therefore, the key issue in applying the developed first principles model to the condition monitoring of AGR graphite cores is to correctly estimate these model parameters by taking advantage of proper nonlinear system identification method.

For each friction model, three numerical experiments are carried out in this study. Among the three numerical experiments, the first and third are used for nonlinear system identification purpose, the second experiment is for validating the nonlinear model with identified parameters.

The experiments are carried out in Matlab using a nonlinear grey-box model estimator. The first step in the system identification process is specifying the nonlinear grey-box model structure, then a *idnlgrey object* (the grey-box model) is constructed, finally using the function *pem* which implement a trust-region approach, the nonlinear parameters are estimated.

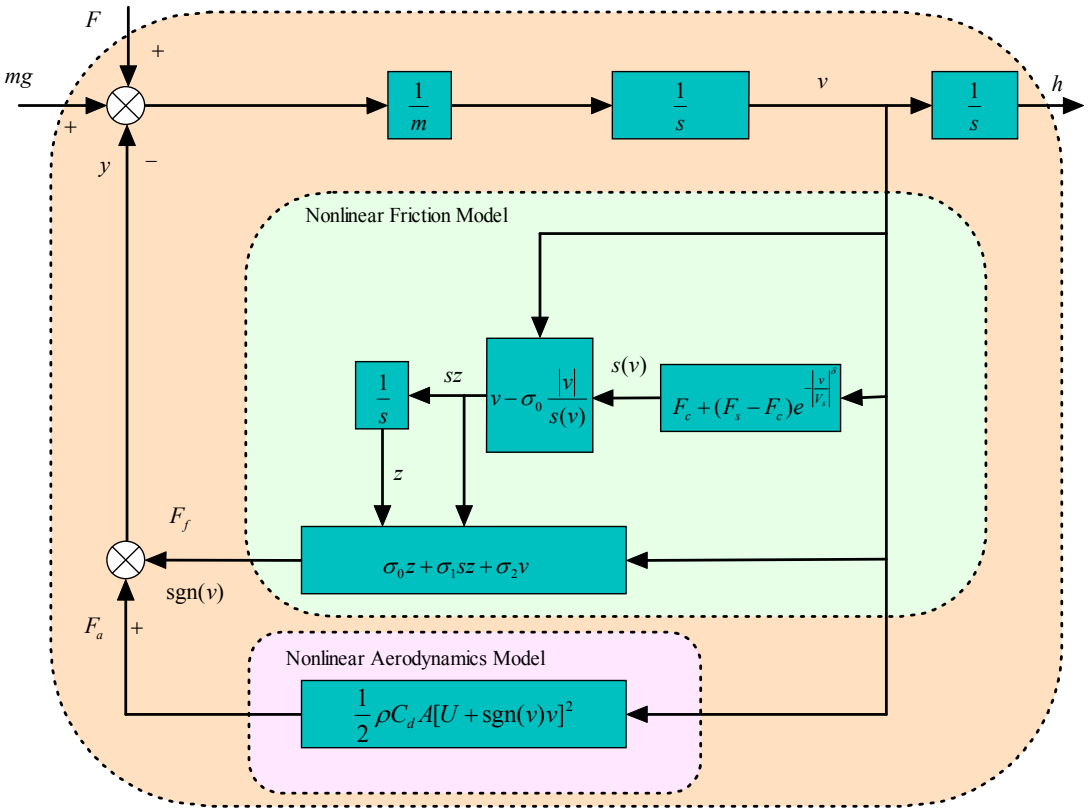

Figure 5.9: Refuelling subsystem

5.3.2.1 **Static Friction Model**

When the static friction model is used with the fuel assembly dynamics and aerodynamic force model, there are in total seven parameters in the subsystem, i.e., the mass of the fuel assembly *m*, the viscous coefficient σ_2, the Coulomb force F_c, the static force F_s, the shape factor δ, the aerodynamic coefficient ψ, and the gas velocity *U*. In many literatures, the shape factor is chosen as 2. Therefore, in all the experiments performed, the shape factor was simply fixed to be 2 in this case study. This can also speed up the process of nonlinear system identification and reduce the complexity of the optimisation problem. So there are six parameters to be identified.

As the static friction model is used, there are two state variables, i.e., the height *h* and the velocity *v* of the fuel assembly. During the refuelling, the velocity *v* of the fuelling assembly is strictly constrained to be about 0.01 m/s when it is in the graphite core region. Therefore, the constrained state is one of the challenging issue when the nonlinear system identification approach is used in the condition

monitoring of AGR nuclear graphite cores. In all our experiments, the velocity v of the fuel assembly is constrained to the range [0.0085, 0.0115] m/s. For the height state variable, its range is [0, 50] m. In comparison with the velocity, the constraint to the height is much relaxed.

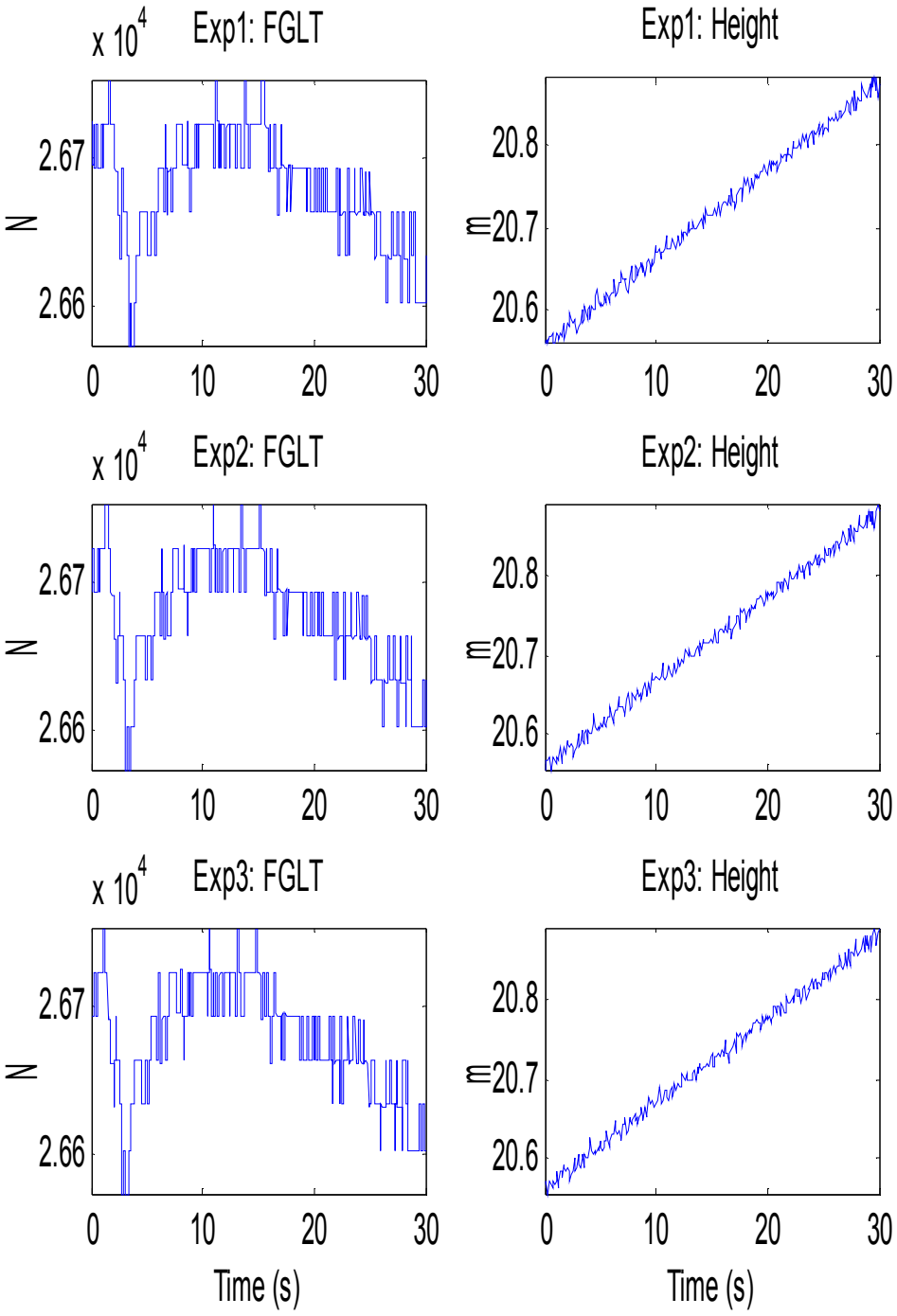

Figure 5.10: FGLT and Height data set for numerical experiments

Figure 5.11 shows the evolutions of cost function in the system identification with the static friction model. It can be seen that the cost function converged very fast. Within a few iterations, it became less than 0.001. This demonstrated that the static friction model can be used to quickly obtain the estimations of the system parameters if the dynamics is not significant in the system under consideration.

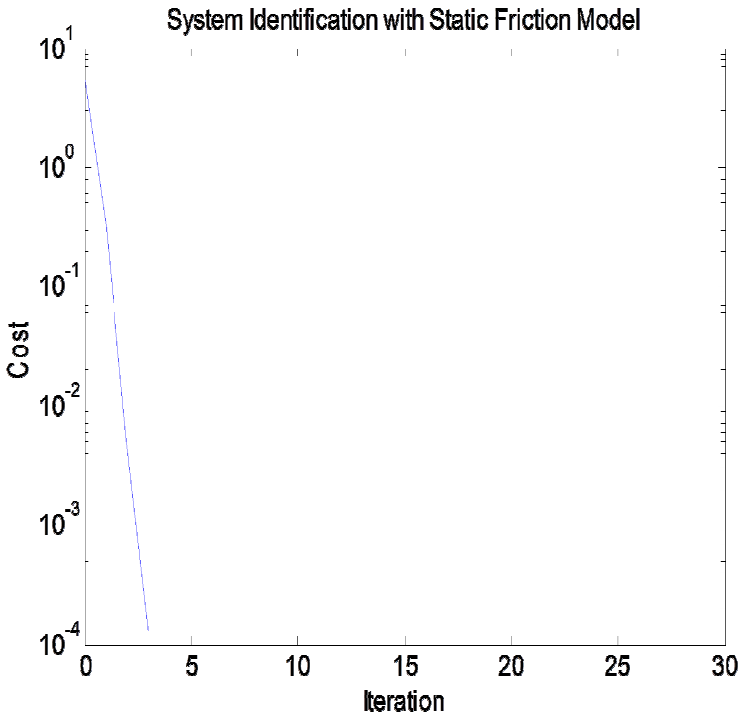

Figure 5.11: The cost function in the system identification with the static friction model.

In Table 5.1 are given all the parameters obtained under the static friction model. In Figure 5.12, the measured and simulated outputs are compared for both the training and validating input-output data sets.

Table 5.1: System parameters under the static friction model

Parameter	Symbol	Unit	Value	Range	Note
Mass	m	kg	2857.06	[2800, 2900]	Identified
Viscous coefficient	σ_2	N.s/m	10008.6	[0, ∞]	Identified
Coulomb force	F_c	N	10.0247	[0, ∞]	Identified
Static force	F_s	N	14.6449	[0, ∞]	Identified
Stribeck velocity	V_s	m/s	0.000977428	[0, ∞]	Identified
Shape factor	δ	N/A	2	Fixed	Fixed
Aerodynamic coeff	ψ	$N.s^2/m^2$	10.5355	[0, ∞]	Identified
Gas velocity	U	m/s	10.6398	[0, ∞]	Identified

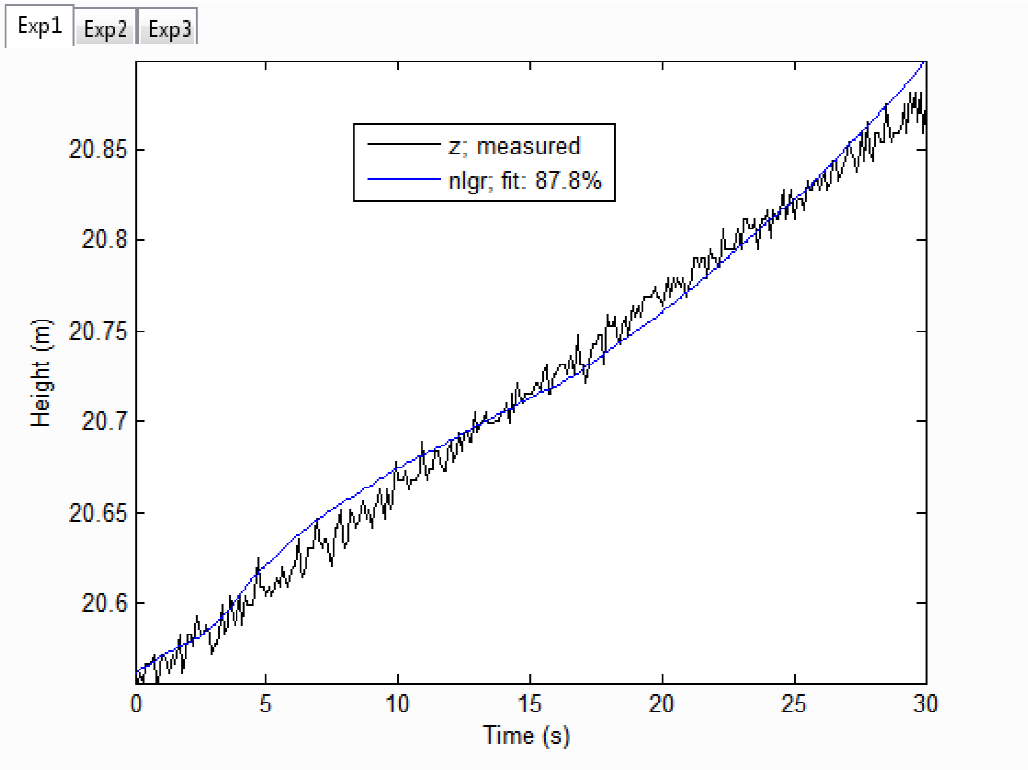

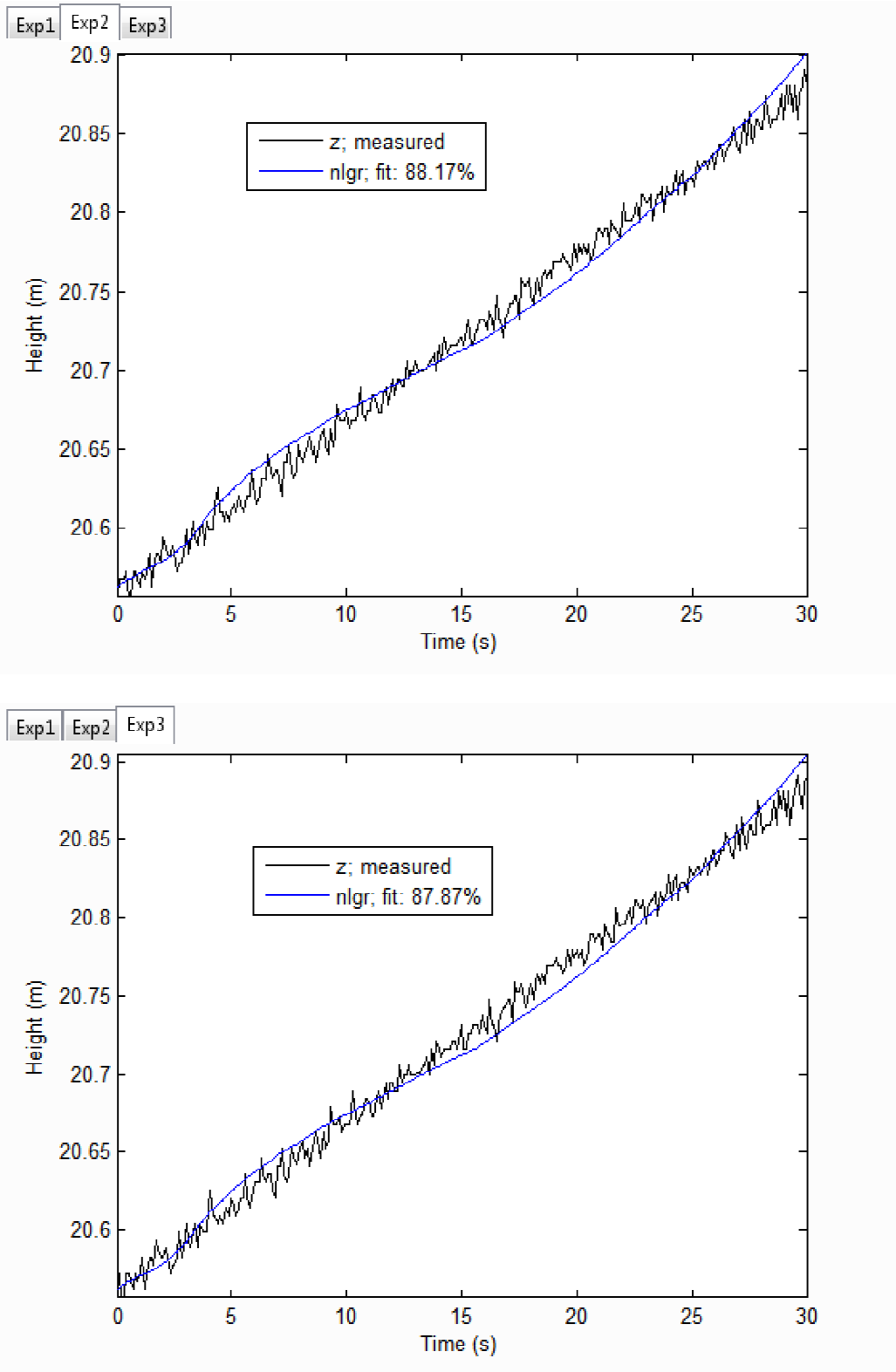

Figure 5.12: Numerical experiments for the static friction model.

5.3.2.2 **Dahl Friction Model**

The Dahl friction model has only a few parameters to be identified and this is an advantage over other friction models. After plugging the Dahl friction model in the fuel assembly subsystem, there are in total 5 parameters meaning there are less to be identified than in the static friction model case, although the Dahl friction model has more state variables. All the constraints to the state variables are similar to the static friction model case; in particular, the velocity v of the fuelling assembly is constrained to the range [0.0085, 0.0115] m/s. Therefore, the challenge raised in the static model by the state constraints remains unchanged in the Dahl friction model case.

The cost function in the system identification with the Dahl friction model are depicted in Figure 5.13. After 8 iterations, the cost function was assuming a steady value of about 0.01 which is far from the optimisation target 0.001. However, the cost could not be further decreased even the iteration number increased up to 50.

The system parameters obtained through the nonlinear system identification approach are listed in Table 5.2. In Figure 5.14, the measured and simulated outputs are compared for all the three numerical experiments. Obviously, the performance of the subsystem with the Dahl friction model is much worse in this case study.

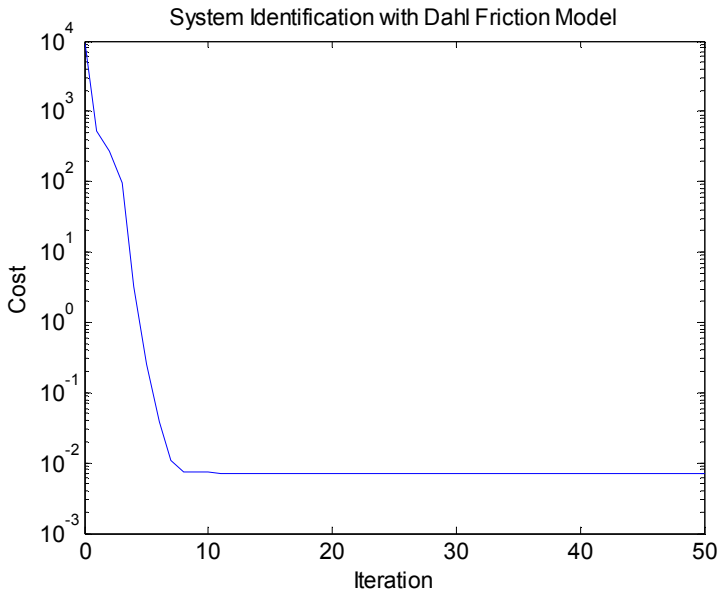

Figure 5.13: The cost function in the system identification with Dahl friction model.

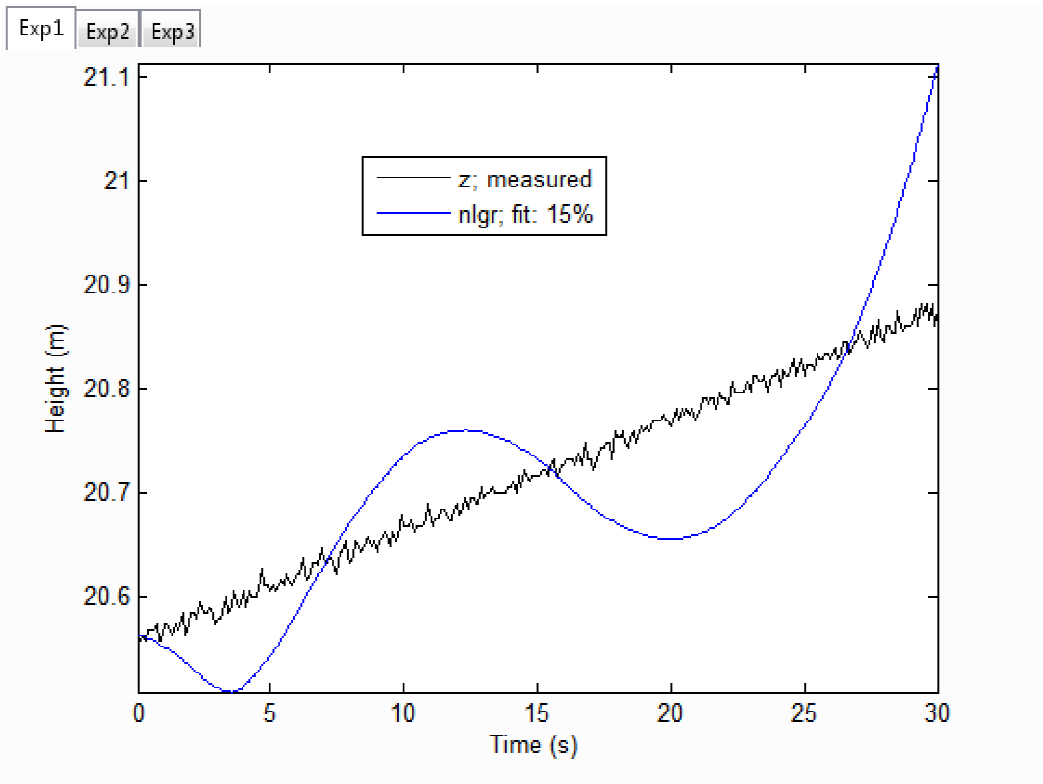
Exp1
Exp2
Exp3
z; measured
nlgr; fit: 15%
Height (m)
Time (s)
21.1
21
20.9
20.8
20.7
20.6
0
5
10
15
20
25
30

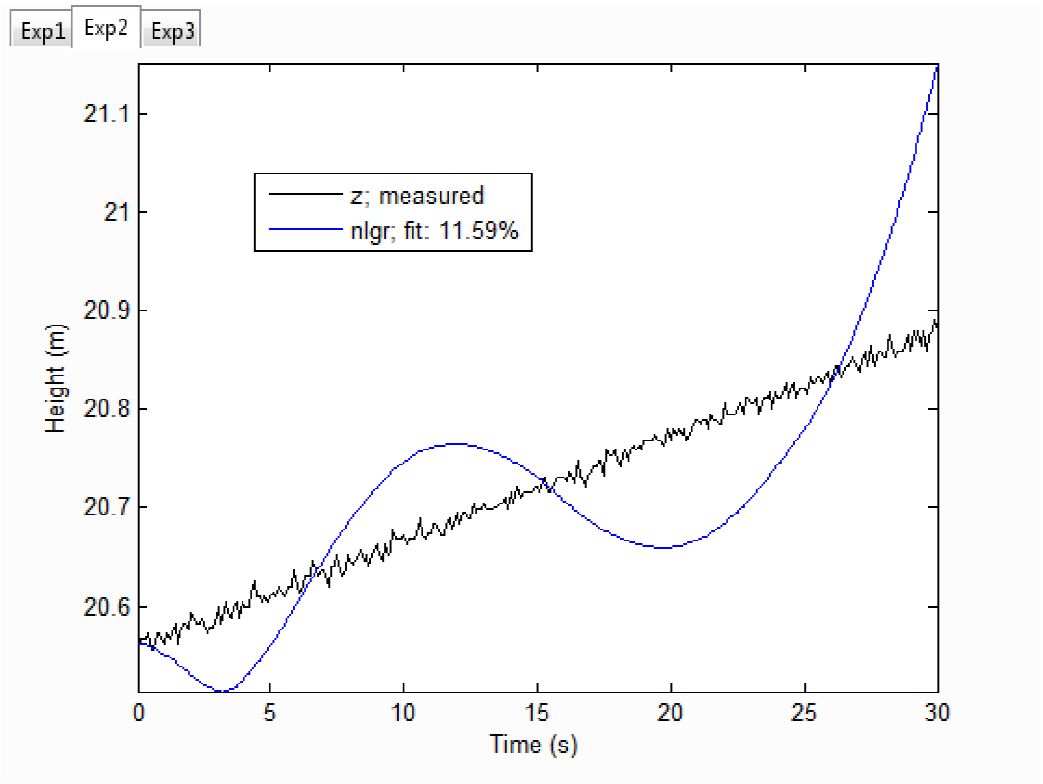
Exp1
Exp2
Exp3
z; measured
nlgr; fit: 11.59%
Height (m)
Time (s)
21.1
21
20.9
20.8
20.7
20.6
0
5
10
15
20
25
30

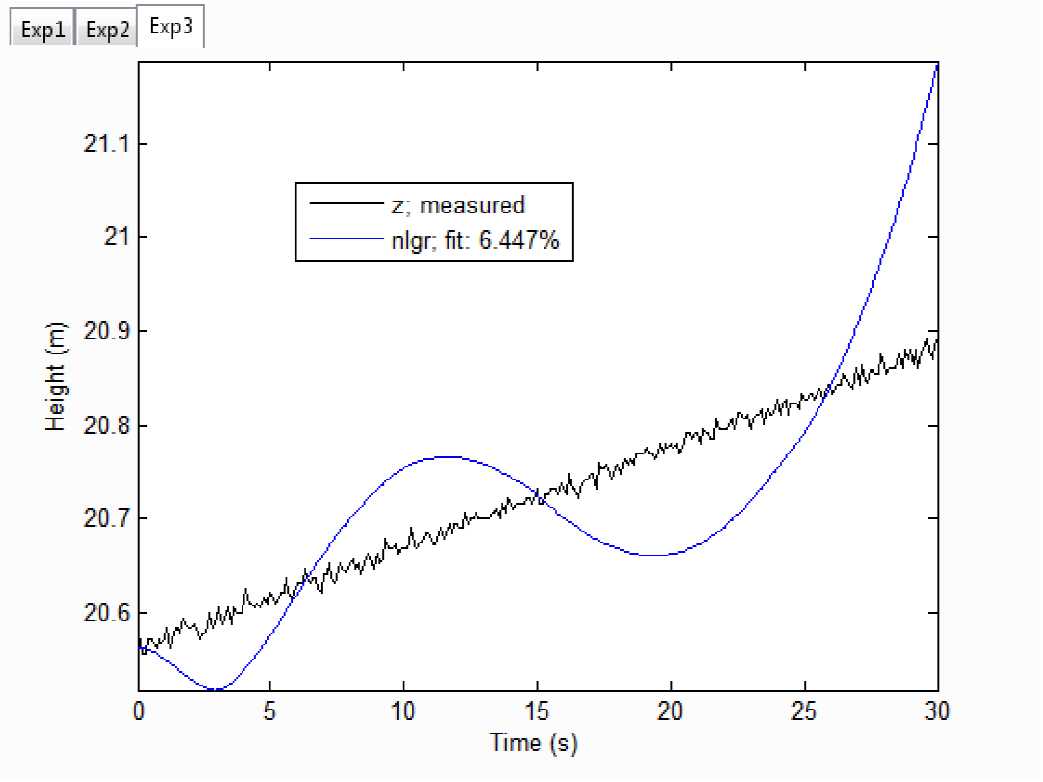

Figure 5.14: Numerical experiments for the Dahal friction model.

Table 5.2: System parameters under Dahl friction model

Parameter	Symbol	Unit	Value	Range	Note
Mass	m	kg	2853	[2800, 2900]	Identified
Stiffness coefficient	σ_0	N/m	658.978	[0, ∞]	Identified
Static force	F_s	N	9.2472	[0, ∞]	Identified
Aerodynamic coefficient	ψ	$N.s^2/m^2$	5.27225	[0, ∞]	Identified
Gas velocity	U	m/s	15.4674	[0, ∞]	Identified

5.3.2.3 **LuGre Friction Model**

Like the Dahl friction model, the LuGre friction model is also designed to describe the dynamic behaviour of friction phenomena. There are seven parameters in the LuGre friction model, i.e., the stiffness coefficient σ_0, the damping coefficient σ_1, the viscous coefficient σ_2, the Coulomb force F_c, the static force F_s, the Stribeck

velocity V_s, the shape factor κ. From the aerodynamic force model, there are another two parameters to be identified, i.e., aerodynamic coefficient ψ and gas velocity U. In addition, the mass of the fuel assembly m also needs to be identified. If the shape factor is fixed, there are 9 parameters to be identified by using the proposed nonlinear system identification approach.

Figure 5.15 shows the evolutions of cost function in the system identification with the LuGre friction model. Although the number of parameters to be identified was increase to 9 in comparison with both the static and the Dahl friction models, the convergence of the optimisation process with the LuGre friction model is much faster. From the figure, the cost can be quickly reduced to 0.0001 with less than 6 iterations.

Table 5.3 gives all the obtained parameters of the fuel assembly subsystem with the LuGre friction model and the aerodynamic model. For all the three numerical experiments, the measured and simulated outputs are compared in Figure 5.16 over the whole input-output data sets.

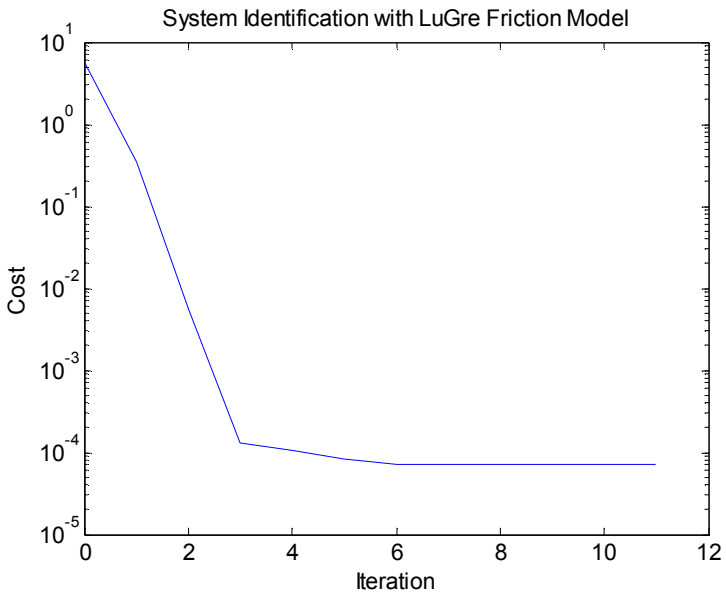

Figure 5.15: The evolutions of cost function in the system identification with the LuGre friction model.

Table 5.3: System parameters under LuGre friction model

Parameter	Symbol	Unit	Value	Range	Note
Mass	m	kg	2859.92	[2800, 2900]	Identified
Stiffness coefficient	σ_0	N/m	18.8273	[0, ∞]	Identified
Damping coefficient	σ_1	N.s/m	2.012	[0, ∞]	Identified
Viscous coefficient	σ_2	N.s/m	22007.9	[0, ∞]	Identified
Coulomb force	F_c	N	14.1654	[0, ∞]	Identified
Static force	F_s	N	15.0422	[0, ∞]	Identified
Stribeck velocity	V_s	m/s	0.00100161	[0, ∞]	Identified
Shape factor	κ	N/A	2	Fixed	Fixed
Aerodynamic coeff	ψ	$N.s^2/m^2$	10.3139	[0, ∞]	Identified
Gas velocity	U	m/s	10.3385	[0, ∞]	Identified

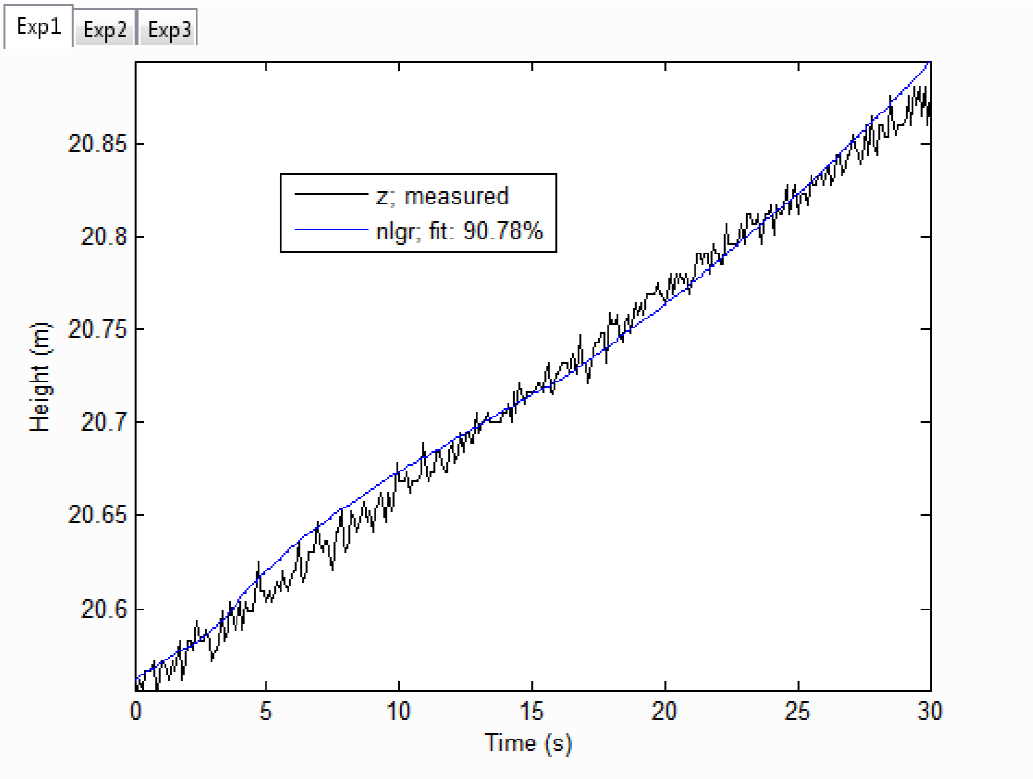

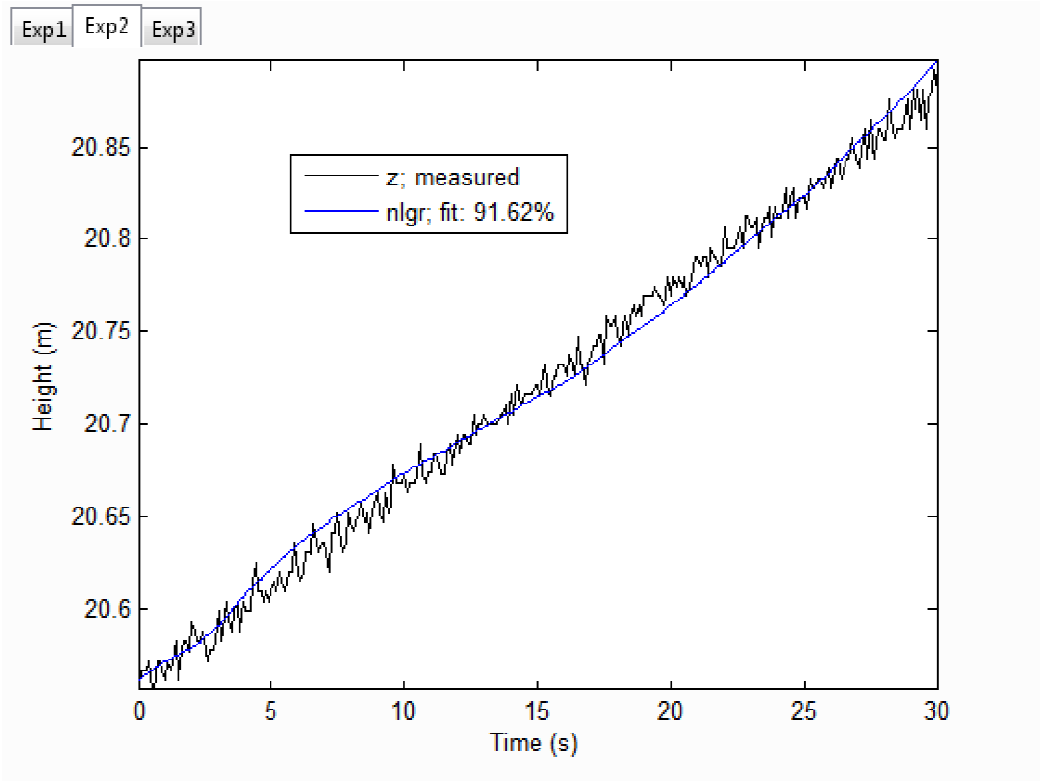

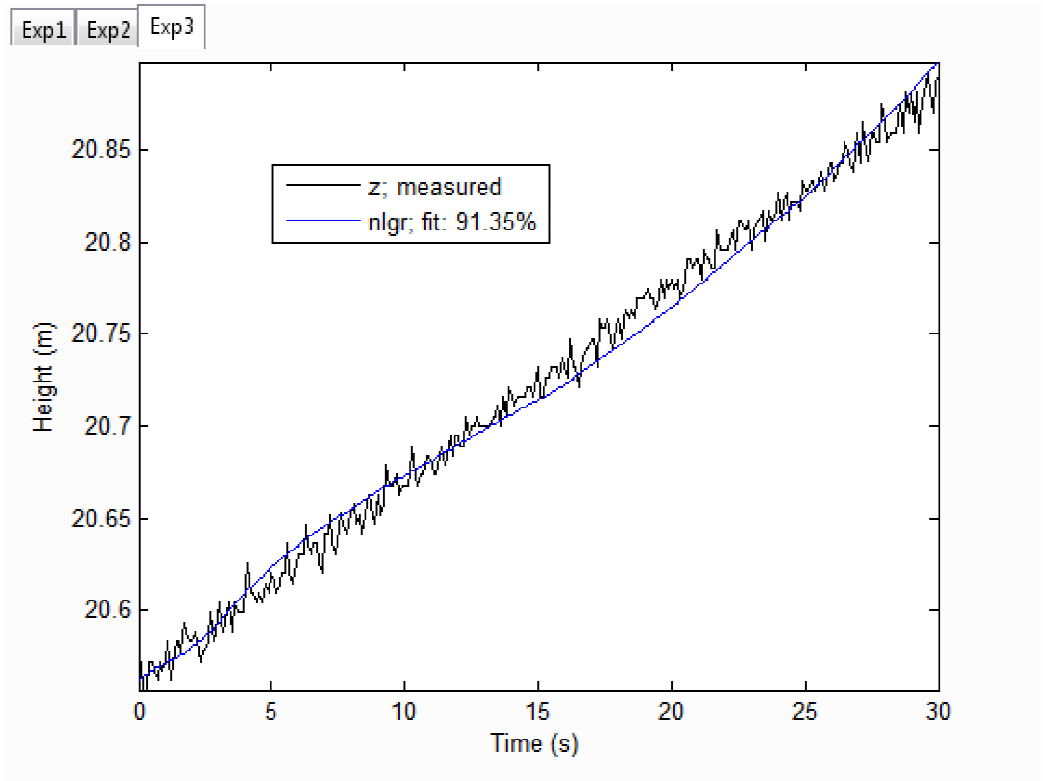

Figure 5.16: Numerical experiments for the LuGre friction model.

5.3.2.4 **Performance Comparison**

In this section the performance of each model is investigated by comparing the true outputs with its simulated outputs under both modelling and validating input-output data sets. If the absolute error between the measured output and the simulated output is less than the specified tolerance, then the modelling accuracy is satisfied at that point. The total modelling accuracy is defined as the percentage (%) of the total satisfaction points against all points.

To compare the performance, the modelling accuracy under the different friction models is given in Table 5.4. From the table, it can be seen that in this case study the LuGre friction model outperformed both the static and Dahl friction models. In the given input-output data sets as shown in Figure 5.10, the velocity of the fuel assembly seems nearly constant, however, it still exhibits some dynamics. Because the LuGre friction model is able to capture this weak dynamics in the nonlinear system, its performance is slightly better than the static friction model.

Table 5.4: Modelling Accuracy under Different Friction Models

Friction Model	Experiment 1	Experiment 2	Experiment 3
Dahl	15%	11.59%	6.447%
Static	87.8%	88.17%	87.87%
LuGre	90.78%	91.62%	91.35%

One of the interesting observations is that although the Dahl friction model was also intended to consider the system dynamic problem, its performance is much worse than the LuGre friction model in this case study. The reason was that the Dahl friction model was mainly designed to describe the presliding behaviours of frictional phenomena. However, all the training and validating input-output data sets were given from the sliding (moving) regime. In addition, the Dahl model does not take the Stribeck effect into account, so it cannot describe the stick-sly motion in the process and this may affect its performance.

5.4 Conclusions

A simplified model for the refuelling system is obtained and mathematically implemented from the first principles of the process. Then its fuel assembly dynamics subsystem is identified to be used in a model based filtering application.

The identification process consists in the unknown model parameters estimation that leads to a nonlinear optimization problem which is solved using the trust-region method.

The identification process is carried out in Matlab using a nonlinear grey-box model estimator for 3 different data sets. The grey-box structure varies depending on which friction model is considered between the static friction model, the Dahl model and the LuGre model. The latter seems to have a better accuracy compared to the other two models likely because in its nature take into account the dynamic of the system and the stick-slip motion.

Chapter 6

H_∞ Friction Estimation for Condition Monitoring of AGR Nuclear Graphite Cores

In this chapter a model-based technique for condition monitoring of an AGR core is introduced. First a state-dependent model and nonlinear operator based approach to estimation and filtering is applied to estimate the friction component of the FGLT data resulting from the interaction of the fuel assembly and the core channel. Then the friction force is estimated by using a H_∞ robust estimator to deal with model uncertainties.

6.1 Friction Estimation by using a State-Dependent NMV Filter

In the previous chapter a nonlinear model for the refuelling operation was implemented starting from the forces acting in the process to form the fuel assembly motion's law then both aerodynamics and friction forces were further investigated in order to have a full physical description that represents the model structure. Finally the model parameters were identified by a trust-region method.

In this section a first attempt to estimate the friction component of the FGLT data is done by using a state-dependent based estimator which is a particular form of the *LPV* estimator developed in chapter 3.

The friction force in the model is not modelled, it is considered as a lump force term instead and this leads to a state-dependent model and state-dependent estimation problem. This choice was undertaken to simplify the parameters identification process which may introduce model uncertainties. It is worth highlighting how in a second instance a robust estimator was used to estimate the friction force to cope with likely model mismatch.

Recall the main contributors to the load recorded during the refuelling process:

a) the weight of the fuel assembly;

b) frictional force generated by the interaction between the stabilizing brushes of the fuel assembly and the channel wall;

c) up-thrust effect of the gas circulating through the core.

Hence we consider the Newton's Law applied to the fuel assembly motion to obtain the general dynamics of the refuelling process:

$$\begin{aligned} \dot{h} &= v \\ \dot{v} &= \frac{1}{m}[mg - F + \text{sgn}(v)F_f - F_a] \end{aligned} \tag{6.1}$$

The aerodynamic force is modelled by the following (recall equ. (5.2))

$$F_a = \psi[U + \text{sgn}(v)v]^2 \tag{6.2}$$

where $\psi = \frac{1}{2}\rho C_d A$, ρ and U are the mass density and speed of the coolant gas, respectively, A is the cross-sectional area, C_d is the drag coefficient.

Thus the overall system is how shown in Figure. 6.1.

.

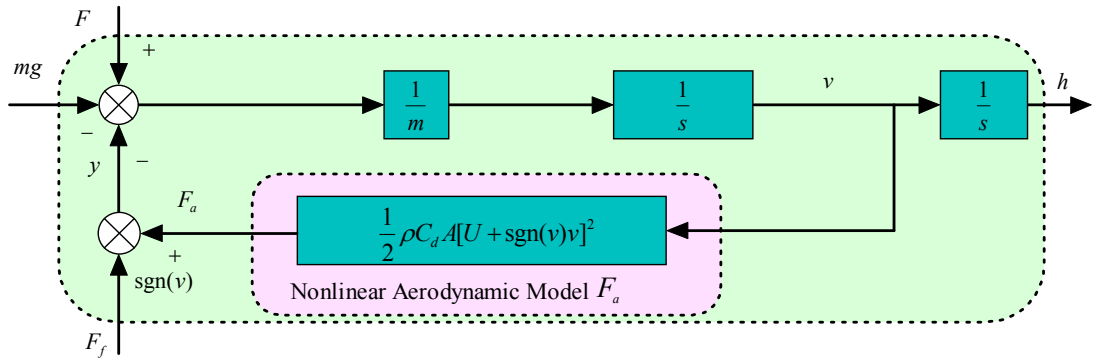

Figure. 6.1: Refuelling process model

6.1.1 State-Dependent System Model

In order to formulate the problem in a state-dependent model, let equation (6.1) be expressed by the following fault-corrupted state-dependent system:

$$\begin{aligned} \dot{\mathbf{x}}(t) &= \begin{bmatrix} \dot{x}_1 & \dot{x}_2 \end{bmatrix}^T = \mathbf{A}(\mathbf{x})\mathbf{x}(t) + \mathbf{B}u(t) + \mathbf{L}v(t) + \mathbf{K} \\ y(t) &= \mathbf{C}\mathbf{x}(t) \end{aligned} \tag{6.3}$$

where the two states x_1 and x_2 are height and speed respectively, $u(t)$ is the FGLT data, $v(t)$ is the unknown friction force, K is an additive matrix term and $y(t)$ is the measured fuel assembly height.

The following matrices are derived by plugging equation (6.2) into equation (6.1) and rearranging in state space form. Note that the matrix A depends on the state x_2.

$$A=\begin{bmatrix}0 & 1\\ 0 & -\frac{2k_{\psi}}{m}\left(2k_u+x_2\right)\end{bmatrix},\quad B=\begin{bmatrix}0\\ -\frac{1}{m}\end{bmatrix},\quad L=\begin{bmatrix}0\\ -\frac{1}{m}\end{bmatrix},$$
$$K=\begin{bmatrix}0\\ g-\frac{2k_{\psi}k_u^2}{m}\end{bmatrix},\qquad C=\begin{bmatrix}1 & 0\end{bmatrix}. \tag{6.4}$$

6.1.2 State-Dependent NMV Filter for Friction Force Estimation

In chapter 3 an *LPV* model based estimator was developed, however, in the following the solution of a state-dependent model and nonlinear operator based filter is used to estimate the friction force component of the measured FGLT data.

LPV and *state-dependent* models appear similar but they are fundamentally different in that a state-dependent model can represent a non-linear system whereas an *LPV* model is a special type of linear time varying system. However, if we consider the particular form of matrix system $\mathcal{A}(x(t), u(t), p(t))$ we can extend the *LPV* solution to the state-dependent based model as highlight in the conclusion of chapter 3.

The refuelling system, as described in the previous section**,** can be expressed by a fault-corrupted state-dependent model (see equation (6.3)), where its term *v(t)* is the unknown input, the friction force, we want to isolate from all the forces involved in the process.

In the numerical experiments the input of the fuel assembly subsystem are the FGLT data and the friction force to be estimated and the output is the height. The FGLT and height data used in this case study, which are measured and collected for each fuel channel during the routine refuelling activities, are chosen from 5 channels in the same AGR nuclear power station. Two channels are used in this section to present the results of the estimation (see those data in Figure 6.3 and Figure 6.4) then the results are validated against the other 3 channels' refuelling process measurements (see Appendix E for simulation plots related to these 3 channels).

The *state-dependent NMV* estimator is used to obtain the friction force generated by the fuel assembly going through the channel and which the value depends on the wall channel geometry. The friction estimation is analysed afterwards in order to gather information about the core condition.

The friction force of the refuelling channel goes through a "communication channel" represented by the state-dependent model and the output from this block is fed to the estimator which gives an estimation of the friction force entering the communication channel.

The overall system and resulting *state-dependent NMV* filter is as shown in Figure 6.2.

Let the sample time 0.1 seconds and the signal and noise models are as follows:

$$W_s = \frac{-09652 + 1081z^{-1} - 01729z^{-2} - 132z^{-3} + 1246z^{-4} + 01349z^{-5}}{1 - 1506z^{-1} + 05374z^{-2} + 02199z^{-3} - 05871z^{-4} + 1028z^{-5} - 06925z^{-6}}$$

$$-> \left[\mathcal{A}_s, \mathcal{D}_s, \mathcal{C}_s, \mathcal{E}_s\right]$$

$$W_n = \frac{0.01393z^{-1}}{1 - 0.8607z^{-1}} \; -> \; \left[\mathcal{A}_n, \mathcal{D}_n, \mathcal{C}_n, \mathcal{E}_n\right]$$

The friction force F_f is indeed thought to be generated by white noise into a colouring filter (the above W_s).

The message signal path transfer function W_c and the estimation error dynamic weighting W_q will be assumed unity.

The estimated signal and the message signal from the model for channel 1 and channel 2 are shown in Figure 6.6 and Figure 6.8 respectively; the estimation error variance is $J = 7.1277\text{e-}004$ for channel 1 and $J = 2.5033\text{e-}003$ for channel 2 (see Table 6.1). The effectiveness of these solutions is more obvious when the observations (measurement from the channel) and the estimate are compared in Figure 6.5 and Figure 6.7.

In Appendix F can been found the software implementation details.

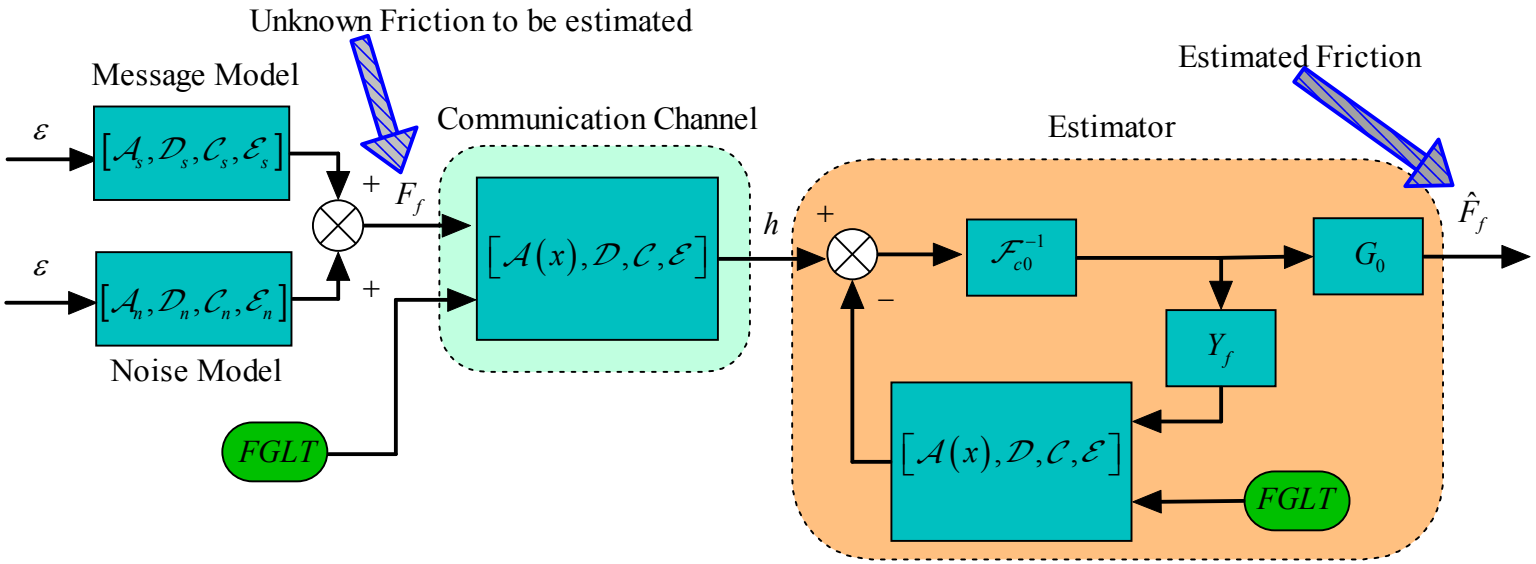

Figure 6.2: Model and State-dependent estimator framework.

Table 6.1: Variance of estimation error for the 5 channels case studies

Channel	Variance of Estimation Error
1	7.1277e-004
2	2.5033e-003
3	4.6828e-003
4	8.6205e-004
5	3.4115 e-003

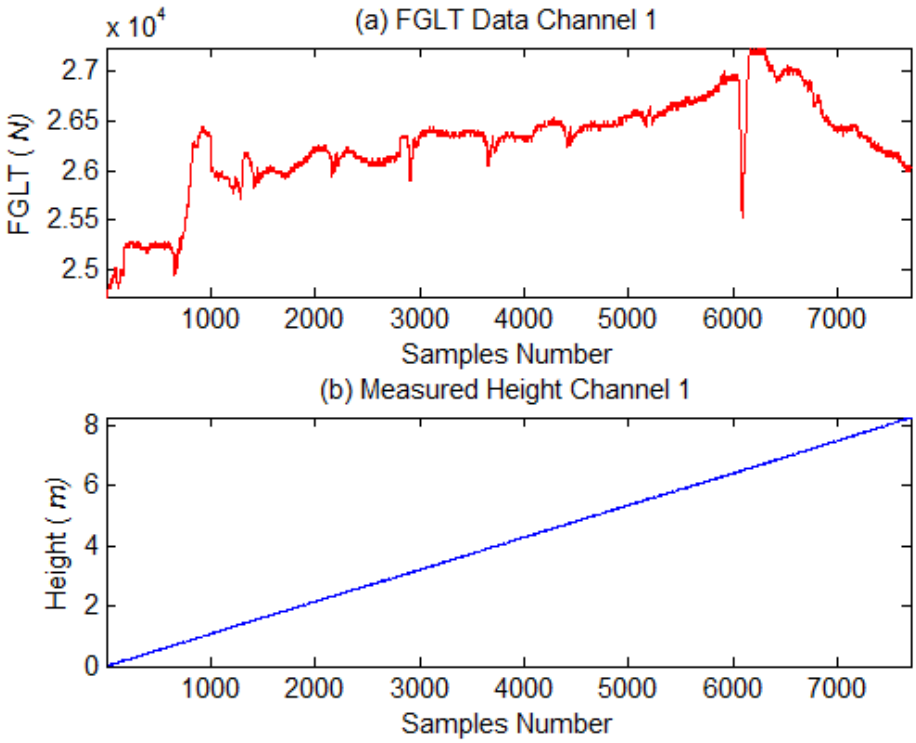

Figure 6.3: Refuelling measurements data channel 1: FGLT data (above) and height (below)

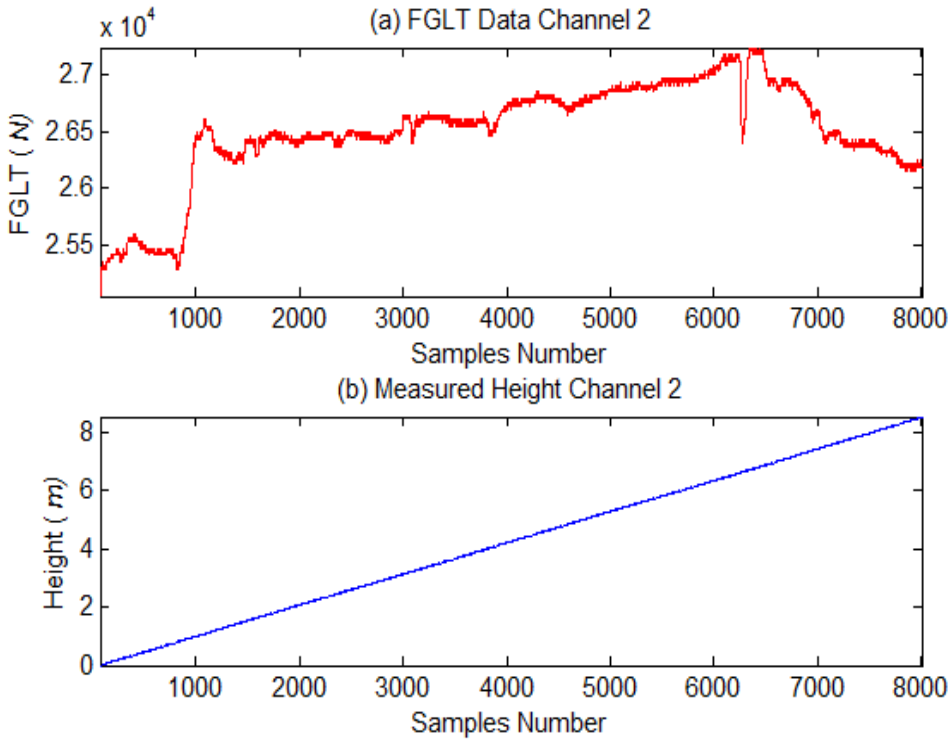

Figure 6.4: Refuelling measurements data channel 2: FGLT data (above) and height (below)

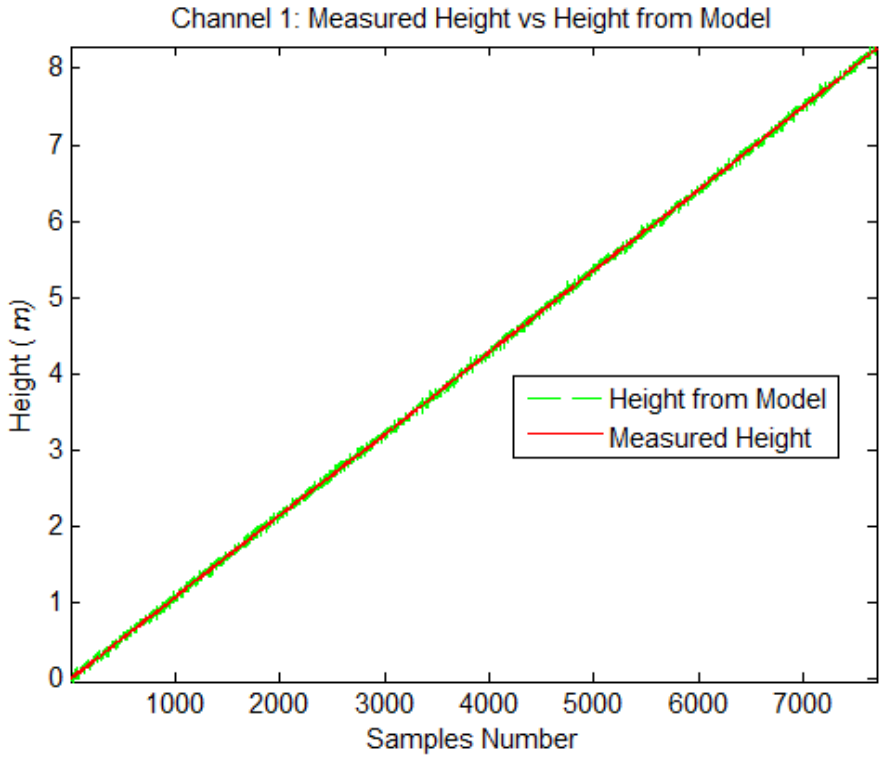

Figure 6.5: Channel 1 measured height vs height from model

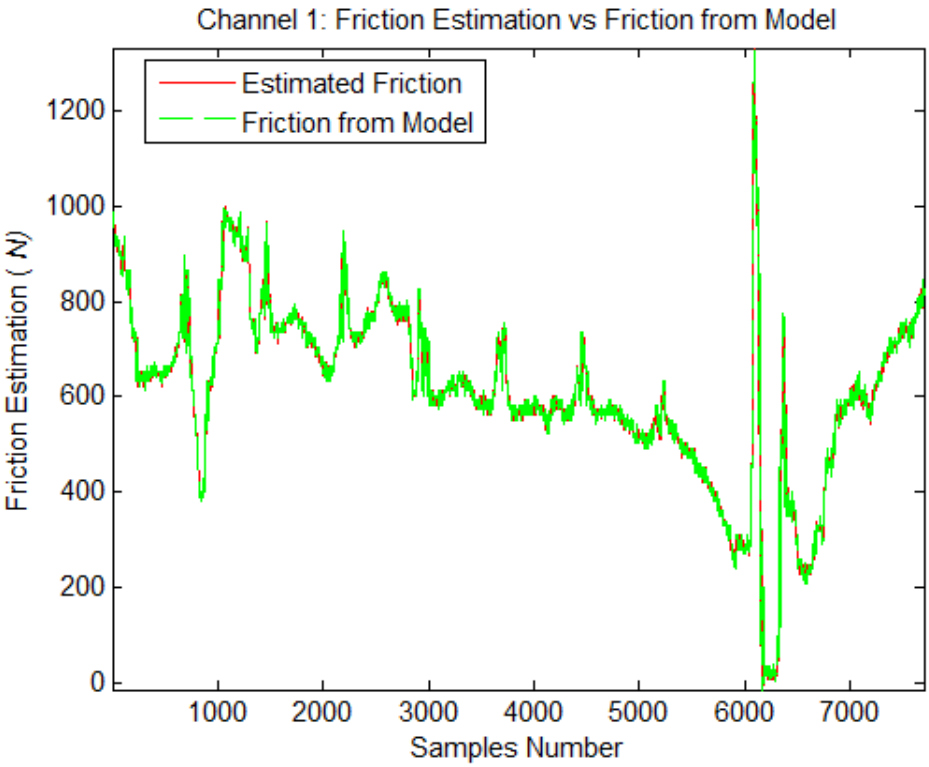

Figure 6.6: Channel 1 friction from model vs estimated friction

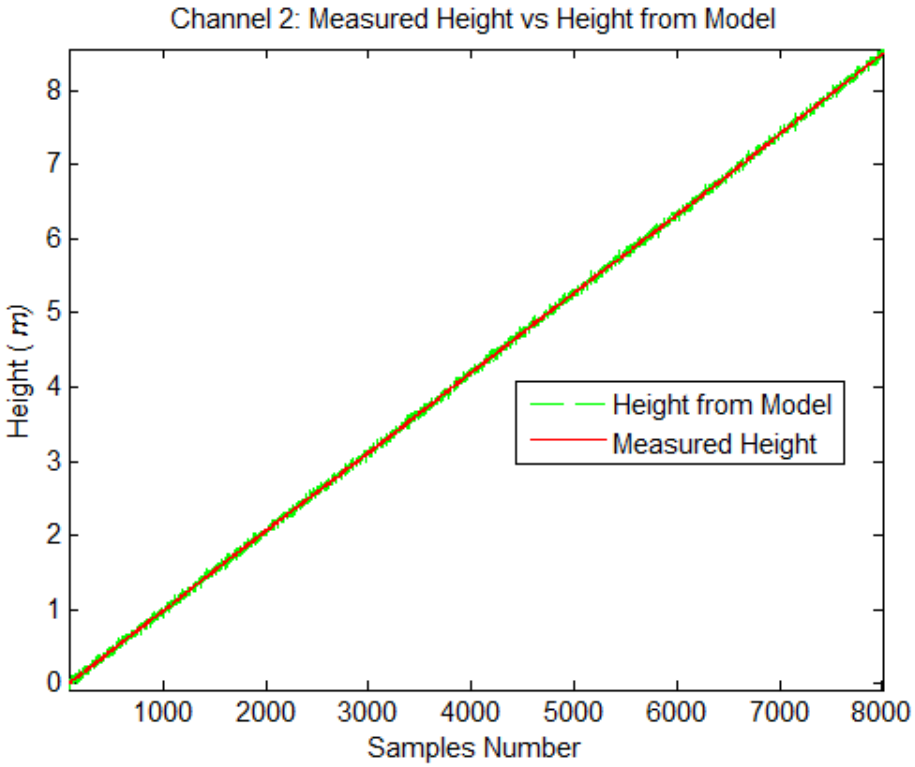

Figure 6.7: Channel 2 measured height vs height from model

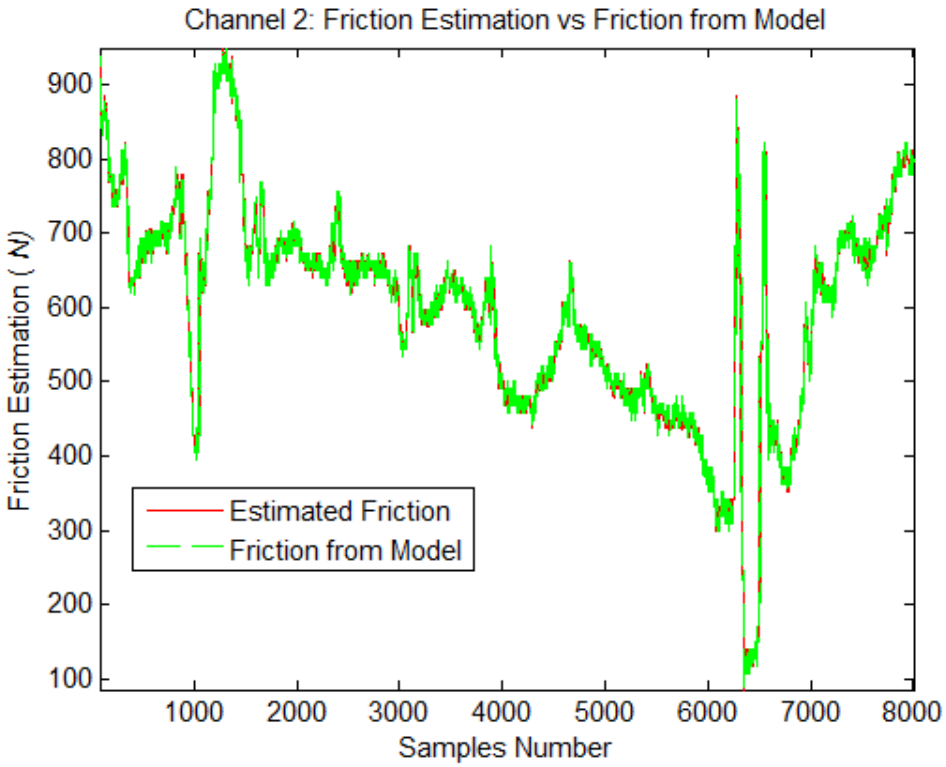

Figure 6.8: Channel 2 friction from model vs estimated friction

6.1.3 Results analysis in terms of core condition assessment

The friction force, component of the FGLT, is well estimated using the state-dependent estimator, as seen in the previous section, however it is important to investigate as the friction force can give details about the wall geometry and consequently about the core condition.

For a better understanding of the friction estimation shape, a physical explanation of the interaction of fuel assembly and the channel is provided in Figure 6.9.

First of all we can observe how the friction forces from various channels have the same shape (see Figure 6.12 and Figure 6.13) and this can help to assess the core condition. The idea, in fact, is to create an envelope of expected behaviour, i.e. an expected trace, and if there is a deviation from the benchmark created, it can be considered as an abnormal condition.

The friction force estimation is first examined to identify peaks; this would represent, for a fault free channel, the locations of the brick layers interfaces. In Figure 6.16 it can be seen that the peaks in the friction force (top) and FGLT

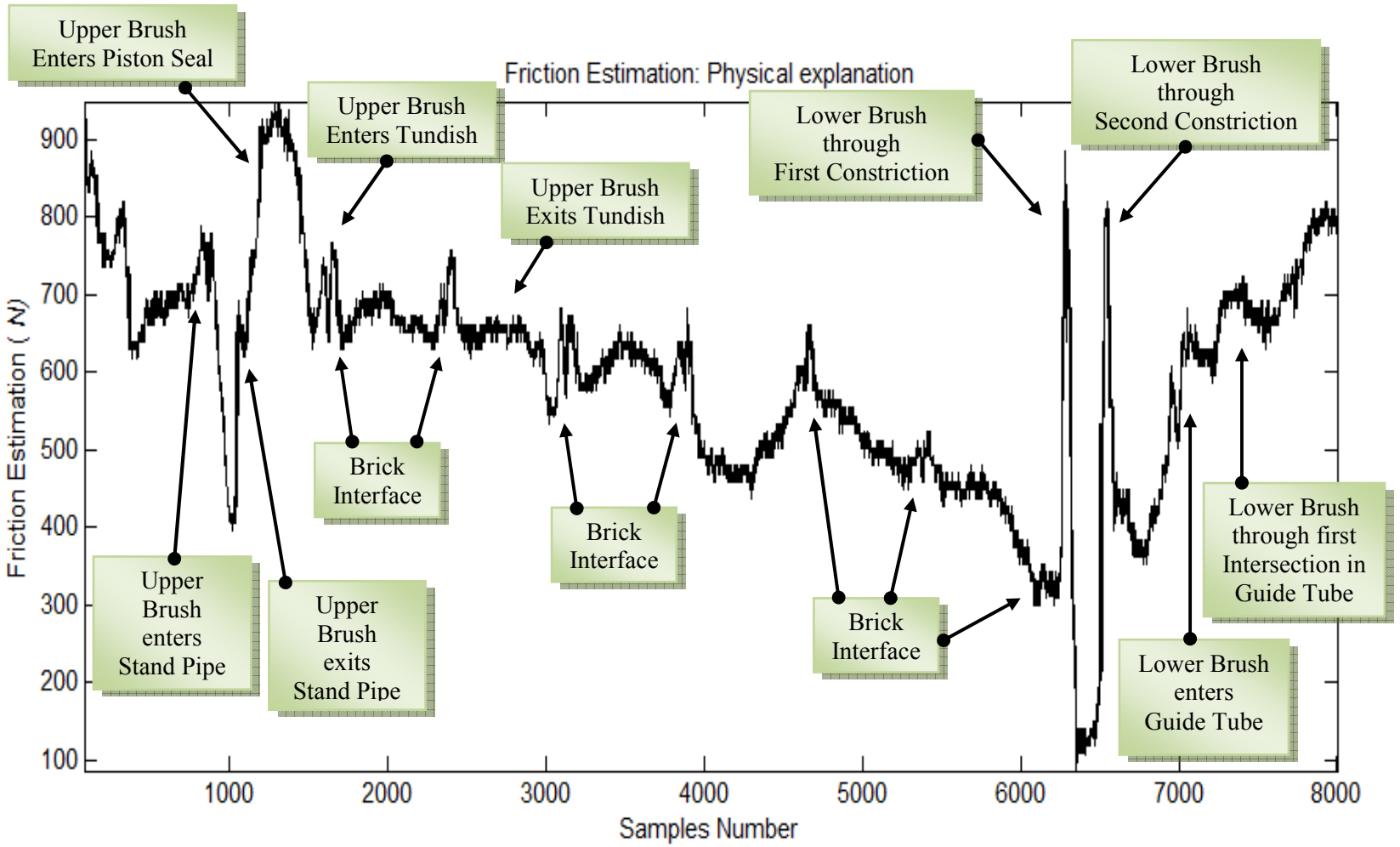

Figure 6.9: Physical explanation of friction estimation shape

(middle) correspond to the brick layer interfaces (see CBMU in the bottom). Then the peaks have to be classified either as brick-layer interfaces or as potential cracks or just noise. This operation is done comparing to the benchmark created, in other words we look for the similarity between the trace analyzed and the average trace. This crack analysis is not within the scope of this thesis and it is undertaken in BETA which uses statistical or ruled-based techniques. The integration of the work developed into the BETA framework can be seen in Figure 6.11. Figure 6.10 shows instead the overall analysis platform used by EDF Energy for the graphite core condition monitoring. The Intelligent Monitoring Assessment Panel System (IMAPS) helps to review the monitoring and inspection information ([99]).

To study the reliability of the condition monitoring of the core using the refuelling data, simulated cracks have been created by Skelton ([94]) using an experimental rig to simulate the FGLT response of different types of cracks. In Figure 6.17, a simulated crack in channel 1 is investigated by comparing the friction estimation, the original FGLT and the CBMU data for that channel. We can see how the crack is spotted by looking at the friction (top) but it is not detected by using the FGLT data (middle).

Figure 6.14 and Figure 6.15 show that the friction estimation is very sensitive to the plant uncertainties, for this reason there is the need to use a robust estimator that can cope well with unavoidable system uncertainties. The different values of the variance errors for the friction estimation of channel 1 and channel 2, for the 4 different plant uncertainties considered in Figure 6.14 and Figure 6.15, can be seen in Table 6.2.

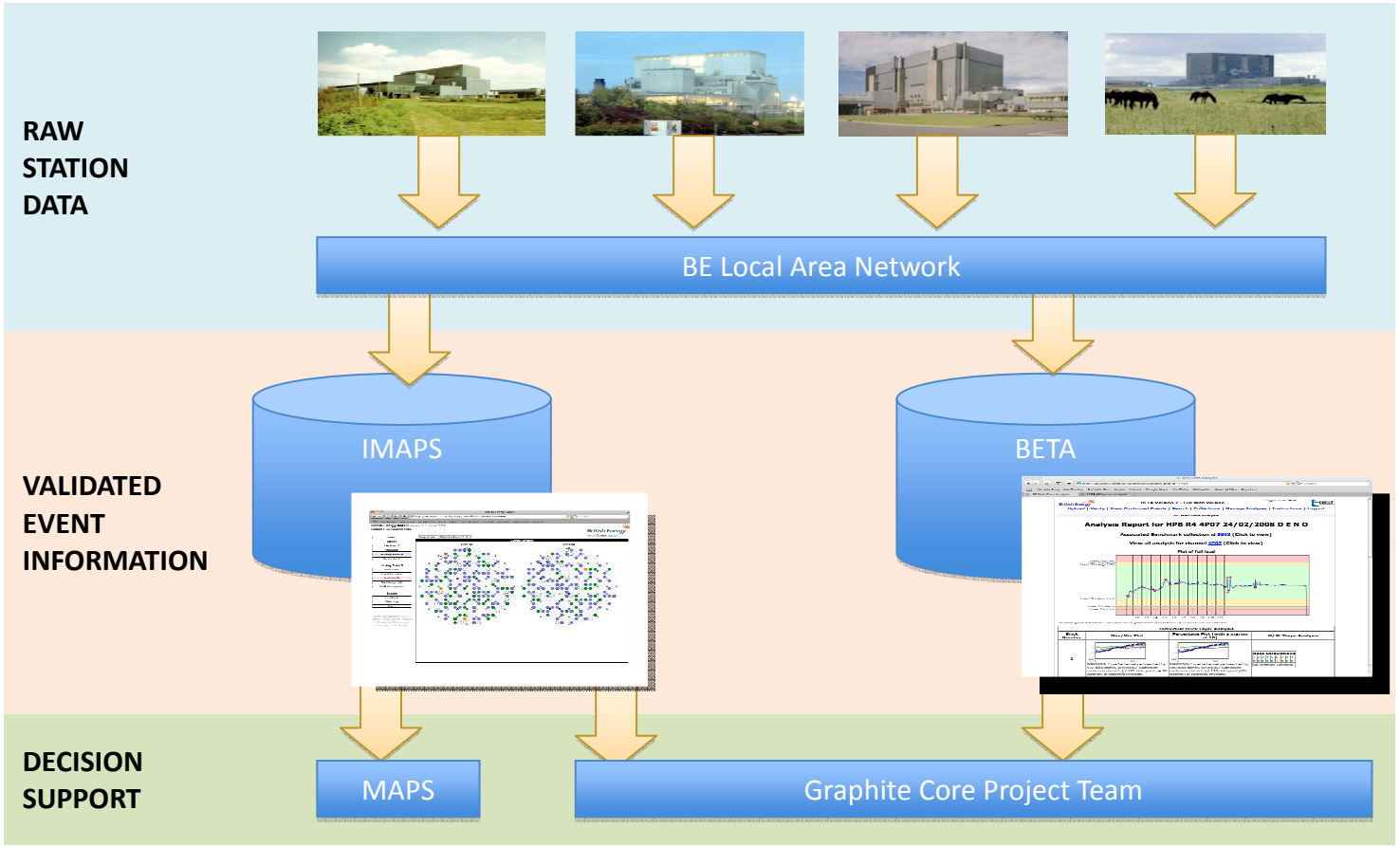

Figure 6.10: The analysis platform used by EDF Energy for core condition monitoring assessment (Source: [100])

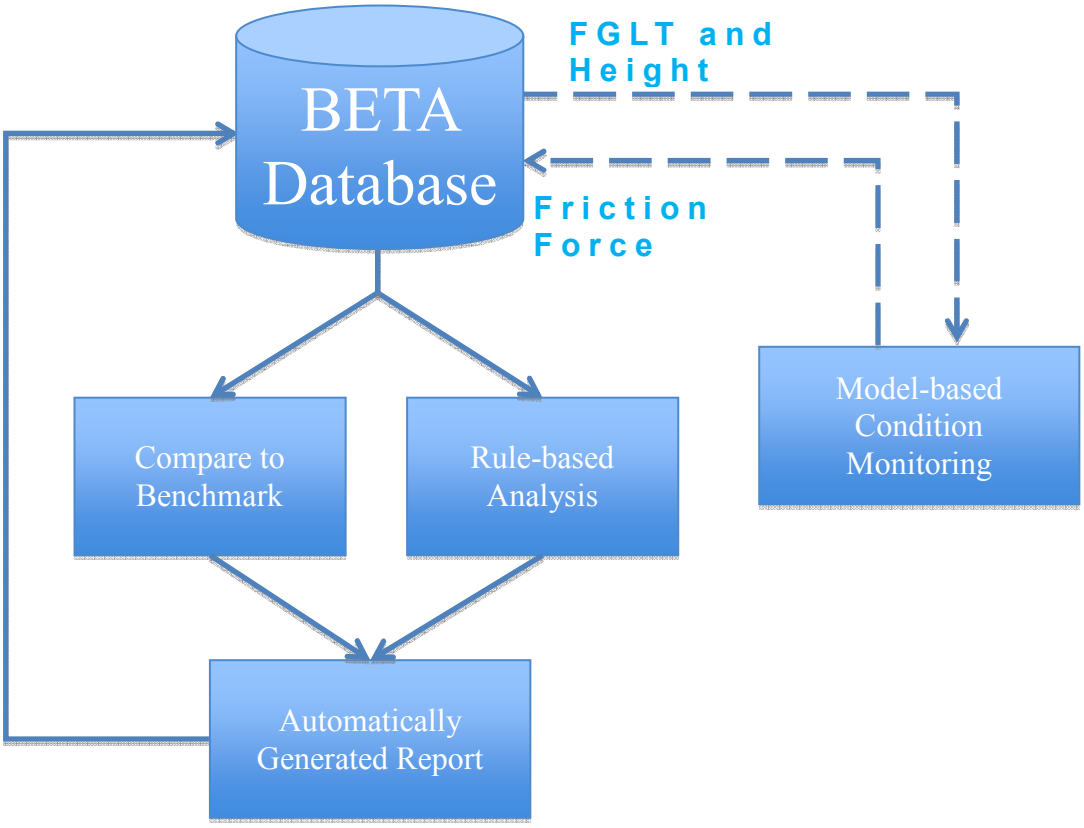

Figure 6.11: Integration of the model-based condition monitoring in BETA framework

Table 6.2: Variance of estimation error for channel 1 and channel 2 for 4 different plant uncertainties

Uncertainty	Variance of Est Error Channel 1	Variance of Est Error Channel 2
$-0.01\frac{\left(3-2.472z^{-1}\right)}{1-0.4724z^{-1}}$	7.1277e-004	2.5033e-003
$-0.1\frac{\left(3-2.472z^{-1}\right)}{1-0.4724z^{-1}}$	0.01086	0.01890
$-10\frac{\left(3-2.472z^{-1}\right)}{1-0.4724z^{-1}}$	3.4289	2.0997
$-100\frac{\left(3-2.472z^{-1}\right)}{1-0.4724z^{-1}}$	7.7151	4.7243

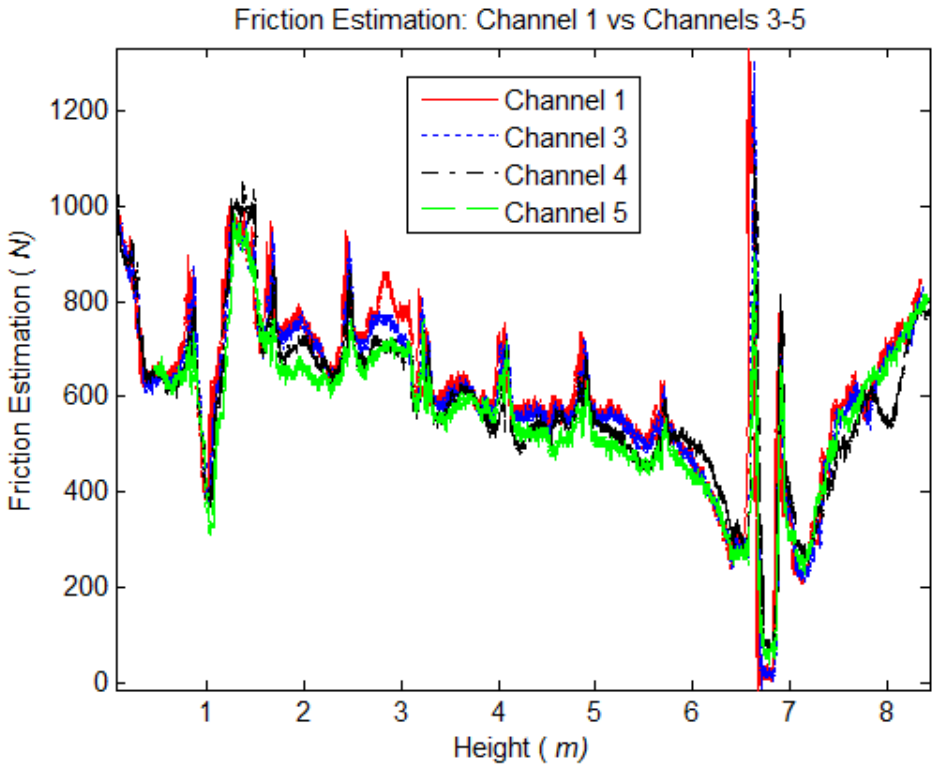

Figure 6.12: Friction estimation for channel 1 vs friction estimation of channels 3, 4 and 5

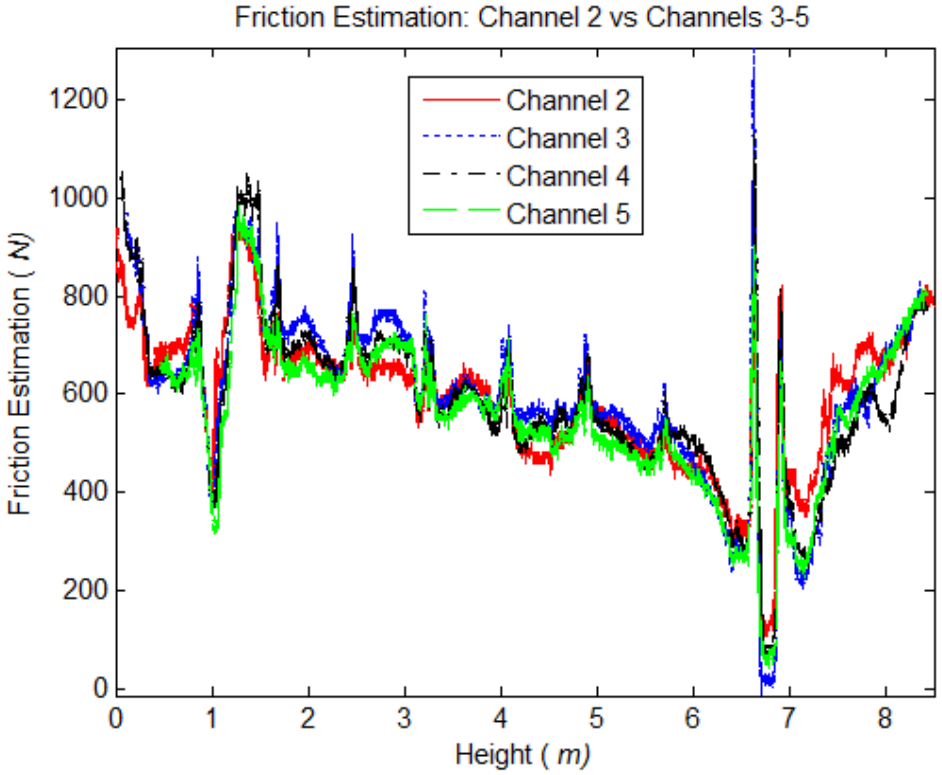

Figure 6.13: Friction estimation for channel 2 vs friction estimation of channels 3, 4 and 5

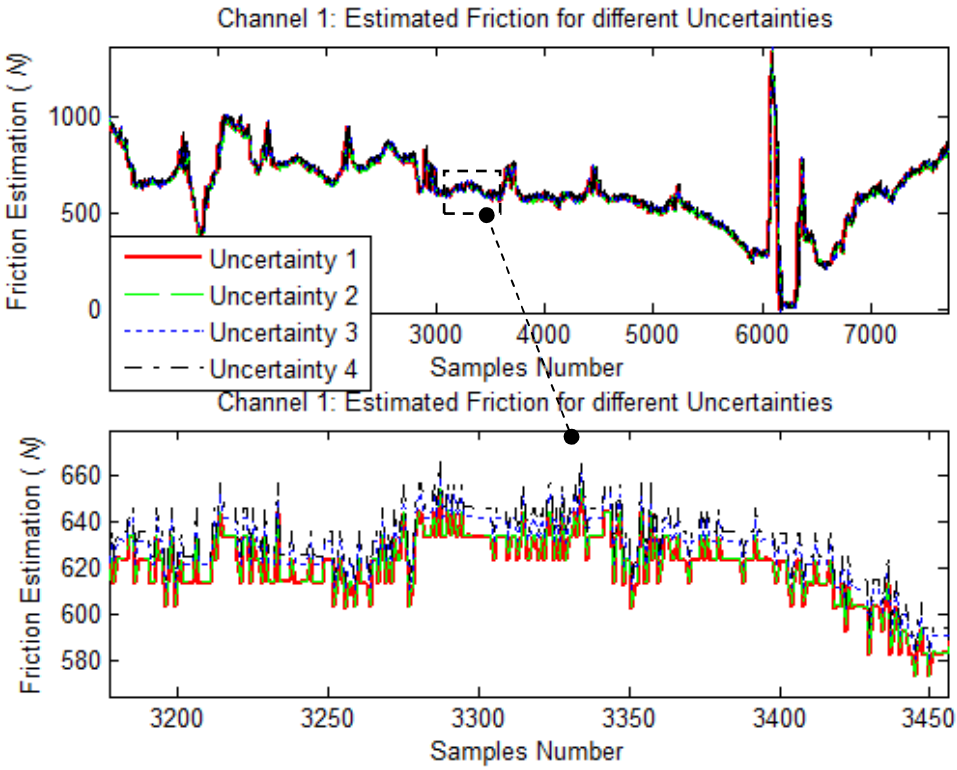

Figure 6.14: Friction estimation for channel 1 for 4 different uncertainties

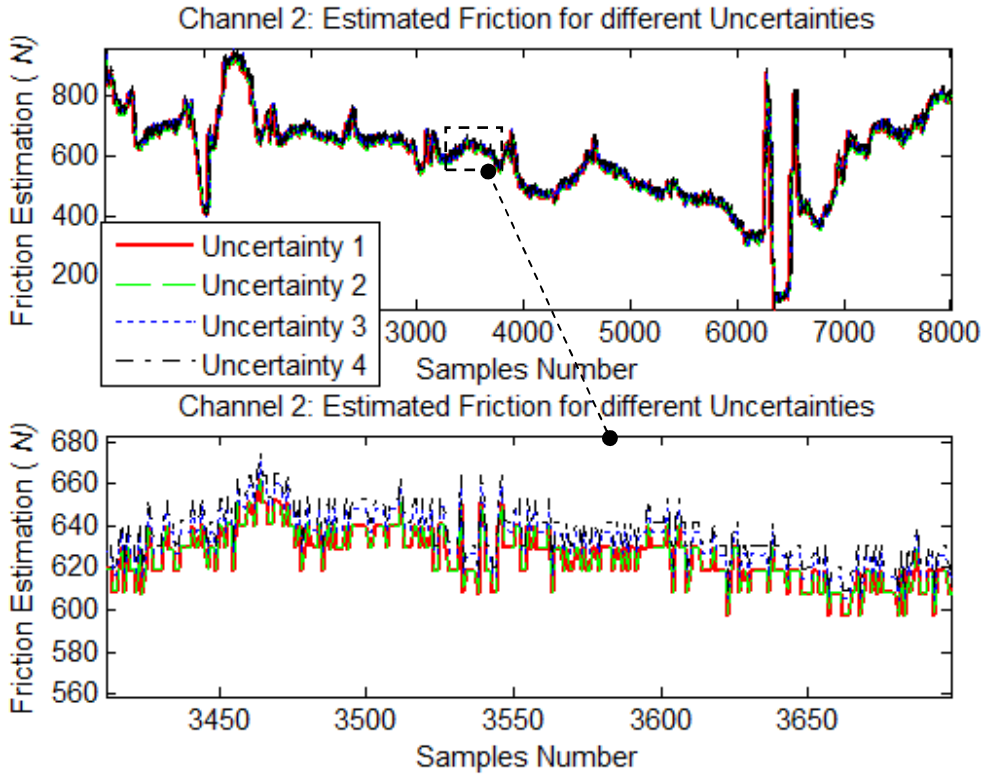

Figure 6.15: Friction estimation for channel 2 for 4 different plant uncertainties

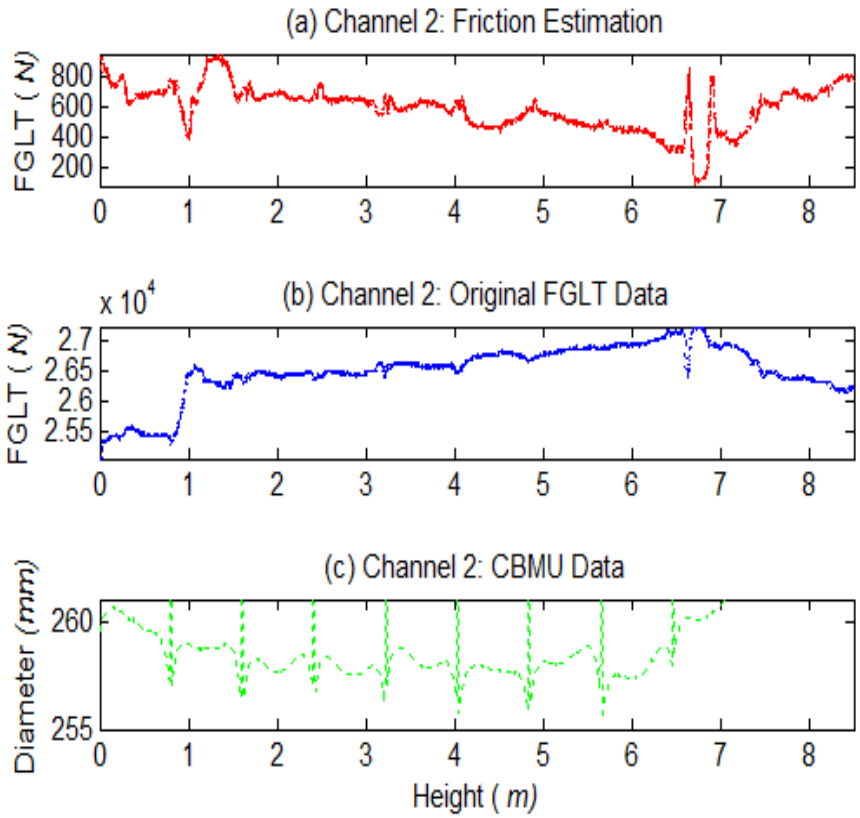

Figure 6.16: Comparison between friction estimation (top), FGLT (middle) CBMU (bottom) of channel 2

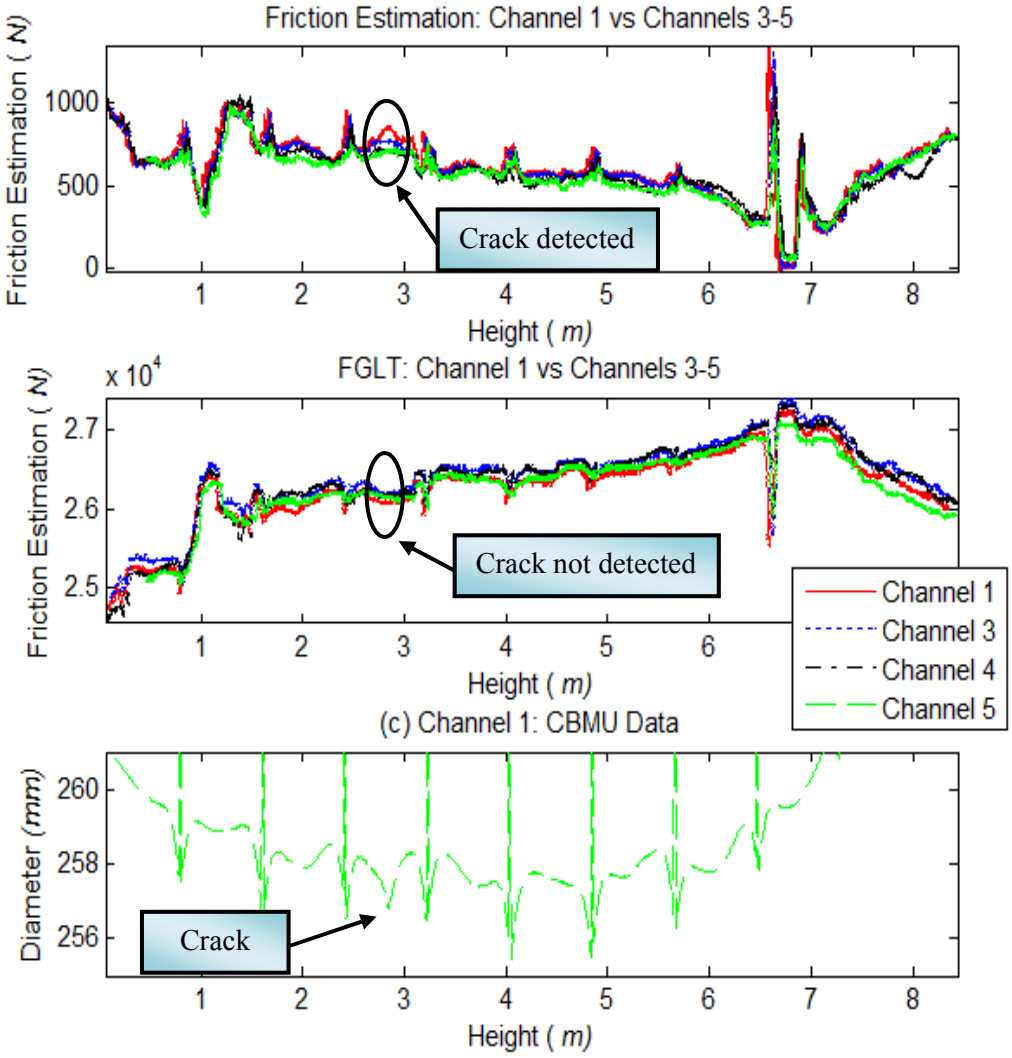

Figure 6.17: Comparison between friction estimation (top) and FGLT (middle) for channels 1, 3, 4 and 5 and the CBMU (bottom) of channel 1

6.2 Friction Estimation by using a H_∞ Robust Nonlinear Estimator

In the previous section the *state-dependent NMV* filter was applied to estimate the friction force, however the drawback is, it presents a sensitivity to model uncertainties. A case study for the fuel assembly subsystem is performed in the rest of the chapter with the objective to produce an estimation that is insensitive to model uncertainties; to this end the H_∞ robust nonlinear estimator introduced in chapter 4 is used.

In the numerical experiments the refuelling model includes, along with the aerodynamics model, the friction model as introduced in chapter 5 (see Figure 5.9). The input and output of the fuel assembly subsystem are, as for the previous section, the FGLT and height respectively (see data in Figure 6.6 and in Figure 6.8).

The friction force from the refuelling channel model goes through a "communication channel" represented by a nonlinear and a linear term, the inverse relation of the friction model F_f (see Equation (5.7)) and an integrator respectively.

The output from this block is fed to the NH_∞ filter which gives an estimation of the friction force entering the communication channel.

The overall system and resulting NH_∞ filter is as shown in Figure 6.18.

Consider, as for the state-dependent filter, that the friction force F_f is generated by white noise into a colouring filter W_s, the sample time is 0.1 seconds, W_n as the noise model (both transfer functions as defined in the previous section) and the message signal path transfer function W_c and the estimation error dynamic weighting W_q are assumed unity.

6.2.1 Friction Estimation Results

The estimated signal and the message signal from the model for channel 1 and channel 2 are shown in Figure 6.20 and Figure 6.22 respectively; the estimation error variance is $J = 1.6876\text{e-}003$ for channel 1 and $J = 2.9134\text{e-}003$ for channel 2 (Table 6.3 shows the estimation error for the 5 channels investigated). The effectiveness of these solutions is more obvious when the height from the channel and its estimation are compared in Figure 6.19 and Figure 6.21.

Table 6.4 illustrates the variance of the estimation error for the 4 dynamic uncertainty cases used in the state-dependent estimator to compare the friction results for the two estimators in term of uncertainty sensitivity. This shows that the variance for the robust estimator would not change significantly for different channel uncertainties and this just confirms that the NH_∞ filter is particularly appropriate for nonlinear uncertain systems. Figure 6.23 and Figure 6.24 show the friction estimation for channel 1 and channel 2 respectively for the 4 different uncertainties.

In Figure 6.25 and Figure 6.26 the friction estimation of channel 1 and channel 2 are compared with the other 3 channels (see Appendix E for simulation plots related to these 3 channels) for validation purpose and it is shown as for the state-dependent case that the friction traces have the same shape. Moreover the friction force from channel 1 and channel 2 are compared to the FGLT data and CBMU (see Figure 6.27 and Figure 6.28) to examine if the estimation gives information about brick-layer interfaces and possible cracks.

The results of applying the robust estimator are almost identical to the ones obtained from the state-dependent filter with the advantage that the estimation is pretty insensitive to model system uncertainties.

Software implementation details can be found in Appendix F.

Table 6.3: Variance of estimation error for the 5 channels case studies

Channel	Variance of Estimation Error
1	1.6876e -003
2	2.9134e-003
3	3.5718e-003
4	1.0405e-003
5	4.4617 e-003

Table 6.4: Variance of estimation error for channel 1 and channel 2 for 4 different plant uncertainties

Uncertainty	Variance of Est Error Channel 1	Variance of Est Error Channel 2
$-0.01\frac{\left(1-0.4724z^{-1}\right)}{3-2.472z^{-1}}$	1.6876e -003	2.9134e-003
$-0.1\frac{\left(1-0.4724z^{-1}\right)}{3-2.472z^{-1}}$	1.6876e -003	2.9134e-003
$-10\frac{\left(1-0.4724z^{-1}\right)}{3-2.472z^{-1}}$	1.6876e -003	2.9136e-003
$-100\frac{\left(1-0.4724z^{-1}\right)}{3-2.472z^{-1}}$	1.7921e -003	3.0156e-003

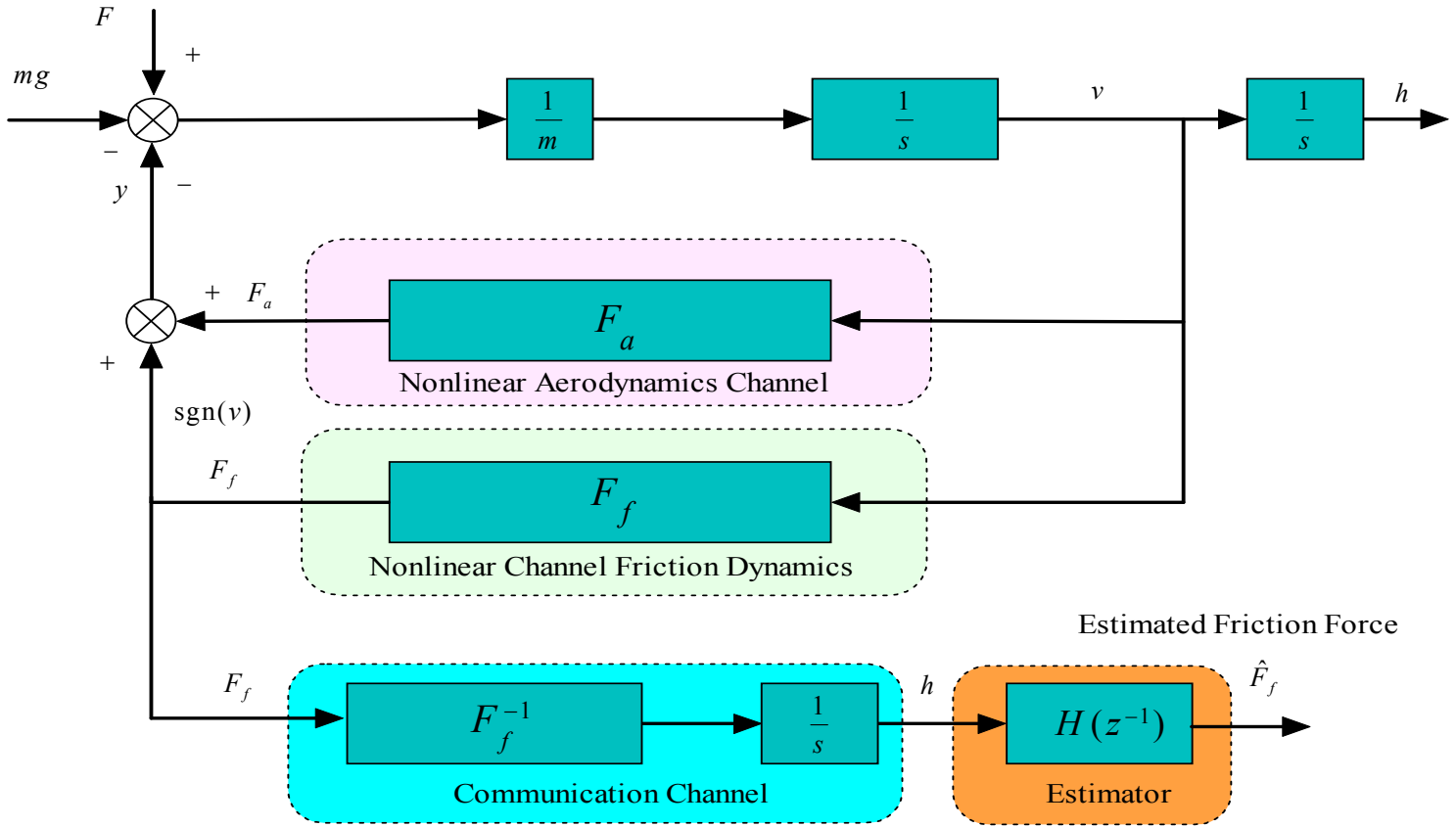

Figure 6.18: Model and NHinf estimator framework

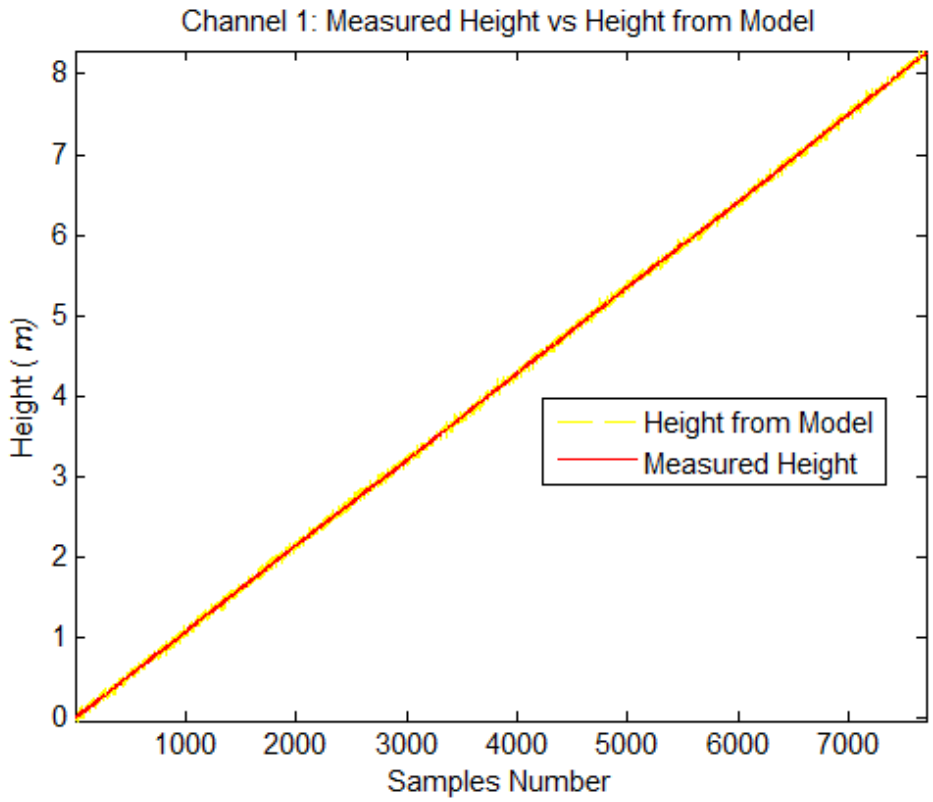

Figure 6.19: Channel 1 measured height vs height from model

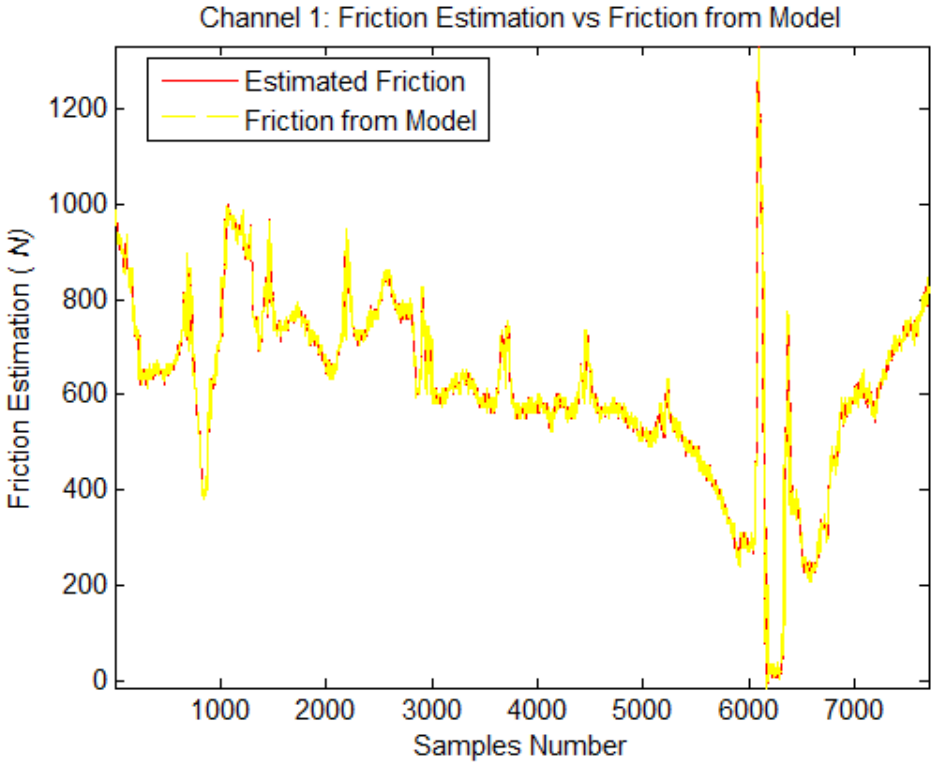

Figure 6.20: Channel 1 friction from model vs estimated friction

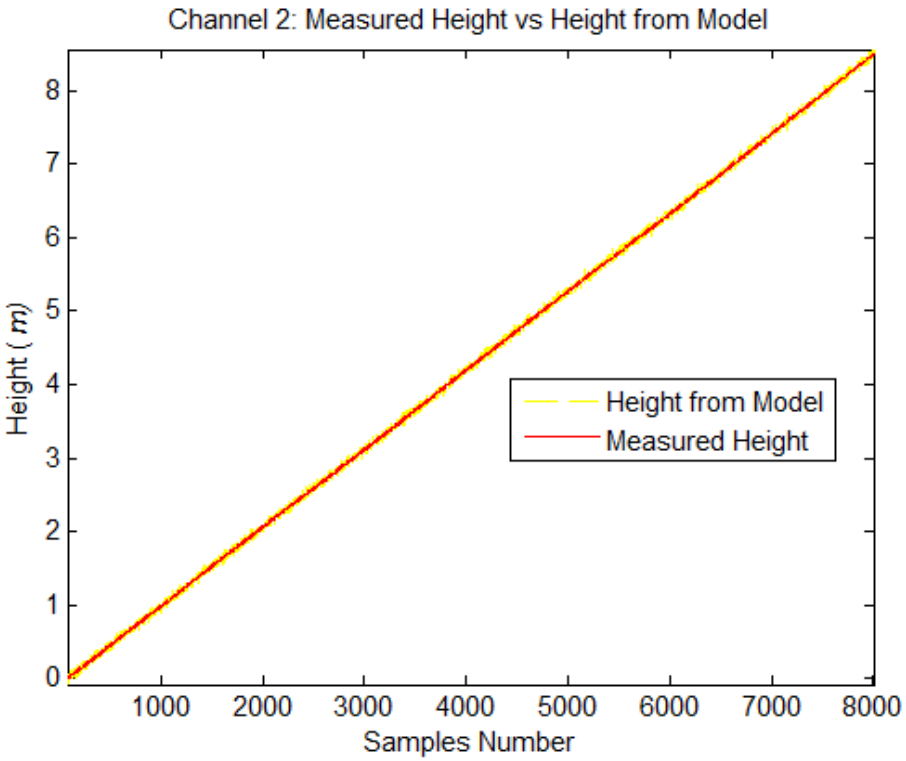

Figure 6.21: Channel 2 measured height vs height from model

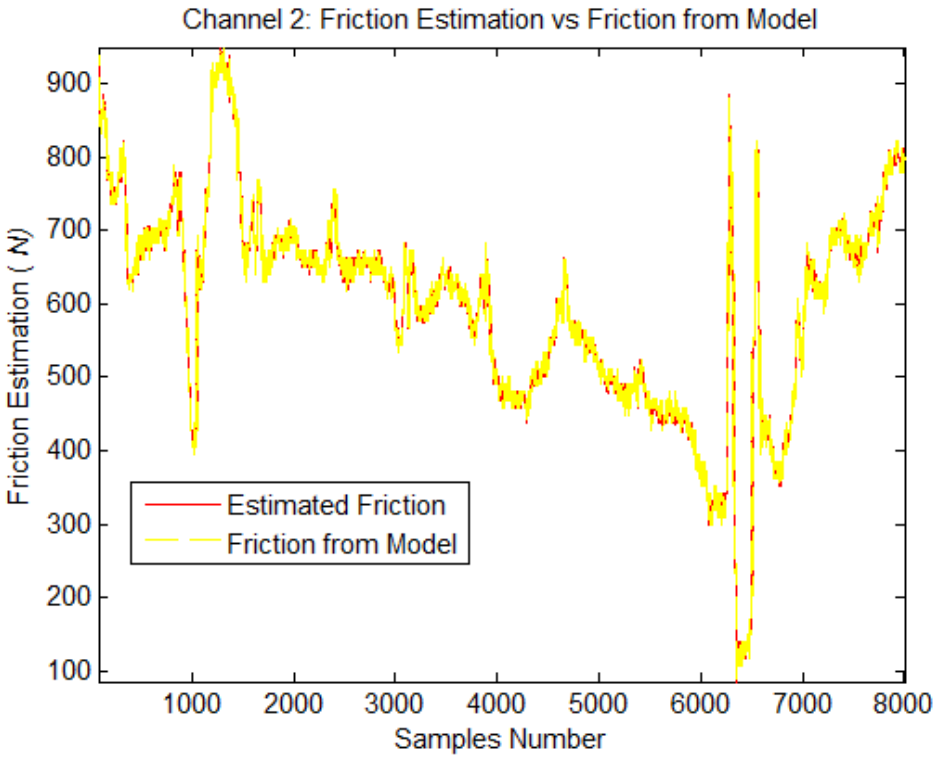

Figure 6.22: Channel 2 friction from model vs estimated friction

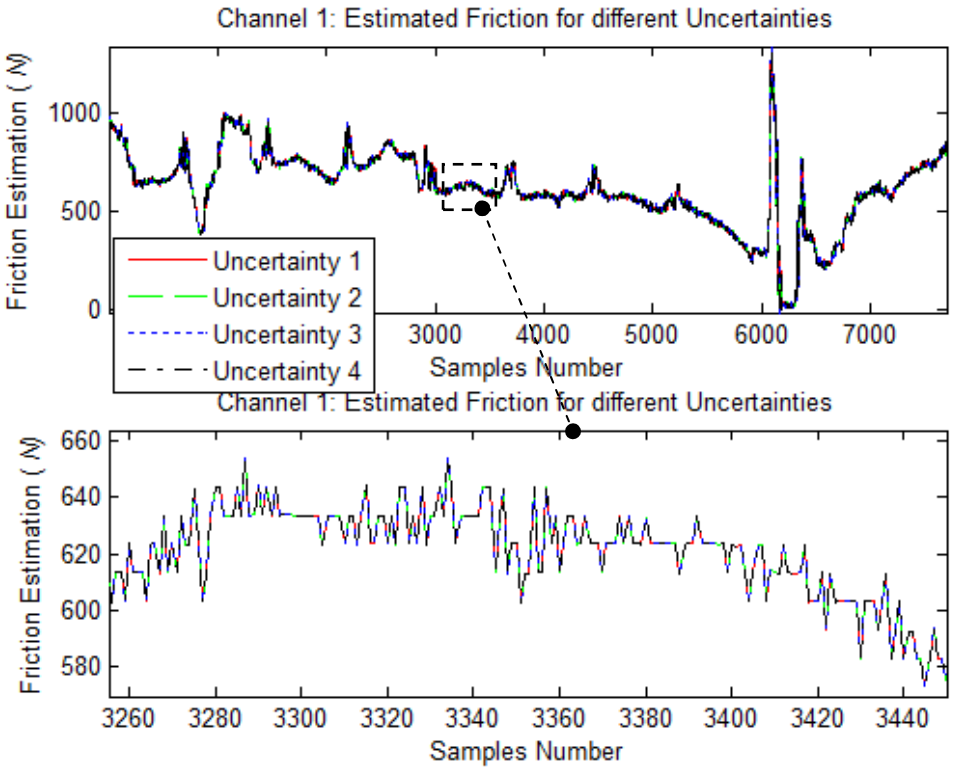

Figure 6.23: Friction estimation for channel 1 for 4 different uncertainties

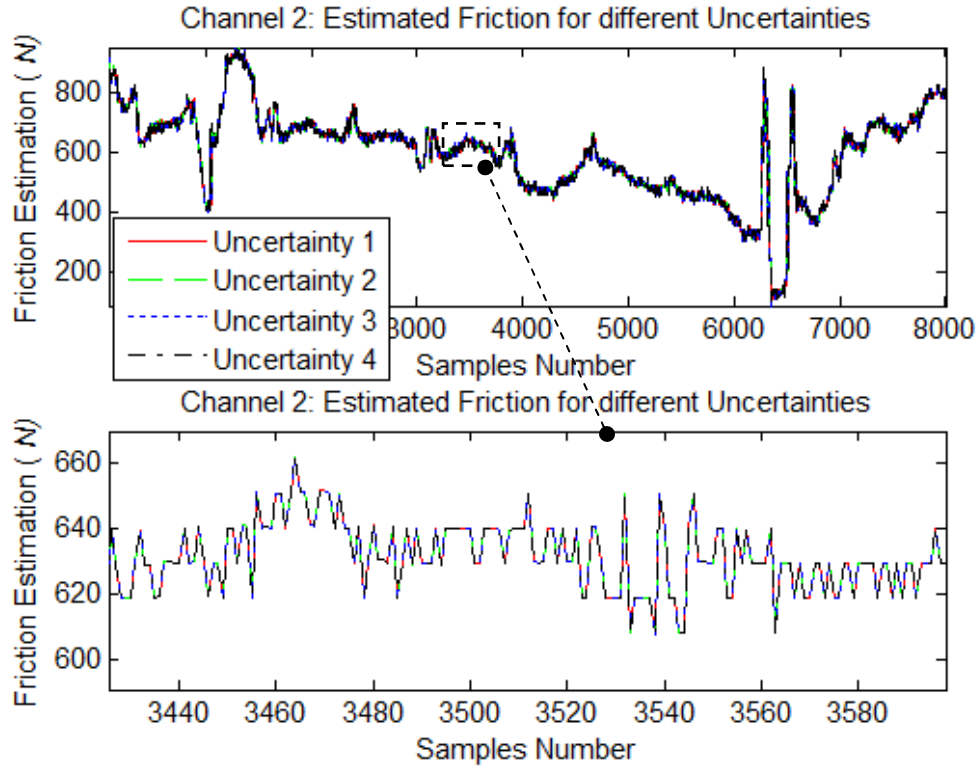

Figure 6.24: Friction estimation for channel 2 for 4 different uncertainties

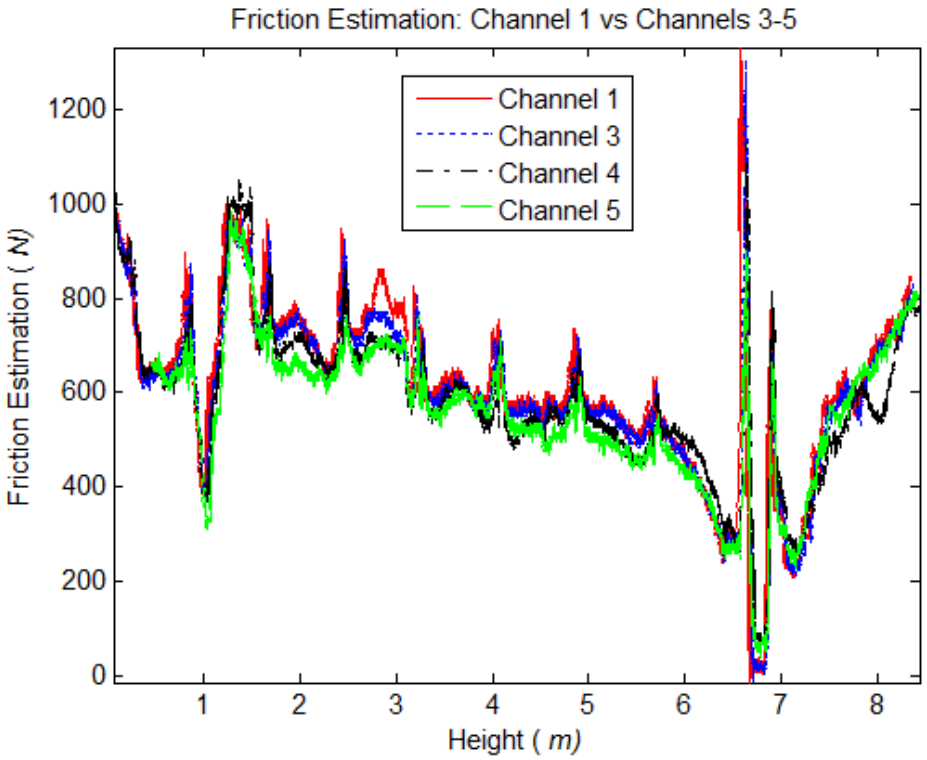

Figure 6.25: Friction estimation for channel 1 vs friction estimation of channels 3, 4 and 5

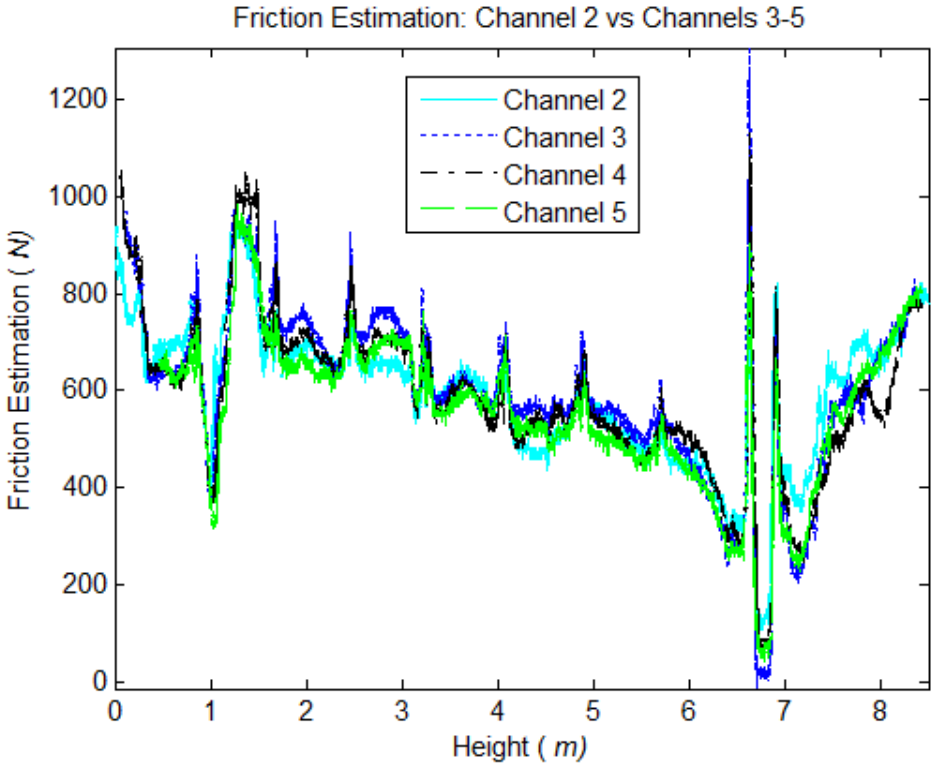

Figure 6.26: Friction estimation for channel 2 vs friction estimation of channels 3, 4 and 5

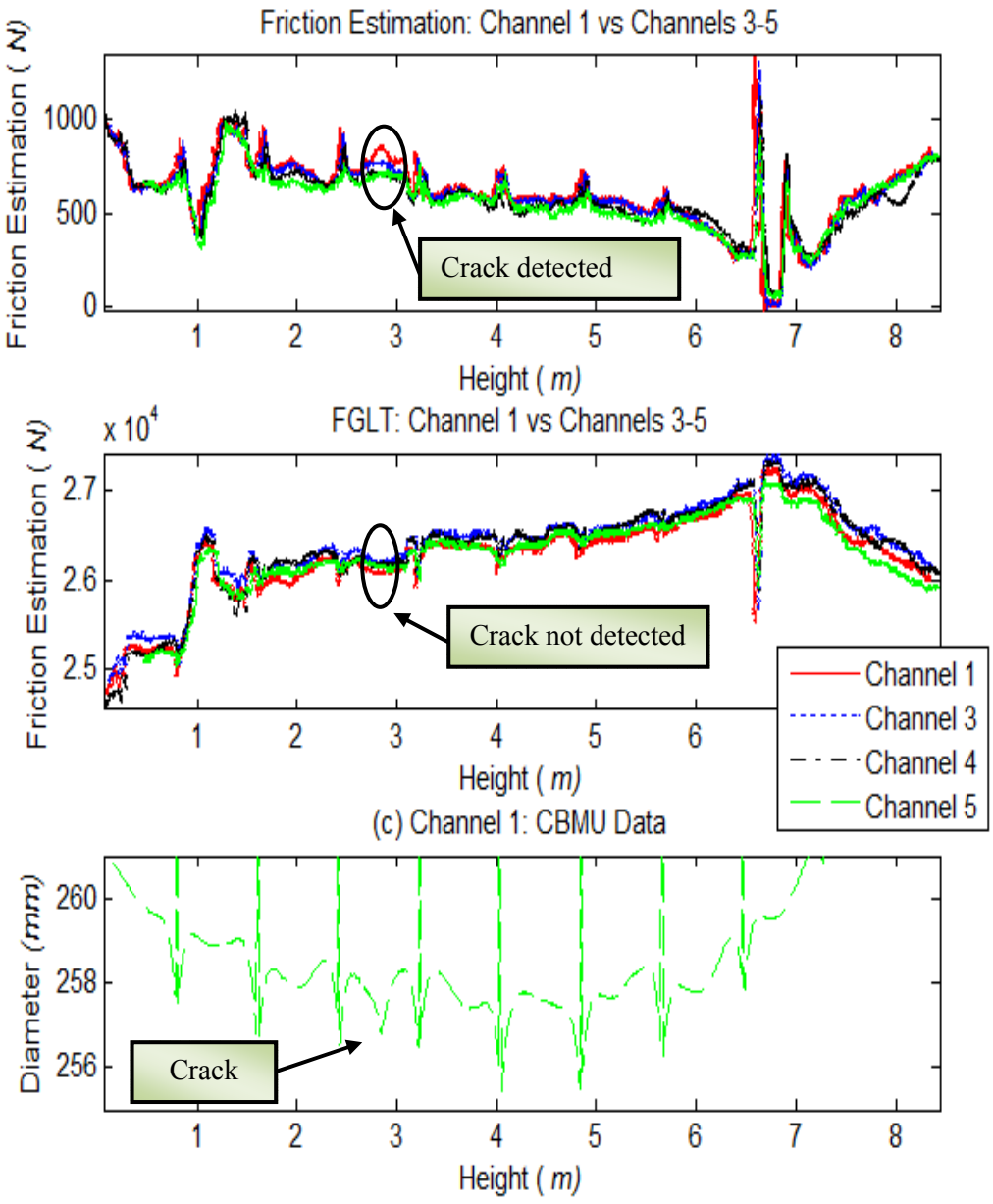

Figure 6.27: Comparison between friction estimation (top) and FGLT (middle) for channels 1, 3, 4 and 5 and the CBMU (bottom) of channel 1

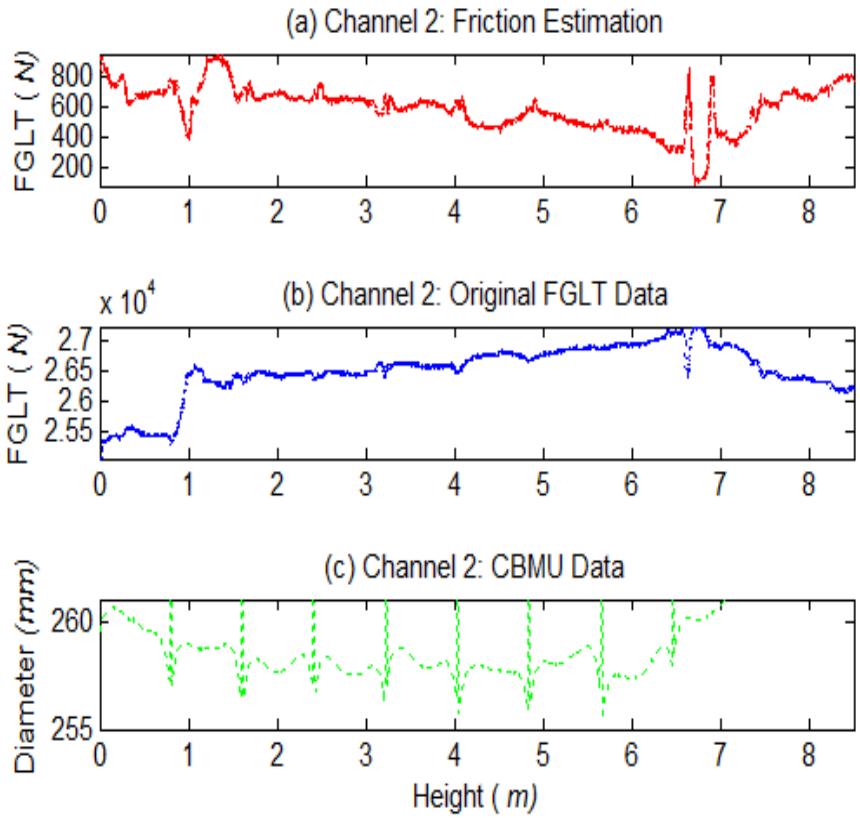

Figure 6.28: Comparison between friction estimation (top), FGLT (middle) CBMU (bottom) of channel 2

6.3 Conclusions

This chapter first presents a new model-based technique for condition monitoring of a nuclear reactor core using a state-dependent filter to estimate the friction component of the fuel grab load trace data resulting from the interaction of the fuel assembly and the core channel. In fact, a key role for brick cracking detection is the analysis of the friction force that provides information of the condition of the reactor core.

The proposed nonlinear filter is easy to understand and to implement and it gives a good friction estimation but it presents a snag, its results are very sensitive to the model uncertainties. This is the reason why a second model-based technique for condition monitoring of a nuclear reactor core is presented. In this approach a H_∞ robust nonlinear filter is used to estimate the friction force.

The results show that the NH_∞ filtering technique is clearly suitable for nonlinear uncertain systems, in fact the results vary only slightly with different uncertainties. The main strength of the robust filter approach is that it is able to predict consistently the friction force from a model which for its complicated physics would unavoidably present uncertainties.

It is also shown how the friction forces can be used to create an envelope of expected behaviour to be used in future comparison to assess the core condition.

Chapter 7

Conclusions and Future Work

7.1 Summary and Conclusions

This thesis has tried to contribute to the theoretical development of nonlinear and *LPV* systems estimation and also to the nuclear plant condition monitoring problem. Both the theoretical developments and the applications are important. Many processes are in fact nonlinear and the type of *LPV* model utilized can provide a much better approximation than switched linear models. The method utilized for dealing with systems represented in *LPV* form is quite generic and the estimate developed is easy to implement.

There is also a useful contribution for robust estimation. Uncertainties are an important feature in real systems and the chapter on robust estimation methods provides a reasonably practical estimation technique. The philosophy adopted is fairly similar for both problems and the benefit in applications is that the theoretical basis required only involves relatively straightforward concepts. These theoretical tools have been shown to be a value in the nuclear reactor condition monitoring problem. In this study the models and the understanding of the physical problem were also important. The feedback from EDF Energy helped to develop the theoretical aspects referred to.

In recent years a lot of research efforts have been made towards extending the lifetime of AGR nuclear power stations in the UK. There is an increasing need to closely monitor the condition of the graphite core within the reactor to ensure its continued safe operation. It has been thought that the FGLT measurements gathered during the nuclear refuelling process can be utilised as a main information source to infer the core condition.

To use the FGLT data for core condition monitoring, the essential and key challenge is how to reliably and accurately separate friction forces from the masked FGLT measurements; in fact the apparent load recorded during the refuelling process

is the combination of different effects. All the forces involved in the process were considered to develop a nonlinear first principles model which include a aerodynamics and LuGre friction models, then a nonlinear identification method was needed to identify its parameters. The identification process, consisting of the unknown model parameters estimation, leads to a nonlinear optimization problem which was solved using the trust-region method. This identification introduces some grade of uncertainty in the model; for this reason initially a more simplified model, where the friction force is not modelled, was considered in order to have less parameters to be identified. This simplified model can be written in state-dependent form, bringing us to the estimation of the friction force for a state-dependent model. To this end an estimator was designed and implemented for *LPV* systems, which in its general form can be used for state-dependent models. The validation of the nonlinear estimator theory was done by using a numerical example and a pursuit-evader problem case study. The friction force was estimated for a few channels to be able to validate one against the others. In other words it was investigated that if the estimation presents the same shape along different channels same wall conditions could be guaranteed. In fact a deformation or crack in the core geometry would be reflected as a peak or as a fall in the friction force.

Inspection data and a simulated crack were also used to validate the data and compare this method to detect cracks with the one that uses the original FGLT data.

Instead of a state-dependent estimator, an *LPV* estimator was designed to deal with future development of the condition monitoring analysis framework.

The proposed nonlinear filter gives a good friction estimation but it presented a drawback its results are very sensitive to the model uncertainties. This is the reason why first a H_∞ robust theory was introduced and implemented where its validation was done for a case study that involves the exhaust gas oxygen sensor or lambda sensor. Then a second model-based technique for condition monitoring of a nuclear reactor core was investigated applying the H_∞ robust nonlinear filter to estimate the friction force. The results show that the H_∞ filtering technique was suitable for nonlinear uncertain systems; in fact the results vary only slightly with different uncertainties.

The estimators presented in this thesis are based on a nonlinear minimum variance estimation problem ([41, 74, 79]). The new *LPV* estimator introduced here adds considerably to the generality of the results, in fact previously only the unstructured channel sub-system $\mathcal{W}_{c1}$ (see Figure 3.1) was assumed to be nonlinear. The potential can be exploited in applications that currently use or are exploring *LPV* models such as in the wind turbine, flight control and the automotive engine control industries.

The potential of this estimator in fault detection applications still has to be explored and there is also a role for the estimator in feedback control systems.

The robust filtering problem is given in the form of a robust Wiener optimal estimator and a H_∞ nonlinear estimator. In the first estimator the uncertainty in signal, noise and plant are represented by a probabilistic system description and the variances are assumed to be given. In the limiting case when the dynamics are linear, the estimator has the form of a Wiener filter in polynomial system description form.

The H_∞ filtering problem is related to the *NMV* through an embedding procedure, where an auxiliary minimum variance filtering problem is solved for a cost function with dynamic weighting and a linking lemma is introduced to relate the two problems. The H_∞ norm minimization exploited in this approach provides different opportunities for tailoring the response of the estimator to uncertainties that can only be frequency response bounded. It may therefore have potential in applications.

7.2 Future Work

To completely rely on the condition monitoring analysis developed in this thesis further study would need to be done.

The fuel assembly is equipped with a pair of stabilizing brushes, however they were considered as one. The friction force is the sum of the effects of both brushes and the brushes acting in different channel areas behave in a different way along the refuelling process. This consideration would require a model modification and the two friction forces to be estimated.

In our model the bristle deflection was considered as constant along the channel however it is thought that as the heat changes in the channel the deflection would change accordingly. In this case an *LPV* model may be used to model the situation where the state matrices vary according to a parameter (i.e. the heat).

The estimators implemented, due their simplicity, could be used in real time applications. This would represent an additional method for EDF Energy to check the core condition. In fact they could check the friction estimation shape against the normal behaviour envelope during the discharge phase so in the case of a possible crack they would not have any stoppage during the charging phase and avoid any additional dynamics in the operation that may introduce noises.

Bibliography

[1] G. B. Neighbour, *Management of ageing in graphite reactor cores*: Royal Society of Chemistry, 2007.

[2] N. McLachlan, J. Reed, and M. Metcalfe, "AGR core safety assessment methodologies," in *Proceedings of the Specialists Meeting on Graphite Moderator Lifecycle Behaviour, IAEA-TECDOC–901*, Bath, UK, 1995 September 24-27, pp. 125–136.

[3] R. Curtis, S. Jones, J. Reed, and A. Wickham, "The Development of Direct Core Monitoring in Nuclear Electric plc, Graphite Moderator Lifecycle Behaviour," IAEA-TECDOC-901, Bath, UK, 1996.

[4] S. He and J. Gotts, "A computational study of the effect of distortions of the moderator cooling channel of the Advanced Gas-cooled Reactor," *Nuclear engineering and design,* vol. 235, pp. 965-982, 2005.

[5] Z. Zou, S. Fok, S. Oyadiji, and B. Marsden, "Failure predictions for nuclear graphite using a continuum damage mechanics model," *Journal of nuclear materials,* vol. 324, pp. 116-124, 2004.

[6] C. Wallace, G. West, G. Jahn, S. McArthur, D. Towle, and G. Buckley, "Control rod monitoring of advanced gas-cooled reactors," 2010.

[7] J. Steele, L. Martin, S. D. J. McArthur, A. Moyes, J. McDonald, D. Howie, R. Elrick, and I. Yule, "An intelligent system for interpreting the nuclear refuelling process within an advanced gas-cooled reactor," *Proceedings of the Institution of Mechanical Engineers, Part A: Journal of Power and Energy,* vol. 217, pp. 159-167, 2003.

[8] G. West, G. Jahn, S. McArthur, and J. Reed, "Graphite core condition monitoring through intelligent analysis of fuel grab load trace data," in *Management of Ageing Processes in Graphite Reactor Cores*, London, U.K, 2007.

[9] G. West, S. McArthur, and D. Towle, "BETA: a system for automated intelligent analysis of fuel grab load trace data for graphite core condition monitoring," presented at the Securing the Safe Performance of Graphite Reactor Cores. Royal Society of Chemistry, Cambridge, pp. 79-87, 2009.

[10] G. West, S. McArthur, J. McDonald, and D. Towle, "An automated intelligent analysis system for analysing reactor refuelling events," in *International Conference on Control and Instrumentation in Nuclear Installations, Manchester*, 2007.

[11] G. West, C. Wallace, S. McArthur, J. McDonald, and D. Towle, "Automated analysis of AGR reactor core condition monitoring data," in *Sixth American Nuclear Society International Topical Meeting on Nuclear Plant Instrumentation, Control, and Human-Machine Interface Technologies NPIC&HMIT* Knoxville, Tennessee, US, 2009.

[12] G. M. West, G. J. Jahn, S. McArthur, J. R. McDonald, and J. Reed, "Data mining reactor fuel grab load trace data to support nuclear core condition monitoring," *Nuclear Science, IEEE Transactions on,* vol. 53, pp. 1494-1503, 2006.

[13] G. West, C. Wallace, G. Jahn, S. McArthur, and D. Towle, "Predicting the ageing of advanced gas-cooled reactor (AGR) graphite bricks," in *Seventh American Nuclear Society International Topical Meeting on Nuclear Plant Instrumentation, Control and Human-Machine Interface Technologies NPIC&HMIT* Las Vegas, Nevada, US, 2010.

[14] C. Wallace, G. West, S. McArthur, D. Towle, and J. Reed, "The effect of reactor parameters on AGR refuelling at Hinkley Point B," presented at the Securing the safe performance of graphite reactor cores. Royal Society of Chemistry, Cambridge, UK, pp. 210-220, 2009.

[15] B. Stephen, G. M. West, S. Galloway, S. D. J. McArthur, J. R. McDonald, and D. Towle, "The Use of Hidden Markov Models for Anomaly Detection in Nuclear Core Condition Monitoring," *Nuclear Science, IEEE Transactions on,* vol. 56, pp. 453-461, 2009.

[16] Y. Pang, M. Grimble, A. Ordys, and J. Reed, "Condition monitoring of the nuclear graphite core using benchmarking techniques," in *Proceedings of the European Control Conference*, Kos, Greece, July 2-5 2007.

[17] C. Bonivento, M. J. Grimble, L. Giovanini, M. Monari, and A. Paoli, "Monitoring a gas-cooled nuclear reactor core integrity," in *17th IFAC World Congress*, South Korea, 2008.

[18] C. Bonivento, M. J. Grimble, L. Giovanini, M. Monari, and A. Paoli, "State and parameter estimation approach to monitoring AGR nuclear core," *G. Marchesini, Ricordo di Antonio Lepschy, Istituto Veneto di Scienze, Lettere ed Arti, Adunanza Accademica del 26 Novembre 2005, Venezia,* pp. 31-56, 2006.

[19] Y. Pang, L. Giovanini, M. Monari, and M. Grimble, "Condition monitoring of an advanced gas-cooled nuclear reactor core," *Proceedings of the Institution of Mechanical Engineers, Part I: Journal of Systems and Control Engineering,* vol. 221, p. 833, 2007.

[20] N. Wiener, "Extrapolation, interpolation, and smoothing of stationary time series: with engineering applications," *Journal of the American Statistical Association,* vol. 47, 1949.

[21] R. E. Kalman, "A new approach to linear filtering and prediction problems," *Journal of basic Engineering,* vol. 82, pp. 35-45, 1960.

[22] R. E. Kalman, "New Methods in Wiener Filtering Theory," in *Proc. of the Symposium on Engineering Applications of Random Function Theory and Probability*, 1963, pp. pp. 270-388.

[23] D. Simon, *Optimal state estimation: Kalman, H [infinity] and nonlinear approaches*: John Wiley and Sons, 2006.

[24] S. J. Julier, J. K. Uhlmann, and H. F. Durrant-Whyte, "A new approach for filtering nonlinear systems," 1995, pp. 1628-1632 vol. 3.

[25] S. J. Julier and J. K. Uhlmann, "A new extension of the Kalman filter to nonlinear systems," in *The Proceedings of AeroSense: The 11th International Symposium on Aerospace/Defense Sensing, Simulation and Controls*, Orlando, FL, USA, 1997.

[26] K. Ito and K. Xiong, "Gaussian filters for nonlinear filtering problems," *Automatic Control, IEEE Transactions on,* vol. 45, pp. 910-927, 2000.

[27] T. S. Schei, "A finite-difference method for linearization in nonlinear estimation algorithms," *Automatica,* vol. 33, pp. 2053-2058, 1997.

[28] M. Nørgaard, N. K. Poulsen, and O. Ravn, "New developments in state estimation for nonlinear systems," *Automatica,* vol. 36, pp. 1627-1638, 2000.

[29] J. L. Crassidis and F. L. Markley, "Unscented filtering for spacecraft attitude estimation," *Journal of Guidance Control and Dynamics,* vol. 26, pp. 536-542, 2003.

[30] F. Hutter and R. Dearden, "The gaussian particle filter for diagnosis of non-linear systems," 2003.

[31] F. Cadini and E. Zio, "Application of particle filtering for estimating the dynamics of nuclear systems," *Nuclear Science, IEEE Transactions on,* vol. 55, pp. 748-757, 2008.

[32] P. M. Djuric, J. H. Kotecha, J. Zhang, Y. Huang, T. Ghirmai, M. F. Bugallo, and J. Miguez, "Particle filtering," *Signal Processing Magazine, IEEE,* vol. 20, pp. 19-38, 2003.

[33] A. Doucet, S. Godsill, and C. Andrieu, "On sequential Monte Carlo sampling methods for Bayesian filtering," *Statistics and computing,* vol. 10, pp. 197-208, 2000.

[34] K. Kastella, "Finite difference methods for nonlinear filtering and automatic target recognition," *Multitarget-multisensor tracking: Applications and advances.,* vol. 3, pp. 233-258, 2000.

[35] V. Beneš, "Exact finite-dimensional filters for certain diffusions with nonlinear drift," *Stochastics: An International Journal of Probability and Stochastic Processes,* vol. 5, pp. 65-92, 1981.

[36] F. Daum, "Exact finite-dimensional nonlinear filters," *Automatic Control, IEEE Transactions on,* vol. 31, pp. 616-622, 1986.

[37] E. A. Wan and R. Van Der Merwe, "The unscented Kalman filter for nonlinear estimation," presented at the Adaptive Systems for Signal Processing, Communications, and Control Symposium, 2000.

[38] S. J. Julier and J. K. Uhlmann, "Unscented filtering and nonlinear estimation," *Proceedings of the IEEE,* vol. 92, pp. 401-422, 2004.

[39] M. J. Grimble, "Non-linear generalized minimum variance feedback, feedforward and tracking control," *Automatica,* vol. 41, pp. 957-969, 2005.

[40] M. J. Grimble and P. Majecki, "Nonlinear generalized minimum variance control under actuator saturation," presented at the IFAC World Congress, Prague, Czech Republic, 2005.

[41] M. Grimble, "NMV optimal estimation for nonlinear discrete-time multi-channel systems," in *IEEE Conference on Decision and Control*, New Orleans, Louisiana USA, 2007, pp. 4281-4286.

[42] J. S. Shamma and M. Athans, "Gain scheduling: Potential hazards and possible remedies," *Control Systems Magazine, IEEE,* vol. 12, pp. 101-107, 1992.

[43] J. S. Shamma and M. Athans, "Guaranteed properties of gain scheduled control for linear parameter-varying plants," *Automatica,* vol. 27, pp. 559-564, 1991.

[44] L. H. Lee and K. Poolla, "Identification of linear parameter-varying systems via LFTs," in *IEEE Conference on Decision and Control, 35th*, Kobe, Japan, 11-13 Dec 1996, pp. 1545-1550 vol. 2.

[45] M. Steinbuch, R. Van De Molengraft, and A. Van Der Voort, "Experimental modelling and LPV control of a motion system," in *Proceedings of the 2003 American control conference, ACC : June 4-6, 2003, Denver, Colorado, USA. Vol. 2*, 2003, pp. 1374-1379.

[46] A. Packard, "Gain scheduling via linear fractional transformations," *Systems & Control Letters,* vol. 22, pp. 79-92, 1994.

[47] P. Apkarian, P. Gahinet, and G. Becker, "Self-scheduled H_∞ control of linear parameter-varying systems: a design example," *Automatica,* vol. 31, pp. 1251-1261, 1995.

[48] M. J. Grimble, *Robust industrial control systems: optimal design approach for polynomial systems*. Chichester: John Wiley & Sons Inc, 2006.

[49] K. D. Hammett, "Control of Non-linear Systems via State-feedback State-dependent Riccati Equation Techniques," PhD Dissertation, Air Force Institute of Technology, Dayton, Ohio, 1997.

[50] T. Moir, "Optimal deconvolution smoother," *Control Theory and Applications, IEE Proceedings D,* vol. 133, pp. 13-18, 1986.

[51] M. Grimble and M. Johnson, *Optimal multivariable control and estimation theory* vol. 1. London: John Wiley, 1988.

[52] B. Kulcsár, J. Bokor, and J. Shinar, "Unknown input reconstruction for LPV systems," *International Journal of Robust and Nonlinear Control,* vol. 20, pp. 579-595, 2010.

[53] J. Shinar, J. Bokor, and B. Kulcsar, "On the detection of unknown input in positional control problems with noisy measurements," in *Proceedings of the 16th IFAC World Congress, Czech Republic*, 2005.

[54] J. Petersen and D. McFarlane, "Robust state estimation for uncertain systems," in *Proceedings of the 30th IEEE Conference on Decision and Control*, 1991, pp. 2630-2631 vol. 3.

[55] L. Xie and Y. C. Soh, "Robust Kalman filtering for uncertain systems," *Systems & Control Letters,* vol. 22, pp. 123-129, 1994.

[56] L. Xie, Y. C. Soh, and C. E. de Souza, "Robust Kalman filtering for uncertain discrete-time systems," *Automatic Control, IEEE Transactions on,* vol. 39, pp. 1310-1314, 1994.

[57] D. Bernstein and D. Hyland, "The optimal projection equations for reduced-order state estimation," *Automatic Control, IEEE Transactions on,* vol. 30, pp. 583-585, 1985.

[58] M. Grimble, "H_∞ design of optimal linear filters," *Linear Circuits, Systems, and Signal Processing: Theory and Application, Eds. Amsterdam The Netherlands: North-Holland,* pp. 533-540, 1988.

[59] A. Elsayed and M. Grimble, "A new approach to the H_∞ design of optimal digital linear filters," *IMA Journal of Mathematical control and Information,* vol. 6, pp. 233-251, 1989.

[60] M. Grimble and A. Elsayed, "Solution of the H_∞ optimal linear filtering problem for discrete-time systems," *Acoustics, Speech and Signal Processing, IEEE Transactions on,* vol. 38, pp. 1092-1104, 1990.

[61] J. C. Doyle, K. Glover, P. P. Khargonekar, and B. A. Francis, "State-space solutions to standard H2 and H∞ control problems," *Automatic Control, IEEE Transactions on,* vol. 34, pp. 831-847, 1989.

[62] U. Shaked, "H_∞-minimum error state estimation of linear stationary processes," *Automatic Control, IEEE Transactions on,* vol. 35, pp. 554-558, 1990.

[63] I. Yaesh and U. Shaked, "A transfer function approach to the problems of discrete-time systems: H_∞-optimal linear control and filtering," *Automatic Control, IEEE Transactions on,* vol. 36, pp. 1264-1271, 1991.

[64] M. J. Grimble, "H_∞ fixed-lag smoothing filter for scalar systems," *Signal Processing, IEEE Transactions on,* vol. 39, pp. 1955-1963, 1991.

[65] I. R. Petersen and A. V. Savkin, *Robust Kalman filtering for signals and systems with large uncertainties*: Birkhauser, 1999.

[66] L. Xie and C. E. de Souza, "On robust filtering for linear systems with parameter uncertainty," in *Proceedings of the 34th Conference on Decision & Control New Orleans* LA, USA, 1995, pp. 2087-2092 vol. 2.

[67] C. E. de Souza, R. Martinez Palhares, and P. L. Dias Peres, "Robust H_∞ filter design for uncertain linear systems with multiple time-varying state delays," *Signal Processing, IEEE Transactions on,* vol. 49, pp. 569-576, 2001.

[68] E. Fridman, U. Shaked, and L. Xie, "Robust H_∞ filtering of linear systems with time-varying delay," *Automatic Control, IEEE Transactions on,* vol. 48, pp. 159-165, 2003.

[69] H. Gao and C. Wang, "A delay-dependent approach to robust H_∞ filtering for uncertain discrete-time state-delayed systems," *Signal Processing, IEEE Transactions on,* vol. 52, pp. 1631-1640, 2004.

[70] H. Kwakernaak and R. Sivan, *Modern signals and systems*: Prentice Hall, 1991.

[71] M. Grimble, "Weiner and Kalman filters for systems with random parameters," *Automatic Control, IEEE Transactions on,* vol. 29, pp. 552-554, 1984.

[72] J. Speyer and D. Gustafson, "An approximation method for estimation in linear systems with parameter uncertainty," *Automatic Control, IEEE Transactions on,* vol. 20, pp. 354-359, 1975.

[73] M. Sternad and A. Ahlén, "Robust filtering and feedforward control based on probabilistic descriptions of model errors," *Automatica,* vol. 29, pp. 661-679, 1993.

[74] S. Ali Naz, "Linear and Nonlinear Polynomial Based Estimators," Ph.D Thesis, Dept. of Elect. Eng., University of Strathclyde, Glasgow, UK, 2009.

[75] M. Grimble and S. Ali Naz, "Optimal minimum variance estimation for non-linear discrete-time multichannel systems," *Signal Processing, IET,* vol. 4, pp. 618-629, 2010.

[76] C. Chi and J. Mendel, "Performance of minimum-variance deconvolution filter," *Acoustics, Speech and Signal Processing, IEEE Transactions on,* vol. 32, pp. 1145-1153, 1984.

[77] K. J. Åström, *Introduction to stochastic control theory* vol. 70: Elsevier Science, 1970.

[78] M. Grimble, "Multichannel optimal linear deconvolution filters and strip thickness estimation from gauge measurements," *Journal of dynamic systems, measurement, and control,* vol. 117, pp. 165-174, 1995.

[79] S. Ali Naz and M. Grimble, "Design and real time implementation of nonlinear minimum variance filter," in *UKACC Conference*, Manchester, UK, 2008.

[80] M. J. Grimble and S. A. Naz, "Nonlinear minimum variance estimation for discrete-time multi-channel systems," *Signal Processing, IEEE Transactions on,* vol. 57, pp. 2437-2444, 2009.

[81] L. Ljung, *System identification*: Wiley Online Library, 1999.

[82] M. Verhaegen and V. Verdult, *Filtering and system identification: a least squares approach*: Cambridge Univ Pr, 2007.

[83] S. Haykin, "Neural networks: a comprehensive foundation, 1999," ed: Prentice-Hall.

[84] J. C. Kantor, "An overview of nonlinear geometrical methods for process control," presented at the In Shell Process Control Workshop, Boston, USA, 1987.

[85] F. J. Doyle, R. K. Pearson, and B. A. Ogunnaike, *Identification and control using Volterra models*: Springer Verlag, 2002.

[86] P. Stoica and T. Söderstrom, "Instrumental-variable methods for identification of Hammerstein systems," *International Journal of Control,* vol. 35, pp. 459-476, 1982.

[87] W. Greblicki, "Nonparametric identification of Wiener systems," *Information Theory, IEEE Transactions on,* vol. 38, pp. 1487-1493, 1992.

[88] P. Gawthrop, J. Jezek, R. Jones, and I. Sroka, "Grey-box model identification," *Control-Theory and Advanced Technology,* vol. 9, pp. 139-157, 1993.

[89] U. Forssell and P. Lindskog, "Combining semi-physical and neural network modeling: an example of its usefulness," *SYSID, July,* pp. 795-798, 1997.

[90] E. Yang, M. Grimble, S. Inzerillo, and M. Katebi, "Nonlinear model-based condition monitoring of advanced gas-cooled nuclear reactor cores," in *7th International Conference on Control & Instrumentation in Nuclear Installations*, Lancaster University, UK, 2011.

[91] A. G. Steer, "AGR core design, operation and safety functions," *SPECIAL PUBLICATION-ROYAL SOCIETY OF CHEMISTRY,* vol. 309, p. 11, 2007.

[92] C. Forsberg, "Refueling Options for LS-VHTRs Based On High-Temperature Reactor Experience," Oak Ridge National Laboratory; , LS-VHTR Meeting, Department of Energy, Germantown, Maryland, US, 2006 (URL: http://www.ornl.gov/~webworks/cppr/y2001/pres/124827.pdf).

[93] B. J. Marsden, "Stresses and Deformations in Graphite Bricks," University of Manchester; (URL: http://web.up.ac.za/sitefiles/file/44/2063/Nuclear_Graphite_Course/Stresses%20and%20Deformations.pdf).

[94] J. Skelton, "Fuel grab load trace applied to the detection of cracks in AGR fuel bricks: Final report on the experimental and analysis programme," AMEC-NNC Report,2005.

[95] P. R. Dahl, "Solid friction damping of spacecraft oscillations," in *Proceedings of AIAA Guidance and Control Conference*, Boston, MA, USA, 1975.

[96] C. Canudas de Wit, H. Olsson, K. J. Astrom, and P. Lischinsky, "A new model for control of systems with friction," *Automatic Control, IEEE Transactions on,* vol. 40, pp. 419-425, 1995.

[97] H. Unbehauen and G. Rao, "A review of identification in continuous-time systems," *Annual reviews in Control,* vol. 22, pp. 145-171, 1998.

[98] M. Niethammer, P. H. Menold, and F. Allgöwer, "Parameter and derivative estimation for nonlinear continuous-time system identification," in *Proceedings of*

the 5th IFAC Symposium on Nonlinear Systems, St. Petersburg, Russia, 2001, pp. 691–696.

[99] G. Jahn, S. McArthur, J. Reed, and D. Towle, "Staged implementation of an agent based advanced gas-cooled reactor condition monitoring system," in *Power Engineering Society General Meeting, Tampa, Florida, USA, 2007, pp 1-4*

[100] G. West and E. Yang, "Graphite Core Condition Monitoring," University of Strathclyde, Internal Report,2010.

[101] A. G. Steer, "Graphite Research and Development," British Energy (URL: http://www.hse.gov.uk/aboutus/meetings/iacs/nusac/031006/presentation3.pdf).

[102] J. J. Moré and D. Sorensen, "Computing a trust region step," *SIAM Journal on Scientific and Statistical Computations,* vol. 4, pp. 553-572, 1983.

[103] D. M. Gay, "Computing optimal locally constrained steps," *SIAM Journal on Scientific and Statistical Computing,* vol. 2, p. 186, 1981.

[104] M. A. Branch, T. F. Coleman, and Y. Li, "A subspace, interior, and conjugate gradient method for large-scale bound-constrained minimization problems," *SIAM Journal on Scientific Computing,* vol. 21, pp. 1-23, 1999.

[105] R. H. Byrd, R. B. Schnabel, and G. A. Shultz, "Approximate solution of the trust region problem by minimization over two-dimensional subspaces," *Mathematical programming,* vol. 40, pp. 247-263, 1988.

Appendix A

AGR Overview

An AGR is enclosed in a concrete pressure vessel that prevents any radiation leak and contains the carbon dioxide (CO2) coolant gas (Figure A.1). The reactor core is a cylinder formed by an array of smaller cylinders which in turn are composed by graphite bricks that host the enriched uranium oxide fuel assemblies and control rods. The latter are steel cylinders, which contain boron, that are inserted or removed from their channels to regulate the chain reaction by absorbing neutrons. The fuel is instead the source of the fissile neutrons, which once moderated by the graphite sustain the fission reaction; therefore the fuel is the source of the heat production. The heat is captured by the coolant gas to be used to drive the generators turbines.

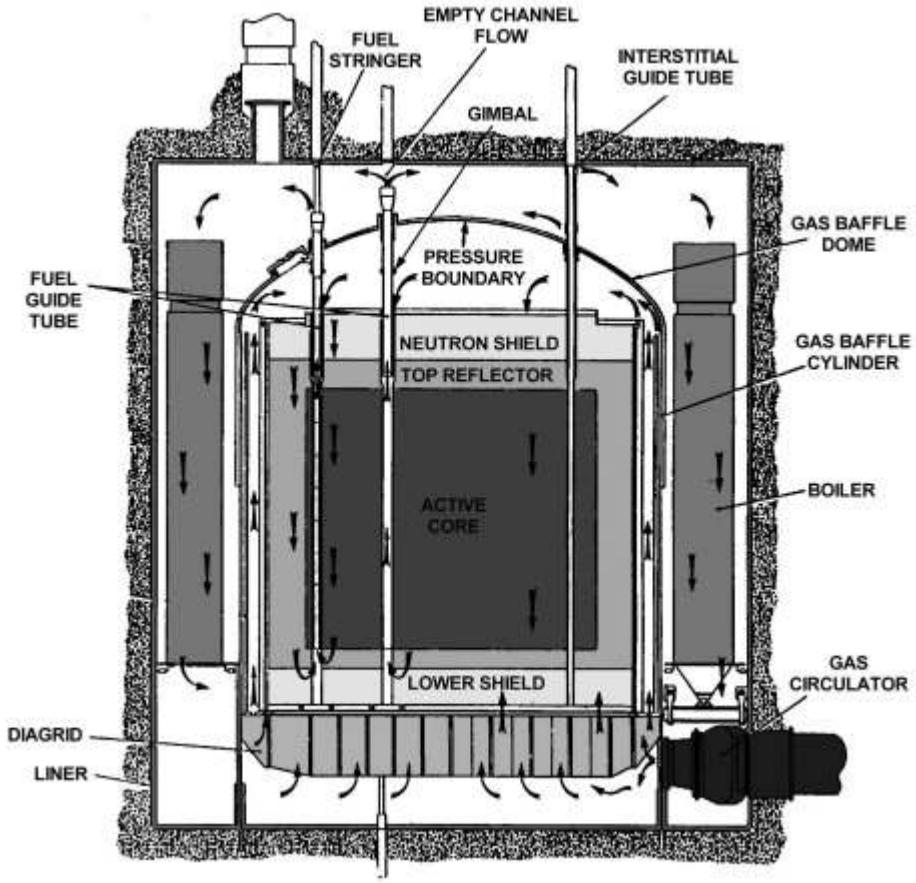

Figure A.1: AGR core internals and coolant flows (Source: [91])

The carbon dioxide was chosen as the gas coolant because it presents some advantages such as it does not corrode, it has a low capture cross section and it is cheap. Although using CO_2 as the coolant gas implies having a large and expensive reactor vessel, the heat transfer is low and the coolant has to be pressurised to 40 bar to give sufficient heat capacity.

The CO_2 is pumped by the gas circulators to enter the bottom of the fuel assemblies where it is heated from the initial temperature of 390°C to a temperature of 630-650°C. This high temperature gas is discharged above the gas baffle dome and goes to the boilers. The heat is then converted within the boilers to steam, which successively passes through the turbines to drive the electricity generators.

Appendix B

Cracks Classification

Due to the prolonged exposure to heat and radiation, the core graphite moderator is ageing, which could cause distortion and possible cracks in the reactor core. Two main types of cracks have been identified, the primary (axial) cracks and the circumferential cracks (see Figure B.1).

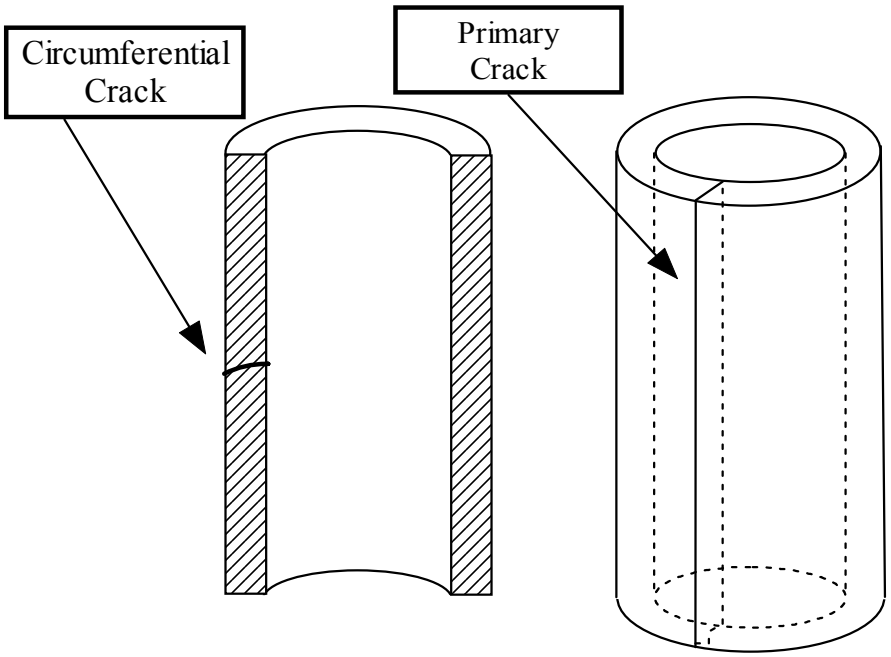

Figure B.1: Two main types of cracks

Primary cracks occur when the crack is extended from the top to the bottom of the brick layer and it may cause the brick to split, ending in a larger internal channel diameter. Although the brick might double crack and shear and in this case we would observe a diameter reduction.

Single and double cracks, however, would most likely have caused the same result, a step change, in the load recorded across the brick layer where the crack is located. The dimension of the change in diameter and the direction of travel of the fuel

assembly, i.e. the refuelling operation performed during the data collection, determine the magnitude and direction of the step change in the FGLT. During the removal of the exhausted fuel assembly (discharge) from the core, the friction force is opposite to the movement of the assembly, therefore the friction is added to the weight of the assembly. In this case a larger diameter would result in a decrement of the friction force, thus of the apparent load of the assembly. Instead during the charge the frictional force supports the weight of the fuel assembly, so a broader fuel channel diameter would cause an increment of the apparent load.

Circumferential cracking refers to cracks that propagate around the inner surface of the channel wall. The stresses built up within the brick cause it to distort at the crack interface, causing a restriction at the crack over time. This manifests itself as a peak on a discharge load trace and as a fall for a charge refuelling operation.

These results have been validated for known cracks against the inspection data, i.e. CBMU.

Appendix C

Core Inspection

Core inspection is an operation that provides information of the core graphite structure condition by investigating the effects of graphite degradation processes in the core brick layers. To assess the core structural integrity, we have to understand how stresses evolve within all the graphite components, and how other factors including neutron damage, ionizing radiation, and temperature affect the core geometry. To this end a trepanning small sample technique has been adopted by EDF Energy ([1]) to reveal the changes in the physical and mechanical properties such as tensile and compressive strength, Young's modulus, and material density. The main advantage of extracting trepanned samples is that it can provide a precise indication of the state of fuel channel graphite.

The channel dimension monitoring equipment specially developed for studies of core and channel geometry is called the channel bore monitoring unit (CBMU). The CBMU is able to provide information on brick ovality, tilt and bow, and overall column tilt and bow as well as the step changes between bricks (see Figure C.1 and Figure C.2).

Figure C.1: Channel Bore Measurement Unit (Source: [101])

To reduce the time required for the measuring and sampling operations, the trepanning, bore measurements along with TV inspection are usually joined and deployed together.

Other approaches have been investigated like in [3] where non-destructive techniques using ultrasound or resistance networks for crack detection were discussed. Ultrasonic imaging is extremely difficult due to both brick geometry and the grain structure of the material as well as the back echoes from the methane holes present in graphite bricks.

It is important to highlight that trepanning unit (TTU), CBMU and TV devices can only be employed during reactor shutdown so they cannot provide core condition information on a frequent basis.

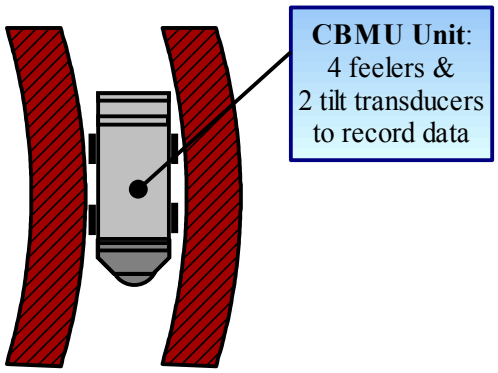

Figure C.2: Cut view of CBMU within a channel during inspection operation

Appendix D

Trust Region Reflective Newton Method

Iterative methods for optimization can be classified into two categories: line search methods and trust region methods. In this appendix a trust-region algorithm for nonlinear optimization problems is presented. The constrained nonlinear optimization problem can be expressed as below:

$$\begin{aligned} &\min_{\mathbf{x}\in R^n} f(\mathbf{x}) \\ &s.t. \qquad l_i \le x_i \le u_i, i = 1, 2, \cdots, n \end{aligned} \tag{D.1}$$

where $f(\mathbf{x})$ is a real scalar function to be minimized, l_i and u_i are the lower and upper bounds for the optimization variable x_i, respectively.

Trust-region algorithms are simple and robust methods which, from a current guess of the solution **x**, constructs an approximate model $q(\mathbf{x})$ of the original model $f(\mathbf{x})$ near this current solution point.

The simpler model $q(\mathbf{x})$ reasonably approximates the behaviour of function $f(\mathbf{x})$ in the trust region, i.e. a neighbourhood N around the current point **x**. A solution of the optimization problem, where the approximated model is employed, gives a trial step **s** used in the next iteration. Such trust-region sub-problem can be written as follow:

$$\begin{aligned} &\min_{\mathbf{s}\in N} q(\mathbf{s}) \\ &s.t. \qquad l_i \le s_i \le u_i, i = 1, 2, \cdots, n \end{aligned} \tag{D.2}$$

If $f(\mathbf{x}+\mathbf{s}) < f(\mathbf{x})$, then the $\mathbf{x}+\mathbf{s}$ becomes the current point; otherwise, the current point remains unchanged and the trust region is reduced to compute a new trial step **s**. This process is repeated until a point can be accepted as a solution.

In trust-region algorithms, the key questions are how to construct the approximation $q(\mathbf{x})$ at the current point **x**, how to decide whether a trial step **s** should be accepted, how efficiently to solve the trust-region sub-problem, and how to choose and adjust the trust region N. Since the trust region N is bounded, the non-convex approximate models can be used in trust-region algorithms. This represents one of the advantages of trust region algorithms over line search algorithms.

In the standard trust-region algorithm ([102]), the trust-region sub-problem is defined by

$$\min\{\frac{1}{2}\mathbf{s}^T\mathbf{H}\mathbf{s}+\mathbf{s}^T\mathbf{g},\|\mathbf{D}\mathbf{s}\|\le\Delta\} \tag{D.3}$$

where $\mathbf{H}$ is the Hessian matrix, $\mathbf{g}$ is the gradient of $f(\mathbf{x})$ at the current point $\mathbf{x}$, $\mathbf{D}$ is a diagonal scaling matrix, and Δ is a positive scalar. The above trust-region sub-problem has been studied by many authors and a well known lemma ([102, 103]) solves it efficiently by computing a full eigensystem and solving the following secular equation by applying a Newton's method:

$$\frac{1}{\Delta}-\frac{1}{\|\mathbf{s}\|}=0 \tag{D.4}$$

To reduce the computation time when the standard trust-region algorithm is applied to solve large-scale problems, a number of new approximation and heuristic strategies have been proposed in the literature. In this study, a two-dimensional subspace strategy ([104, 105]) is adapted to solve the nonlinear system identification problem for the model-based condition monitoring of AGR nuclear graphite cores. The key idea is to restrict the trust-region sub-problem to the two-dimensional subspace $S=<s_1,s_2>$ where $\mathbf{s}_1$ is in the direction of the gradient $\mathbf{g}$ and $\mathbf{s}_2$ is either in the direction of negative curvature

$$\mathbf{H}\times\mathbf{s}_2=\mathbf{-g}$$

or an approximate Newton direction found by solving the following equation:

$$\mathbf{s}_2^T\cdot\mathbf{H}\cdot\mathbf{s}_2<0$$

By constructing such a two-dimensional subspace S, the global convergence can be reached via the steepest descent direction or the negative curvature. Instead through the Newton step, a fast local convergence can also be achieved.

Appendix E

Friction Force Estimation Results Plots

E.1 Input and Output Data for Channel 3, 4 and 5

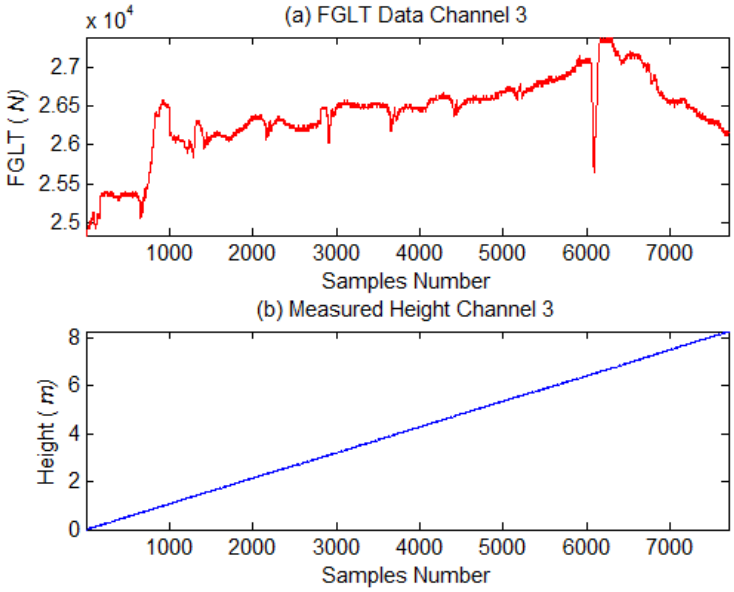

Figure E.1: Refuelling measurements data channel 3: FGLT data (above) and height (below)

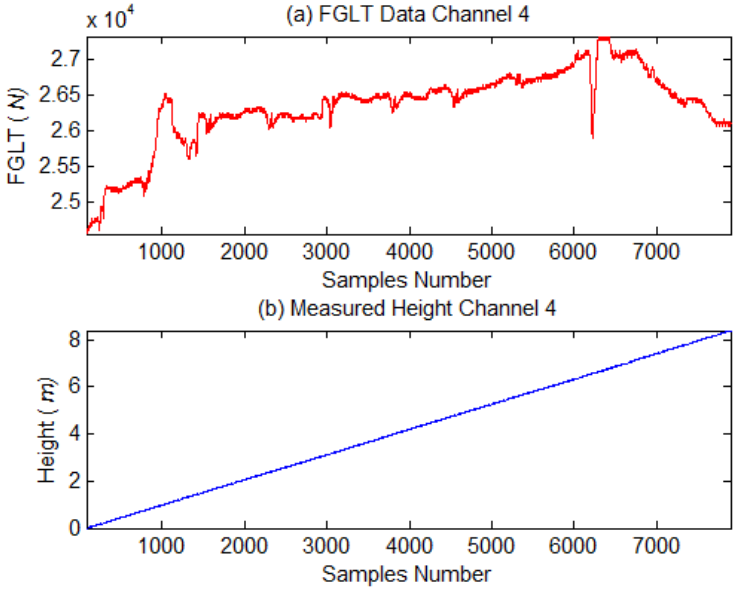

Figure E.2: Refuelling measurements data channel 4: FGLT data (above) and height (below)

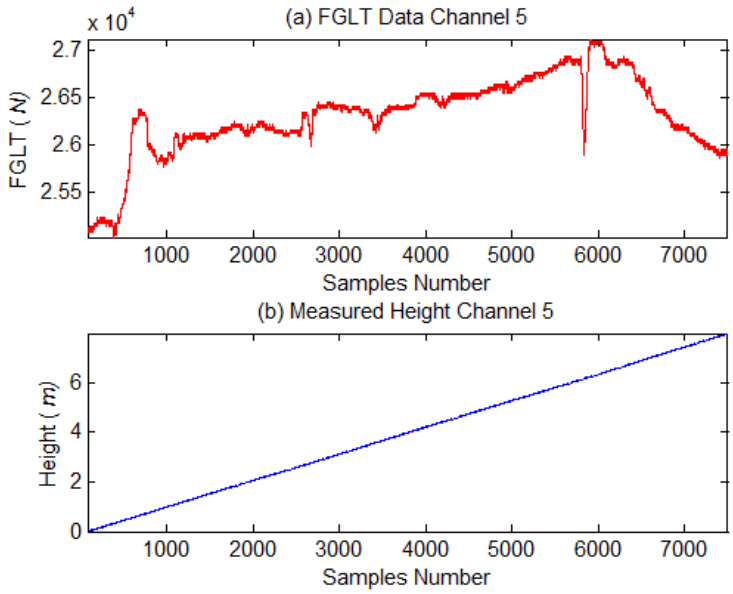

Figure E.3: Refuelling measurements data channel 5: FGLT data (above) and height (below)

E.2 Friction Estimation by using the state-dependent estimator

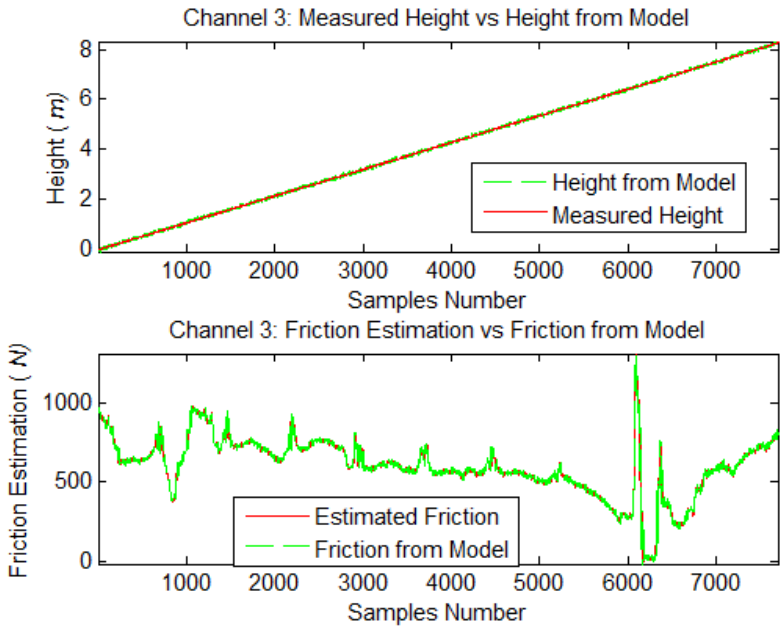

Figure E.4: Channel 3 measured height vs height from model (above) and friction from model vs estimated friction (below)

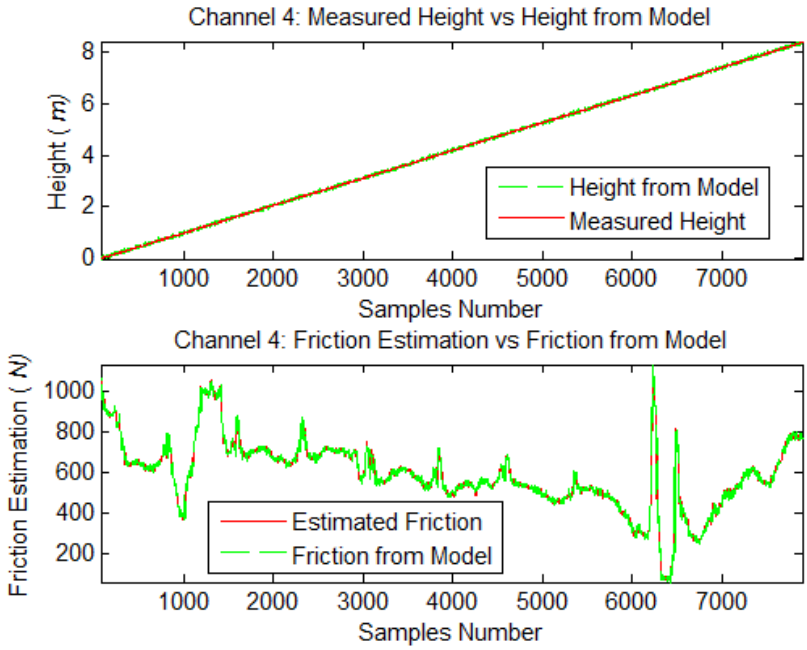

Figure E.5: Channel 4 measured height vs height from model (above) and friction from model vs estimated friction (below)

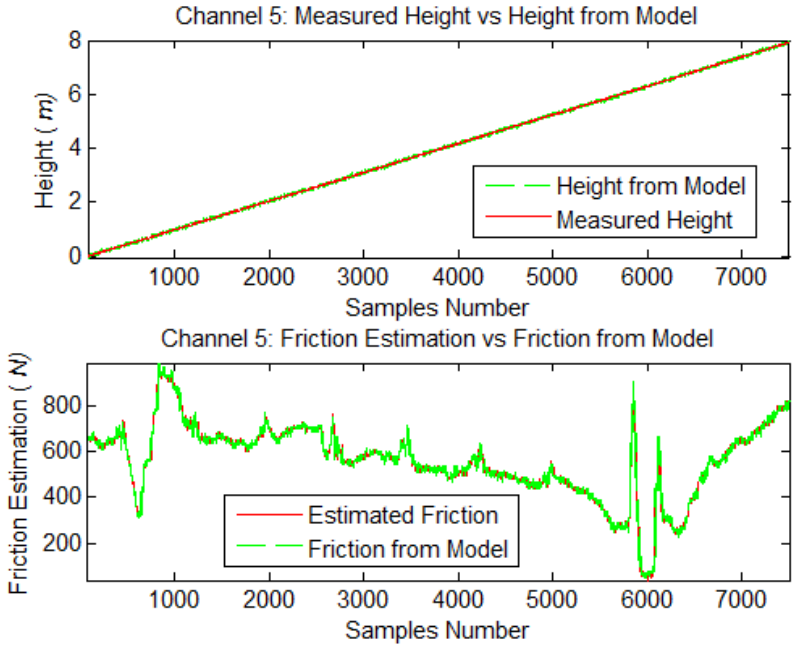

Figure E.6: Channel 5 measured height vs height from model (above) and friction from model vs estimated friction (below)

E.3 Friction Estimation by using the robust estimator

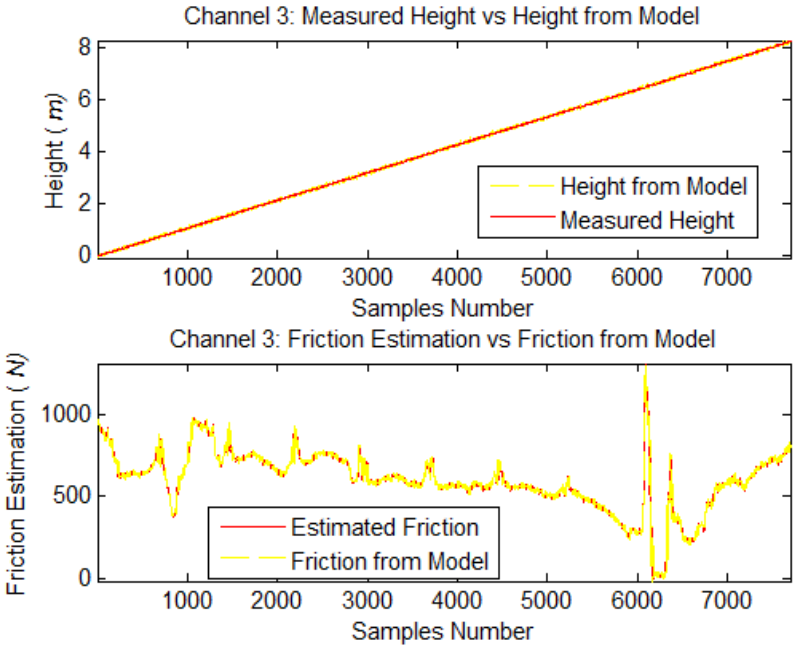

Figure E.7: Channel 3 measured height vs height from model (above) and friction from model vs estimated friction (below)

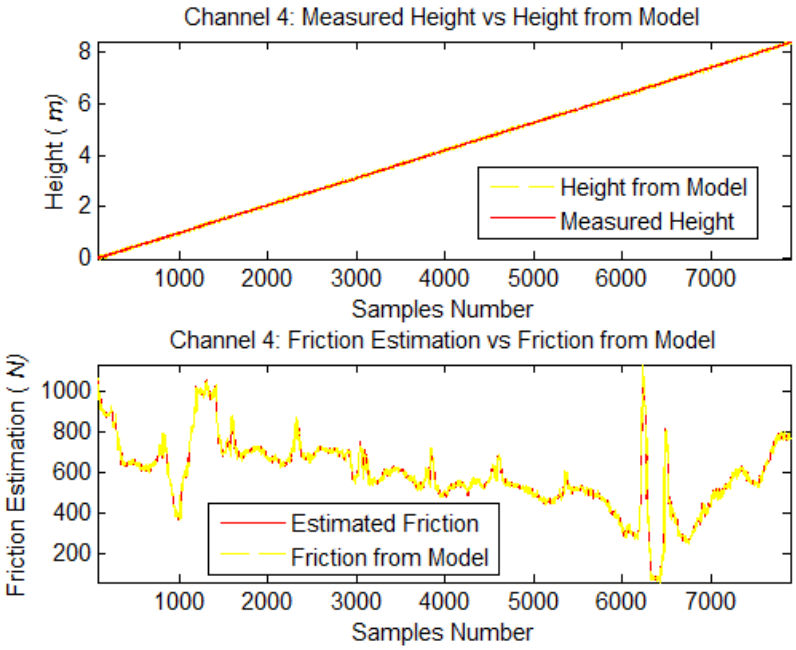

Figure E.8: Channel 4 measured height vs height from model (above) and friction from model vs estimated friction (below)

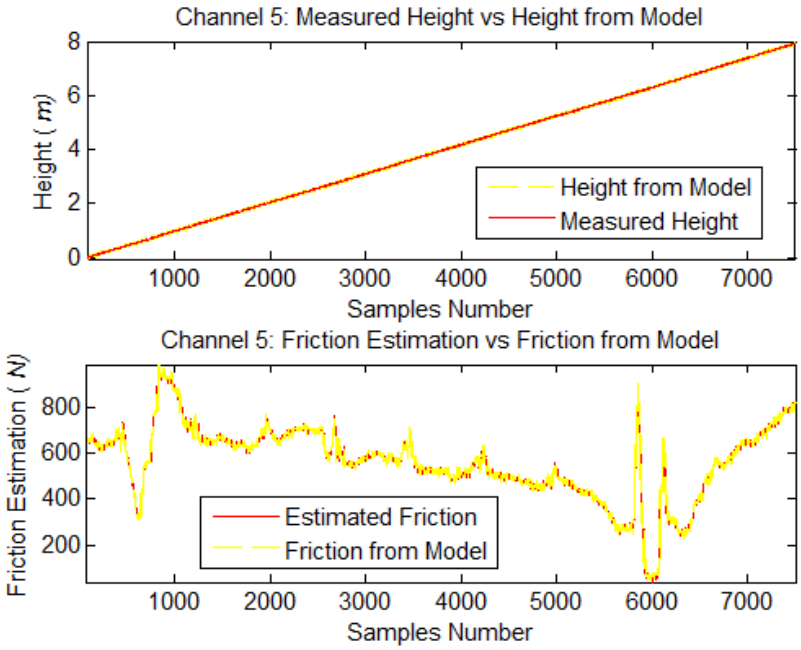

Figure E.9: Channel 5 measured height vs height from model (above) and friction from model vs estimated friction (below)

Appendix F

Overview of Software Developed

F.1 LPV Estimation Software (Evader-Pursuit Problem)

master_file_LPV.m

Define System Specifications
Define Models
Define Weighting Dynamics
Call Function lpv_nmv_estimator.m
Run Simulation: lpv_estimator.mdl
Plot Results

calcMatrices.m
Calculate Matrices Runtime
Called from simulink

lpv_nmv_estimator.m
Calculate Spectral Factor Y_f
Design Filter L_0

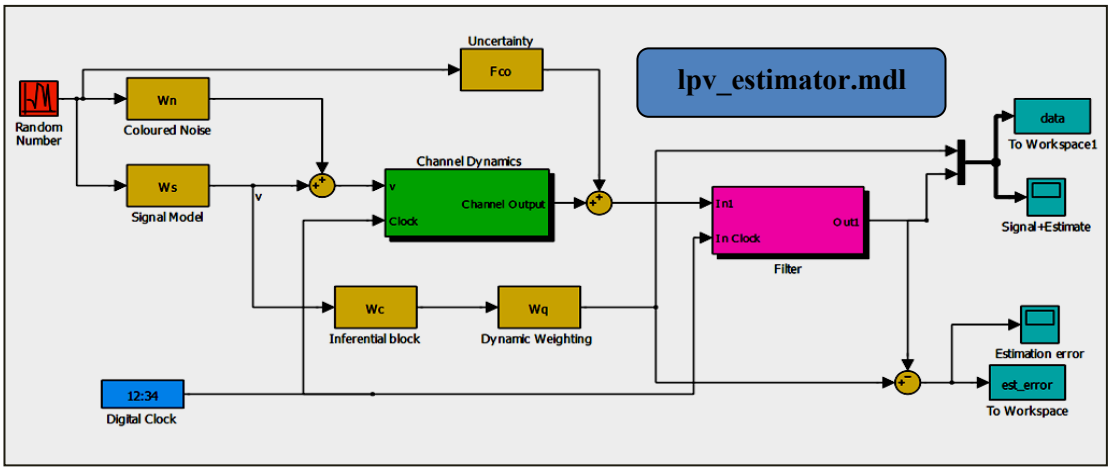

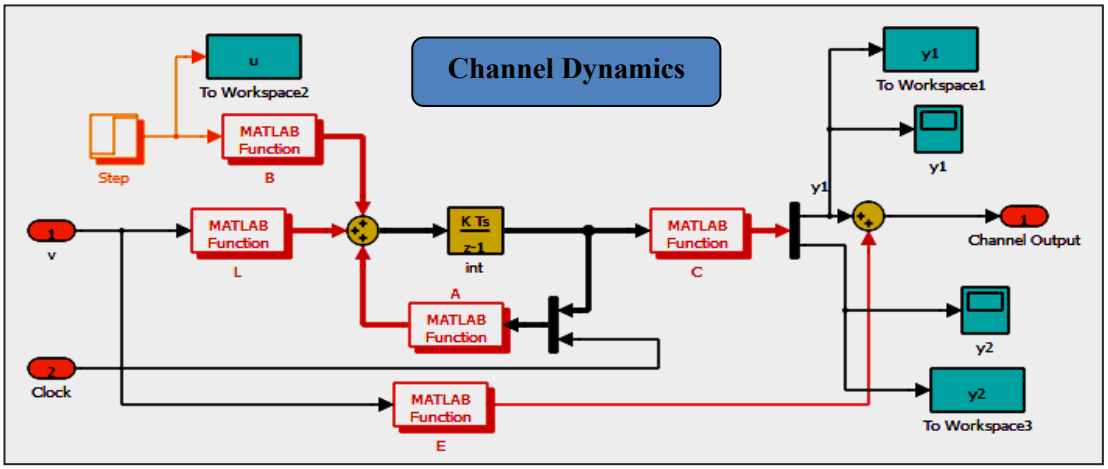

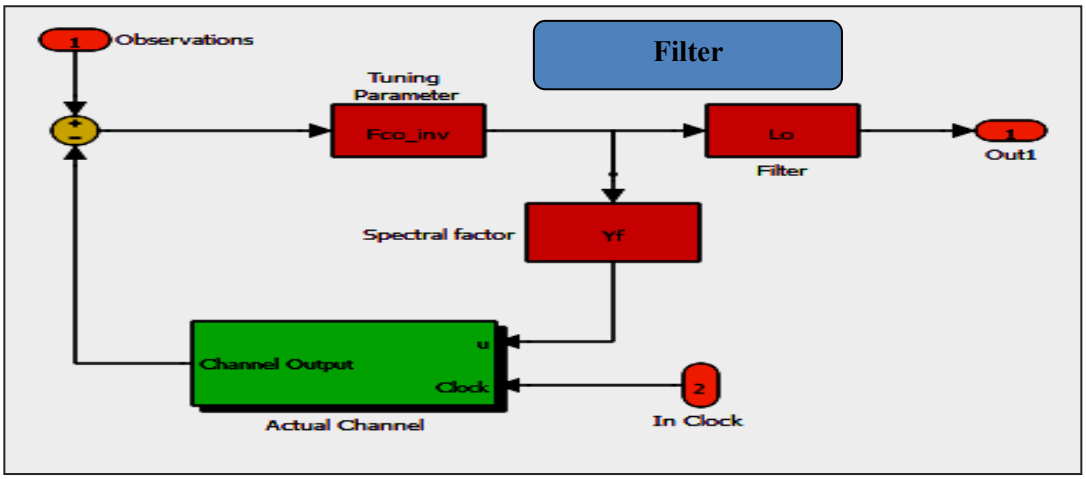

F.2 H_∞ Robust estimation Software (UEGO & EGO Sensors Case Studies)

master_hinf_ego_sensor.m

Define System Specifications
Define Models
Define Weighting Dynamics
Call Function nmv_estimator.m
Call Function hinf_estimator.m
Run Simulation:
hinf_ego_sensor.mdl
Plot Results

master_hinf_uego_sensor.m

Define System Specifications
Define Models
Define Weighting Dynamics
Call Function nmv_estimator.m
Call Function hinf_estimator.m
Run Simulation:
hinf_uego_sensor.mdl
Plot Results

hinf_estimator.m

Calculate Spectral Factor Y_f

Call function siso_dio_gep.m
Calculate Filter L_0

siso_dio_gep.m

Solution of the generalized eigenvalue problem

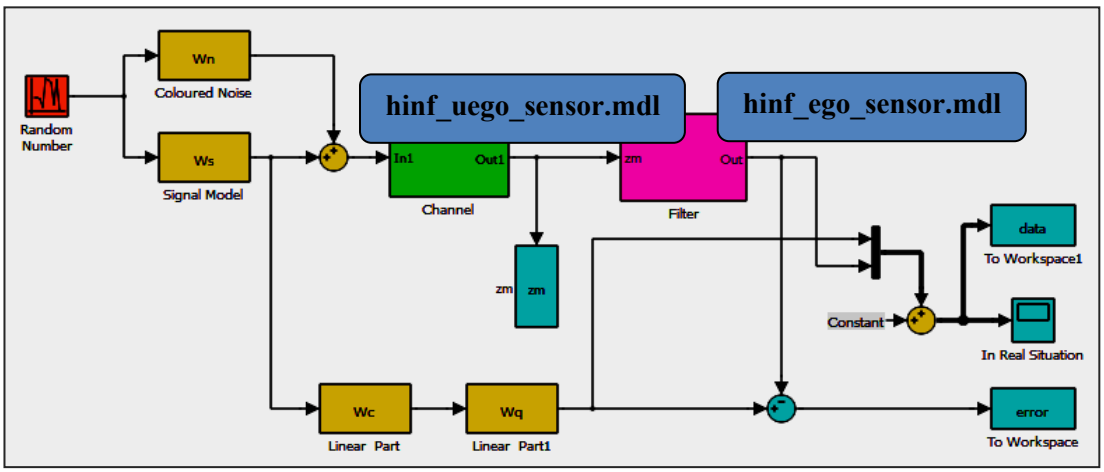

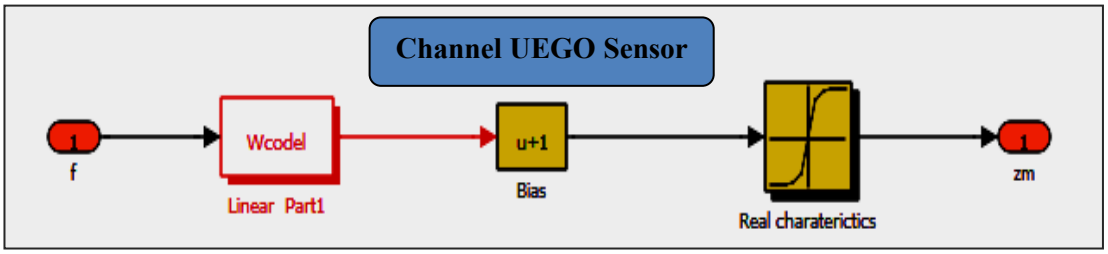

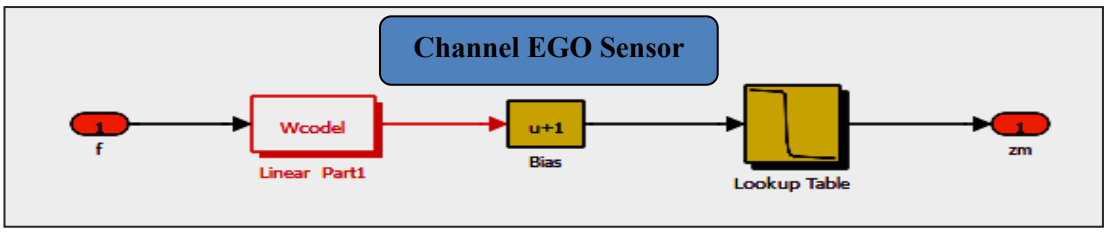

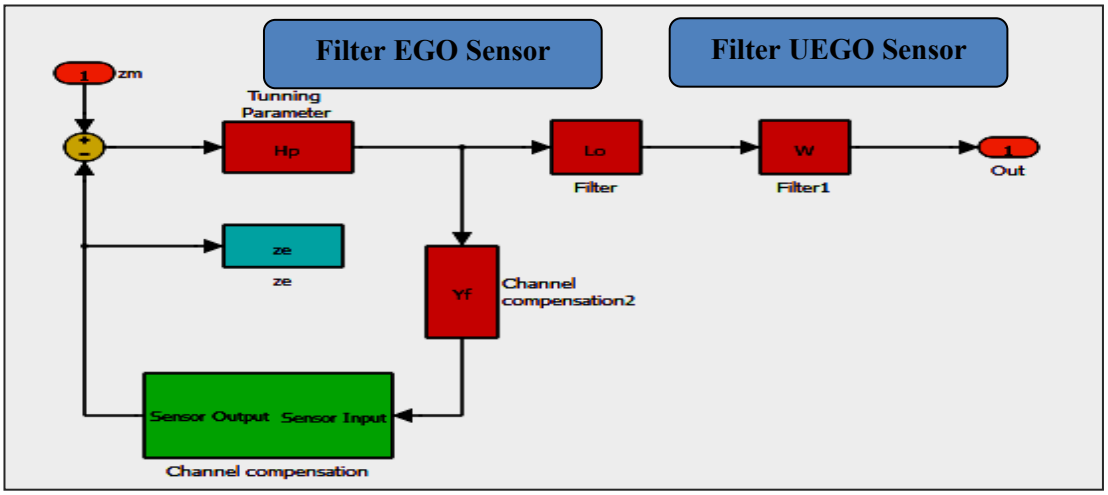

F.3 Robust Wiener estimation Software (Channel Equalization Case Study)

master_rob_wnmv_NL_ChEqual.m

Define System Specifications
Define Models and Parameter Covariances
Define Weighting Dynamics
Call Function wnmv_estimation.m
Run Simulation:
wnmv_NL_ChEqualPr.mdl
Plot Results

wnmv_estimation.m
Calculate Averaged Spectral Factor $\bar{Y}_f$
Design Filter L_0

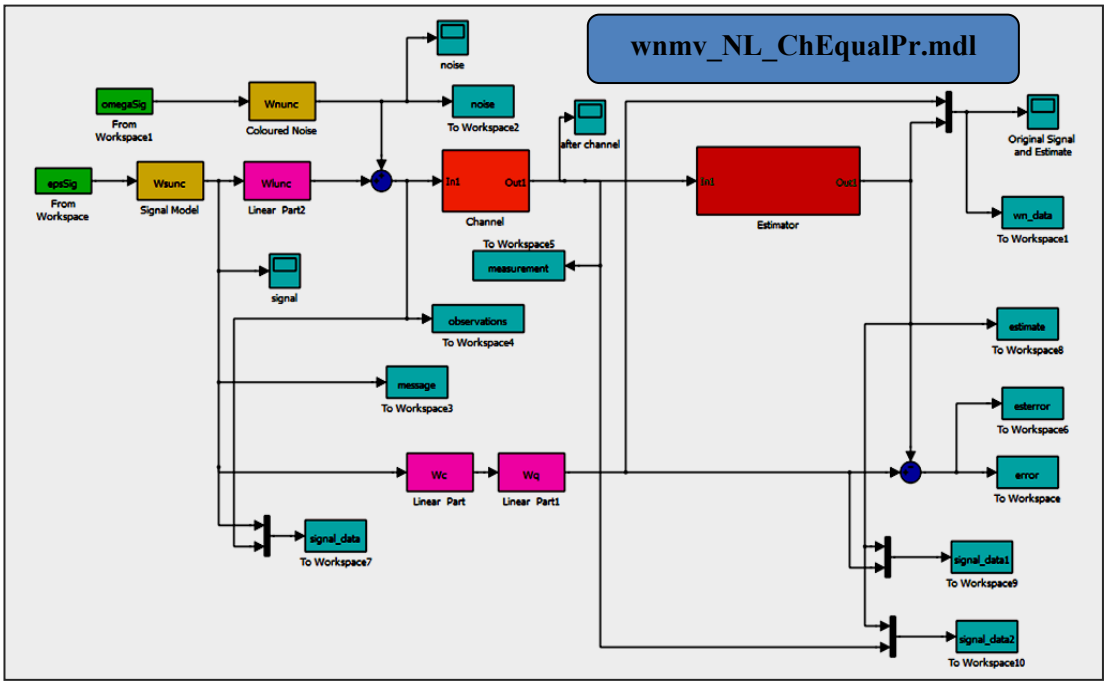

F.4 Nonlinear System Identification Software

Friction_Model_LuGre.m
Define the model structure through an external file (Model_LuGre_c.c)

Create an IDNLGREY object reflecting the modelling situation

Identify the unknown parameters using real plant data

Plot Results

Save parameters

Model_LuGre_c.c

Define first principles model of the refuelling subsystem

F.5 Friction Estimation by using the State-dependent estimator

master_stdep_friction_estim.m
Define System Specifications
Load Model Parameters
Define Weighting Dynamics
Call Function stdep_nmv_estimator.m
Run Simulation:
stdep_friction_estimation.mdl
Plot Results

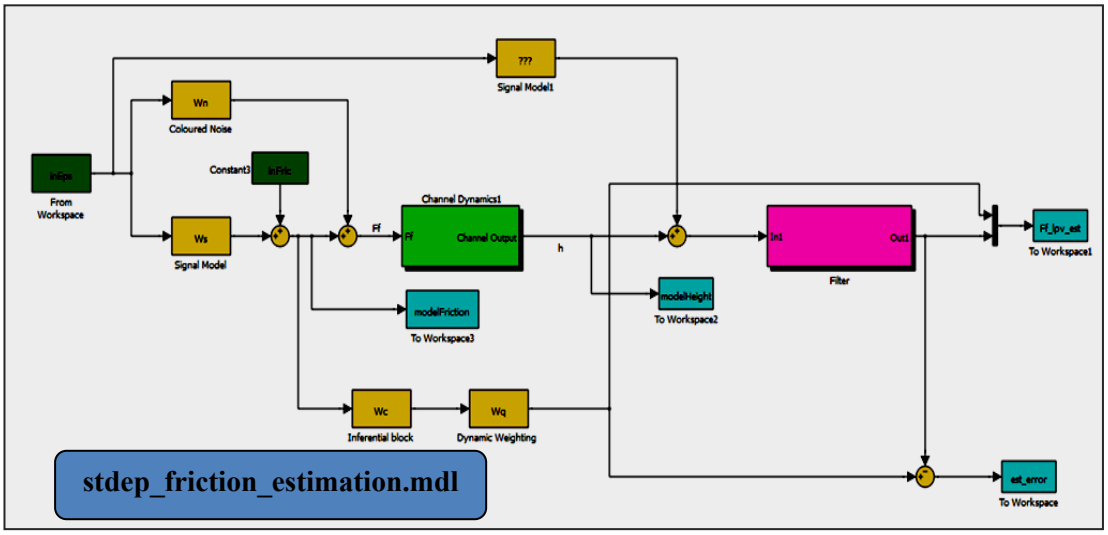

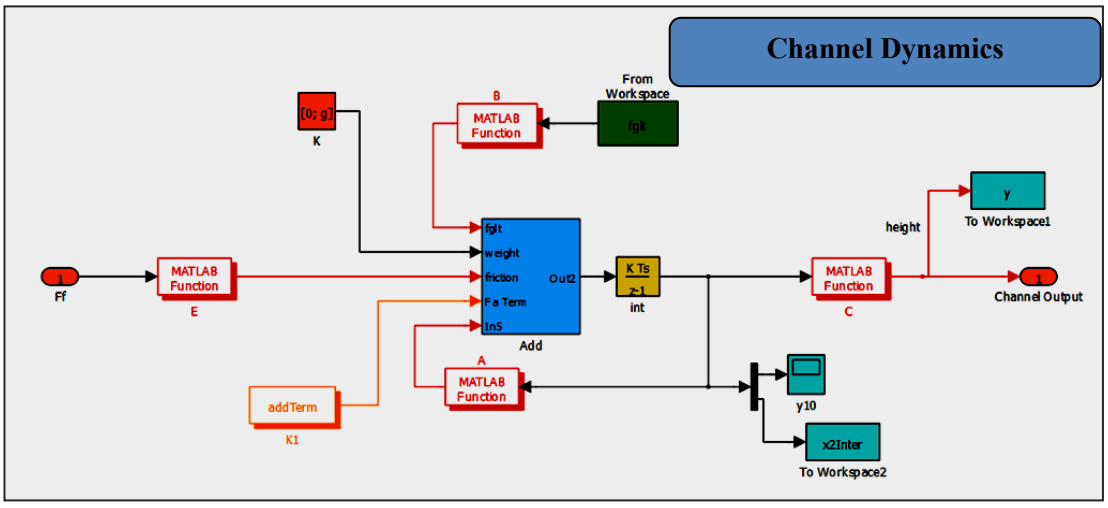

F.6 Friction Estimation by using the Robust estimator

master_hinf_friction_estim.m
Define System Specifications
Load Model Parameters
Define Weighting Dynamics
Call Function hinf_estimator.m
Run Simulation:
NHinf_friction_estimation.mdl
Plot Results

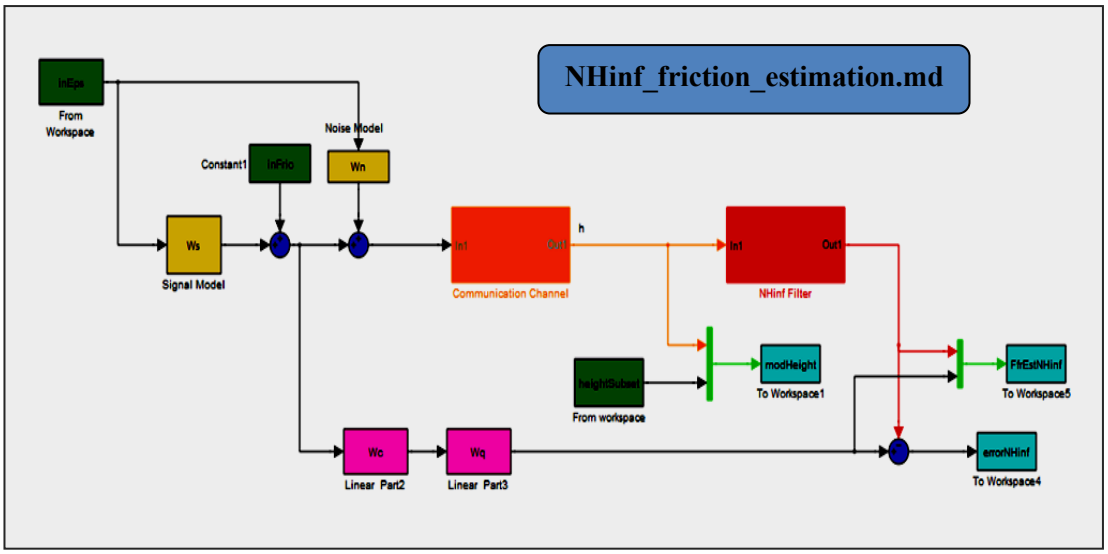

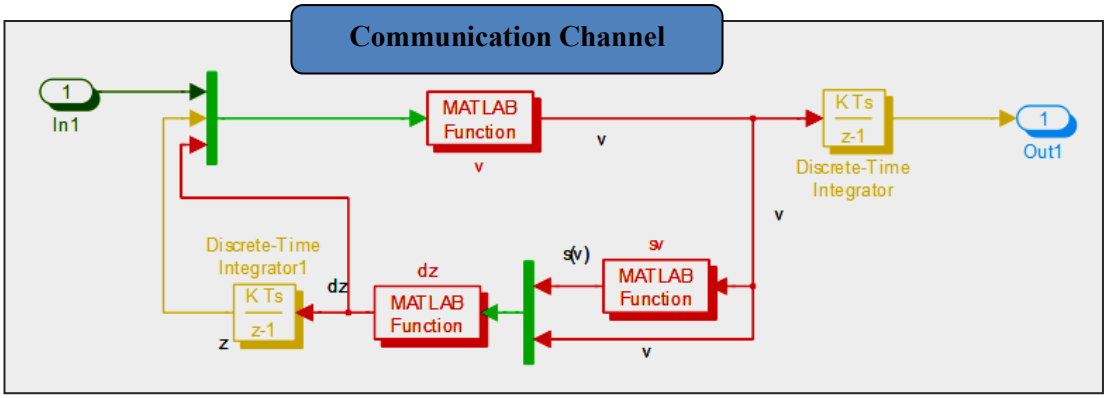

Appendix G

Implementable Nonlinear Inverse Operator Block Diagram

Let us consider the system in Figure G.1 where F_{ip} is a nonlinear channel selected by the designer that has a stable inverse, W_l and W_{nl} are a linear channel (it may be the unit matrix) and a nonlinear operator respectively. Note that the above mentioned matrices are of appropriate dimensions.

We can derive the procedure that follows, which constructs an inverse for the nonlinear operator $(F_{ip}+W_lW_{nl})$:

$$y(t)=F_{ip}^{-1}(m-n)^{-1} \tag{G.1}$$

$$m=(F_{ip}+W_lW_{nl})\varepsilon(t); \quad n=W_lW_{nl}y(t) \tag{G.2}$$

Substituting equation (G.2) into (G.1) yields:

$$F_{ip}y(t)=(F_{ip}+W_lW_{nl})\varepsilon(t)-W_lW_{nl}y(t) \tag{G.3}$$

$$(F_{ip}+W_lW_{nl})y(t)=(F_{ip}+W_lW_{nl})\varepsilon(t)=m \tag{G.4}$$

From the above equation we can see that the parallel blocks on the right of Figure G.1 produce an inverse of the operator $F_{ip}+W_lW_{nl}$ with the assumption that F_{ip} is chosen in a way that the inverse of the operator is stable.

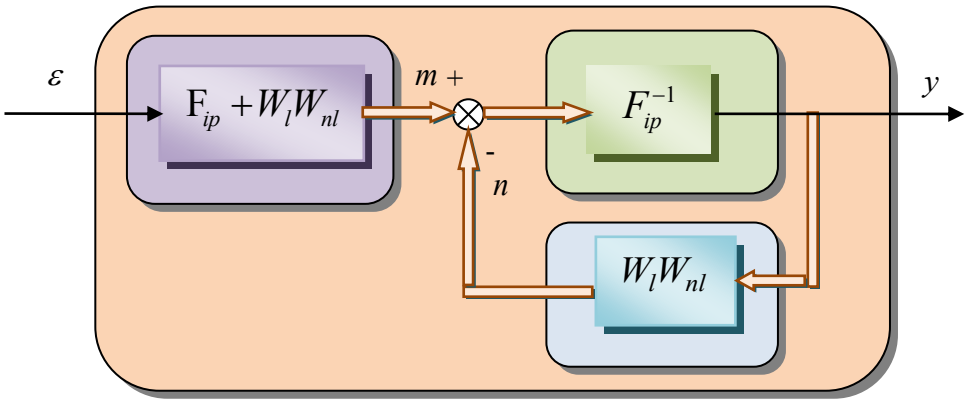

Figure G.1: Block diagram of the construction of the inverse operator

From the above consideration and a proper choice of F_{ip} which guarantees the operator $(F_{ip} + W_{nl})$ to have an inverse stable, by construction we can produce an inverse of this operator that can be therefore be implemented for simulation (e.g. simulink blocks).